Titre: Title:	Geologically constrained inversion modeling of titan magnetotelluric and induced polarization survey results at Kidd Creek Mine
Auteur: Author:	Jean M. Legault
Date:	2005
Type:	Mémoire ou thèse / Dissertation or Thesis
Référence: Citation:	Legault, J. M. (2005). Geologically constrained inversion modeling of titan magnetotelluric and induced polarization survey results at Kidd Creek Mine [Master's thesis, École Polytechnique de Montréal]. PolyPublie. https://publications.polymtl.ca/7409/

UNIVERSITÉ DE MONTRÉAL

GEOLOGICALLY CONSTRAINED INVERSION MODELING OF TITAN MAGNETOTELLURIC AND INDUCED POLARIZATION SURVEY RESULTS AT KIDD CREEK MINE

JEAN M. LEGAULT
DÉPARTEMENT DES GÉNIES CIVIL,
GÉOLOGIQUE ET DES MINES
ÉCOLE POLYTECHNIQUE DE MONTRÉAL

MÉMOIRE PRÉSENTÉ EN VUE DE L'OBTENTION
DU DIPLÔME DE MAÎTRISE ÈS SCIENCES APPLIQUÉES (M.SC.A)
(GÉNIE MINÉRAL)
AVRIL 2005

Your file Votre référence
ISBN: 0-494-01355-9
Our file Notre référence
ISBN: 0-494-01355-9

UNIVERSITÉ DE MONTRÉAL

ÉCOLE POLYTECHNIQUE DE MONTRÉAL

Ce mémoire intitulé:

GEOLOGICALLY CONSTRAINED INVERSION MODELING
OF TITAN MAGNETOTELLURIC AND INDUCED
POLARIZATION SURVEY RESULTS AT KIDD CREEK MINE

présenté par: LEGAULT Jean M.
en vue de l'obtention du diplôme de: Maîtrise ès sciences appliquées
a été dûment accepté par le jury d'examen constitué de:

M. MARCOTTE Denis Ph.D., président
M. CHOUTEAU Michel Ph.D., membre et directeur de recherche
M. KEATING Pierre Ph.D., membre

ACKNOWLEDGEMENTS

This thesis was drawn from a project that was sponsored by the Ontario Mineral Exploration Technology (OMET) through the Ontario Ministry of Northern Development and Mines, in partnership with Falconbridge Ltd. and Quantec Geoscience Ltd. (Toronto). These groups kindly gave permission for the use of the data and survey results. The data processing and data presentation computer software and hardware were provided by Quantec Geoscience Ltd.

I would first like to acknowledge my gratitude to Prof. Chouteau, for introducing me to the magnetotelluric technique, in 1982, for encouraging me to persevere with my quest for my degree, throughout these many years, and for accepting to become my thesis advisor, once again, after previous attempts and more than a decade hiatus on my part. I would also like to express my appreciation to others who assisted: Dr. R. Bazinet, who first invited me to graduate studies at École Polytechnique; M. Jean Dansereau, director of graduate studies at École Polytechnique, for his generosity in recognizing my previous course-credits and for facilitating the return to my M.Sc.; Dr. Ransom Reddig who oversaw the Kidd Creek project data acquisition, assisted, reviewed and mentored me during the 2D inversion work, in particular the MT, while at Quantec; David J.W. Dawson undertook the smooth unconstrained 2D DCIP inversions, while at Quantec; Vince Gerrie undertook the Logtrans™ statistical analysis of the borehole physical property results, while at Quantec; Elaine Slama, of Mira Geoscience (Montreal) created the 3D Gocad common earth model and its many images included here; my employer, Quantec Geoscience Ltd., for allowing me to use this work; as well as facilitating the time off to complete this thesis, and Keith Morrison, in particular, who stood by me during the lengthy but informative report stage, that spawned this thesis study, and; Robert Gordon, my colleague for his help with the original interpretation report; and finally, my wife Lori, my family and my brother Marc, for their unflagging support throughout these many years.

RÉSUMÉ

Cette thèse concerne l'interprétation des résultats de levés MT et DCPP venant du système d'acquisition distribuée Titan-24 obtenus par Quantec Géoscience Inc. pour Falconbridge Ltée sur le site de la mine Kidd Creek près de Timmins, Ontario. Le levé a été entrepris en décembre 2001 et a été subventionné par OMET, Falconbridge et Quantec. Le levé a consisté de 5 profils de 4800 mètres de longueur, séparés de 200 m, avec stations aux 100 m et situé à 500 m du puis à ciel ouvert de Kidd Creek. Les lignes étaient orientées approximativement d'est en ouest, soit perpendiculaires et obliques aux orientations géologiques prédominantes. Les levés avaient pour buts de démontrer et d'évaluer les capacités du système Titan de cartographier la géologie et de détecter les minéralisations anomaliques en sulfures et en graphite (massifs ou disséminés), sous une épaisse couverture de mort terrain et dans l'environnent complexe du Bouclier Canadien Ontarien.

Le Titan est un nouveau système d'acquisition distribué à multicanaux, développé par Quantec Geoscience, capable d'enregistrer des données magnétotelluriques tensorielles (AMT/MT) à large bande de fréquences, ainsi que les données de résistivité DC et de polarisation provoquée. Le système Titan consiste de 3 éléments principaux: 1) son système d'acquisition, 2) son traitement de données digitales, et 3) sa capacité d interprétation, utilisant l'inversion 2D non contrainte et contrainte à la géologie. Cette thèse a pour but de documenter cette nouvelle approche scientifique d'interprétation, qui se sert aussi de modélisation géologique 3D pour fournir l'information géologique sous la surface pour contraindre les inversions 2D et pour mieux comparer les résultats géophysiques directement avec la géologie connue.

L'étude commence avec une analyse des propriétés physiques géoélectrique des roches à Kidd Creek. Les données pétrophysiques ont été obtenues de divers sources, soit in situ (diagraphies en trous de forage) et indirecte (archi-

ves d'études en laboratoire et inversions 2D) for chacune des unités géologiques. Cette information quantitative venant du modèle géologique permet les contraintes géo référenciées pour l'inversion de données MT et DCPP venants du Titan. Les images de résistivité et de chargeabilité respectent donc l'information géologique et dans les régions où ces différences existent entre le modèle géologique et l'inversion géo référenciées représentent des cibles distinctes. Ces différences sont mises en meilleure évidence en utilisant les techniques d'analyse de ratio-M et de delta-M.

Cette étude inclut elle aussi une analyse de sensibilité, utilisant le modèle 3D Gocad du dépôt de Kidd Creek, pour tester la profondeur d'investigation des levés MT et DCPP Titan, ainsi que les limites de détection des inversions 2D. L'analyse de sensibilité a démontré que la MT Titan était capable de détecter un dépôt comme Kidd Creek jusqu'à 2 km de profondeur. La résistivité DC pouvait détecter et définir le gisement Kidd Creek de 500 m jusqu'à plus de 750m. La chargeabilité PP pouvait potentiellement détecter et définir le dépôt à des profondeurs suffisamment moindre que 500 mètres due à de plus moindres contrastes.

Les données DCPP et MT Titan ont été interprétées quantitativement utilisant des codes d'inversions 2D par ordinateurs. Les inversions ont été fait de deux façons distinctes: 1) non contrainte utilisant un demi-espace simple comme modèle partant et 2) contrainte utilisant un modèle géologique comme guide pour l'inversion.

Les inversions 2D initiales ont démontré une excellente corrélation entre la géologie connue, enfouie sous plus de 70 m de mort terrain glaiseux, et les zones courbées et linéaires de basse résistivité et de haute chargeabilité qui caractérisent les horizons rhyolitiques ciblées. Cependant, les inversions contraintes se sont démontrées comme les outils plus bénéfiques pour l'exploration à faible et à grande profondeur sur la propriété de Kidd Creek.

Les inversions contraintes géo référenciées des données du Titan-24 ont amélioré de façon significative les résultats du levé, en faisant parvenir de plus ample détail le long et en biais des unités lithologiques, particulièrement le long des pendages. Ce processus a permis d'identifier un nombre significatif d'anomalies et une interprétation à des profondeurs en excès de 1,5 km. Les anomalies de plus haute priorité sont concentrés le long des horizons rhyolitiques clefs. Le système a défini des réponses sur chacun profils qui ne sont pas expliquées dans le modèle géologique. Plusieurs de ces anomalies sont consistantes avec des réponses de sulfures massifs ou minéralisation graphitique.

L'AMT/MT s'est démontrée l'indicateur le plus fiable de variations en conductivité épaisseur le long et sur le pendage d'unités rhyolitiques. Bénéficiant de profondeur d'investigation supérieur (>1,5 km) et d'algorithmes d'interprétation avancées, les résultats d'inversion MT, en particulier, ont permis d'identifier des anomalies profondes d'intérêt le long de l'horizon North Rhyolite. Ces anomalies paraissent comme les plus intrigantes de tous celles identifiées par le levé Titan-24 à Kidd Creek. Il y a cinq anomalies profondes (>750m) de plus haute prioritée qui sont associées avec 2 à 3 cibles distinctes alignés dans le volume relevé. Toutes sont situées le long de l'horizon North Rhyolite. Cela inclut une anomalie profonde centrée sur la ligne 11400N à 1,5 km de profondeur.

D'autres anomalies MT profondes ont été identifiées le long d'autres unités rhyolitiques, comme l'horizon Chance, cependant elles sont comparativement plus faibles et aussi n'ont pas la même étendue en profondeur. Comme résultat, elles ont étés assignées une plus faible priorité.

Un plus grand nombre de signatures à haute priorité ont été identifiées proche de la surface (<250m). Ces anomalies ont tendance à être plus petites (<100 x100m) mais elles combinent la haute chargeabilité, ainsi qu'une baisse de résistivité DC et MT. A des profondeurs moyennes (250-750m) il y a cinq

anomalies à haute priorité additionnelles qui ont été identifiées principalement avec la MT et la résistivité DC.

Le paramètre de chargeabilité PP, tel que l'a prédit l'analyse de sensibilité par modélisation 2D, semble faire parvenir de l'information fiable sur des cibles allant jusqu'à environ 350 mètres. Pareillement, il y a généralement une bonne corrélation entre les anomalies identifiées par la résistivité DC et MT allant à des profondeurs de 500-750m. En delà de ces profondeurs, la MT Titan est le seul outil utile d'exploration.

ABSTRACT

This thesis concerns the interpretation of Titan-24 distributed array MT and DCIP survey results obtained by Quantec Geoscience Inc. for Falconbridge Ltd at their Kidd Creek Mine Site near Timmins, Ontario. The survey was carried out in December of 2001 and was funded by OMET, Falconbridge and Quantec. The survey consisted of 5 lines, each 4800 m long, separated by 200m and with 100m-station interval and located just 500m north of the Kidd open pit. These lines are oriented approximately E – W. The lines run both orthogonal and oblique to the predominant geological strike. The primary objectives of the surveys were to demonstrate and evaluate the Titan system's capability of mapping geology and detecting anomalous graphite or sulphide mineralization (massive or disseminated) in areas of thick overburden and Palaeozoic cover within Ontario's complex environment.

The Titan system is a newly developed, multi-channel, distributed array survey (DAS; Sheard, 1998), recording broad band Magnetotelluric data (AMT/MT), D.C. Resistivity data and Induced Polarization data. The Titan system consists of 3 main elements: 1) its acquisition system, 2) its digital signal processing, and 3) its interpretation capability, using unconstrained and geologically constrained 2D inversion. This thesis documents this novel, integrated scientific interpretation process. It included the use of a Gocad common earth model to provide geological subsurface information to constrain the 2D inversions and to better compare the geophysical results directly with the known geology.

The study starts with a geoelectric physical property analysis of the Kidd Creek rocks. Petrophysical data were collected from several sources, both in-situ (borehole logging data) and indirect (archival laboratory studies and 2D inversions) for each of the geological formations. This quantitative information within the earth model provided geo-referenced constraints for inverting the Titan

MT and DCIP data. The resulting subsurface resistivity and chargeability images therefore respect the geological information and areas where differences between the geologic model and the geo-referenced inversion exist, represent distinct areas for follow-up. These differences are highlighted using ratio-M and delta-m analyses.

The study also includes a sensitivity analysis, using the Gocad model of the Kidd Creek deposit, which tested the depth of investigation capability of the Titan DCIP and MT surveys, as well as their detection limits using 2D inversion. The sensitivity analysis proved that Titan MT would be capable of detecting Kidd Creek orebody down to 2 km. The DC resistivity should detect and image Kidd Ck. to depths of 500 to 750m. The IP would potentially detect and image the orebody to depths significantly less than 500 metres due to weaker contrasts.

The Titan DCIP and MT data were interpreted quantitatively using computerized 2D inversion codes. The inversions were done in two distinct ways; 1) unconstrained using a mathematical half-space as a starting model and 2) constrained using a geological model as the starting point for the inversion.

Initial, unconstrained 2D inversions demonstrate excellent correlation between the known geology, buried beneath up to 70m of clay overburden, and curvi-linear zones of resistivity low and chargeability high, which characterize the targeted rhyolitic horizons. However, the constrained inversions have proven the most effective targeting tools for shallow and deep exploration at the Kidd property.

Constrained geo-referenced inversions of the Titan 24 data have significantly improved the results of the survey, providing better detail along, and across the lithologic units and particularly down dip. This has enabled interpretation to depths in excess of 1.5 km. This process has identified a number of significant anomalies. The highest priority anomalies are concentrated along the key Rhyolitic horizons. The system delineated responses on each line that are

unexplained in the geological model. Several of these anomalies are consistent with the response of massive sulphide or graphite mineralization.

AMT/MT has proven to be the most reliable indicator of conductivity thickness variations both along strike and down dip of the Rhyolitic units. Benefiting from superior depth-penetration (>1.5 km+) and advanced interpretation algorithms, the MT inversion results, in particular, have identified deep anomalies of interest within the north Rhyolite horizon. These anomalies appear to be the most compelling signatures identified in the Titan 24 surveys at Kidd Creek. There are five high-priority deep anomalies (>750m) associated with 2 to 3 distinct targets along strike identified within the survey volume. All are situated along the north Rhyolite. This includes a deep anomaly centred on line 11400N at 1.5km depth.

Other deep conductive MT anomalies have also been identified along other rhyolitic units, such as the Chance horizon, however they are comparatively weaker and do not have the same depth extent and, as a result, have been assigned a lower priority.

A greater number of high priority signatures have been identified within the near surface (<250m). These anomalies tend to be small (<100x100m) but they represent combined high chargeability, DC and MT low resistivity. In the mid depth range (250-750m) there are five additional high priority anomalies, which have been identified using primarily the DC and MT resistivity.

The IP chargeability parameter, as predicted by the 2D forward modeling sensitivity analysis, seems to provide reliable information on targets to approximately 350m depths. Similarly, there is generally a good correlation between anomalies identified by the DC resistivity and the MT resistivity to depths of 500-750m. Below these depths, Titan MT is the only effective exploration tool.

CONDENSÉ EN FRANÇAIS

Cette thèse concerne l'interprétation des résultats de levés MT et DCPP venant du système d'acquisition distribuée Titan-24 obtenus par Quantec Géoscience Inc. pour Falconbridge Ltée sur le site de la mine Kidd Creek près de Timmins, Ontario. Le levé a été entrepris en décembre 2001 et a été subventionné par OMET, Falconbridge et Quantec. Le levé a consisté de 5 profils de 4800 mètres de longueur, séparés de 200 m, avec stations aux 100 m et situé à 500 m du puis à ciel ouvert de Kidd Creek. Les lignes étaient orientées approximativement d'est en ouest, soit perpendiculaires et obliques aux orientations géologiques prédominantes. Les levés avaient pour buts de démontrer et d'évaluer les capacités du système Titan de cartographier la géologie et de détecter les minéralisations anomaliques en sulfures et en graphite (massifs ou disséminés), le long d'horizons de rhyolites favorables, sous une épaisse couverture de mort terrain et dans l'environnent complexe du Bouclier Canadien Ontarien.

Le Titan est un nouveau système d'acquisition distribué à multicanaux, développé par Quantec Geoscience, mais basé sur celui décrit par Sheard (1998), capable d'enregistrer des données magnétotelluriques tensorielles (AMT/MT) à large bande de fréquences, ainsi que les données de résistivité DC et de polarisation provoquée. Le système Titan consiste de 3 éléments principaux: 1) son système d'acquisition, 2) son traitement de données digitales, et 3) sa capacité d interprétation, utilisant l'inversion 2D non contrainte et contrainte à la géologie. Cette thèse a pour but de documenter cette nouvelle approche scientifique d'interprétation, qui se sert aussi de la modélisation géo-intégrée 3D Gocad pour fournir l'information géologique sous la surface pour contraindre les inversions 2D et pour mieux comparer les résultats géophysiques directement avec la géologie connue.

Le levé Titan consiste de deux techniques de profilage et de sondage géoelectriques: 1) la magnétotellurique (MT) tensorielle et 2) la combinaison de résistivité DC et la polarisation provoquée (DCPP). Les sondages MT tensoriels ont été obtenus simultanément aux 100m continus, utilisant une configuration électro-tellurique selon celle décrite par Torres-Verdin et Bostick (1992), avec une référence lointaine (30km au NO) et dans la bande de fréquences de 10kHz à 0.1Hz. Le résultats DCPP ont été obtenus avec ce même configuration d'électrodes fixe, avec injections selon une configuration hybride à pole centrale (Qara), décrite par Kingman et Garner (2003).

La mine Kidd Creek est situé à environ 25 km au nord de Timmins, Ontario. Le levé occupe un aire d'environ 5km est-ouest par 800m nord-sud, situé à 500m du puit No. 1. Le site est caractérisé d'un terrain plat, sans affleurements et recouvert de jusqu'à 70m de mort terrain glaiseux. La géologie consiste de roches volcaniques Archéennes de l'Assemblage Kidd-Munro. Les gîtes de sulfures massifs de Kidd Creek se situent en haut d'un empilement de roches felsiques, qui s'aminci et s'étend vers le nord où il s'appelle le «Rhyolite Nord» et devient plissé. A l'ouest, d'autres unités de roche felsiques forment un pli synforme et s'appellent «Rhyolites Chance». Selon le modèle d'exploration ces stratigraphies rhyolitiques sont les cibles principales et renferment sulfures et graphite – dont les plus grandes concentrations sont les indices de dépôts de cuivre et zinc. Ailleurs se retrouvent des argilites graphitiques conductrices et des volcanites coussinés à pyrrhotine qui sont des sources de bruit géologique.

L'étude commence avec une analyse des propriétés physiques géoélectrique des roches à Kidd Creek. Les données pétrophysiques ont été obtenues de divers sources, soit in situ (diagraphies en trous de forage) et indirecte (archives d'études en laboratoire et inversions 2D) for chacune des unités géologiques. Cette information quantitative venant du modèle géologique permet les contraintes géo référenciées pour l'inversion de données MT et DCPP venants du Titan. Les images de résistivité et de chargeabilité respectent donc

l'information géologique et dans les régions où ces différences existent entre le modèle géologique et l'inversion géo référenciées représentent des cibles distinctes. Ces différences sont mises en meilleure évidence en utilisant les techniques d'analyse de ratio-M et de delta-M.

Cette étude inclut elle aussi une analyse de sensibilité, utilisant le modèle 3D géo-intégré (common earth model; Morrison and McGaughey, 2001) Gocad du dépôt de Kidd Creek, pour tester la profondeur d'investigation des levés MT et DCPP Titan, ainsi que les limites de détection des inversions 2D. Des inversions non contraintes et contraintes ont été calculées à partir de données synthétiques DCPP et MT en simulant l'enfouissement progressif du dépôt de Kidd Creek en modifiant les modèles de référence. Cette technique d'analyse est similaire aux style études de Oldenburg et Li (1999) et de White et al. (2003). L'analyse de sensibilité, à l'aide d'inversions 2D, a démontré que la MT Titan était capable de détecter un dépôt comme Kidd Creek au moin jusqu'à 2 km de profondeur, sinon plus. La résistivité DC pouvait détecter et définir le gisement Kidd Creek de 500 m jusqu'à plus de 750m. La chargeabilité PP pouvait potentiellement détecter et définir le dépôt à des profondeurs suffisamment moindre que 500 mètres due à de plus moindres contrastes. La profondeur de détection s'est vue plus élevée avec les inversions non contraintes plutôt que contraintes – démontrant l'utilité des deux techniques d'analyse.

Les données DCPP et MT Titan sont de très grandes qualités, en dépit de la proximité des installations de la mine et la période hivernale du levé. Elles ont été interprétées quantitativement utilisant des codes d'inversions 2D par ordinateurs. Les inversions ont été fait de deux façons distinctes: 1) non contrainte utilisant un demi-espace simple comme modèle partant et 2) contrainte utilisant un modèle géologique comme guide pour l'inversion. Les inversions 2D initiales ont démontré une excellente corrélation entre la géologie connue, enfouie sous plus de 70 m de mort terrain glaiseux, et les zones courbées et linéaires de basse résistivité et de haute chargeabilité qui caractérisent les horizons rhyolitiques ci-

blées. Cependant, les inversions contraintes se sont démontrées comme les outils plus bénéfiques pour l'exploration à faible et à grande profondeur sur la propriété de Kidd Creek.

Les inversions contraintes géo référenciées des données du Titan-24 ont amélioré de façon significative les résultats du levé, en faisant parvenir de plus ample détail le long et en biais des unités lithologiques, particulièrement le long des pendages. Ce processus a permis d'identifier un nombre significatif d'anomalies et une interprétation à des profondeurs en excès de 1,5 km. Les anomalies de plus haute priorité sont concentrés le long des horizons rhyolitiques clefs. Le système a défini des réponses sur chacun profils qui ne sont pas expliquées dans le modèle géologique. Plusieurs de ces anomalies sont consistantes avec des réponses de sulfures massifs ou minéralisation graphitique.

L'AMT/MT s'est démontrée l'indicateur le plus fiable de variations en conductivité épaisseur le long et sur le pendage d'unités rhyolitiques. Bénéficiant de profondeur d'investigation supérieur (>1,5 km) et d'algorithmes d'interprétation avancées, les résultats d'inversion MT, en particulier, ont permis d'identifier des anomalies profondes d'intérêt le long de l'horizon North Rhyolite. Ces anomalies paraissent comme les plus intrigantes de tous celles identifiées par le levé Titan-24 à Kidd Creek. Il y a cinq anomalies profondes (>750m) de plus haute prioritée qui sont associées avec 2 à 3 cibles distinctes alignés dans le volume relevé. Toutes sont situées le long de l'horizon North Rhyolite. Cela inclut une anomalie profonde centrée sur la ligne 11400N à 1,5 km de profondeur.

D'autres anomalies MT profondes ont été identifiées le long d'autres unités rhyolitiques, comme l'horizon Chance, cependant elles sont comparativement plus faibles et aussi n'ont pas la même étendue en profondeur. Comme résultat, elles ont étés assignées une plus faible priorité.

Un plus grand nombre de signatures à haute priorité ont été identifiées proche de la surface (<250m). Ces anomalies ont tendance à être plus petites (<100 x100m) mais elles combinent la haute chargeabilité, ainsi qu'une baisse de résistivité DC et MT. A des profondeurs moyennes (250-750m) il y a cinq anomalies à haute priorité additionnelles qui ont été identifiées principalement avec la MT et la résistivité DC.

Le paramètre de chargeabilité PP, tel que l'a prédit l'analyse de sensibilité par modélisation 2D, semble faire parvenir de l'information fiable sur des cibles allant jusqu'à environ 350 mètres. Pareillement, il y a généralement une bonne corrélation entre les anomalies identifiées par la résistivité DC et MT allant à des profondeurs de 500-750m. En delà de ces profondeurs, la MT Titan est le seul outil utile d'exploration.

Parmi les recommandations les plus importante de cette étude, les inversions contraintes pourraient être améliorées à l'aide de «poids» variables qui reflèteraient la fiabilité des informations contenues dans le modèle Gocad. Les résultats DCPP devraient être réinterprétés à l'aide d'inversions 3D. Les inversions MT devraient être corrigées pour l'angle de dé rotation. L'analyse de sensibilité devrait inclure d'autres configurations d'électrodes ainsi qu'avec des cibles de plus petite taille et aussi avec des données synthétiques de modèles 3D qui seraient donc plus réalistes. Ils devraient peut-être aussi inclure du bruit synthétique. Des inversions des données synthétique MT devraient aussi être calculées, comme l'a été fait pour la DCPP.

TABLE OF CONTENTS

LIST OF TABLES

LIST OF FIGURES

LIST OF SYMBOLS AND ABBREVIATIONS

Abbreviation or Symbol	Definition
AMT	Audio magnetotelluric
A/D	Analog to digital conversion
B	Magnetic induction
DAS	Distributed acquisition system
DC	Direct current (Resistivity)
DCinv2D	UBC 2D DC and IP inversion algorithm
DCIP	DC resistivity and induced polarization
Dpdp	Dipole-dipole array (DCIP)
EAL	Electric array logging
E-field	Electric field (MT)
EVA	Eigen vector analysis (MT)
H-field	Magnetic field (MT)
IC	Inductive conductivity
IP	Induced polarization (DCIP)
M	Chargeability (DCIP)
Mrad	Milliradians (DCIP)
MT	Magnetotelluric
Pha	Phase
PP	Polarisation provoquée (DCPP)
Pldp	Pole-dipole array (DCIP)

Abbreviation or Symbol	Definition
PROQ	Phase rolling out of quadrant (MT)
Pz	Phase (IP effect)
PW2dinv	Plane wave 2D MT inversion algorithm
Qara	Quantec center-pole array (DCIP)
Rho	Resistivity
RLM	Smooth conjugate 2D MT inversion algorithm
S-grid	3D stratigraphic grid (Gocad)
SPR	Single point resistivity
1D, 2D, 3D	One-dimensional, two-dimensional, three-dimensional
UBC	University of BC (Geophysical Inversion Facility)
Vp	Primary voltage (DCIP)
Voxet	3D volumetric grid (Gocad)
$\alpha_S, \alpha_X, \alpha_Z$	Alpha parameters (DCinv2d misfit function)
m_0	Starting model (DCinv2d misfit function)
μ	Magnetic permeability (SI units)
ρ	Resistivity (ohm-metres)
ρ_a	Apparent resistivity (ohm-metres)
σ	Conductance (siemens per metre)
σt	Conductivity thickness (siemens)
φ	Phase (MT Electric/Magnetic field)
Ω-m	Ohm-metres (resistivity)

LIST OF APPENDICES

CHAPTER 1 INTRODUCTION

This thesis concerns the results of joint tensor magnetotelluric and dc resistivity\induced polarization surveys that were undertaken, during the period of December 11TH to 22ND, 2001, in an area immediately adjoining the Kidd Creek Mine, near Timmins, ON, using the Titan-24 distributed acquisition system (DAS; Sheard, 1998; Rutley et al., 2001), newly developed by Quantec Geoscience Inc., of Waterdown, ON (Quantec, 2004). The study was the first of a 4-part survey program, sponsored through the Ontario Mineral Exploration Technologies (OMET) Program, the Ontario Ministry of Northern Development and Mines, in partnership with Falconbridge Ltd. The results were subsequently submitted in the form of a logistics report by Quantec, in Legault et al. (2002a), in which the general survey details are described and both the raw and final-processed results, including preliminary 2D smooth inversion modeling, were presented, and in a final interpretation report by Quantec, in Legault et al. (2002b).

The objective of the OMET Titan survey program at Kidd Creek was primarily to demonstrate the new technology's ability to map general geology, including lithology, alteration, structural control and, in particular, mineralization, from surface to 2km depths, below thick conductive overburden, during the winter season and in a noisy, mine-site environment. The exploration targets sought after were conductive anomalies, potentially associated with copper-zinc volcanogenic massive sulphides adjacent to the Kidd Creek Mine and the nearby Chance Deposit – specifically, along several known, favourable rhyolitic units which are subvertically- dipping and variably sulphide-mineralized to graphitic.

This thesis focuses on the interpretation of the Titan survey results, which is based on an integrated approach, whereby the geology, their physical rock properties and the geophysics are combined, using the Gocad 3D common-earth platform (Morrison and McGaughey, 2001), culminating in constrained or refer-

enced 2D geophysical inversions – the results of which are compared directly against standard unconstrained inversions and drilling results.

This thesis presents both the unconstrained (non-geologically referenced) and constrained DCIP and MT inversions, as presented in Legault et al. (2002b). The physical properties used to characterize the geologic units used as inversion constraints have been obtained using petrophysical analysis of in-situ borehole results and laboratory analyses of representative samples. Using the Gocad model, a 2D sensitivity analysis has been performed by calculating the inverse response of 2D forward models of a simulated Kidd Creek orebody, progressively buried at depths from surface to 2km, in order to test the system's limits of detection and inversion-imaging. The study is heavily reliant on the Gocad common earth model that was constructed, for not only extracting the inversion constraints from the known geology, but for also reintroducing the present inversion results, for closer scrutiny, examination and comparison against the geologic model by others.

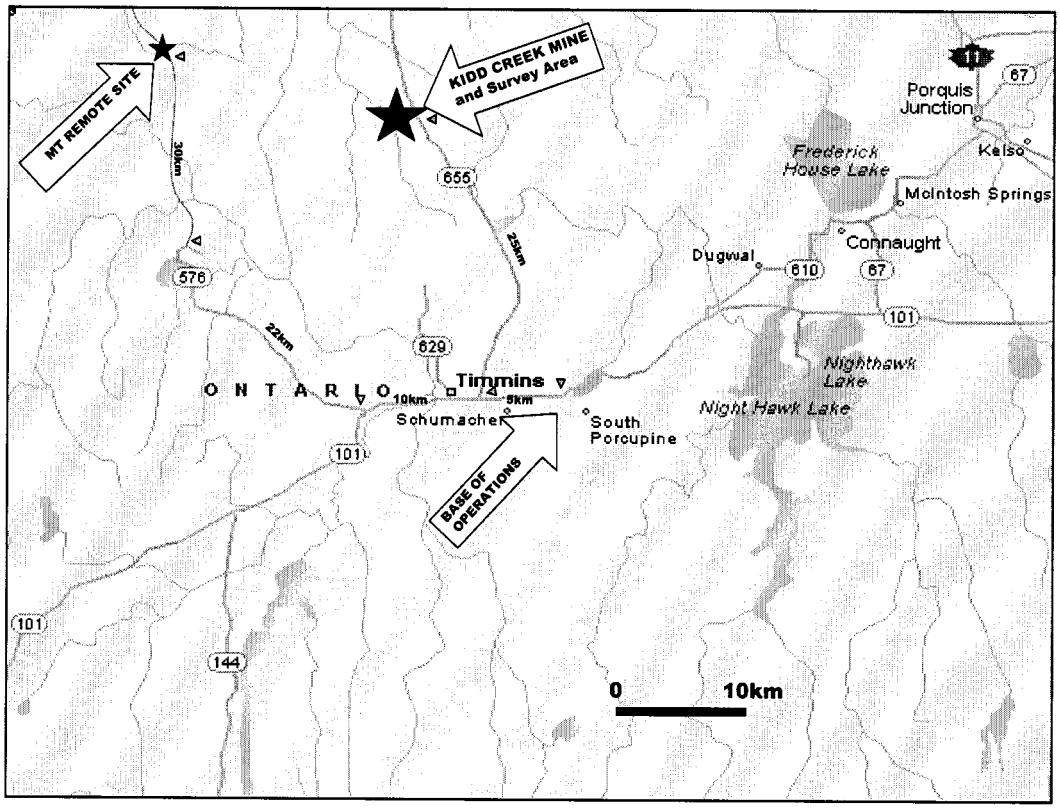

Figure 1.1: General Kidd Creek Property Location

1.1 OMET Titan Survey Overview

The Kidd Creek Titan survey area, lying just 500m northwest of the mine site (Figure 1.2), is overlain by a thick (20-50m) layer of conductive overburden, which has significantly limited exploration by conventional geologic mapping and geophysical methods, requiring a reliance on costlier diamond-drilling. The close proximity of the active mine-site and all its associated cultural noise sources also pose significant impediments to high signal-to-noise ratios required for deep exploration, locally, particularly in consideration of the weak nature of the natural electromagnetic fields used in MT, whose sources are worldwide thunderstorm activity, which are largely attenuated during the winter months.

The survey consisted of 5 parallel survey lines (Table 1.1 and Figure 1.2), roughly 5km in length, spaced 200m apart and at 100 metre station intervals, that

were oriented approximately east-west, which ran both orthogonal and oblique to the predominant geological strike. The Titan surveys used two different geoelectric sounding and profiling technologies: i) tensor magnetotellurics (MT) and ii) DC resistivity and induced polarization (DCIP). The MT method was chosen based on its high resolution and deep penetration (depths up to and exceeding 10km) characteristics, as well as its advanced 2D-3D interpretative capability, using 2D inversion. The large dipole/large-array DCIP surveys were chosen to provide more shallow to moderate geoelectric depth control (<1km depths), with the added benefit of detection of possible disseminate (non-conductive) mineralization using the chargeability parameter.

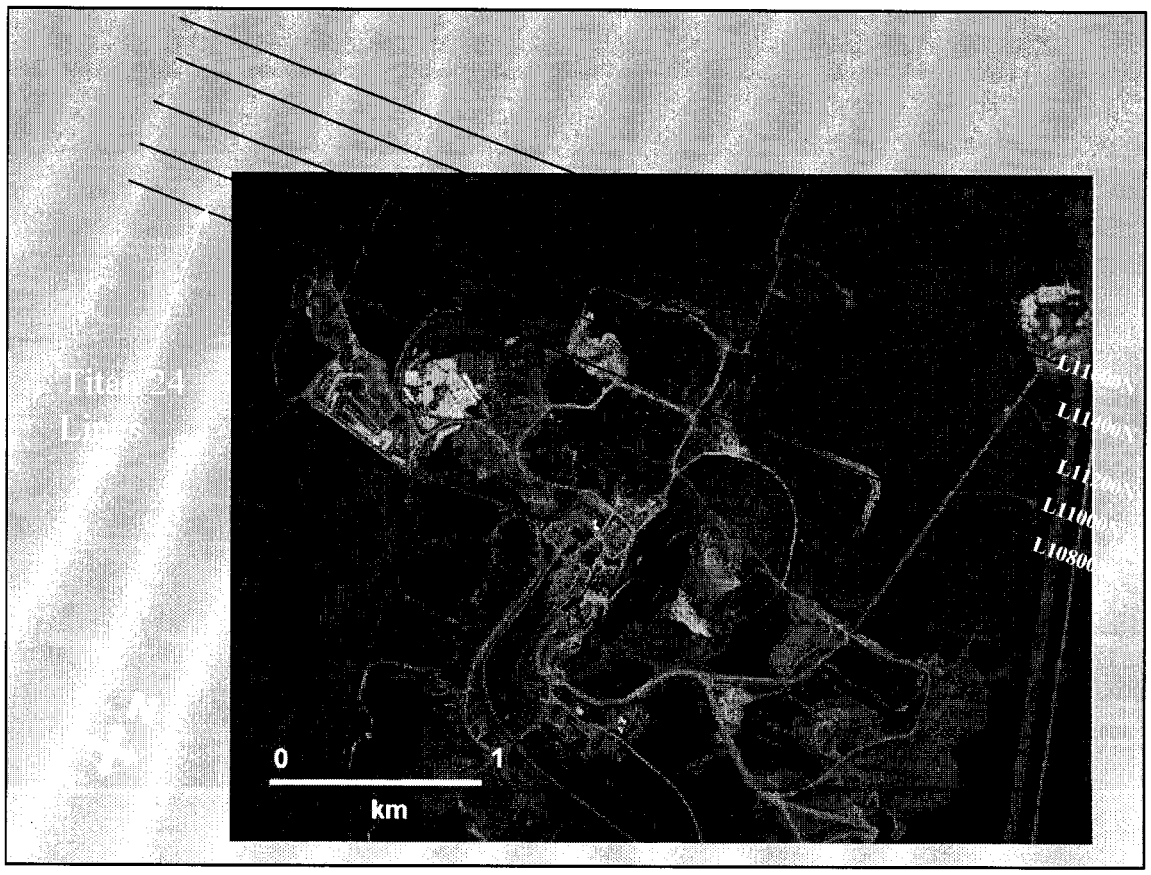

Figure 1.2: Titan Survey Lines at Kidd Creek (courtesy Falconbridge Ltd.)

The Titan tensor MT survey results were simultaneously obtained at 100 metres for all stations along the line, using a hybrid electro-telluric array, where

the multiple in-line and orthogonal electric field dipole measurements are normalized using a single set of magnetic field measurements, similar to that described in Torres-Verdin and Bostick (1992) and Word et al. (1986). The tensor MT surveys were fully referenced using a remote magnetic field site that was situated approximately 30 km west-northwest, in a culturally quiet area. Full tensor spectral measurements ($\rho_A + \Phi_A$) were obtained across an effective frequency bandwidth of 0.1-10k Hz.

The Titan DCIP survey results were obtained using a hybrid center-pole array (Kingman and Garner, 2003), where a fixed array of multiple in-line and orthogonal voltage measurements were simultaneously obtained from a fixed current injection pole and mobile current injection points at the dipole-midpoints. The full waveform data (240 samples per sec.) were obtained using transmitter base repetition rate of 30/356 Hz (~8.6 sec full duty cycle) and the chargeability decays were obtained across a ~2100 millisecond window, using an 800 millisecond delay.

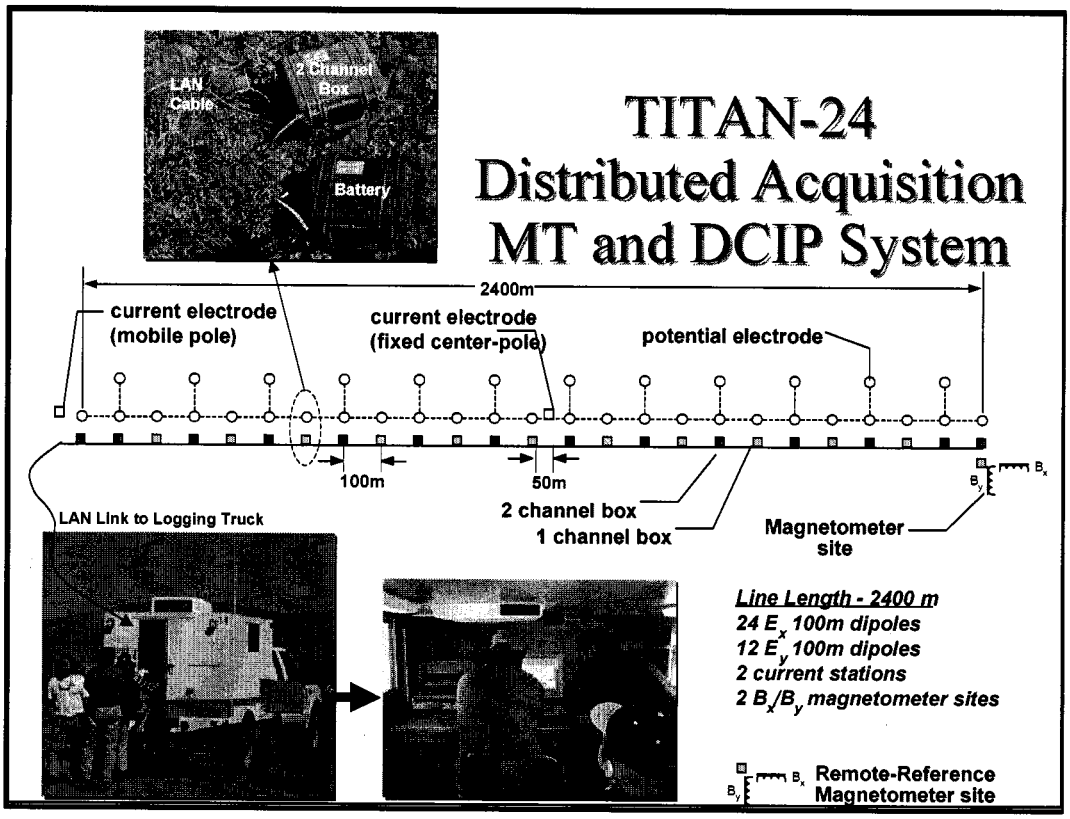

Figure 1.3: Titan-24 General Survey Layout for Tensor MT and DCIP.

The Titan study involved a 3-component approach, starting with high quality data acquisition using the Titan-24 distributed acquisition system, which uses state-of-the-art, broad-band, 24-bit A/D digital conversion, and multi-channel data sampling, in conjunction with advanced full waveform, time-series spectral data processing and robust noise rejection. The second phase involved the incorporation of geologic and physical property elements into a common earth model, using *Gocad*. The third and final element was the interpretation, which relied heavily on geologically-constrained 2D inversions, using the common earth models previously developed, in order to extend the application from being a conventional anomaly-finder to a more advanced, geologic and structural mapping tool. Differences in the resulting 2D inversion model and the known geology were compared, in *Gocad*, through *delta-M* and *ratio-M* studies (for the chargeability

and resistivity parameters, respectively), in order to further refine the geologic model or, hopefully, to define new potential drill targets.

1.2 Survey and Line Location

The Kidd Creek Mine property is situated approximately 25 kilometres north of Timmins, in northwest Ontario, at Lat. 48°42'00"N and Long. 81°22'30"W (UTM 471900mE, 5394000mN). The survey area occupies a roughly 5km east-west by 800m north-south region immediately north-west of the Kidd Creek deposit – just 100m north of the No. 1 mine open pit (Figure 1.2). The area is characterized by typically flat terrain, at a uniform elevation of 279m above mean sea level, devoid of outcrop and features up to 70m of conductive clay overburden cover. The survey control for the geophysical profiles at Kidd Creek is presented in Table 1.1.

Table 1.1: Survey Line Locations and UTM Reference

Line No.	Array Coord. Start	Array Coord. End	UTM Coord. Start	UTM Coord. End
108+00N	7400E	12200E	469538mE, 5393601mN	474322mE, 5393613mN
110+00N	7400E	12200E	469527mE, 5393828mN	474318mE, 5393828mN
112+00N	7200E	12000E	469336mE, 5394027mN	474119mE, 5394016mN
114+00N	7200E	12000E	469332mE, 5394230mN	474111mE, 5394216mN
116+00N	7800E	12000E	469962mE, 5394425mN	474108mE, 5394485mN

1.3 General Geology

The Kidd Creek deposit occurs within a generally east-west trending steeply dipping sequence of Archean mafic, ultramafics, and felsic metavolcanics known as the Kidd Munro Assemblage (Hannington et al., 2004; Falconbridge, 2002). The Kidd Creek Cu-Zn massive sulphide orebodies occur at the top of a thickened felsic file consisting of massive rhyolite flows, felsic fragmental rocks, and epiclastic deposits. The felsic sequence attains its maximum thickness of 300m within the Kidd Creek mine horizon but thins to the north (where it is known as the North Rhyolite) and south of the mine, suggesting that volcanism and mineralization were localized within a paleo-topographic depression, resembling a linear graben-like feature. Felsic volcaniclastics, fragmentals and debris flows interbedded with tuffaceous rhyolite, siltstone and argillite fill the graben and are the principal hosts to ore. The footwall rocks below the mine rhyolites are mainly comprised of ultramafics flows and sills, with minor rhyolite intercalations. Pillow basalts and breccias give way to clastic metasediments to form the hanging wall rocks to the west of the mine horizon.

At Kidd Creek, the mine sequence occupies an anomalous S-shaped fold structure (see Figure 1.4), with younging directions to the west. Northwest of the mine, underlying much of the western survey area, the rocks form an open syn-form, in the nose of which the Chance Deposit, a small (180,000 T, 12.8% Zn), subeconomic massive sulphide resource, is situated, approximately 1km west of Kidd Creek (Opawica, 2004). The Chance rhyolites extend to the NW, centrally and NE of the survey area – the latter eventually merging with the North Rhyolite units just north of our survey lines. Much of the geology along the furthest western extent of the survey are not included in the Gocad model, however other intercalated rhyolitic and basaltic sequences are implied, based on regional geology (L. Martin, Falconbridge, pers. comm., 02-02). Based on evidence from the Gocad model, geologic dips vary from subvertical to steeply east-dipping along the southern lines, whereas the geology for the northern survey lines generally

dips steeply towards the center – implying a synform. In general, current exploration targets the rhyolitic stratigraphies within the survey area, which, due to their increased sulphide and graphite content, are likely to provide reliable markers for both resistivity and induced polarization – similarly for the graphitic argillite bands to the east. However pyrrhotite, commonly found in the pillowed mafic volcanic units and unaccounted for in the Gocad model, is also likely to provide unwanted geologic noise (S. Taylor, Falconbridge, pers. comm., 01-02).

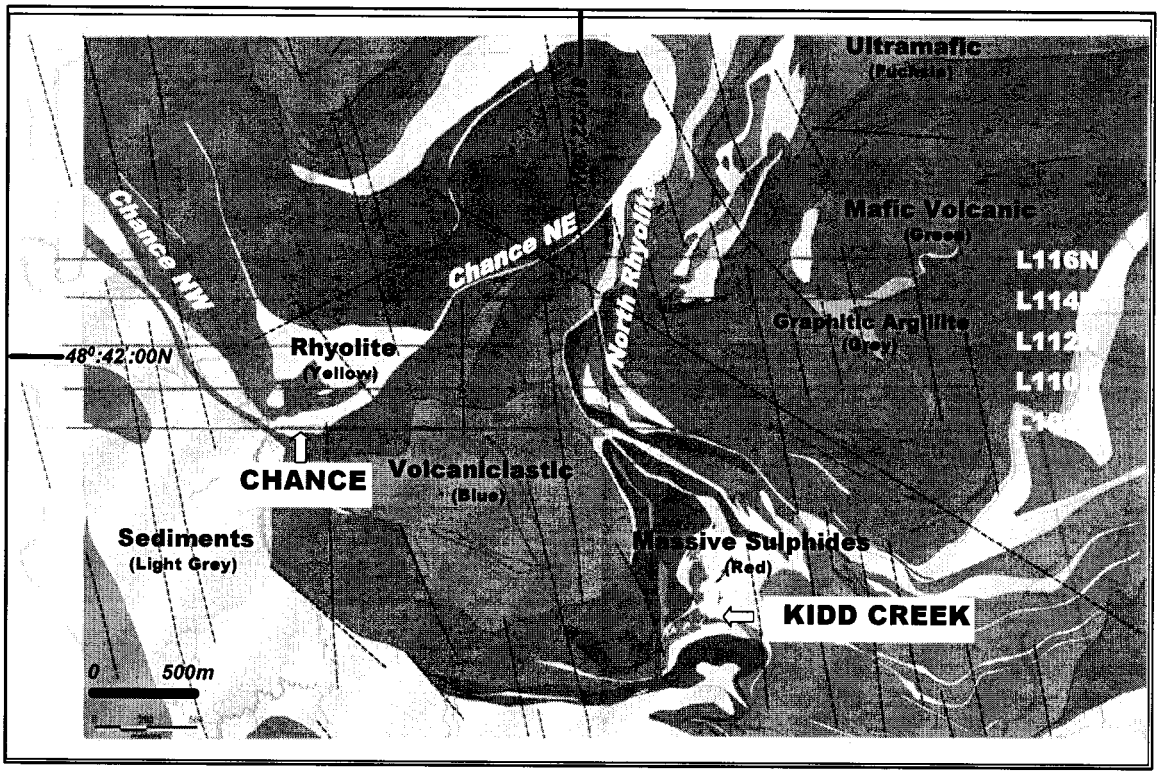

Figure 1.4: Kidd Creek General Geology (courtesy Falconbridge Ltd.)

CHAPTER 2 THEORY AND METHODOLOGY

2.1 DCIP Survey

2.1.1 Introduction

The resistivity is among the most variable of all geophysical parameters, with a range exceeding 10^6. Because most minerals are fundamentally insulators, with the exception of massive accumulations of metallic and submetallic ores (electronic conductors) which are rare occurrences, the resistivity of rocks depends primarily on their porosity, permeability and particularly the salinity of fluids contained (ionic conduction), according to Archie's Law. In contrast, the chargeability responds to the presence of polarizeable minerals (metals, submetallic sulphides and oxides, and graphite), in amounts as minute as parts per hundred. Both the quantity of individual chargeable grains present, and their distribution within subsurface current flow paths are significant in controlling the level of response. The relationship of chargeability to metallic content is straightforward, while the influence of mineral distribution can be understood in geologic terms by considering two similar, hypothetical volumes of rock in which fractures constitute the primary current flow paths. In one, sulphides occur predominantly along fracture surfaces. In the second, the same volume percent of sulphides are disseminated throughout the rock. The second example will, in general, have significantly lower intrinsic chargeability.

More detailed descriptions on the theory and application of the IP/Resistivity method can be found in Coggon (1973), Langore, Alikaj and Gjovreku (1989) and Telford et al. (1976). A full description of the Titan survey methodology is included in Legault et al. (2002a).

2.1.2 Halverson-Wait Chargeability

The Titan-24 DCIP chargeability decays are described using the Halverson-Wait spectral model (Halverson et al., 1981), which is not well known,

but is similar to the Cole-Cole model proposed by Pelton et al. (1978) which is a simple relaxation model that fits complex (frequency-dependant) resistivity results.

The time domain chargeability, originally proposed by Siegel (1959), is defined (Telford et al., 1976) as

$$M = \frac{1}{V_C} \int_1^2 V(t)dt$$

Where $V(t)$ is the residual or secondary voltage at a time t, that is decaying after the current is cut off, between time t_1 and t_2, with the steady voltage V_C during the current flow interval. The ratio $V(t)/V_C$ is expressed in millivolts per volt.

In the frequency domain, the "frequency effect" is defined as:

$$fe = (\rho_{DC} - \rho_{AC}) / \rho_{AC}$$

Where ρ_{DC} and ρ_{AC} are apparent resistivities measured at d.c. and "very high" frequency, usually in the 0.1 to 10 Hz range.

The Cole-Cole model for the chargeability m, as defined by Pelton et al. (1978) is given by the following:

$$Z(\omega) = R_0 \left[1 - m \left(1 - \frac{1}{1 + (i\omega\tau)^c} \right) \right]$$

Where $Z(\omega)$ is the complex impedance, R_0 is the DC resistivity, m is the chargeability in volts per volt, ω is the angular frequency in Hz, τ is the time constant in seconds, and c is the frequency dependence (unitless). The latter two physical properties describe the shape of the decay curve in time domain or the phase spectrum in frequency domain, and commonly range between 0.01s to +100s and 0.1 to +0.5, respectively (Johnson, 1984).

The Halverson-Wait model was proposed by Halverson et al. (1981) as an extension to the Wait (1959) model of the impedance of "volume loading" of spheres, given by:

$$Z(\omega) = \frac{\rho}{G}\left[1 - 3v\left(1 - \frac{3\delta}{1+2\delta}\right)\right]$$

Where ***G*** is a geometric factor, ***ρ*** is the resistivity of the media, ***v*** is the volume loading (the volume fraction of chargeable "spheres"), δ is the sphere surface impedance. The Wait model was designed to provide an explanation of the differences in the shape of decay curves from different polarizeable targets, but does not describe very well the physical attributes of the rocks.

The Halverson-Wait model expands the Wait coated sphere IP model to include a new formulation of the sulphide-rock interface impedance, based on field studies and laboratory tests on samples (Kingman, 2000a). It is closely correlated to the Pelton et al. (1978) Cole-Cole model and is given by:

$$Z(\omega) = \frac{\rho}{G}\left[1 - 3v\left(1 - \frac{3/2}{1+r[i\omega]^K}\right)\right]$$

Where ***r*** is the sphere radius and is equivalent to τ - the Cole-Cole time constant ($r = \tau^K$). The ***v*** volume loading compares well to ***m*** – the Cole-Cole

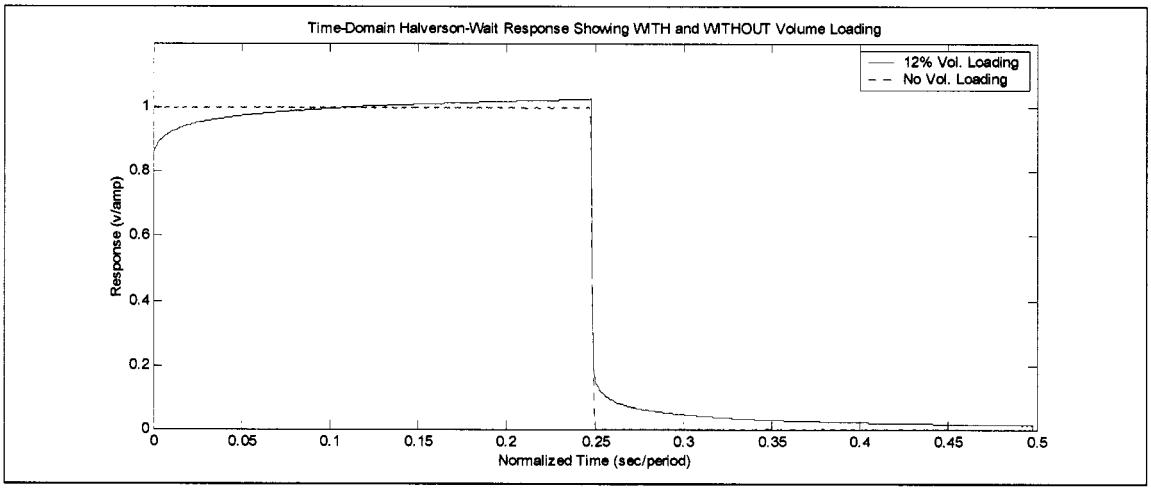

chargeability (see equation below) – and the exponent ***k*** is equal to ***c*** - the Cole-Cole frequency dependence (Halverson et al., 1983). For sulphide systems, the *r*-factor reflects the size or interconnection of the sulphide grains and the *k*-factor reflects the electrical characteristics of the sulphide surfaces. An example of time domain Halverson-Wait model responses is shown in Figure 2.1.

Figure 2.1: Polarizeable versus Non-Polarizeable Time-Domain Response using Halverson-Wait Model (from Kingman, 2000b)

In practice the Titan chargeability decays are fit to a Halverson-Wait model. In order to solve for the volume loading *v*, the *r*-factor and *k*-factor are set to the standard (typical) Halverson-Wait values of 1.0 and 0.2, respectively. In the Halverson-Wait model the theoretical PFE (for infinite bandwidth), which equates to the theoretical chargeability in the Cole-Cole equation, is thereby defined by the volume loading:

$$PFE_0 = m_0 = \frac{9v}{(2+3v)}$$

and ***m*** is output in units of milliradians (Kingman, 2000b).

2.1.3 2D Inversion Procedure

The following discussion of Titan 2D DCIP inversion procedure is drawn from Reddig (2002): As a result of the relatively complex responses that are obtained from the center-pole array, the visual interpretation of pseudosections is not possible. Rather, the interpretation of the Titan DCIP data relies primarily on 2D inversions. There is little pre-processing of the data. The steps are:

1. Edit data to remove extreme outliers. This is commonly done by deleting data where the repeatability errors are > 10% of the dc voltage data value, and > 3 milliradians error for the ip data values.

2. Assign realistic data errors. The calculated repeatability errors from the Titan field observations are, by their nature, much smaller than the data – owing, in large part, to the 24 bit A/D sampling and advanced post-processing (for example, for line 10800N, avg Vp error = 0.000076 or 1 part in 13,0000; avg ip error $\approx$ 0.1 milliradians or 1 part in 105). This contrasts the expected data errors for MT and DCIP inversions, which are typically in the 2-5% range for the resistivity and 0.5 milliradians for the chargeability. As a result, because industry standard inversion algorithms are not designed to such high tolerances, they typically fail to achieve the desired numerical convergence using the actual data errors assigned. In reality, these small repeatability errors are dominated by many other factors, including uncertainty in electrode positioning, topographic effects, multidimensional effects, and inaccuracies in the modeling and inversion programs. In order to correct for this, more realistic data errors are assigned either by: a) adding additional errors to the Titan calculated error values, b) multiplying the Titan errors by a factor, or c) in the present case, assigning a minimum error floor. Typically, error floors of 3-5% of the measured data value,

for the voltages and 0.5-2 milliradians for the phase error, often work well, and are consistent with the expected numerical modeling errors.

3. Invert the data.

4. Evaluate "convergence" of the inversion. The inversion approach focuses initially on fitting the data. Once convergence is obtained (the data are "fit") additional iterations of the inversion are necessary to reduce the model norm – remove structure from the inversion that is not required by the data. Presuming the inversion has not converged, the remaining procedure includes either a) changing the "chi factor", b) further adjusting the data errors or c) the data are "culled". Culling involves removing a small percentage of the data that are most inconsistent with the inversion model. These are, presumably, data that are biased or have 3D effects. However, some care must be taken as this approach presumes that the inversion has fit the "good" data.

5. Re-invert the "culled" data, starting from the original (halfspace or geologic) model. This will generally provide the necessary convergence.

   Several inversions are run on the "culled" data, using different "model norms", or target models. This is important in exploring the range of models consistent with the data.

Several different inversion models are produced. Several models are "smooth" inversions starting from a half-space. These models will vary in the "model norm", the balance between model smoothness and data misfit. Finally, Gocad geologically constrained inversion models are calculated. The geophysicist selects one, representative, model as "the" inversion.

2.2 MT Survey

2.2.1 Introduction

The magnetotelluric (MT) method, first proposed by Cagniard (1953), is an electromagnetic technique which allows the investigation of crustal resistivity structure through measurements of orthogonal electric (*E*) and magnetic (*H*) components of horizontally incident EM fields at the earth's surface. Although these electromagnetic fields may be artificially induced (controlled source MT (CSMT); Goldstein and Strangway, 1975), magnetotelluricists more commonly employ the naturally occurring and worldwide time-varying source fields of both solar and atmospheric origin. Scalar audio-magnetotellurics (SAMT) is a simplified version which limits itself to the upper bandwidth of the MT spectrum and, by measuring only a single component of the horizontal EM field, permits the use of portable equipment, making it a low-cost and speedy high resolution, deep penetration geophysical tool. However, technological advances in the last decade have completely supplanted SAMT and CSMT, in favour of full tensor audio-magnetotellurics (AMT).

A detailed description of the Titan MT survey methodology is given in Legault et al. (2002a).

2.2.2 Source Fields

A broad spectrum of frequencies (f), or periods ($T = 1/f$), are available for magnetotelluric studies: at frequencies below 1 to 0.0001 Hz (periods of 1 sec. to 48 hours and beyond) the source fields are magnetospheric and are linked to solar winds and sunspot activity, as well as the relative motions of the earth, sun and moon (Kaufman and Keller, 1982); at higher frequencies (1-10,000 Hz), the ambient EM field is contributed to by natural oscillations in the earth-ionospheric cavity, due to electromagnetic radiations of lightning discharges originating mainly from equatorial regions and other meteorological activity, and from

man-made power distribution systems (culture) and radio-communications networks (VLF). At great distances from the source, the waves are modified as they travel in the earth-ionospheric wave-guide, resulting in discrete, peak energy, Schumann resonances (8,14,20,25,32 Hz) and a strong absorption band centred at 2 kHz (Keller and Frischknecht, 1966; Hoover et al., 1976; Strangway and Koziar, 1979). Although, strictly speaking, MT encompasses all these frequencies, when we are specifically concerned with audio-frequency range signals ($1 < f < 20{,}000$ Hz), the technique is known as audio-magnetotellurics or AMT (Strangway et al., 1973). For AMT measurements between 300Hz and 3kHz there is a "dead-band" where the signal does not propagate well. Despite hardware and signal processing improvements this dead-band remains problematic. When signal (atmospheric activity) is present within several hundreds of miles of the survey area the data is quite good. When no signal is being generated in the vicinity data quality is poor.

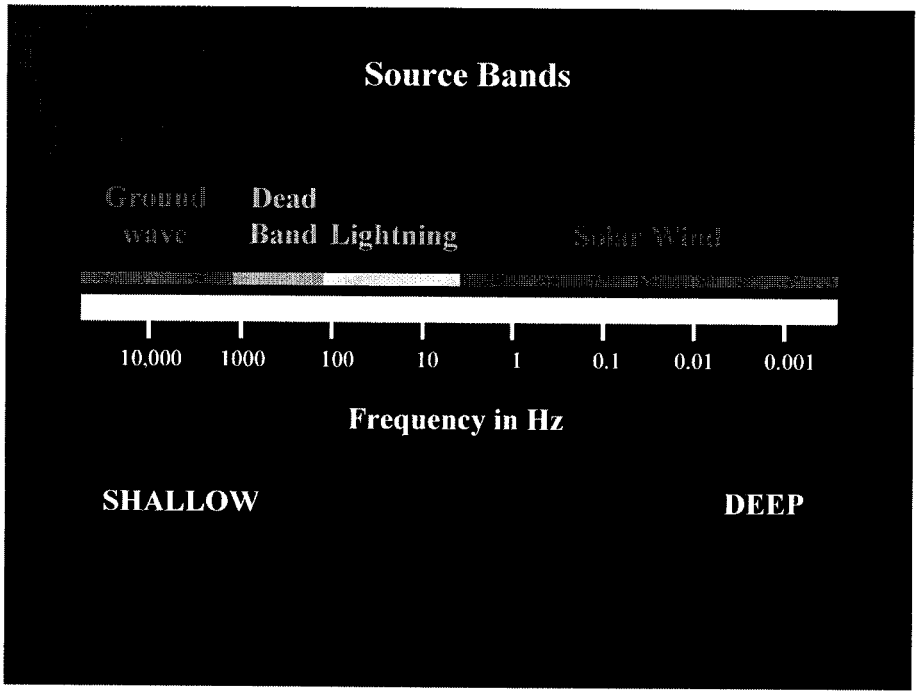

Figure 2.2: Magnetotelluric Source Bands
(after Reddig, 2002)

2.2.3 Basic Equations

Three basic laws of physics can help us understand how we derive apparent resistivities from separate measurements of components of horizontal EM fields (Garland, 1979; Vozoff, 1972). First of all, oscillating (time-varying) magnetic and electric fields are mutually inclusive, i.e. one cannot exist without the other; this phenomenon is governed by both *Ampere's Law*, which states that a magnetic field (**B**, **H** – see pages xxvii-xxviii) is generated in space by a current (**I**) flow ($d\mathbf{B}\cdot d\mathbf{l} = \mu_o \mathbf{I}$, $\mathbf{B} = \mu\mathbf{H}$); and by *Faraday's Law*, which states that an electric field (**E**) exists in the region of a time-varying magnetic (φ) field ($d\mathbf{E}\cdot d\mathbf{l} = d\varphi/dt$, $\varphi = \int \mathbf{B}\cdot d\mathbf{S}$). Moreover, the electric and associated magnetic components of an electromagnetic field are perpendicular in space ($\mathbf{E}\cdot\mathbf{H} = 0$), by *Maxwell's Equations*. These notions also provide explanations for the origin of ionospheric currents and the occurrence of telluric currents within the earth's crust.

In MT, the incident plane wave is horizontal, so that it travels downward into the earths. The deeper the EM wave penetrates, the more information it collects about materials at greater depths. The penetration mechanism of these fields is not by wave propagation but diffusion because the wavelengths (λ) are quite long ($\lambda = (10\rho T)^{1/2}$ km) - the attenuation is the same in either case (Waeselynck, 1974). The penetration of EM fields is limited by the physical properties of the earth: when an electromagnetic wave travels in a conductive medium, energy is dissipated as heat - consequently the wave is gradually weakened (attenuated) with increasing depth. The amplitude attenuation is directly related to the angular frequency (ω) of the wave ($\omega = 2\pi f$), and the medium's electrical conductivity ($\sigma = 1/\rho$) and magnetic permeability (μ). The depth where the EM field is reduced to 37% (1/e) of its original value is known as the skin depth and is commonly used as a rule of thumb depth of penetration:

MT Skin Depth:

$$\delta_s = \frac{\sqrt{2}}{\sqrt{\mu\sigma\omega}} = 503 * \sqrt{\frac{\rho_a}{f}} \ \textit{metres}$$

A similar depth estimator, the Niblett-Bostick depth, is used for calculating magnetotelluric resistivity-depth distributions in half-spaces. The value of this approximation is less than the skin depth because the attenuation factor of ½ is used instead of 1/e (Jones, 1983):

$$\textit{Niblett-Bostick Depth:} \qquad \delta_s = \sqrt{\frac{1}{\mu\sigma\omega}} = 356 * \sqrt{\frac{\rho_a}{f}} \ \textit{metres)}$$

The relation between the two components of an EM field is called the electric impedance ($Z = E/H$), which is a concept well-known to electrical engineers and physicists involved in domains outside of geophysics. The impedance is a complex number due to the fact that the E and H fields are not in phase; the magnetotelluric impedance provides us with both an amplitude (the apparent resistivity $\rho_a = (1/5f)\times|Z|^2$) and a phase (the apparent phase $\varphi_a = \arg(E/H)$) component. Combining all these notions together we arrive at the magnetotelluric resistivity: By simultaneously measuring horizontal (at the earth's surface) electric and magnetic fields (using two electrodes, a voltmeter and a magnetometer) at right angles to each other (orthogonal) at a select frequency ($f=\omega/2\pi$), the scalar or Cagniard apparent resistivity (ρ_a) is calculated:

$$\textit{Scalar Apparent Resistivity:} \qquad \rho_a = \frac{1}{\mu\omega}\left|\frac{E_x}{H_y}\right|^2 = \frac{1}{5f}\left|\frac{E_x}{H_y}\right|^2 \ \textit{ohm-metres}$$

By measuring these fields at various frequencies, we get a resistivity-depth distribution of the earth without having to change the instrument set-up (parametric sounding). The result looks much like a smooth electrical log from a borehole measurement. The phase and amplitude components are interdependant, ρ_a and φ_a being related to the resistivity through the Hilbert Transform (Young, 1981). The phase distinguishes MT in particular as it is unavailable to conventional DC resistivity methods (geometric sounding), its behaviour is different from ρ_a, and it can be used to increase the precision of model estimates. However, too often, it is under-utilized because, as an abstract parameter, φ_a is

conceptually less appealing than ρ_a, and also because it is not well understood (Fischer, 1985).

Another, less familiar, MT measurement is the anomalous vertical field (H_z), which is a linear function of the horizontal magnetic components (Chouteau, 1985):

Secondary Vertical Field: $$H_z = A \cdot H_x + B \cdot H_y + \vartheta$$

where H_z, H_x, H_y, A, B and ϑ are frequency dependant; A and B are complex magnetic transfer functions; and ϑ is the vertical residual field, being the residual error in the response equation (Prugger and Woods, 1984). Although it is always less than the two horizontal components, H_z occurs in the presence of lateral electrical heterogeneities; a plot of the magnitude and direction of the A and B define induction arrows which point to the source of anomalous conductivity, hence help determine the geoelectric strike (Garland, 1979). However, despite the promotion of the tipper (H_z/H_x-max) as an exploration tool, the vertical field's high sensitivity to noise and strong bias in the presence of polarized source fields are not easily overcome.

The magnetotelluric impedance is actually a tensor quantity, which rotates and scales a vector magnetic field into a vector electric field - such that the electric and magnetic fields are related by a more complex 2ND order linear tensor expression than is given in the Cagniard equation (Eq. 3). The frequency domain relations between the Fourier-resolved tangential components of the surface electromagnetic fields are defined as:

MT Impedance: $$\begin{aligned} E_x &= Z_{xx} H_x + Z_{xy} H_y \\ E_y &= Z_{yx} H_x + Z_{yy} H_y \end{aligned}, \quad E = Z H, \quad \begin{vmatrix} E_x \\ E_y \end{vmatrix} = \begin{vmatrix} Z_{xx} & Z_{xy} \\ Z_{yx} & Z_{yy} \end{vmatrix} * \begin{vmatrix} H_x \\ H_y \end{vmatrix}$$

where the column vectors $|E|$ and $|H|$ are the tangential electric and magnetic field vectors and the dyad $|Z|$ is the rank two tensor electrical impedance - whose on-diagonal elements are defined as Z_{ii}, and Z_{ij} are the off-diagonals

(Word et al., 1971). This is used to extend the method because the simple Cagniard linear relation breaks down for laterally inhomogeneous structures. The *Z* impedance is however an abstract quantity without readily apparent physical significance (Eggers, 1982). We can extract the scalar parameters from *Z* by rotating the axis to the geoelectric strike direction. Moreover, the tensor equation simplifies with the decreasing n-dimensionality or structural complexity of the environment (Vozoff, 1972):

1) In the simplest case, the resistivity varies only with depth ($\rho = \rho\{z\}$) and the earth is referred to as one-dimensional. In layered 1-D earths the tensor relation is reduced: the on-diagonal elements (Z_{ii}) equal zero and the off-diagonals (Z_{ij}) equal each other such that the scalar equation is always exact. Hence, the scalar measurement of ρ_a in any direction will always give the same result - a condition known as isotropy:

1-D Earth: $$Z_{xx} = Z_{yy} = 0, \quad Z_{xy} = -Z_{yx}, \quad Z = \begin{vmatrix} 0 & Z \\ -Z & 0 \end{vmatrix}, \quad \rho_a = \frac{1}{\omega\mu}|Z|^2 = \frac{0.2}{f}\left|\frac{E_x}{H_y}\right|^2$$

2) When the earth's resistivity is uniform along only one of two horizontal axes (the geologic strike), the earth is two-dimensional ($\rho = \rho\{(x,z\}$). In 2-D earths the scalar resistivity is accurate only when the sensor orientations are parallel and perpendicular to the geologic strike, because the fields are linearly polarized parallel to the symmetry. This results in the Z-impedance's on-diagonal elements equalling zero and the remaining scalar pair being the maximum and minimum values of apparent resistivity (ρ_{max} and ρ_{min}); the sensor-oriented difference in ρ_a is called anisotropy:

2-D: $$Z_{xx} = Z_{yy} = 0, \quad Z_{xy} \neq -Z_{yx}, \quad Z = \begin{vmatrix} 0 & Z_{xy} \\ -Z_{yx} & 0 \end{vmatrix}, \quad \rho_{xy} = \frac{0.2}{f}|Z_{xy}|^2, \quad \rho_{yx} = \frac{0.2}{f}|Z_{yx}|^2$$

3) In the most complex case, the three-dimensional earth's conductivity varies in all, or at least two horizontal directions regardless of the coordinate system chosen ($\rho = \rho\{x,y,z\}$). In 3-D environments, the impedance tensor cannot be

coordinate-rotated so that the on-diagonal elements are zeroed. The electric and magnetic fields therefore are never orthogonal and, as a result, the scalar equation never approximates the apparent resistivity:

3-D Earth: $$Z_{xx} \neq Z_{yy} \neq 0,\ Z_{xy} \neq -Z_{yx},\ \rho_{ij} \neq \frac{0.2}{\ddot{u}} \left| Z_{ij} \right|^2$$

In the sensor-miss-oriented 2-D and the 3-D case, the advent of non-zero on-diagonal elements means that the measured apparent resistivity is dependant on the polarization of the source fields and results in E_i and H_j being uncorrelated. This arises because, as shown in the general equation for the MT impedance, that adjacent to a structure of a given strike, the E field (E_i) measured is in part due to the H field perpendicular to it (H_j) and also partially due to H_i, whose currents are deflected by the structure. Therefore, unless the source fields are circularly polarized, the measured scalar apparent resistivity may not necessarily be repeatable with time and the data scatter will also increase. So it is necessary to reorient the reference system until the principle elements are maximized and the on-diagonal elements are minimized (3-D) or zeroed (2-D or 1-D) - this can be done either by: a) pivoting the field sensors during data acquisition, or b) if at least four orthogonal components (E_i, E_j, H_i, H_j) are measured simultaneously, by rotating the impedance tensor mathematically, during data processing:

Rotation: $$Z'(\theta) = \theta Z \theta',\ \theta = \begin{vmatrix} \cos\theta & \sin\theta \\ -\sin\theta & \cos\theta \end{vmatrix},\ \begin{matrix} E_x \_ Z_{xy}(\theta) \cdot H_y(\theta) \\ E_y \_ Z_{yx}(\theta) \cdot H_x(\theta) \end{matrix}$$

2.2.4 2D Inversion Procedure

The following discussion on 2D inversion procedure is drawn from Reddig (2002): The primary interpretation tools for Titan MT are 2D inversions. Problems emerge when the real world, complex, data are not consistent with the simplistic 2D assumptions. In a perfect world we would use modeling and inversion programs capable of reflecting the full complexity of the subsurface. However, in practice incorporating too much complexity in the modeling and inversion pro-

grams results in very coarse models which are incapable of resolving exploration targets. Instead, we must find ways to remove some of the complexity from the actual data. A number of techniques are employed to this end:

- Rotation to principal coordinates. The inversion algorithms presume that we have acquired a profile that is perpendicular to the true geologic strike. In reality, geologic strike is often difficult to define, and seldom known prior to acquisition. However, because we have acquired full tensor data we can rotate our data to the geologic strike direction after acquisition.
- Eigenvector processing. 3D structures can introduce complex "rotations" of the electrical currents. These rotations produce effects, such as excessively steep resistivity curves and out-of-range phases, that would be impossible to fit with 2D modeling programs. By relaxing the assumption that the electric and magnetic fields are orthogonal eigenvector analysis provides a unique and trivial methodology for simplifying complex 3D data.
- 1D Occam inversion for curve fitting. Real data are often noisy, and inconsistent. Out-of-range phases are a typical example of features seen in real data that can not be fit using 2D inversion. It is often best to make use 1D inversion to make interpretative decisions about how to "best" fit the data, rather than letting the 2D inversion thrash trying to fit inconsistent data.

Once these data processing techniques have been completed the data are inverted. Generally, two inversions of the MT data are done. The first inversion uses a model norm that explicitly looks for the "smoothest" model consistent with the data. This approach essentially finds the minimal subsurface structure consistent with the data. The second inversion uses a different model norm that looks for a model most consistent with the known geology.

For the geologically constrained inversion we use a proprietary approach developed by Dr. Phil Wannamaker (de Lugao and Wannamaker, 1996). This approach uses the geologic constraints as a target, while not imposing any intrinsic smoothing on the inversion. The approach finds the maximum structural information, at the risk of sometimes including structure not required by the data. It represents an effort to extract the maximum exploration information from the data.

Both approaches are valid, and important. A smooth model approach to inversion can be viewed as finding the least possible useful exploration information. However, it does provide an independent assessment of what the data actually require. The geologically constrained inversion will provide a much sharper subsurface image. But it will also reproduce the known geology where the data does not require a change to the model. Without an independent smooth model inversion it can be hard to determine whether a geologically constrained inversion has confirmed the geologic interpretation, or simply doesn't have any information either way.

2.3 Inversion Theory

The following discussion on inversion theory is drawn from Reddig (2002): An excellent overview and introduction to both the philosophy and use of inversions in geophysics is available on the University of British Columbia (UBC) website (http://www.geop.ubc.ca/ubcgif/; Oldenburg et al., 1998).

Several points, detailed on the website, are crucial to understanding the Titan-24 approach to exploration:

- Inversion is a powerful 'tool', not a 'solution'.
- Inversion is not normally "unique". Given noisy and incomplete data of inherently limited resolution there are usually an 'infinite' range of models that 'fit' the data equally well. Recognition of this inherent non-uniqueness is why inversion must be viewed as a tool rather

than a solution. Understanding and exploration of this non-uniqueness is an important part of the interpretive process.

- Inversion finds a model that 'fits' the data. The precise definition of 'fit' can be critical in the actual model that is found.
- The inversion depends on the data, and the data errors. The importance of the data errors is often overlooked.
- Inversion depends on a "model norm" – the mathematical definition of which model the inversion should try to find. This definition is almost as important as the actual data in determining the final inversion model.

Mathematically, inversion is the process of minimizing a function. The choice of which function to minimize ultimately defines the inversion model. Schematically, this function might be expressed:

$$\phi = \phi_d + \beta \phi_m = \text{(misfit)} + \beta\,\text{(model norm)}$$
$$0 < \beta < \infty \text{ is a constant}$$

This defines a function to be minimized that consists of some function that minimizes the data misfit, combined with some function that finds a "smooth" model. Beta represents a relative weighting between fitting the data and smoothing the model.

Clearly, the data misfit function must be defined in more detail. One approach might be:

$$\phi_d = \sum_{i=1}^{N} \left(\frac{F_i[m] - d_i^{obs}}{\varepsilon_i} \right)^2$$

This function defines the data misfit as the sum of the individual misfits squared, normalized by the errors associated with each data point. It is a very common, and stable, definition of the data misfit.

An important point not made on the UBC website is that the errors depend on many factors. The most common measure of data errors is simply the repeatability of the voltage and current measurements in the field. This may be misleading as there are also "errors" associated with electrode positioning, geologic complexity (2D vs 3D, but also coupling of shallow and deeper structure), and errors in the numerical calculation of model responses and inversion.

Another point not sufficiently detailed on the UBC site is the importance of not overestimating the data errors and fitting the data as closely as possible. Most geophysical techniques, but particularly electrical techniques, have large responses to shallow structure. This is expressed as "pant legs" in DC/IP, or "statics" in MT. The response to deep structure is generally a very subtle component of the data, compared to the sensitivity to shallow structure. Without excellent data, and an excellent match between the data and model response, the deep structure will not be imaged to the degree necessary for commercial exploration.

The model misfit function must also be defined in more detail. One of the most flexible definitions is the one used by UBC:

$$\phi_m(m,m_0)=\alpha_s\int_{vol}(m-m_0)^2dv+\alpha_x\int_{vol}\left(\frac{\partial(m-m_0)}{\partial x}\right)^2dv+\alpha_z\int_{vol}\left(\frac{\partial(m-m_0)}{\partial z}\right)^2dv$$

In this definition there are three components to the "model norm" (or "smoothness" constraint, or "regularization"), each of which contains an α constant (α_S, α_X, α_Z) that are commonly referred to as "alpha parameters". The first component is simply an overall difference between the model and a "target" model, the second component is a horizontal smoothness, and the third component is a vertical smoothness. The three "alpha" parameters (α_S, α_X, α_Z) represent a relative weighting of each component. A fourth variable, m_0, refers to the starting or reference model – either a half-space or geophysical constraint – that also has a profound influence on the model-misfit.

The UBC website provides an excellent example of the importance of selecting an appropriate "model norm", reproduced here:

In this example the expected response of the top figure was computed. These 'data' were then inverted six times, using different "model norms" (α_S, α_X, α_Z, m_0). The lower six figures show the range of valid inversion models that can be produced. Note that six of these models are essentially mathematically equivalent, they all "fit" the data.

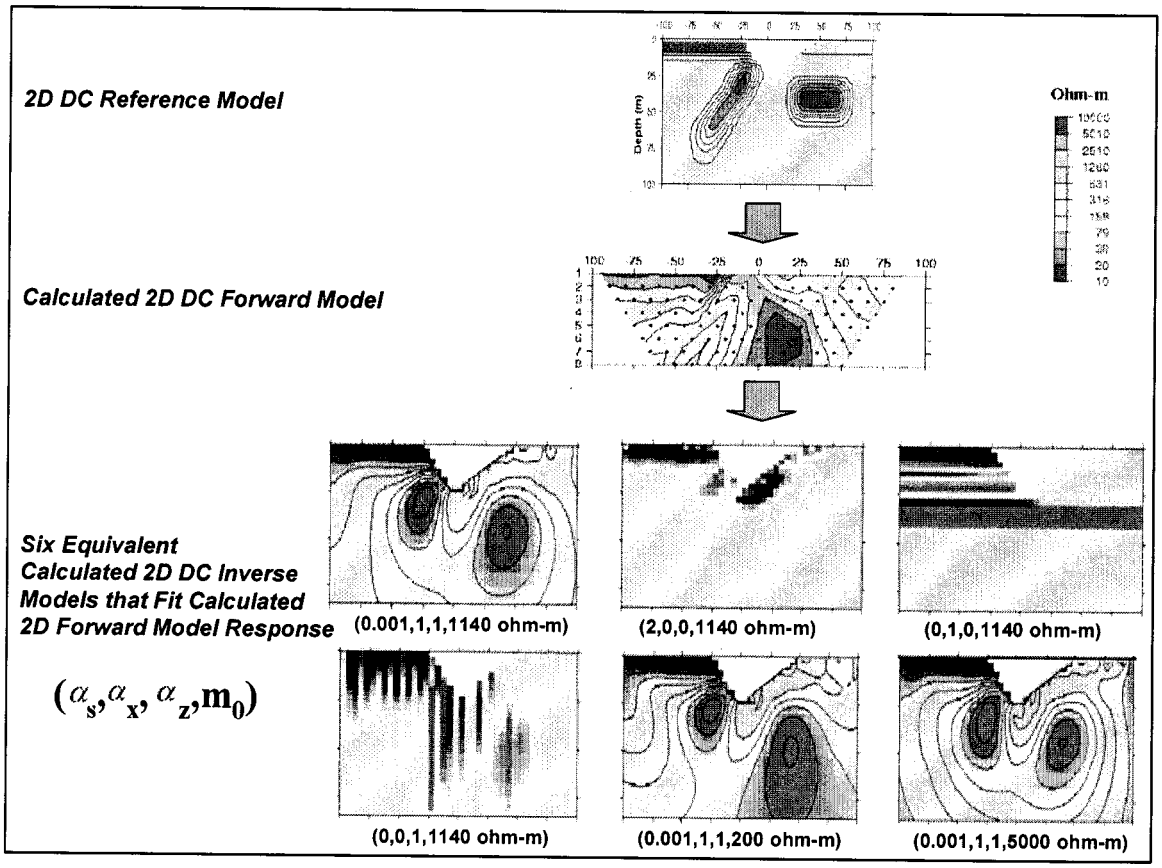

Figure 2.3: Effects of Model Norm and Starting Model on Inversion Results (modified after Oldenburg and Jones,1998).

An important philosophy, driving much of the academic communities approach to inversion for the last two decades, is that the "best" model is the "smoothest" model consistent with the data. There are good reasons for taking this approach. However, from an exploration viewpoint this philosophy can be rephrased to "find the model with the least exploration value" – perhaps not reflecting the real goal of an exploration program.

Recently, several groups have taken major steps towards developing inversion approaches more tuned to exploration needs. Instead of using "smooth" model norms, they are being replaced with "focused (minimum transition zone) inversion, or smoothing to a geologic "target" model.

For exploration smoothing to a geologic target model makes sense. It requires good geologic control, and some understanding of the rock physical properties. There are three drawbacks to the geologic target approach:

- The geologic information is incomplete or inaccurate.
- Physical property data are incomplete.
- It is difficult to determine whether the geophysical data support the geologic model, or simply provide no information.

The most sensible approach is to combine smooth model inversion with geologic target inversion. For now, we are focusing on providing inversions using both approaches. It is up to the project geologist and geophysicist to review these inversions and develop a final interpretation.

2.3.1 Ratio-M and Delta-M Analysis

An accurate measure of the degree to which a constrained inversion has identified new, geologically unexplained elements is by calculating the difference between the final inversion model and the reference model. For 2D inversions, this procedure is achieved simply by differencing the corresponding cell elements in the mesh solutions.

For parameters such as IP chargeability, density and magnetic susceptibility, which vary linearly, the difference is referred to as Delta-M, which is defined as follows:

$$\textbf{\textit{Delta-M}} = \textbf{\textit{Value}}_{\textbf{\textit{Inversion}}}\ \textbf{\textit{minus}}\ \textbf{\textit{Value}}_{\textbf{\textit{Reference}}}$$

For parameters such as Resistivity, which vary logarithmically, the difference is referred to as Ratio-M, since by definition, the difference in two logarithms is equal to their ratio. The Ratio-M for resistivity is defined as follows:

$$\textbf{\textit{Ratio-M}} = \textbf{\textit{Value}}_{\textbf{\textit{Inversion}}}\ \textbf{\textit{divided by}}\ \textbf{\textit{Value}}_{\textbf{\textit{Reference}}}$$

Due to its simplicity and compatibility with multi-dimensional inversion, the use of Delta-M and Ratio-M products is routine in the Gocad common earth modeling platform (Morrison and McGaughey, 2001).

The following Titan case-history example (Figure 2.4; Legault et al., 2003) well illustrates the benefits of the Ratio-M and Delta-M products, which are: a) better highlighting geologically unexplained targets, and b) providing insight on the depth of investigation, analogous to the methodology outlined in Oldenburg and Li (1999).

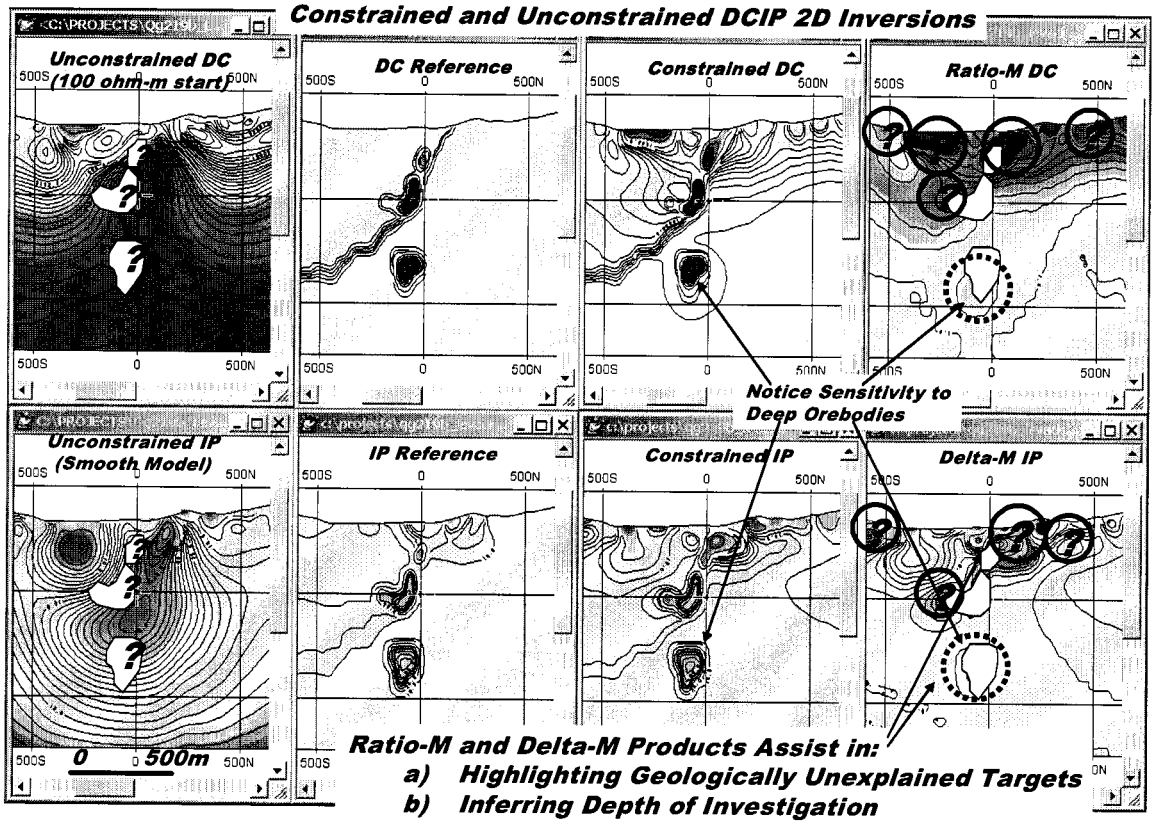

Figure 2.4: Case-History Examples Showing Delta-M and Ratio-M Products of 2D DCIP Inversion

CHAPTER 3 RESULTS AND DISCUSSION

3.1 Overview

The Titan-24 system acquires three types of geophysical data, magneto-telluric (MT), direct current (DC) resistivity and induced polarization (IP). The MT and DC both measure the same physical property, resistivity, in two different ways, whereas the IP measures the chargeability, which is an indicator of metallic mineralization, either massive or disseminate.

DCIP is an electrical method which uses the injection of current and the measurement of voltage and decay to determine subsurface resistivity and chargeability. Depth of investigation is controlled by array geometry and transmitted current. The Titan surveys image DC resistivity to depths of 500-750 metres, while the IP images to 350-500m. The difference in penetration is a function of relative physical property contrasts and relative signal-to-noise levels between the two measurements. A sensitivity analysis which studies the depth of investigation limits of the Kidd Creek Titan data and DCIP inversion models is presented in Section 3.3.

MT is an electromagnetic method which measures the subsurface resistivity to great depths, using natural EM signal sources from worldwide thunderstorms and the ionosphere. Depth of investigation is controlled primarily by the frequency of measurement and the bedrock resistivity, and it can be to great depth. Depth estimates from individual soundings can easily exceed 20km. However, the data can only be interpreted, using inversion, when the "aperture" of the array is comparable to the depth of investigation, which is about half the length of the profile. In the present survey, this equates to 2-2.5 km depths. A sensitivity analysis which studies, in detail, the depth of investigation limits of the Titan DC, IP and MT data and corresponding 2D inversions at Kidd Creek is also presented in Section 3.3.

The primary tool for evaluating Titan-24 data is two-dimensional (2D) inversion. The critical points are that inversion models depend on the data, as well as the data errors and the model objective function. The inversion models are not unique, may contain "artefacts" of the inversion process, and may also not accurately reflect all the information apparent in the actual data. Inversions are a tool, sometimes very powerful, but not a "solution". Inversion models need to be reviewed in the context of the data, model fit, and with an understanding of the model objective functions used.

The present analysis and interpretation of the Kidd Creek Titan-24 survey results has followed 5 stages/steps:

First, unconstrained 2D inversion (non-geologically referenced), using smooth DC and IP inversions (Oldenburg and Li, 1994) and smooth-conjugate MT inversions (Rodi and Mackie, 2001) were calculated, independent of each other, using solely the raw DCIP and MT geophysical data, immediately following the acquisition and data processing stage - most of which were performed on-site during the survey. This allowed for an assessment of data quality and a preliminary geologic mapping capability. These unconstrained DCIP and MT inversions are described below and are also documented in Appendix A and C.

Additional, unconstrained 2D inversions were later performed, using more advanced inversion processing techniques – for the DCIP, this consisted adjusting error floors, in order to maximize the number of data input into the convergent models, as well as using an alternate model-objective function in the UBC DCInv2d algorithm, in order to "sharpen" the resulting DC and IP images. For the MT, this first involved applying more rigorous post-processing, termed "EVA", which consists of component de-rotation into the geologic strike directions, the selection of the in-line and cross-line modes, static correction of apparent resistivity curves, and curve fitting to a 1D Occam inversion model – along with additional data editing as required. An advanced 2D inversion algorithm (PW2dinv), developed by Quantec and described in de lugao and Wannamaker (1996), us-

ing a finite-element, Gauss-Newton solution, was then used to obtain sharper, deeper, high resolution cross-sectional resistivity images. These unconstrained DCIP and MT inversions are described below and are also documented in Appendix A and C.

Second, a physical property analysis stage, where rock properties were assigned to the respective geologic units in Gocad, combined in-situ data available from borehole petrophysical surveys and, where required, archival evidence from laboratory analyses of representative rock samples, as well as preliminary 2D inversion results. This stage is described in Sections 3.2.1.

Third, a 3D Gocad common earth model (Morrison and McGaughey, 2001) was constructed which best represented the known geology underlying the survey area, based on drill evidence. This stage is described in Section 3.2.5. 2D geoelectric sections, based on the 3D geologic model and populated with resistivities and chargeabilities obtained during the physical property analysis stage, were input directly as references for the constrained 2D inversions and sensitivity analyses. The results of each geophysical inversion stage were then reintroduced into the Gocad model for easy comparison against the geology.

Fourth, constrained 2D inversions (geologically referenced) were performed, upon obtaining the geologic and physical property constraints from the Gocad model, and immediately following the final unconstrained modeling and data processing stages. This type of inversion relates the geophysics directly to the known geology. The DCIP inversions utilized the UBC DCInv2d algorithm and both "smooth" and "sharp" model were calculated. The MT inversions used the Quantec PW2dinv algorithm and "EVA" processed data, used in the advanced unconstrained modeling stage.

After an initial round of constrained inversions, the physical property constraints were reviewed and the values for rhyolite and mineralization were adjusted to better fit the observed data. The constrained 2D DCIP and MT inver-

sions were again repeated. Following the referenced inversions, the interpretation results were re-introduced into the Gocad model, to precisely target unexplained geophysical responses, using Ratio-M and Delta-M analyses. These constrained DCIP and MT inversions are documented in Appendix B and D.

Fifth, a sensitivity analysis was performed, using 2D geophysical forward models of a simulated Kidd Creek orebody and geology, in its original unmined state, obtained directly from the Gocad model - with its assigned physical properties, as it is progressively buried from surface to 200m, 500m, 1km and 2km depths. The objectives were to: a) simulate the expected Titan-24 MT and DCIP responses from a world class orebody, for comparison with the present survey results, b) test the depth-detection and resolution limits of the DCIP and MT techniques, as well as c) test the predicted behaviour of resulting 2D unconstrained and constrained DCIP inversions. These results are described and documented in Section 3.3

3.2 Physical Properties Analysis and Gocad Modeling

An important first step in the 3D Quest process is the assignment of representative physical properties to the various geologic units in the Gocad model. However, not all Gocad model units are specifically represented in any single database available, the physical properties used to populate the Gocad common-earth model, as well as to geologically-constrain the geophysical inversions shown in this study, were drawn from several sources. For the resistivity values used in the present study at Kidd, rock properties were obtained from both a) Borehole single-point resistivity (SPR) logging results provided by the client (ref., W. Hughes, Falconbridge, pers. comm., Prpinfo.doc, Feb-02), and b) Borehole electric array logging (EAL) data and Logtrans™ (see Sec. 3.2.3) statistical analyses for Hole 4509, performed by Quantec Logging Services (S. Coulson, QLS, pers. comm., Jan-2002; C. Drielsma, QLS, pers. comm., Feb-02). As well, for the chargeability, because DCIP data were unavailable for the Kidd area, val-

ues were inferred based on archival evidence of laboratory physical property testing for Timmins-area, Archean rocks, provided by Quantec Geoscience Inc. (ref. P. Alikaj, QGI files, 09/99-01/02). Lastly, in the case of the overburden, where direct physical property evidence was unavailable, values were inferred based on preliminary 2D inversion results.

3.2.1 Borehole Single Point Resistance Logging Results

The borehole single-point resistivity data, made available by Falconbridge, were previously obtained, independently of the present study, and also include AC conductivity, natural gamma as well as magnetic susceptibility. The borehole results provided, however, are entirely archival and consist solely of tabled statistical means and standard deviations according to roughly 20 lithologic units – as such, neither the raw borehole logging data nor details regarding the statistical population (number of points, holes, etc.) are available to the author. As a result, more robust Logtrans^{TM} borehole statistical analyses, as with EAL data, were not performed. While there is some degree of correlation between the 20 geologic units represented SPR database and those in the Gocad model, however, there also are several omissions, for mineralization (massive sulphide, graphite), in particular, and many overlapping units (i.e., 7 mafic volcanic types). In fact, only 3 of the 8 Gocad model units (see Table 3.3) are represented in the SPR data: mafic and felsic volcanics, and argillite/sediments. Finally, while SPR resistances are widely used to map borehole lithology, based on relative variations in contact resistance between the borehole probe electrode at depth and the grounding point at surface, in fact, these measurements, by their nature, differ significantly from the formational resistivities required for the Gocad model and those values obtained in electric array logs. Furthermore, due to their uncalibrated nature (i.e., direct dependence to grounding points), these are liable to show a wide variance – likely explaining, in large part, the results shown in Figure 3.1). Nevertheless, in spite of these cautions, the SPR values presented for the various rock types appear to correlate well with the range of resistivity

values those obtained in subsequent EAL logs, as well as in preliminary 2D inversions. And so the SPR results have been included in the present statistical analysis - albeit weighted accordingly.

As shown in Figure 3.1, based on the SPR results, surprisingly, it appears that, the mafic volcanic units are more resistive (≈11k Ω-m) than the felsic volcanics and metasediments, which both have similar resistance averages (≈8.5k Ω-m) – likely explained by the presence of sulphide and graphite generally found in these units. Note also the large variances in the data, which easily span the narrow range in SPR values.

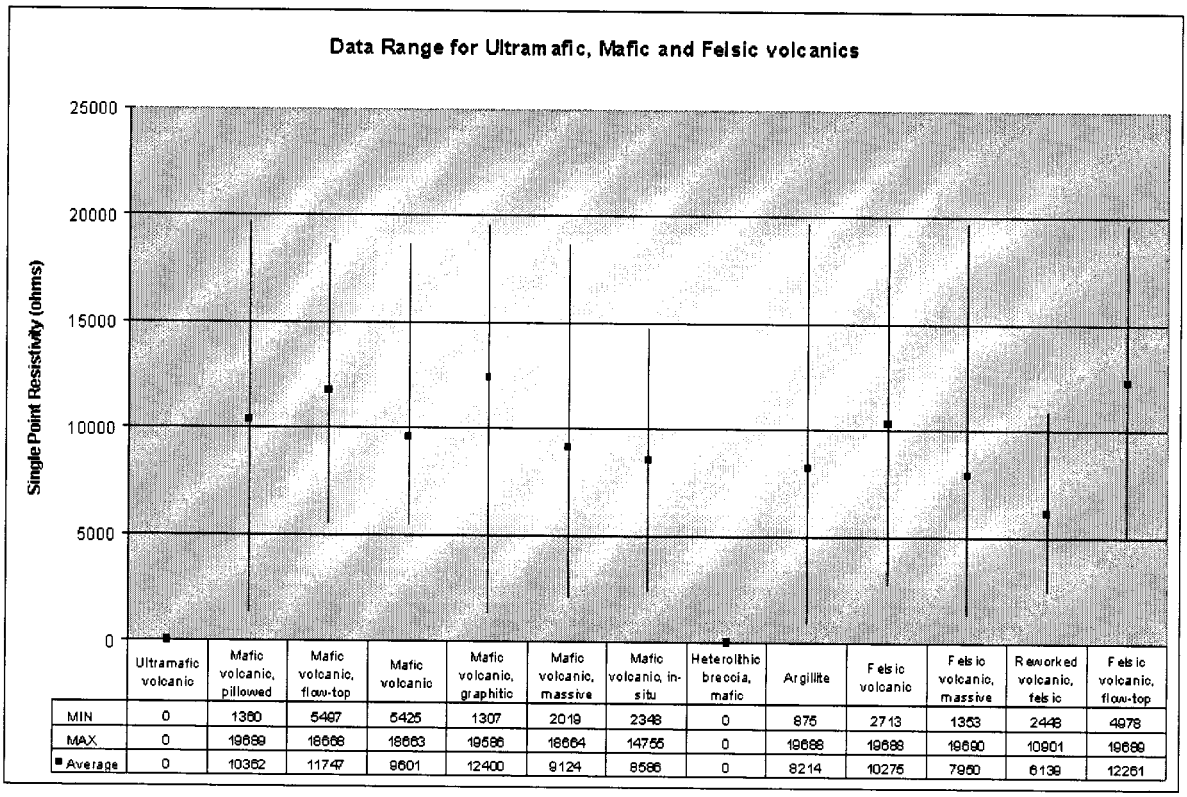

	Ultramafic volcanic	Mafic volcanic, pillowed	Mafic volcanic, flow-top	Mafic volcanic	Mafic volcanic, graphitic	Mafic volcanic, massive	Mafic volcanic, in-situ	Heterolithic breccia, mafic	Argillite	Felsic volcanic	Felsic volcanic, massive	Reworked volcanic, felsic	Felsic volcanic, flow-top
MIN	0	1360	5497	5425	1307	2019	2348	0	875	2713	1353	2448	4978
MAX	0	19689	18668	18663	19586	18664	14755	0	19688	19688	19690	10901	19689
Average	0	10362	11747	9601	12400	9124	8586	0	8214	10275	7950	6139	12261

Figure 3.1: Statistical summary showing the single point resistance range for the ultramafic, mafic and felsic rocks of the Kidd Creek area (from W. Hughes, Falconbridge, pers. comm., 02-02).

3.2.2 Borehole Electric Array Logging

In mid January, 2002, prior to the submission of the Titan-24 survey logistics report, hole 4509, was surveyed, at Kidd, by Quantec Logging Services (QLS), with a multi-spaced electric array log (EAL), using the 8in, 11in, 13in, 16in-normal and long-normal (LN) spacings, as well as for inductive conductivity (IC). Hole 4509 is collared at approx. 10540E/10975N, in local grid coordinates (UTM 474666mE / 5393786mN), just south of profile 110N, is oriented southward (180^{O}-200^{O}) and dips at 70^{O}-45^{O}. It was surveyed, at approx. 10cm intervals, in both directions (down/up) nearly over its entire length of 883m, for a total of 852m surveyed. Hole 4509 was chosen for logging, based on its vicinity to the present Titan survey area and the fact that it spans nearly all (5 of 8 – see Table 3.3) lithologic units found in the Gocad model – with the notable exception of massive sulphides and graphite. In contrast with the SPR result, however, mafic and ultramafic units represent a relatively small portion (<0.1%) of the 4509 drillhole lithology.

Borehole normal-resistivity logs, such as that for hole 4509, record the electrical resistivity of the borehole environment and surrounding rocks and water as measured using a fixed transmitter electrode pair and variably spaced potential electrodes on the logging probe. Typical spacings for potential electrodes are 16 inches or less for short-normal resistivity and 64 inches for long-normal resistivity. The data values for EAL and IC logs are output directly into units of ohm-meters and siemens/m, respectively. In the case of the 4509 log, the 16inch spacing results, shown in Figure 3.3, were considered the most reliable measure of formational resistivity, and least affected by borehole diameter and fluid conductivity, relative to the other, shorter spacings acquired (V. Gerrie, QLS, pers. comm., 02/02). It is worthwhile noting that, although for many applications, in-situ measurements using normal-resistivity logs are nearly equivalent to true formational resistivities, borehole electrical measurements are nevertheless affected by bed thickness, borehole diameter, and borehole fluid resistivity – in the

same way that surface geoelectric soundings are affected by the thickness and resistivity of the overburden. In fact, the effect of the correction is strongest for higher resistivity rocks and higher conductivity borehole fluids – shown to approach 3x-10x. It is also worthwhile noting that, unlike EAL logs which can be easily corrected for the effects borehole fluids, this is not the case for SPR logs – providing another mitigating factor in their use as indicators of formational resistivity.

An illustration of the extent of this effect is shown in Figure 3.2, which describes the formational resistivity correction applied to normal electrical logs, using hole diameter and fluid resistivity results, obtained using Caliper and Fluid Conductivity logs, respectively. Although, typically, these variations are ignored, particularly in qualitative borehole log interpretation, based on relative contrasts, the effects of fluid resistivity and hole-diameter are more likely to be more strongly felt in quantitative analyses, combining multiple holes – resulting in underestimates in resistivity and larger statistical scatter. In the case of hole 4509, appropriate corrections could not applied, as the necessary calliper and fluid conductivity logs were not obtained. However, while it is likely that the 16inch EAL data likely underestimate the true formational resistivities, in fact, as was the case for the SPR, the values obtained in Logtrans analyses (see below) appear to correlate well with those obtained in preliminary 2D DC and MT inversions.

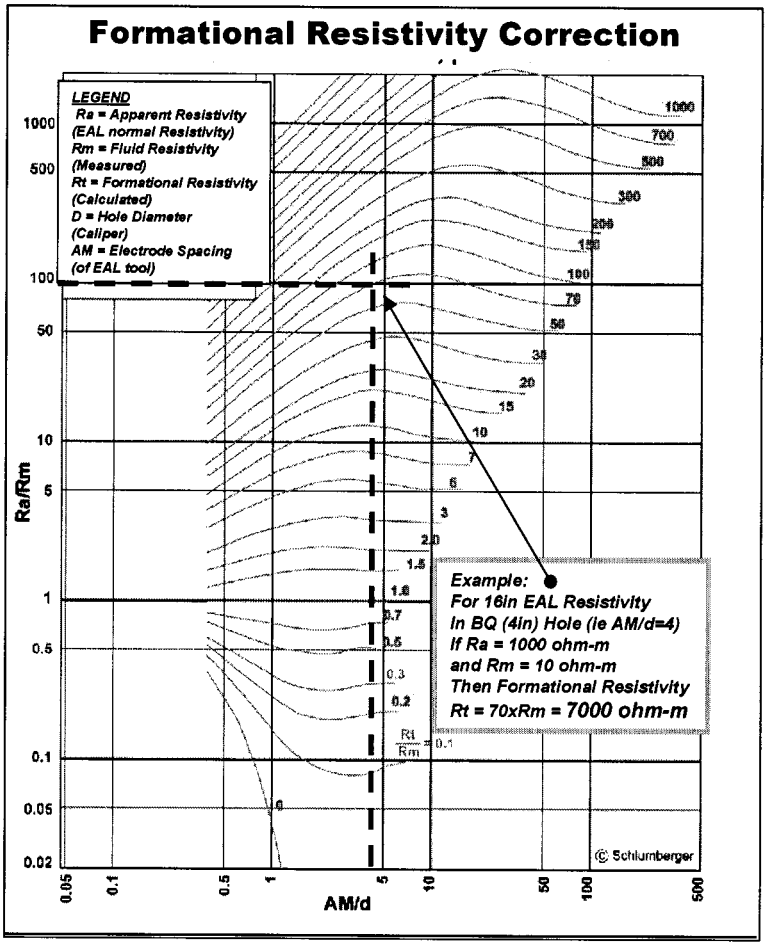

Figure 3.2: Formational Resistivity Correction for Electric Array Logs (courtesy J. Stowell, Mount Sopris Instruments, Dec-2001).

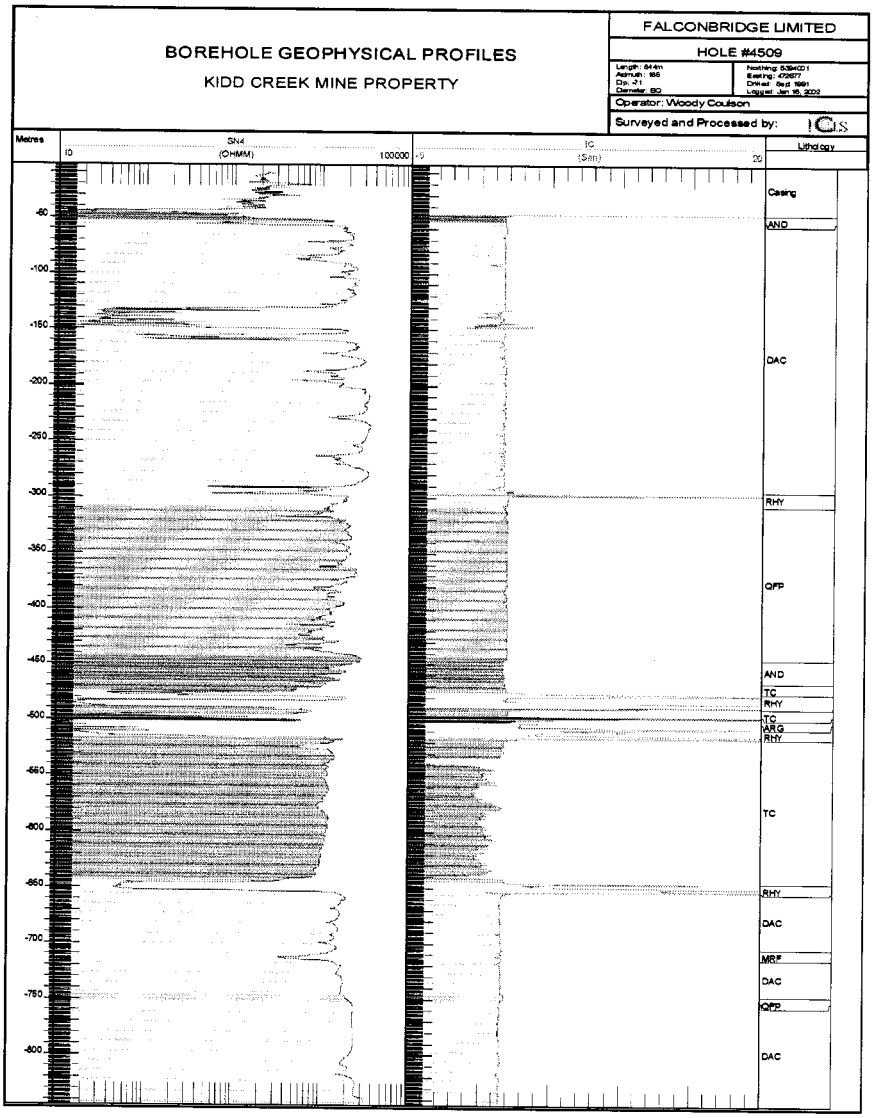

Figure 3.3: Viewlog™ Plot[1] Showing Electric Log (16in) Resistivity Log , Inductive Conductivity and Lithology for Hole 4509.

As highlighted in Figure 3.4, a visual analysis of the EAL results for 4509 would suggest that the Dacites are generally more resistive (>≈20k Ω-m) than the other units, but contain highly conductive portions, likely relating to pyrrhotite (S. Taylor, Falconbridge, pers. comm., 01/02), based on the associated high levels

[1] Viewlog™, Viewlog Systems, Toronto, Ontario.

of inductive conductivity. In contrast, the talc-chorite schists and MRF units appear to be the least resistive(≈10k Ω-m), with quartz-feldspar porphyry and andesite falling into the mid-range. More significantly, the rhyolitic units consistently correlate with high levels of inductive conductivity, exceeding 20 siemens/m, and appear to be marker horizons for mineralization, both graphitic and sulphides. It is clear, however, that portions of the rhyolite are also moderately resistive. Although quantitative statistical analyses of the EAL logs are possible using simple spread-sheet methods, robust analyses are more easily and reliably obtained using semi-automated software programs, such as Logtrans.

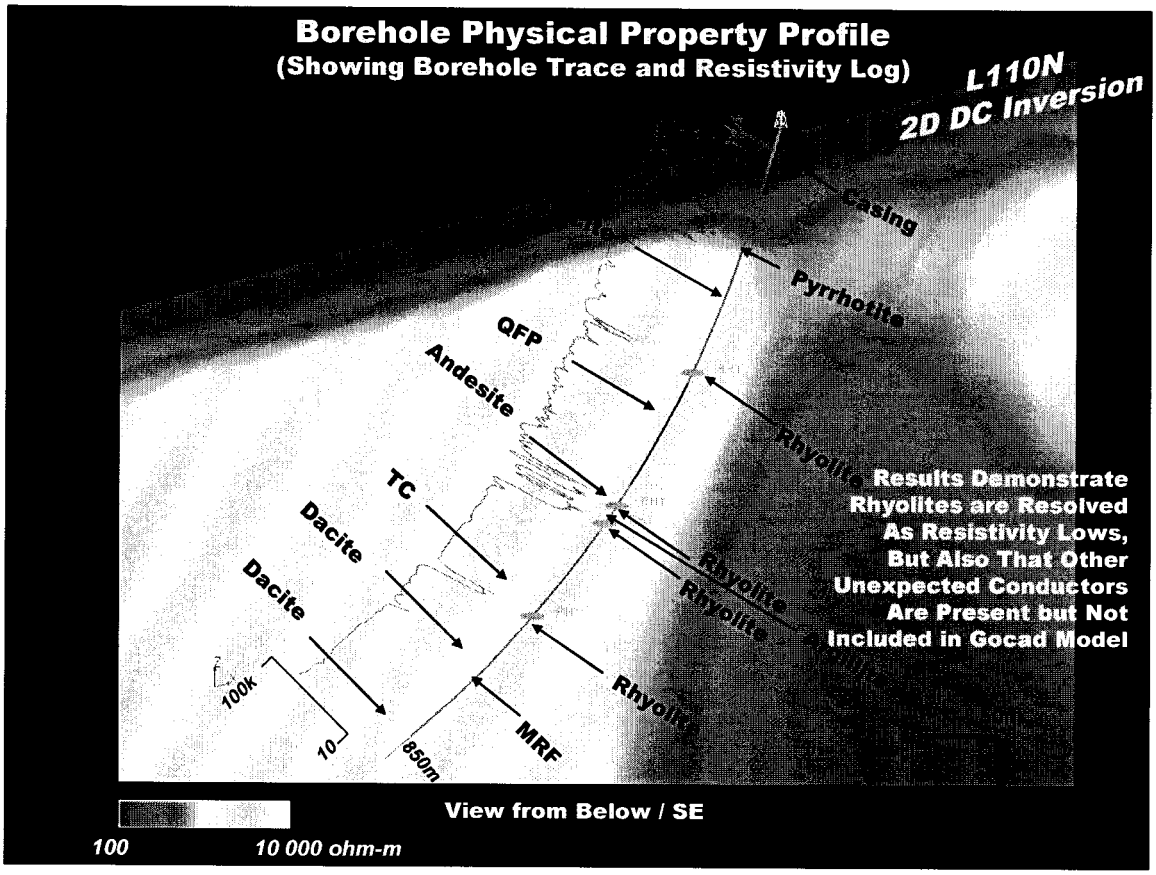

Figure 3.4: Borehole Electric Array Log, Drill-hole Trace and Geology for 4509 inside Gocad Model

3.2.3 Logtrans Borehole Statistical Analyses

Borehole physical property logs are easily correlated to geology, both visually and statistically, using software algorithms, such as Logtrans[2], which utilizes geo-statistical means and spreads of each of the physical properties, which then allow for the unique identification of each lithology subset – potentially, using multi-parameters for predictive auto-interpretative applications. In the present case, however, Logtrans analyses are used for the sole purposes of obtaining statistically accurate resistivity constraints used in advanced inversion analysis of Titan-24 distributed acquisition array data.

Logtrans utilizes composite (multi-parameter) LAS (log ascii standard) files generated in Viewlog™, the borehole logging processing and plotting platform (Figure 3.3). Logtrans analysis is based on a statistical characterization, where the statistical centroids (means or medians) and standard deviations of the resistivity distributions for each lithologic class are calculated using LAS data from either a single hole or a suite of control holes.

As shown in Figure 3.5, additional geophysical subcategories of each lithologic unit found in 4509 can been interpreted, based on visual analyses of borehole petrophysical logs, though not uniquely from the resistivity parameter (V. Gerrie, QLS, pers. comm., 02-02), and the results used for comparison purposes. For hole 4509, the more conductive and resistive portions of both the rhyolite and dacite have been subdivided into barren and mineralized, resulting in 2 separate and distinctive statistical populations, with smaller variances, within these two lithologic units – possibly reflecting a bimodal distribution. It appears that this may have also been warranted for andesite, due to the large standard deviation shown. Overall, the Logtrans borehole log statistical analyses shown in Figure 3.5 and Table 3.1 demonstrate that our subdivision of obvious conductive,

---

[2] Logtrans™, Fullagar Geophysics Pty Ltd., Taringa, QLD, Australia.

presumably mineralized sections of the borehole log results in both a) relatively smaller variances, hence better accuracy for formational resistivity estimates, and b) clear separation between mineralized and non-mineralized lithologies at Kidd Creek.

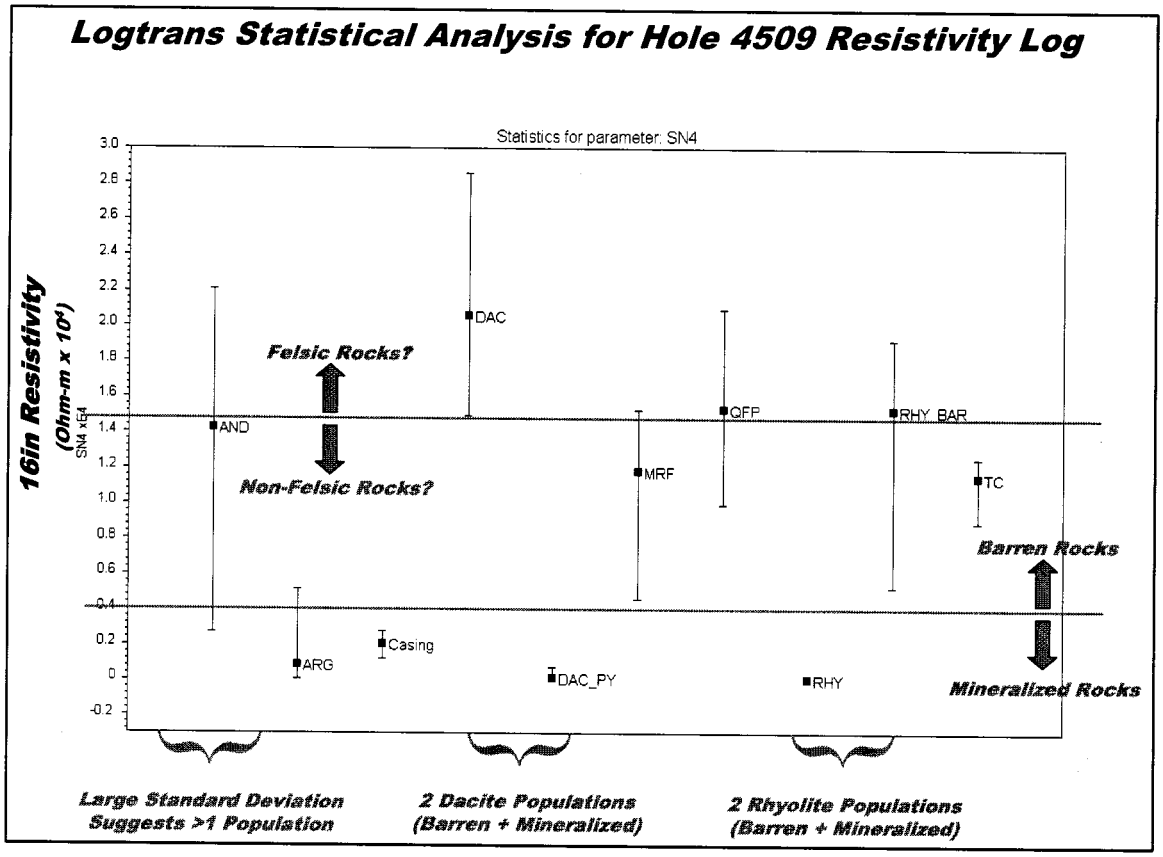

Figure 3.5: Logtrans™ Box-and-Whisker Plots Showing Composite Statistical Analysis.(Hole 4509, 16 inch Resistivity Parameter – uncorrected).

Table 3.1: Logtrans Statistical Analysis for Hole 4509 (see Figure 1.1).

Class ID	16 inch Median[3]	16 inch LDEV	16 inch RDEV	NPTS
ANDESITE	14213.6514	11538.7109	7843.71	277
ARGILLITE	822.8751	803.3351	4294.144	58
Casing	2024.29	878.7903	739.0398	365
DACITE	20534.8223	5622.9062	8002.5703	3923
DAC_PYRITIC	96.265	67.485	607.3149	222
MRF	11779.1318	7219.0112	3428.1523	96
QTZ FELDSPAR POPRPHYRY	15297.665	5362.5732	5635.4189	1425
RHYOLITE	34.57	20.57	54.77	307
RHY_BARREN	15237.9033	10021.124	3926.5713	185
TALC CHLORITE SCHIST	11423.0898	2555.8594	1086.9053	1452

The Logtrans analyses highlight several differences between the EAL and SPR results – notably, a greater range in values between rock types (≈3 log-decades vs 0.3 for SPR), smaller variances within rock types, greater contrasts shown between lithologic units and more reasonable geophysical behaviour. For example, the EAL statistics confirm that the dacites are distinctively resistive (20k Ω-m) relative to the other units, possibly reflecting their more felsic composition, whereas the argillites (800 Ω-m) are the least resistive among the lithologies – presumably due to their graphitic nature. Other felsic units (QFP and rhyolite) are also relatively resistive in comparison with the more mafic-ultramafic units (andesite, MRF and talc-chlorite schists). Finally, as expected, the Logtrans analyses show that the mineralized units are >100x more conductive than the non-mineralized rocks, on average, and are likely to provide easily detectible contrasts for surveys and 2D inversions. These results therefore confirm the im-

[3] Note: In Table 3.1, 16 inch refers to diameter of EAL array, Median refers to value in statistical population, LDEV refers to Median value minus 1 standard deviation, RDEV refers to Median value plus 1 standard deviation, NPTS is number of points.

proved results obtained by electric array logging and Logtrans borehole log statistical analyses over the more primitive SPR logging technique.

More importantly, the definition of distinctive, high conductivity sub-units (bi-modal) in the EAL logs, which were not subdivided in the drill-hole geology but are likely attributed to non-massive sulphides, pyrrhotite and graphite (S. Taylor, Falconbridge, pers. comm., 01/02), has potentially significant ramifications to the Gocad model and constrained inversions: a) anomalous conductivity is present within the rhyolitic bands and country rocks, b) the conductivity is unrelated to massive sulphide ore or graphite and, as such, is not specifically identified in the Gocad model, and c) conductors will likely be detected in Titan surveys and 2D inversions which will be unexplained in the Gocad model, but which may have some explanation in drill-hole logs. Moreover, the high degree of correlation in the EAL results suggests that the rhyolites may be best characterized as weakly conductive and likely polarizeable horizons for modeling and inversion purposes.

3.2.4 Physical Rock Properties for Gocad Model

The borehole electric array results and petrophysical analyses, using the Logtrans^{TM} statistics, were successful in providing improved resistivity references, on a lithology by lithology basis, to most (5), but not all 8 units included in the Gocad model. For some units, which are underrepresented in the EAL results, such as mafic volcanics, these are augmented by single-point resistance values, which appear to be in a similar range, in spite of their uncalibrated and indirect nature. Still, resistivity values for ultramafics and, more importantly, massive sulphides and graphite, as well as overburden are not characterized in the available borehole data. Furthermore, in-situ chargeability data are entirely absent for characterizing the IP parameters of the Gocad model.

To augment the available data, resistivity and chargeability values were, in part, obtained from archival evidence of laboratory physical property testing for

45 representative, Timmins-area, Archean rocks samples, provided by Quantec Geoscience Inc. (ref. P. Alikaj, QGI files, 09/99-01/02). These data are tabled below, listing values of resistivity and chargeability, along with corresponding source, according to 14 rock types - divided into various mineralized and non-mineralized volcanics, intrusives and sediments. Log averages of the resistivity and linear averages for the chargeability are presented in Table 3.2 and Figure 3.6 & Figure 3.7. Notice the progressive increase in resistivity from barren mafic to intermediate felsic volcanic rocks, which contrasts the more contradictive results from the SPR data. Notice also the unexpectedly weak conductivity for massive sulphides – possibly reflecting the Zn-rich nature of the laboratory samples tested.

Table 3.2: Summary of Petrophysical Properties from All Sources.

No.	Lithology/Gocad Unit	Resistivity Log-Average	N-pts/ Samples	Chargeability Average	N-pts/ Samples
1	Mafic volcanic	10122	11	5.6	6
2	Mafic volcanic, mineralized	3361	15	55.1	14
3	Intermediate volcanic	11784	5	n/a	--
4	Intermediate, mineralized	96	1	n/a	--
5	Felsic volcanic	15922	10	n/a	--
6	Felsic volcanic, mineralized	154	4	n/a	--
7	Ultramafic volcanic	1528	5	3.9	3
8	Ultramafic, mineralized	204	1	12.0	1
9	Greywacke-argillite	3266	4	37.9	1
10	Graphitic sediment	61	2	160.4	1
11	Mafic intrusive	8780	1	n/a	--
12	Felsic intrusive	7506	9	3.8	5
13	Felsic intrusive, mineralized	1695	5	47.9	5
14	Massive sulphides	45	6	83.4	6

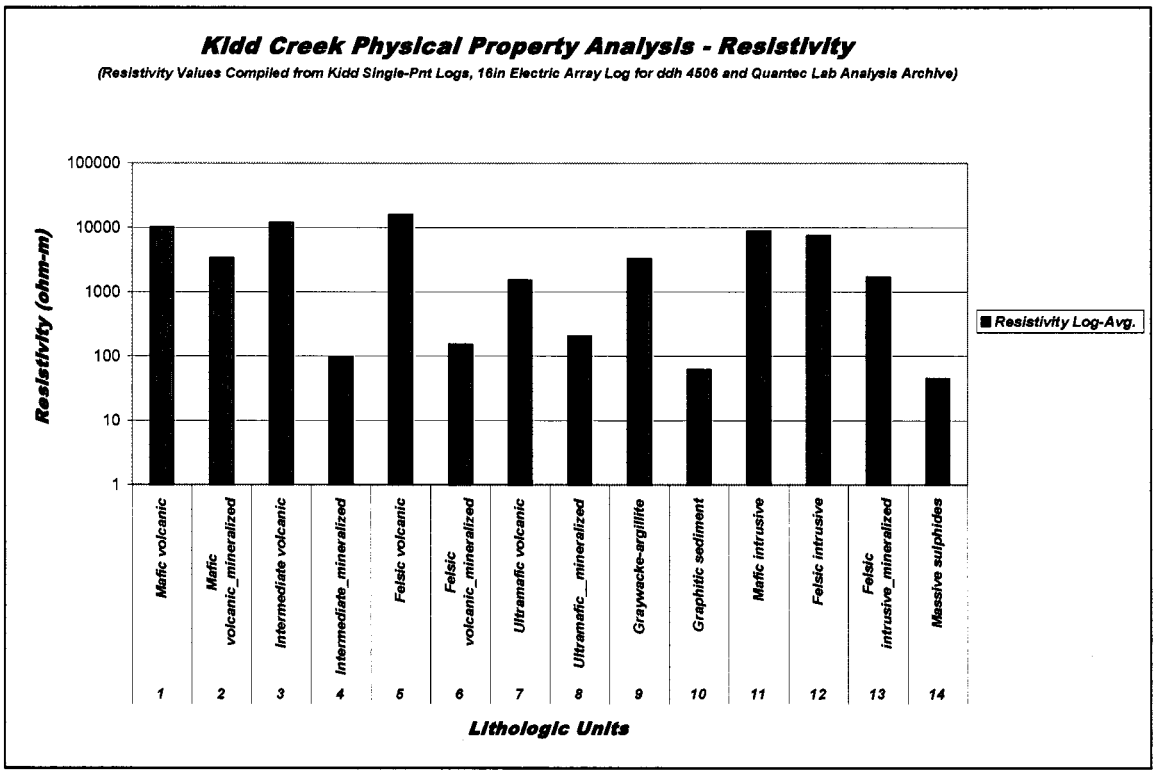

Figure 3.6: Resistivity Values from Composite Physical Property Analysis for Gocad Model

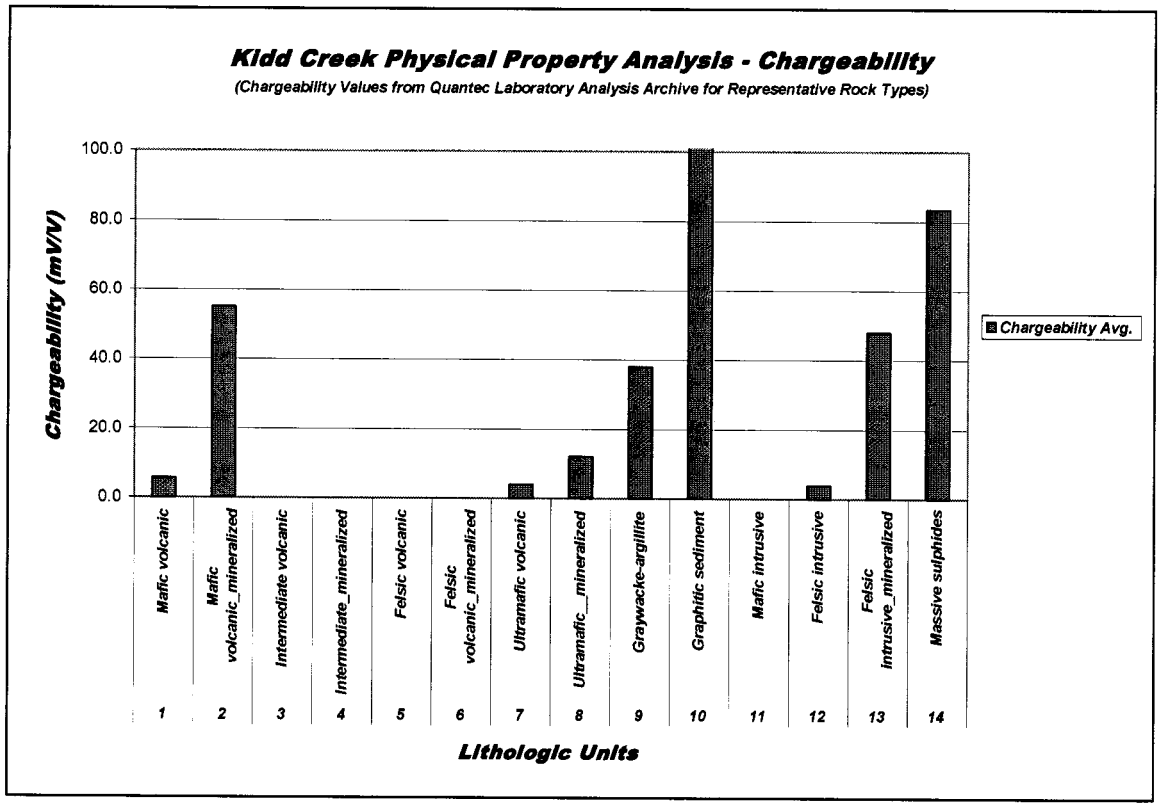

Figure 3.7: Chargeability Values from Composite Physical Property Analysis for Gocad Model.

In a final step, the results of the petrophysical analyses have been assigned to Gocad units is given in Table 3.3. First, the values for mineralized geologic subsets (mineralized mafic volcanic, mineralized intermediate volcanic, etc.) were removed and the resulting, barren/unmineralized reference values were assigned the remaining 8 Gocad units presented. For the lithologic units, the more resistive, non-anomalous values, attributed to barren rocks, were assigned to the Gocad model; whereas for the mineralization and graphite, the more conductive values were chosen – explaining some the discrepancies between Table 3.2 and Table 3.3. We expect, however, that the variations that were observed in the petrophysical profiles, both conductive and resistive, will be expressed in later, constrained, referenced inversion model and subsequently attributed to the effects of alteration and mineralization. For overburden and rock types which re-

main poorly characterized (notably intermediate, ultramafic and felsic volcanics, massive sulphides), and particularly in the chargeability, 2D inversions were compared directly against the geologic cross-sections and more representative values were substituted into the Gocad model.

The results suggest that while barren and mineralized units should be easily differentiable, based on up 300x contrasts in the resistivity and 20x for the chargeability, weaker contrasts within the main volcanic units will make them difficult to differentiate on the basis of resistivity or chargeability. Following an initial round of constrained inversion models, using 50 ohm-m and 50 milliradians for the rhyolite, these were later changed to 1k ohm-m and 20 milliradians, based on final model comparisons and behaviours. This was considered appropriate, given the absence of in-situ evidence for this unit, in particular. Similarly, chargeability estimates for graphite and massive sulphides, neither of which based on hard, in-situ evidence, were subsequently lowered from 150 and 100, respectively, to 75 milliradians in final models. The values chosen for the reference models are as follows:

Table 3.3: Resistivity and Chargeability Constraints Assigned to Gocad Reference Models.

No.	Lithologic Unit	Resistivity (Conductivity)	Chargeability
1.	Overburden	30 ohm-m (0.03s/m)	0.1mrad
2.	Mafic Volcanic	10,000 Ω-m (0.0001 s/m)	5 mrad
3.	Intermediate Volcanic	8,000 Ω-m (0.000124 s/m)	10 mrad
4.	Ultramafic Volcanic	7,000 Ω-m (0.000143 s/m)	3 mrad
5.	Sediments	5,000 Ω-m (0.0002 s/m)	10 mrad
6.	Rhyolite	50 to 1,000 Ω-m (0.001 s/m)	50 to 20 mrad
7.	Graphite	10 ohm-m (0.1 s/m)	150 to 75 mrad
8.	Massive Sulphides	10 ohm-m (0.1 s/m)	100 to 75 mrad

3.2.5 Gocad Model Creation

The Gocad common earth modeling software was developed by the Gocad research consortium, an industry-university alliance that has brought together more than thirty resource companies and more than forty universities since 1989 in developing the methods and software for achieving the common earth model (Morrison and McGaughey, 2001). The resulting software has been available commercially since 1999, and is distributed in Canada by Mira Geoscience Inc. (Montreal, QC).

Gocad is a very general earth-modeling application that has been used in both soft-rock and hard-rock applications at scales ranging from large regional compilations to detailed reservoir and ore body modeling. Largely based on a novel, patented geometric modeling algorithm that successfully allows "data-fitting" rather than the CAD approach of "designing" modeled objects, Gocad is fully 3D, fully topological, and provides the most sophisticated geometry and property modeling functionality currently available. It is available as both a user application and as object libraries for building custom applications. It is fully customizable at the user level and is easy to link to third-party applications. Its uses have been reported in the literature to vary from providing the basis for advanced geophysical processing, to structural geology, to advanced geostatistical applications, to resource risk analysis.

The Gocad model construction was undertaken by Mira Geoscience Inc., in late-January, 2002, based on geologic data provided by Falconbridge, Kidd Creek Mine Division, as well as an existing, on-going, separate Gocad model of the Kidd Creek orebody developed by Mira and the Kidd Creek staff. The Gocad model cube for the Kidd Creek Titan Project, shown in Figure 3.8, has dimensions of approximately 6.5km EW x 1.2km NS x 2.2km vertical, which matches the approximate aerial coverage of the survey lines and the depth-extent of exploration interest.

As shown in Figure 3.10, in plan, the Gocad model includes geologic elements extending 1km east, and 500m further north and south of the existing survey coverage. However, the known geology does not extend further west than approx. 78+00E, which is 600m east of the westernmost tip of our survey lines – and so, beyond this point, a mafic volcanic geology has been assumed for this region of the Gocad model. In total, the Gocad geologic model consists of 8 elements, including 5 geologic units, 2 mineralized units and overburden, as described in Table 3.3. Faults structures, alteration and drill-hole elements are also not included in the current Gocad model or as references for the 2D geophysical inversions.

The Gocad model was constructed from geologic contacts extracted from the Kidd Creek geologic database, at 1500, 1900, 2300, 2700, 3100 and 3320m mine levels (spanning approx. 1.8km vertically), as separate layers, in DXF-format. Overburden topography was also recovered from the Kidd Creek diamond-drill database. Gocad S-grids[4] of the surfaces were then constructed by linearly interpolating the contacts, vertically, between the mine-levels, and from the overburden-bedrock interface to 2km depths, as shown in Figure 3.9. Following this, the Gocad 3D Voxet[5], for the 2x1x5 km cube (see Figure 3.11), was created by volume-rendering the various geologic lithologies between the S-grid surfaces into $25m^2$ x12.5m cubic volumes. Each individual 3D volume in the Voxet was then populated with the physical properties, obtained previously, and 2D S-grids were then extracted, along east-west cross-sections (see Figure 3.12), in order to provide geophysical reference models for the constrained 2D inversion stage of the project, as shown in Figure 3.13.

---

[4] 3D stratigraphic grid. Cells follow stratigraphic horizon or 2D surface; G. Perron, Mira Geoscience, pers. comm., 12/04).

[5] 3D volumetric grid. Cells follow normal block parameterization (IBID).

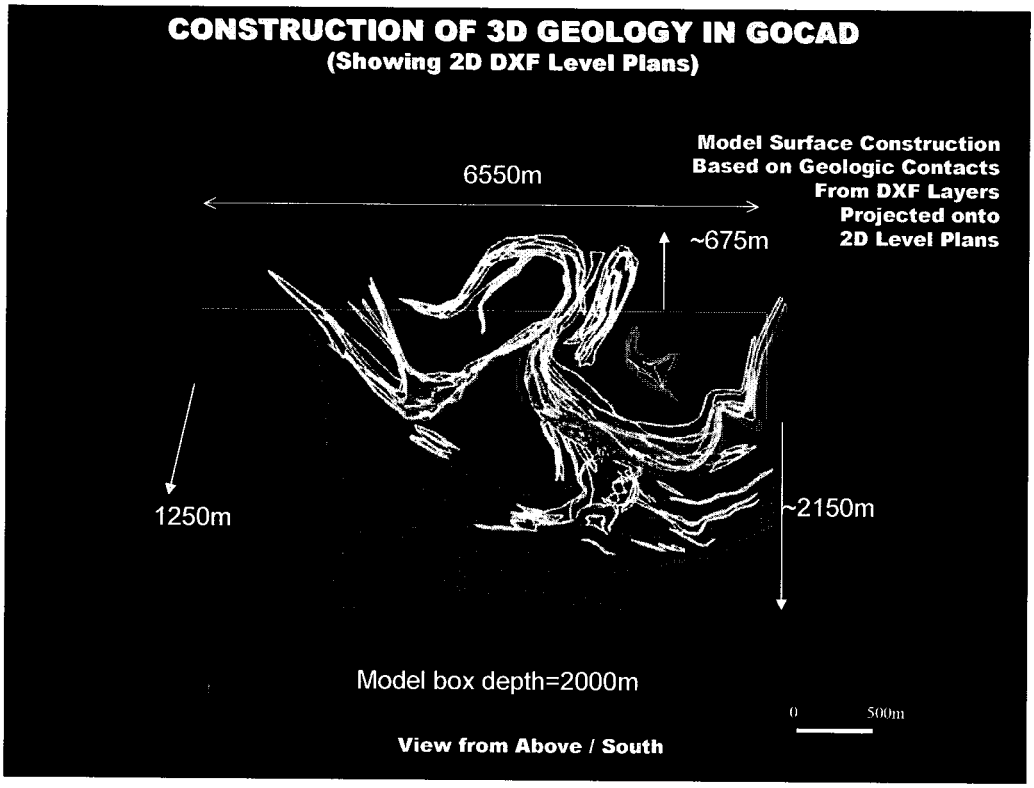

Figure 3.8: 3D Geologic Model Construction in Gocad.

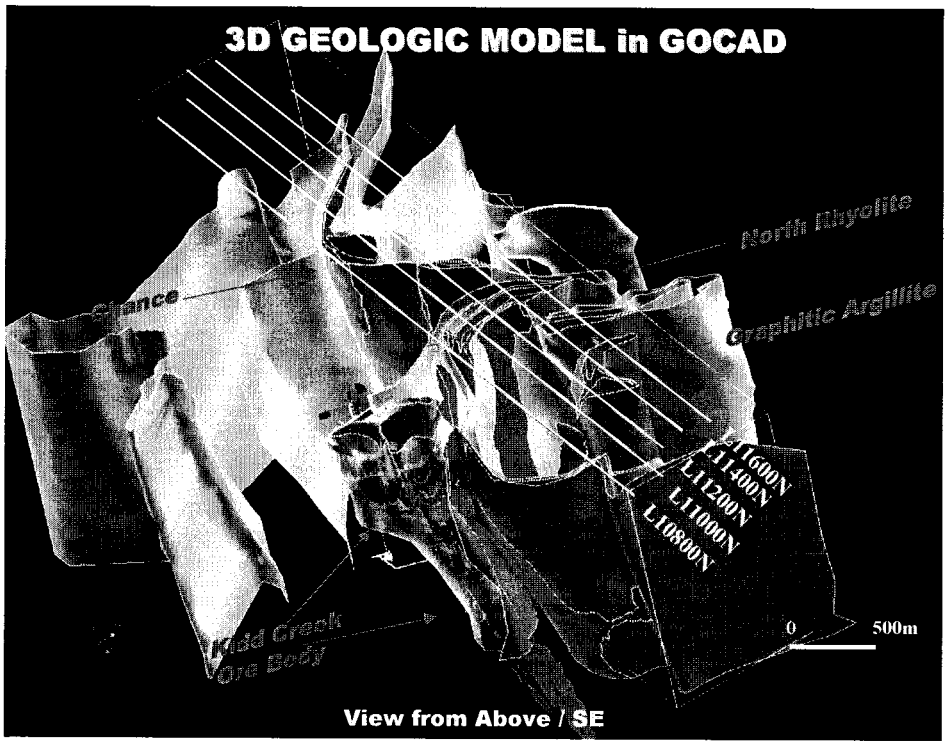

Figure 3.9: Gocad Model Showing Geology and Titan-24 Line Locations.

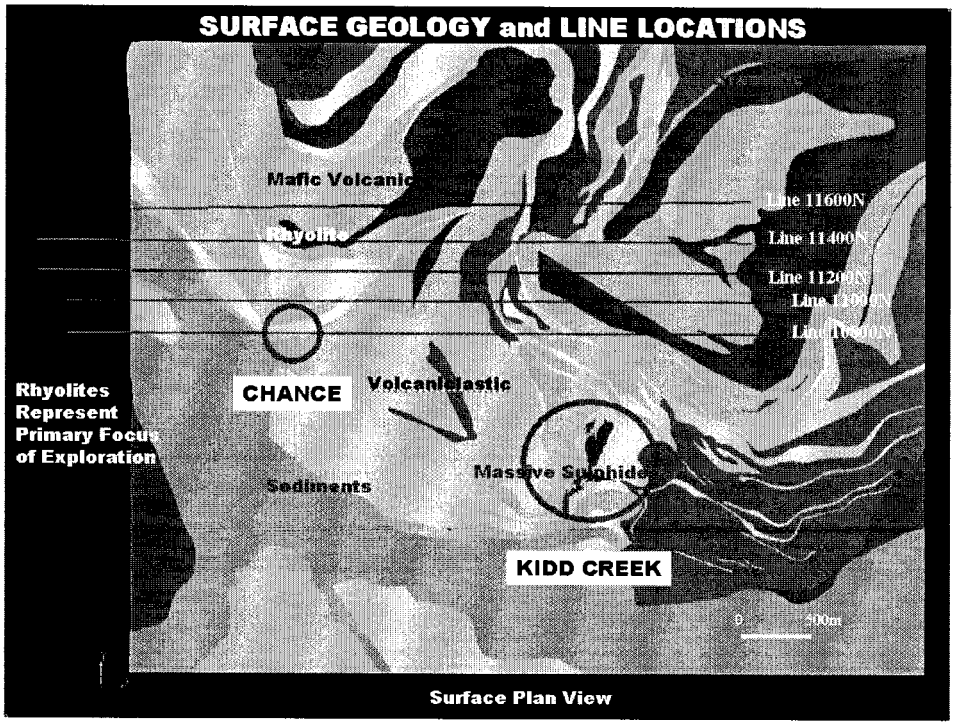

Figure 3.10: Gocad Model in Plan Showing Geology and Titan-24 Line Locations

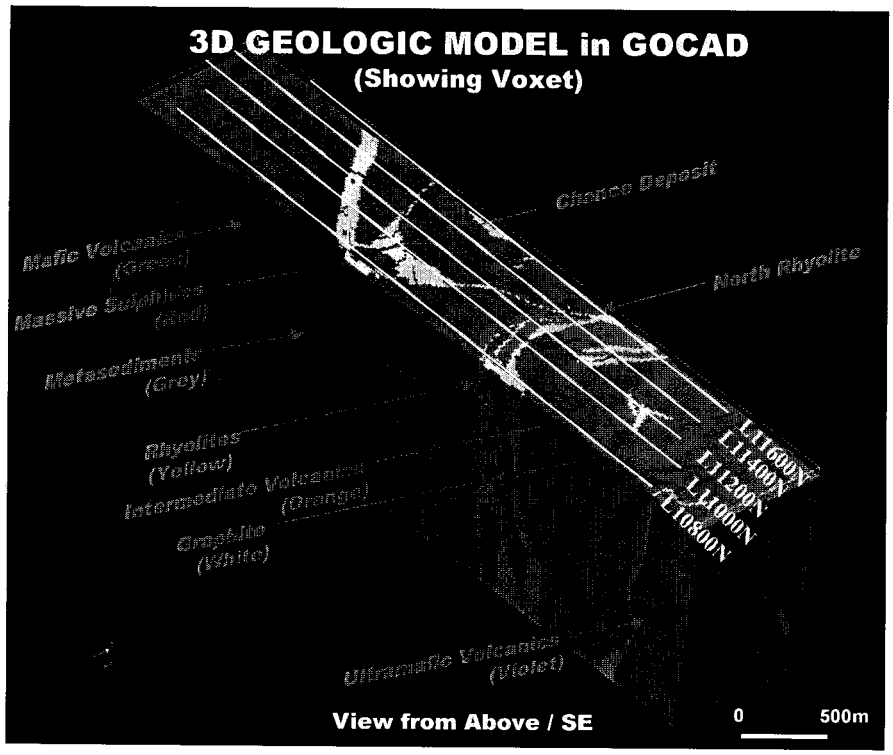

Figure 3.11: Gocad Model Showing 3D Voxet Containing Physical Properties.

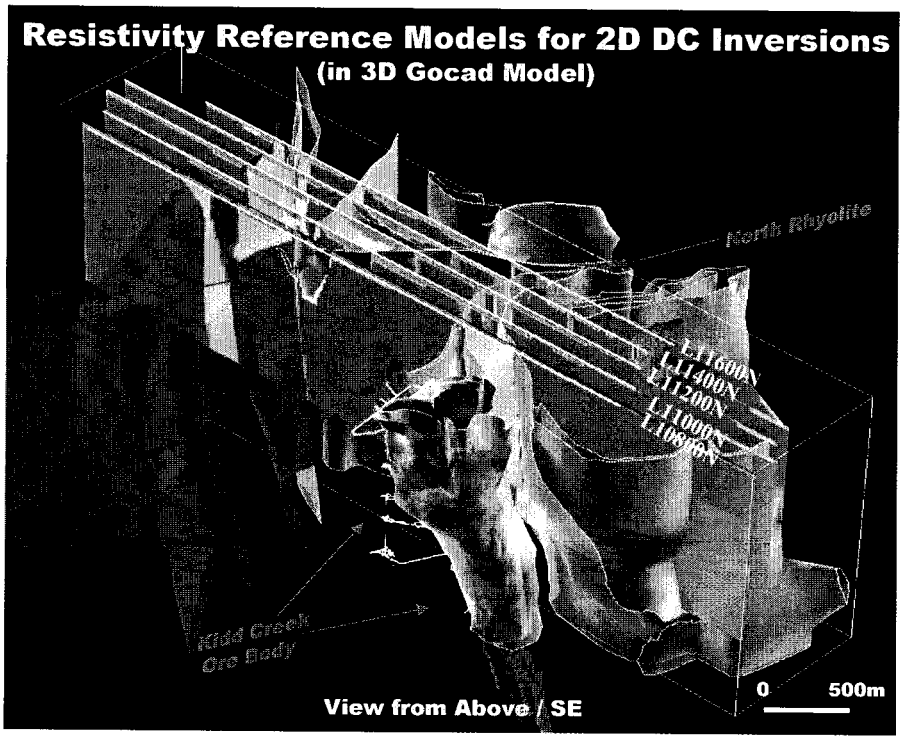

Figure 3.12: Gocad Model showing 2D DC Resistivity Reference Models.

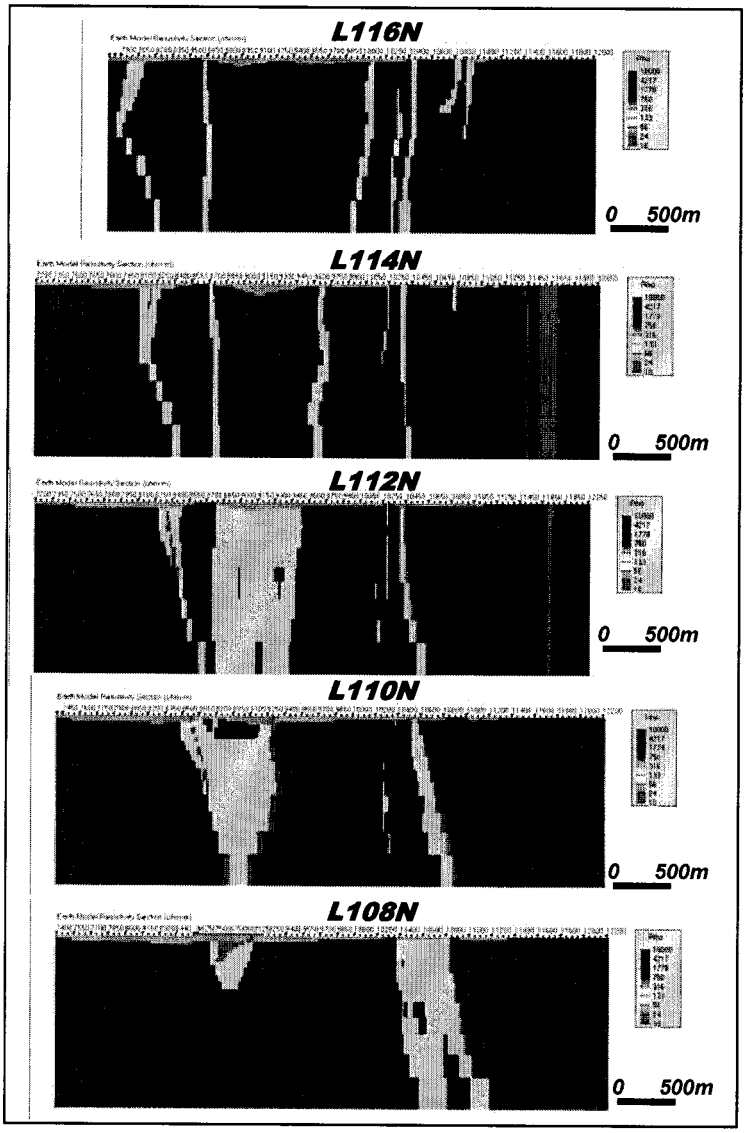

Figure 3.13: Gocad Resistivity Reference Models for Constrained 2D Inversions

3.3 Sensitivity Analysis using 2D Model Studies

Using the Gocad geologic model for Kidd Creek and the constraining physical properties used to populate the 3D voxet, 2D forward modeling studies were performed, as a sensitivity analysis, to determine the expected responses of Titan-24 DC Resistivity and Induced Polarization, as well as Magnetotelluric methods, for a realistic, world class exploration target. Furthermore, by progressively burying the target orebody, further showcases the depth of investigation characteristics of the Titan distributed acquisition system. In addition, 2D DCIP inversions were performed to simulate expected model responses for both unconstrained (non-geologically referenced) and constrained (Gocad-referenced) models. It is important to remember that while the majority of the original Kidd Creek orebody has been mined out and replaced with backfill, from surface to >2 km depths, it is still worthwhile to understand and recognize the kinds of responses which might be expected from potential virgin orebodies on-site, or elsewhere on the Kidd Creek property.

The Kidd Creek profile (L10300N), used in the following 2D models, was created using L10800N, the southernmost Center-pole array profile lying closest to the Kidd Creek deposit, as a template for the electrode layout. In order to place it approximately right-of-center of the existing Kidd Creek deposit in the Gocad model, the survey coordinates were translated by subtracting 500m to the L10800N Northing and adding 500m to its Easting, using a spreadsheet editor. A 2D DC inversion mesh was then created inside the UBC *Dcinv2d* platform and used as a template to create a cross-sectional S-grid in Gocad. After being populated with physical properties identical to those used to constrain the Titan-24 DCIP and MT survey 2D inversions, a 2D reference model was then output from Gocad, in both UBC and Geotools formats. These were later modified, as required using a text editor, to create additional reference models for sulphides buried at the 200m, 500m, 1km and 2km depths, as well as a non-sulphide bearing rhyolite. 2D DC and IP forward models were calculated for a 4.8km length (2-spread x 32

channel max) native center-pole array configuration (see Figure 1.3) and its superposed dipole-dipole array - equivalent to 100m a-spacing, n≈1-30 maximum separations, with 2x (a=50m) overlapping coverage (see Figure 3.15a). These forward model responses were then used as observed data for both unconstrained and constrained 2D inversions that follow.

3.3.1 2D DC Resistivity Modeling and Inversion

a) Depth = 0m / DC Model and Inversion

The model for the Kidd Creek deposit profile is shown in Figure 3.14, using the resistivity constraints presented in Table 3.4 below. This model is designed to simulate the theoretical Titan-24 DC response and resulting 2D inversions over Kidd Creek orebody, in its original state, before being mined out.

Table 3.4: Reference Resistivities for DC Models and Constrained Inversions

LITHOLOGY	RESISTIVITY	COLOUR
Mafic volcanic	10k ohm-m	Purple
Ultramafic volcanic	7k ohm-m	Navy-blue
Sediments	5k ohm-m	Blue
Rhyolite	1k ohm-m	Light blue
Overburden	30 ohm-m	Red
Graphite/Massive Sulphide	10 ohm-m	Pink

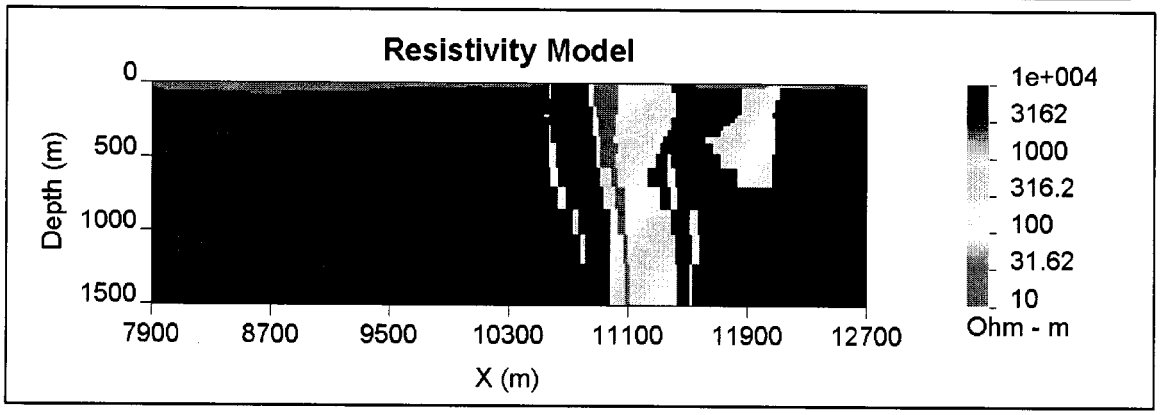

Figure 3.14: 2D DC Resistivity Reference Model for Kidd Creek from Gocad.

The 2D DC resistivity forward model in superposed dpdp array format and calculated from the Gocad reference model, using the UBC *Dcinv2d* (Oldenburg and Li, 1994) platform, are both shown in Figure 3.15. Notice the well-defined resistivity low at shallowest n-spacings, directly coincident with the up dip edge of Kidd Creek massive sulphides. The dipole-dipole pseudosection resistivity low, however, appears as a compound anomaly, suggesting 2 separate conductive bodies – a smaller, subcropping 10 ohm-m zone and another, larger 10 Ω-m feature which appears offset 200m West and buried at 200m depths (see Figure 3.15a). In fact, this is a 2D effect, resulting from the overprint of the high resistivity mafic volcanics in subvertical contact with moderate resistivity rhyolite host-rocks, immediately west of the Kidd Creek deposit.

Based on the asymmetric conductive anomaly, a moderate east dip suggested for the conductive horizon(s) agrees with the geologic model. As well, the dipole-dipole results also reflect the thickening of the conductive overburden blanket towards the west. However, none of the remaining litho-geologic features in the reference model appear to be resolved in the raw data. Similar features are also discernable, though less well resolved, in the analogous 2D forward model calculated for Center-pole array, shown in Figure 3.16ab – except that the buried (fictitious) anomaly, due to 2D overprint, appears deeper and further offset west. Clearly, therefore, a response of this type could have led to a largely incorrect interpretation of the true bedrock resistivity structure, based on a reliance of the raw data alone.

An unconstrained 2D inversion of 2D forward model results, in Center-pole array, for this Kidd Creek (depth = 0m) model is shown in Figure 3.16c. This inverse model was calculated using a relatively small alpha-s ($\alpha_S < 10^{-6}$) parameter in the UBC model norm function (see Section 2.3), which produces "smooth" resistivity images. All other parameters used were the default UBC parameters – in-

cluding a voltage error equal to 5% of the primary voltage that is assigned for the input forward model data[6].

Note that, owing to the high level of data quality expected from Titan surveys (i.e., average Vp error[7] at Kidd = <0.1%), no additional "noise" (such as the 5% Gaussian, commonly used for geologic noise) has been added to these synthetic model data. This differs from standard practice (M. Chouteau, pers. comm., 11/2004) but is justifiable in light of the very high Titan data quality.

The DC inversion results in Figure 3.16c shows a well defined conductive, subcropping feature corresponds well to the actual width, strength, depth of burial and dip-direction of the Kidd Creek deposit model. As well, the effect of the 2D overprint signature is noticeably absent. Moreover, in spite of the apparent pinching-out at 350m-depths for the conductive zone and the poorly resolved lateral resistivity structure, relating to geo-lithologic contacts, significant vertical extent for the orebody is indicated and the depth of investigation for the inversion appears to approach 500-700 metres across much of the profile. Furthermore, the inversion also appears to accurately map the overburden across the length of the profile.

Another unconstrained 2D inversion of the same 2D forward model results is presented in Figure 3.17, for Kidd Creek at surface, which represents another comparable "sharp" model inversion – one which emphasizes fitting the data over the model smoothness. This is simply achieved by using a large alpha-s parameter in the UBC model norm function (see Section 2.3). All other parameters were set to the UBC default values. The differences are dramatic. In contrast with the smooth model, the sharp model defines 2 separate anomalies: 1) a small (400 x 200m), shallow, moderate strength resistivity low which, in spite of gener-

---

[6] In the UBC DCinv2D code, the input data format requires both a normalized Vp voltage and a voltage error, in millivolts.

[7] Based on statistical analysis of all Titan DC data collected at Kidd Creek (7791 points), Avg Vp error = 0.09%.

ally corresponding to the width, dip-direction and depth of burial of the actual Kidd Creek deposit, is nonetheless clearly too short, vertically – barely extending to 250m depths; and 2) a large, moderate to weakly resistive anomaly, which remains open at depth, but which is also clearly 500m too far west of the actual Kidd Creek orebody. Indeed, the sharp model appears to be responding to the 2D overprint effects identified in the raw dipole-dipole and Center-pole results – including the false artefact. As well, the depth of investigation appears to be 300-400m – much less than the smooth model results. We conclude therefore that, for unconstrained inversions, the smooth model appears to best represent the resistivity structure, where size, strength, vertical continuity and depth of investigation are possibly better estimated than in the sharp unconstrained 2D models.

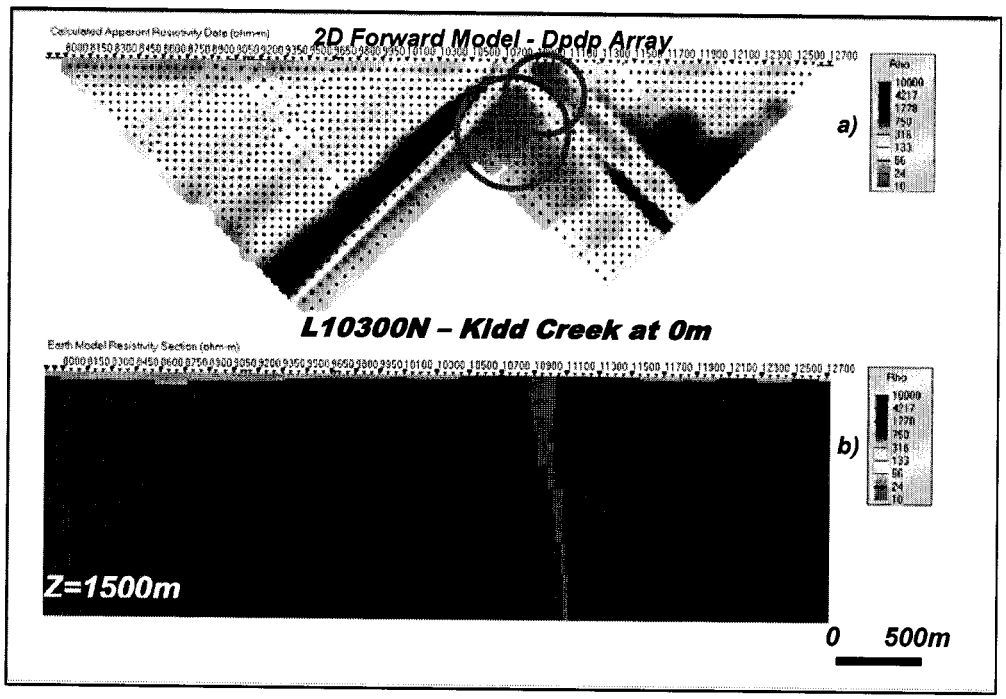

Figure 3.15: 2D DC Resistivity Forward Model, in Dpdp Array Format, for Kidd Creek at Surface (view looking north).

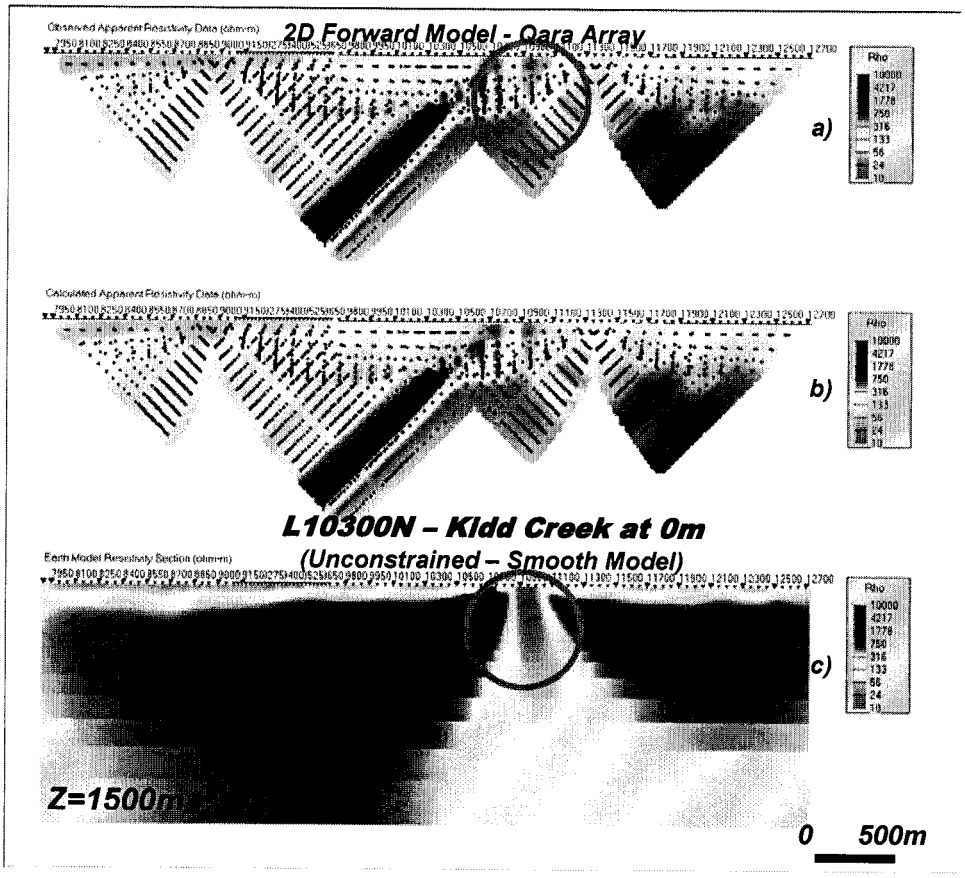

Figure 3.16: Smooth 2D Unconstrained DC Resistivity Inversion for Kidd Creek at Surface.

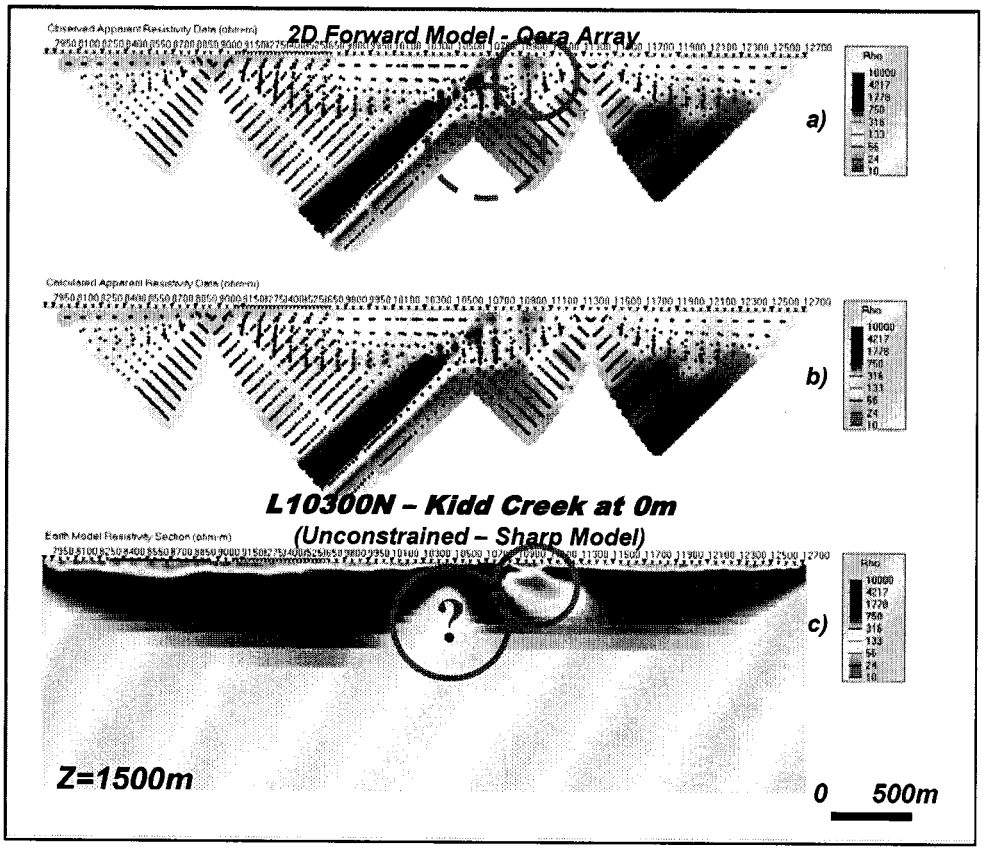

Figure 3.17: Sharp 2D Unconstrained DC Resistivity Inversion for Kidd Creek at Surface.

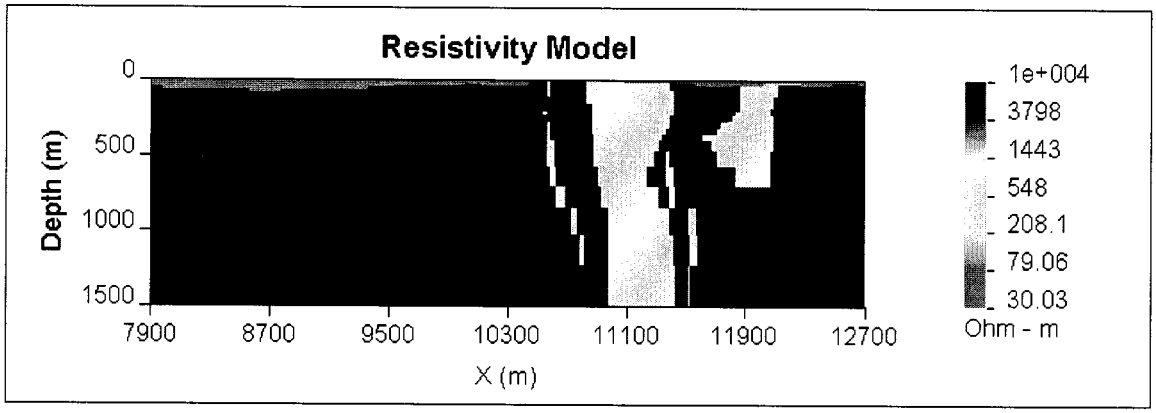

Figure 3.18: 2D DC Reference Model (Kidd Creek w/o Sulphides) for 2D Constrained Inversions.

In a final comparative imaging test over the Kidd Creek orebody, simulated in its original (depth = 0m) state, a constrained 2D inversion of 2D forward model results, in Center-pole array format, was performed using a non-sulphide bearing rhyolite reference model for the Kidd horizon -shown in Figure 3.18. The constrained 2D inversion, shown in Figure 3.19, used modeling parameters identical to the first inversion (smooth model norm) but has been weighted/guided by the geologic reference model and petrophysical constraints from Gocad. The 2D inversion returns a subcropping conductive body which corresponds well to the actual Kidd Creek orebody, in terms of depth of burial, vertical extent, dip angle, dip-direction, width at surface and position inside the rhyolite host rocks. However, in contrast, the zone is also clearly more weakly conductive (10-100 ohm-m), yet broadens at depth – possibly resolving the conductivity-thickness product, rather than the width and conductivity alone. The anomaly is also a complex one, featuring two conductive centers – a stronger yet smaller zone at surface, and another, larger, weaker body centered at 700m depths (see Figure 3.19c), which differs from the original model. Moreover, like Kidd Creek, the modeled conductive zone also appears to extend below 1.5km depth - however this is unexpected, given reasonable penetration limits of the Titan array DCIP surveys. Similarly, while most the litho-geologic features in the original reference model have been largely preserved in the constrained 2D inversion, the thinner rhyolitic units and basalts surrounding the main Kidd Creek horizon are somewhat more conductive, particularly at >500m depths – beyond its expected effective range.

Overall, therefore, the constrained inversion appears to benefit from improved lithologic mapping capability, depth of investigation, and better vertical and lateral resolution in comparison with the conductor's unconstrained inversion, particularly for the sharp model. On the other hand, the constrained inversion is incapable of restoring the original geometric constraints of the Kidd orebody, and while perhaps resolving its conductivity-thickness, its resistivity contrasts are much weaker than the unconstrained model. Moreover, it may also

exaggerate the depth-resolution capabilities of the DCIP technique. Nevertheless, these results highlight the fact that the constrained inversions have successfully outlined a region of increased conductivity, within the rhyolite, which is unexplained by the geologic model, and which therefore merits potential follow-up.

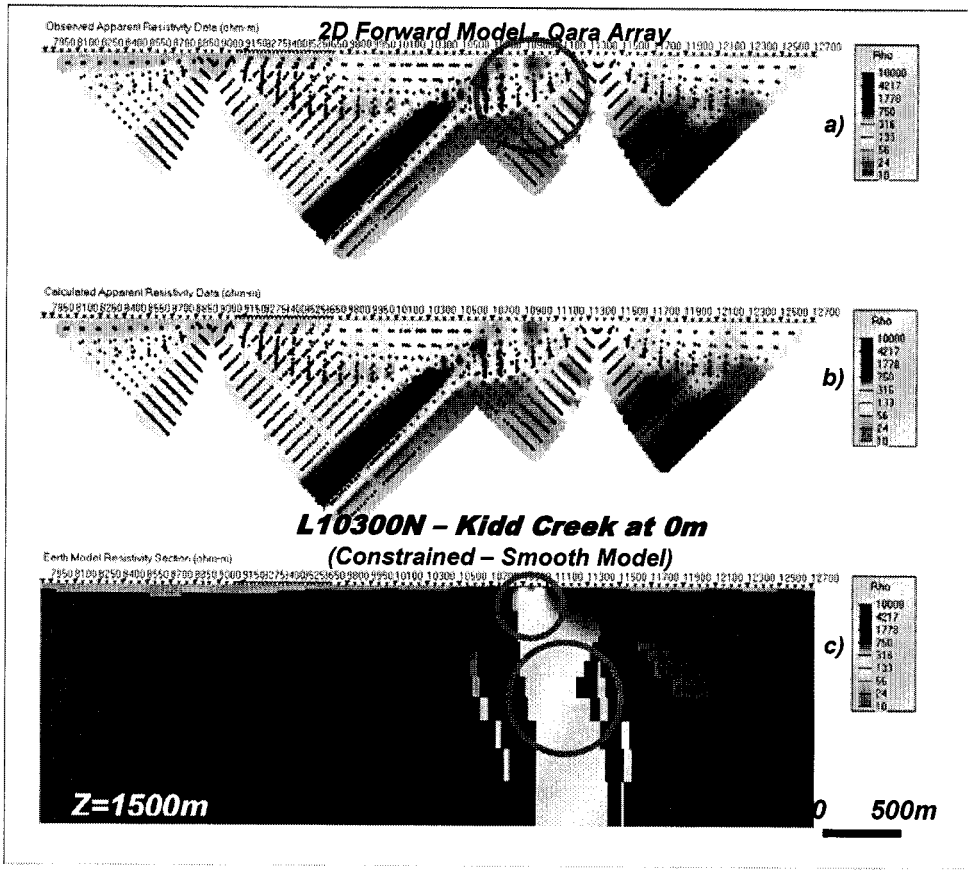

Figure 3.19: Smooth 2D Constrained DC Resistivity Inversion for Kidd Creek at Surface.

b) *Depth = 200m / DC Model and Inversion*

The 2ND model shown in Figure 3.20, using identical resistivity parameters as previous, has been altered to simulate the Kidd Creek deposit at 200m depths, by replacing the values for sulphides with those for rhyolite in the reference model.

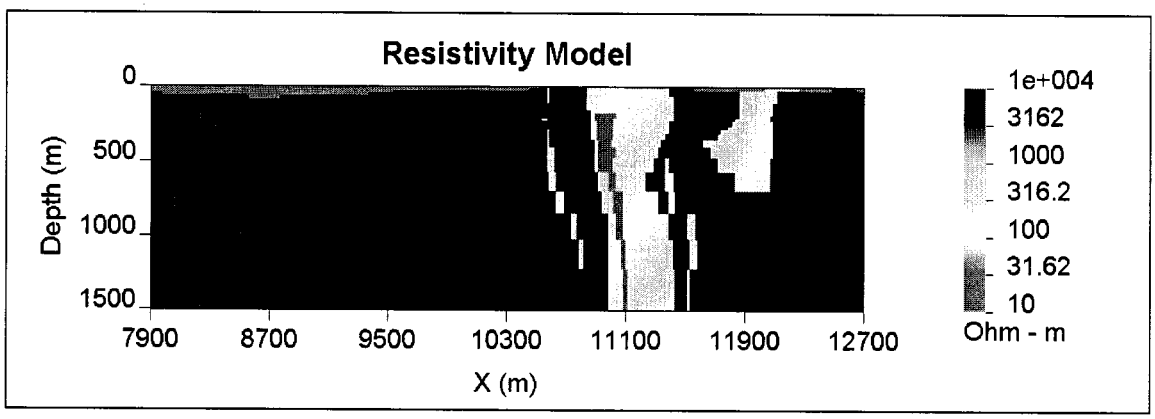

Figure 3.20: 2D DC Resistivity Reference Model for Following Inversions, with Kidd Creek at 200m.

The 2D DC forward solution for this reference model is presented in Figure 3.21a, in dpdp array format. In comparing the 200m depth response to the original (Figure 3.15a), the compound resistivity low anomaly is noticeably absent, the anomaly is deeper (>n=3-6), weaker (100 Ω-m vs 30 Ω-m) and more asymmetric (east dip), and offset 300m west of the known target. The shallow overprinting, V-shaped, high resistivity contact feature is also present in this model and is clearly causing this apparent visual offset. These characteristics are also shown in the Center-pole array forward model (Figure 3.22ab) – except that the low resistivity feature is better centered over the known target and also appears to be more deeply (>300m) buried. The conductive anomaly, associated with Kidd Creek at 200m, would therefore be easily recognized in the raw results – although possibly interpreted too far westward, using the dpdp results, or too deep, if relying on the Center-pole results, alone.

The unconstrained 2D DC inversion of the 200m depth forward data, shown in Figure 3.22c, identifies a weakly conductive target at depth which corresponds very well to the depth of burial and dip-direction of the Kidd Creek model provided. In particular, the inversion also correctly images the upper rhyolitic cap rock, in terms of thickness and resistivity (1k Ω-m), as well as providing indications of significant vertical extent (>1km). However, the anomaly strength is significantly weaker (100 Ω-m vs 10 Ω-m actual) and is also much wider – possibly reflecting the inversion's greater sensitivity to the conductivity-thickness product, as described previously. Nevertheless, the unconstrained resistivity anomaly is clear-cut – there is no doubt that the zone has been identified at depth.

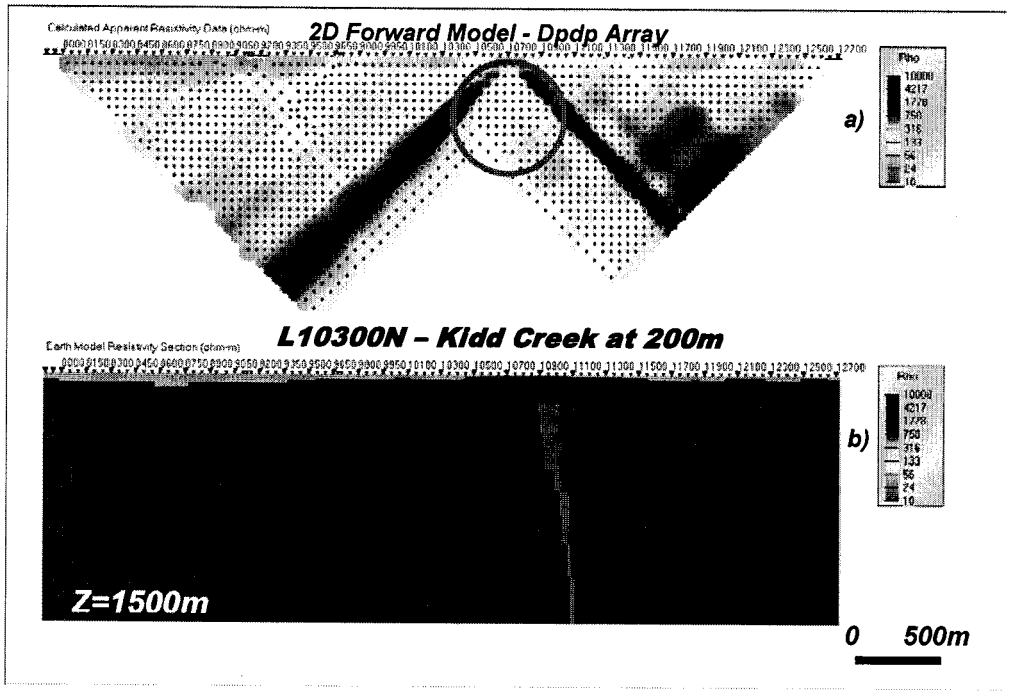

Figure 3.21: 2D DC Resistivity Forward Model, in Dpdp Array Format, for Kidd Creek at 200m Depth.

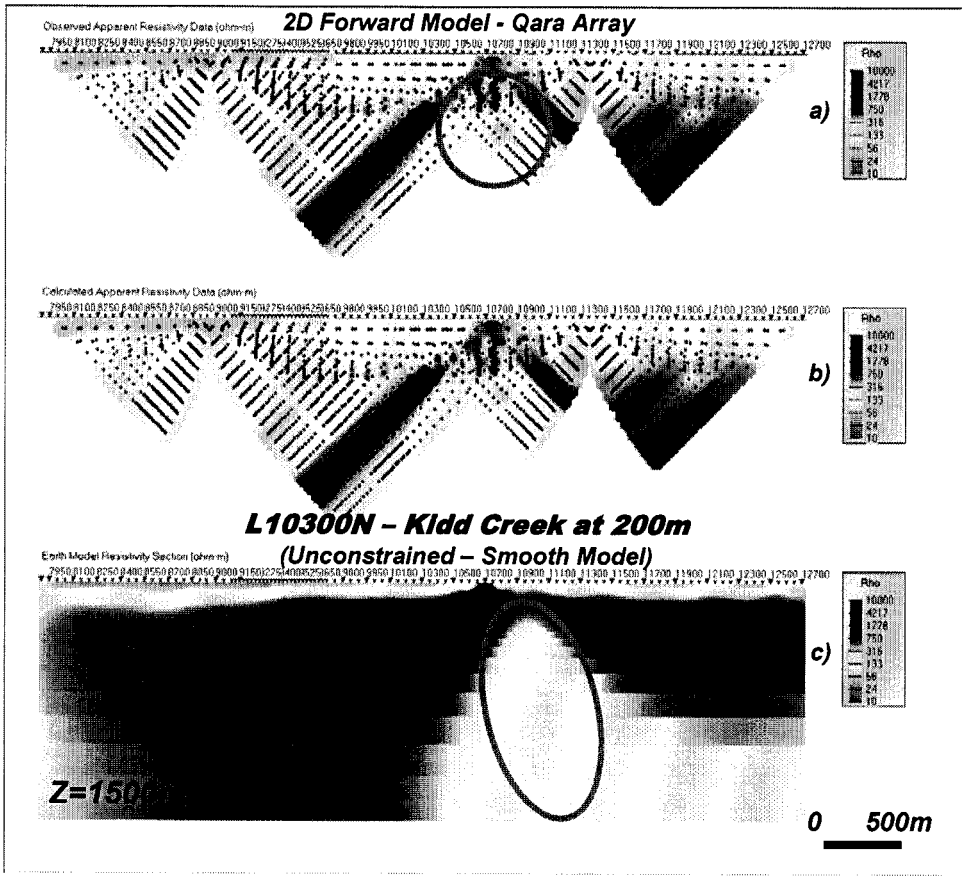

Figure 3.22: Smooth 2D Unconstrained DC Resistivity Inversion for Kidd Creek at 200m.

The constrained 2D inversion of the 2D forward results, shown in Figure 3.23, uses the same, non-mineralized reference model (Figure 3.18) and parameters that were tested earlier. The inverse solution clearly defines a weakly conductive target at depth which corresponds very well to the depth of burial, dip-direction and vertical depth-extent of the Kidd Creek model provided. In spite of the fact that, as with the unconstrained solution, the conductive anomaly is also much weaker and broader than expected, its position inside the rhyolite host rocks is well defined. Thus, the constrained inversion has successfully outlined a zone of increased conductivity, of significant size and buried at 200m depths within the rhyolite host. However, the anomaly is significantly weaker than the expected value for sulphides (~100 ohm-m vs 1 ohm-m) and is also more diffuse. This un-

derestimation of strength and relatively diffuse nature suggest that this target might be misconstrued as a lithologic feature –and as a result, possibly not targeted. In contrast, the unconstrained result seems to provide better resistivity contrasts is also somewhat sharper than the constrained inversion, as also suggested in the earlier modeling results. These inversion artefacts should therefore be properly considered when assessing buried features identified in constrained inversion results.

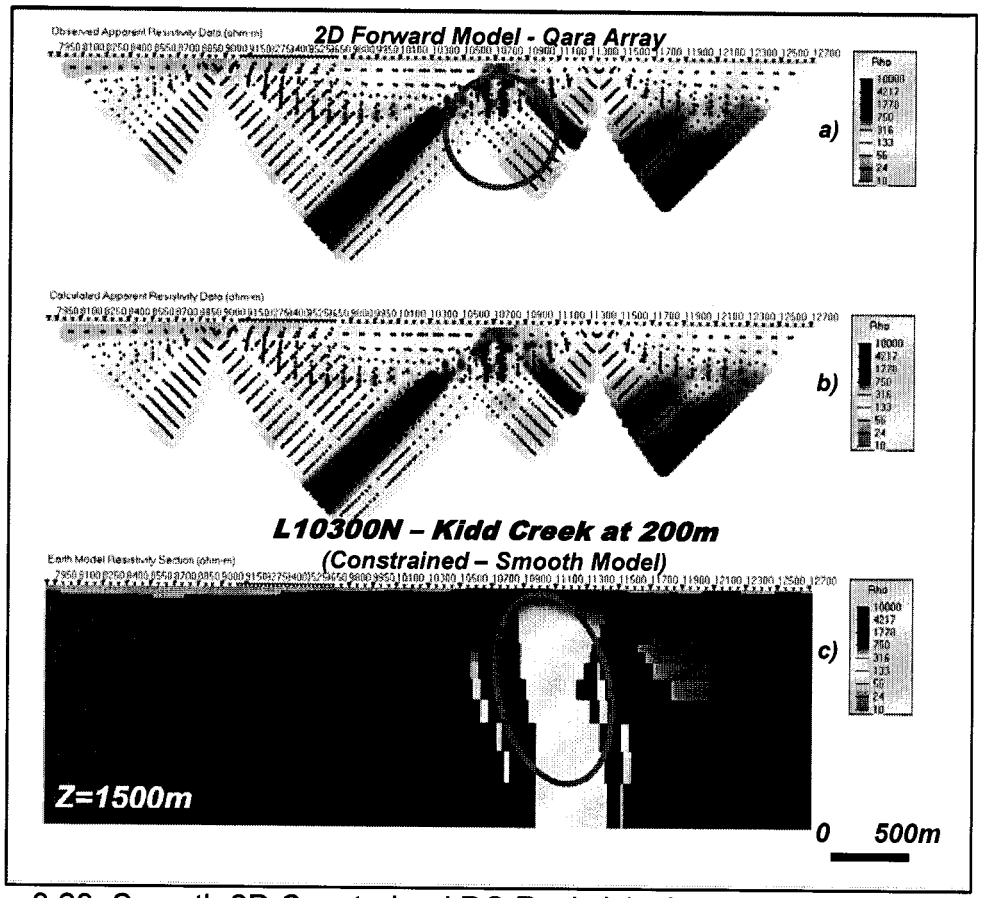

Figure 3.23: Smooth 2D Constrained DC Resistivity Inversion for Kidd Creek at 200m.

c) *Depth = 500m / DC Model and Inversion*

A 3RD model, shown in Figure 3.24, represents the Kidd Creek deposit which as been eroded to 500m depths below surface – again, by replacing mas-

sive sulphides for rhyolite in the reference model. The target is visibly small in relation to the geologic cross-section. In order to fairly test the Titan-24 DC system's ability to detect and resolve such deeply buried targets, the resistivity contrast has been increased, by setting the value for massive sulphide from 10 to 0.1 ohm-m. The 2D DC forward solution, in dpdp array format, for this reference model is presented in Figure 3.25. It is surprisingly similar to the 200m dpdp response (see Figure 3.21), suggesting at first glance that the 500m depth of burial poses no problem for detection in the Titan array DC data. However, upon closer examination, the uppermost anomaly in Figure 3.25a is clearly too shallow (top at n=3) and offset 300m west to represent the deep Kidd deposit.

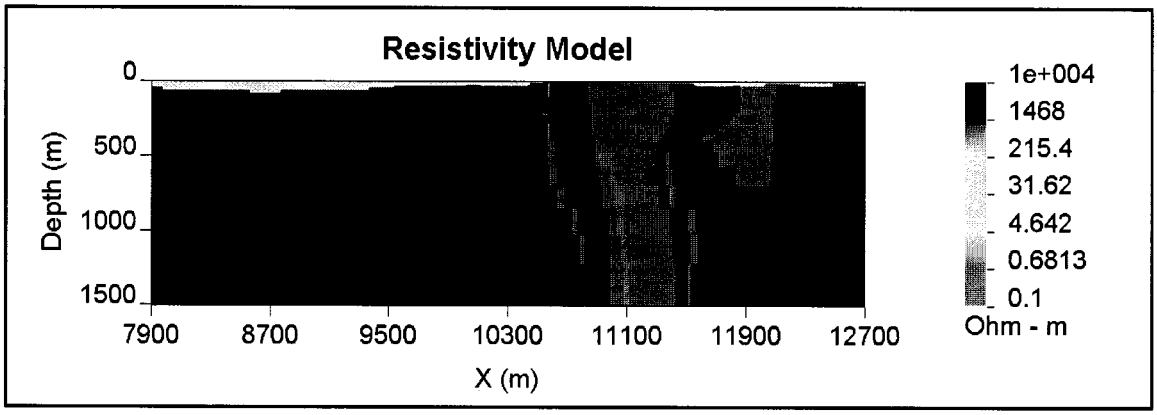

Figure 3.24: 2D DC Resistivity Reference Model for Following Inversions, with Kidd Creek at 500m.

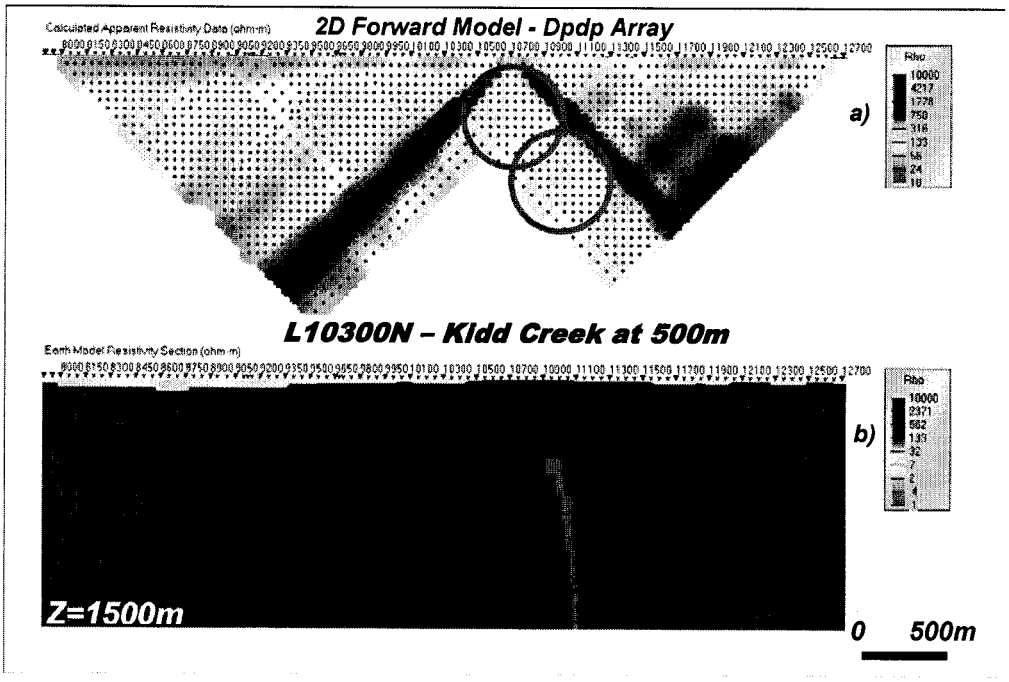

Figure 3.25: 2D DC Resistivity Forward Model, in Dpdp Array Format, for Kidd Creek 500m Depth.

To resolve this ambiguity, another forward model for the non-mineralized Kidd horizon is also shown in Figure 3.26, for comparison. From these results it is now clear that the response from the deep Kidd orebody is resolved as a weak (100 Ω-m) resistivity low, correctly centered over the target below n=10, as shown in Figure 3.25a. Moreover, the shallower dpdp response is, in fact, a false anomaly relating to the near-surface high resistivity contact, described previously. Of note, this ambiguity is not present in the Center-pole array pseudosection and a deep anomaly is more clearly resolved (see Figure 3.27a). It is likely, however, that reliance on the raw dpdp results alone could contribute to a misinterpretation, which might result in incorrectly targeting the proper anomaly.

The unconstrained 2D DC inversion of the 500m depth forward data, in Figure 3.27, identifies a weakly conductive target at depth, matching very well the position, depth of burial, dip-direction and vertical depth extent of the Kidd Creek model provided. Moreover, as with the previous 200m model, the unconstrained

inversion also correctly images the rhyolitic cap-rock above the deposit. However, the anomaly strength is considerably less (300 Ω-m vs. 0.1 Ω-m actual) and is also much wider – making it easily misconstrued as a formational-like conductive unit, of limited exploration interest. Nevertheless, any lack of certainty as to whether the unconstrained inversion is correctly imaging the massive sulphide or simply the rhyolite itself is proven by Figure 3.28, which presents the unconstrained 2D DC inversion for the Kidd horizon without massive sulphides. In this example, the rhyolite is correctly resolved as a weakly resistive (1k Ω-m) unit, without any conductive artefacts associated.

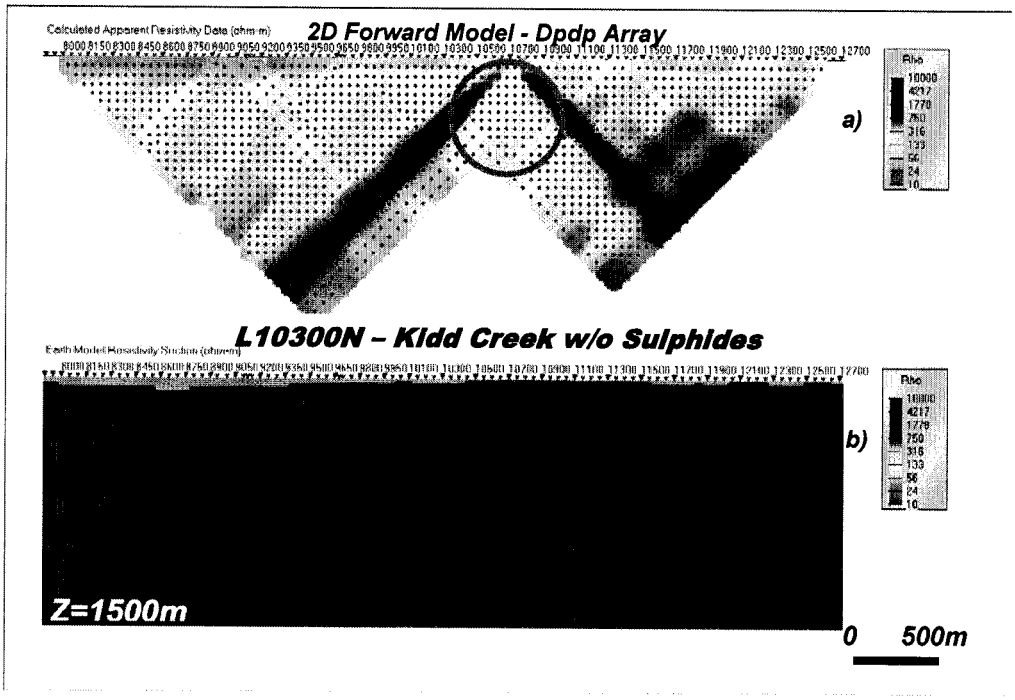

Figure 3.26: 2D DC Resistivity Forward Model for Kidd Creek without Massive Sulphides (DC reference for constrained inversions)

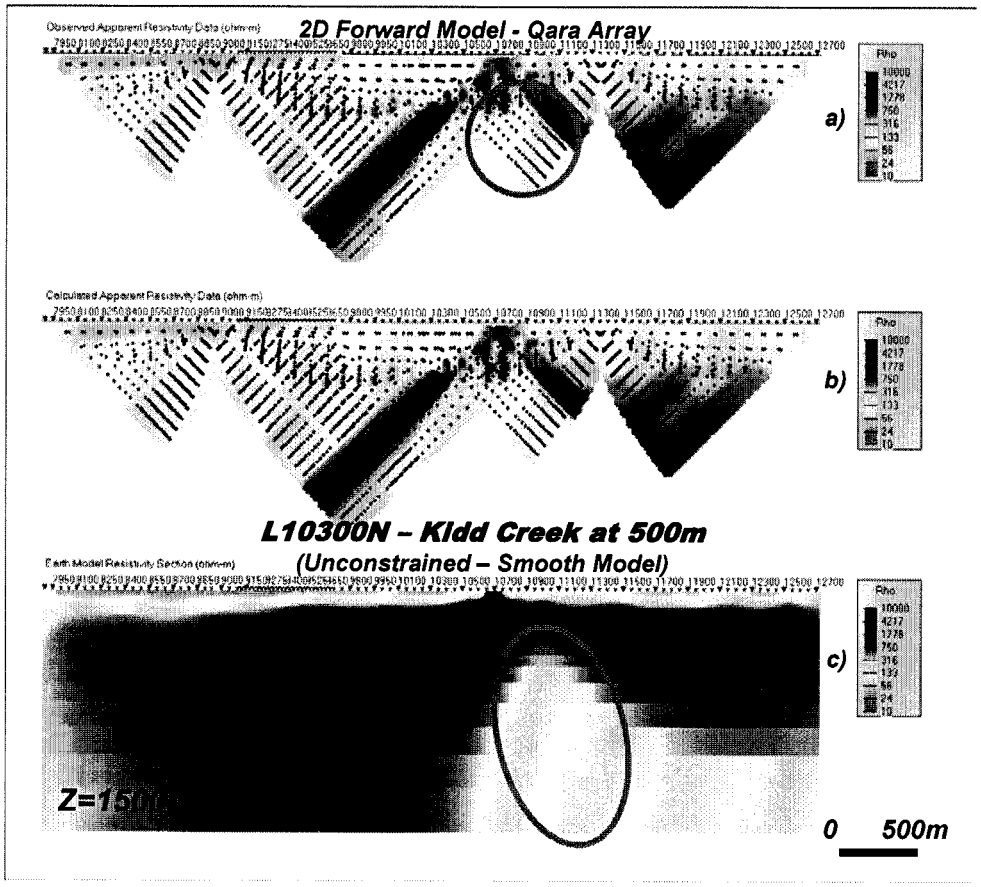

Figure 3.27: Smooth 2D Unconstrained DC Resistivity Inversion, for Kidd Creek at 500m.

We can therefore safely conclude that, providing there is a sufficiently high contrast between the host and massive sulphide, that a large tabular, steeply dipping and relatively narrow target, similar to Kidd Creek, can not only be detected at 500m depths using the Titan-24 arrays, but can also be resolved in unconstrained 2D inversions, even while using basic, default inversion parameters.

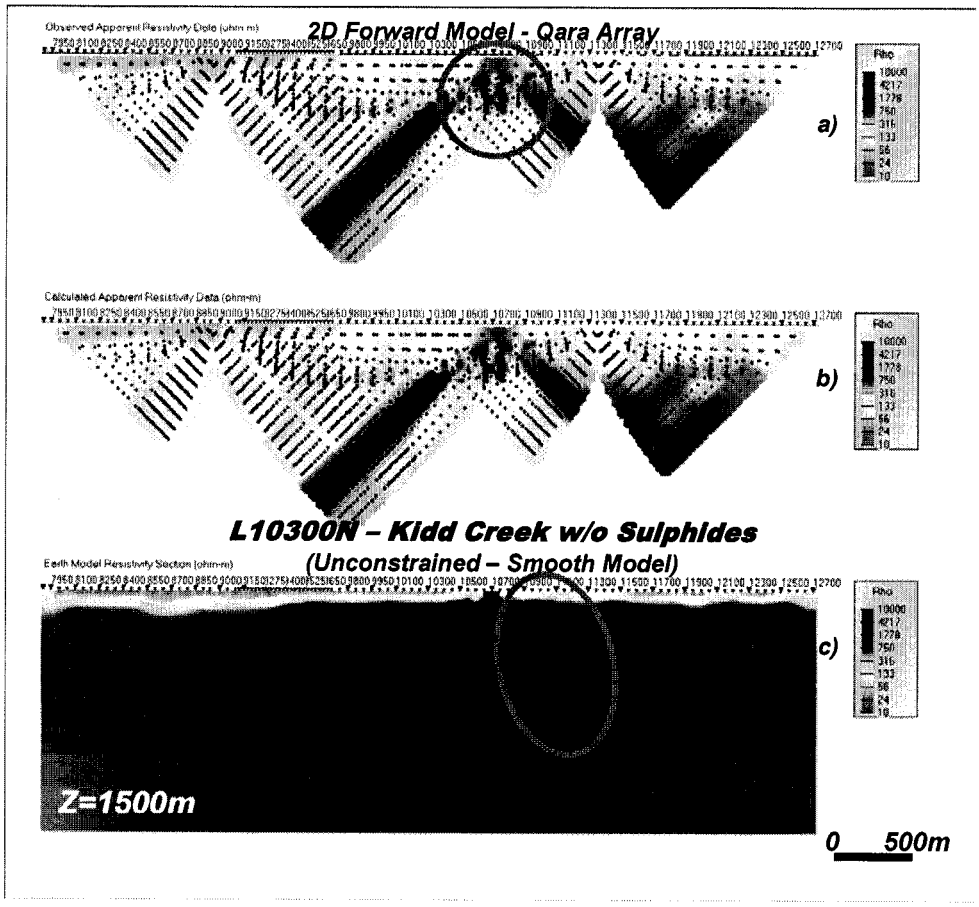

Figure 3.28: Smooth 2D Unconstrained DC Inversion for Kidd Creek without Massive Sulphides.

Figure 3.29 presents the constrained 2D inversion of the 2D forward results for a 500m deep target, using the non-mineralized reference model (Figure 3.18) used earlier. The inverse solution has defined a broad, diffuse, very weakly conductive anomaly at depth which corresponds roughly to the position of the intended Kidd Creek model. However, in contrast with the unconstrained solution, response is much less well defined. This suggests that the 500m depth represents a possible threshold of the depth-resolution limit for the constrained inversion, i.e., that below this depths, the constrained inversion might not image the Kidd Creek. The unconstrained inversion, therefore, appears to provide better depth of resolution than the constrained model, as similarly indicated in the earlier, 200m model inversions.

A final constrained inversion model for the 500m deep orebody is shown in Figure 3.30, which differs from the previous by using a reference model with Kidd Creek at the surface (rather than the barren sulphide model), i.e., using the model from example 1 (see Figure 3.14) as the geologic constraint. All inversion parameters were held the same as in the previous models. The inverse solution appears to have correctly compensated for the incorrect starting model by replacing the conductive (0.1 ohm-m) sulphides, found in the reference, with resistive (100-1k Ω-m) material, within the first 500m, while maintaining lower resistivities at depth – albeit more weakly conductive than predicted. We conclude therefore that in the event where the reference model clearly does not fit the data – either through an incorrect geologic model or incorrect physical property assignment – that the constrained inversion can be still relied upon to compensate for this and return a reasonably accurate model based on information contained in the measured results, i.e., we can afford to start with an improper reference model.

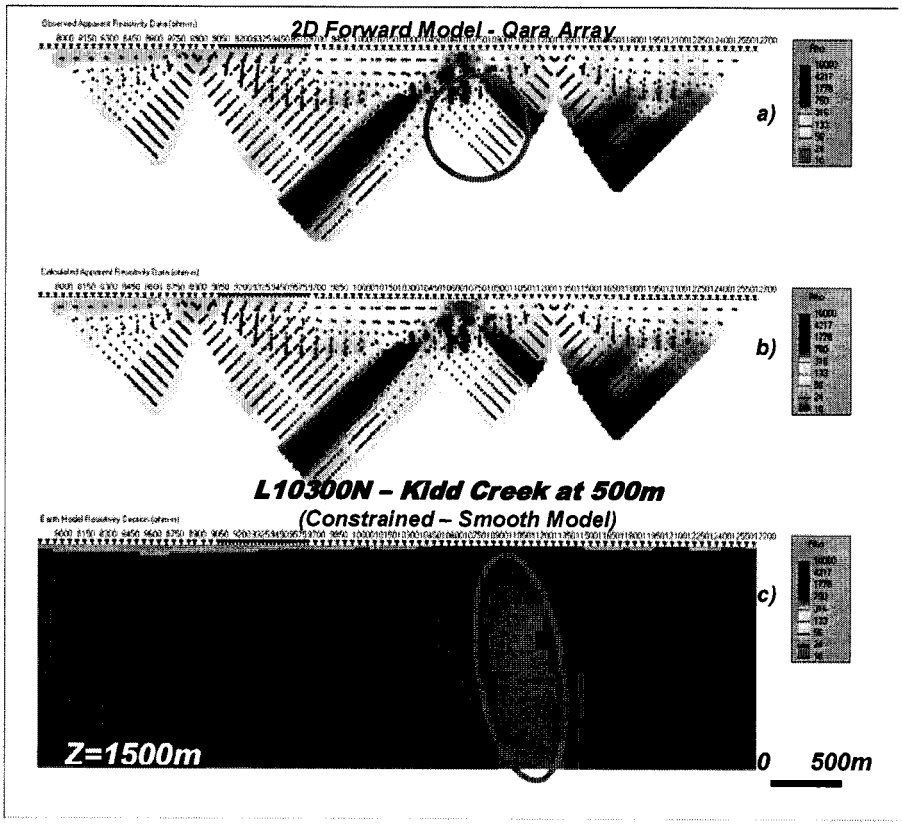

Figure 3.29: Smooth 2D Constrained DC Resistivity Inversion for Kidd Creek at 500m.

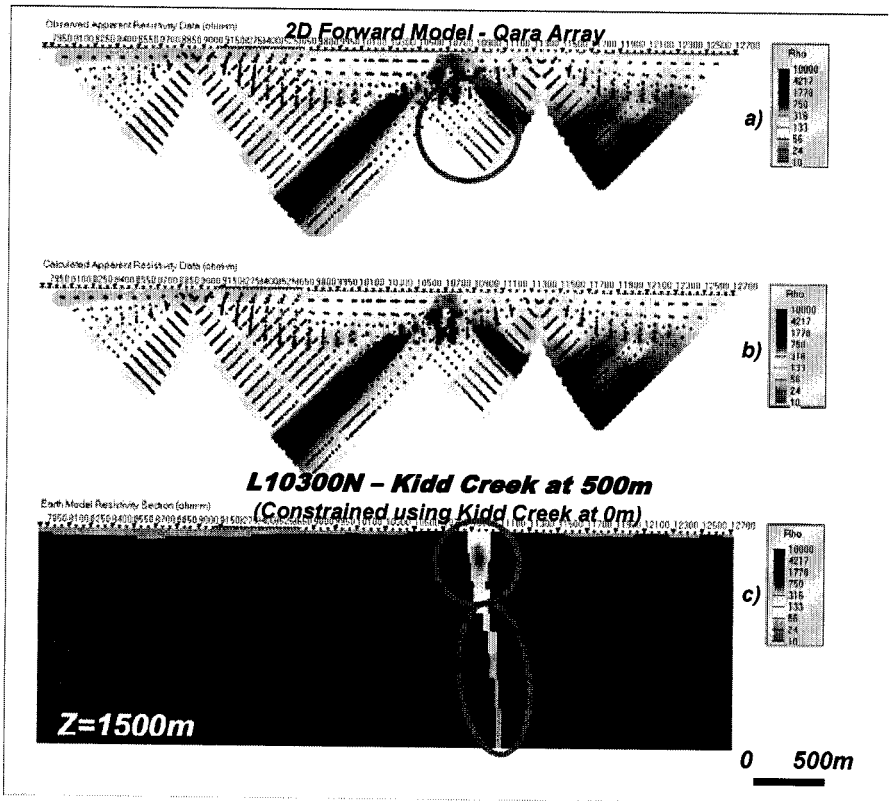

Figure 3.30: Smooth 2D Constrained DC Resistivity Inversion, for Target at 500m, Referenced using Model for Kidd Creek at Surface (see Figure 3.14).

d) *Depth = 750m / DC Model and Inversion*

The fourth model (Figure 3.31b) represents the Kidd Creek deposit which has been further eroded or buried to 750m depths below surface. This was achieved by replacing the upper 750m of conductive (0.1 Ω-m) massive sulphides with moderately resistive (1k Ω-m) rhyolite in the 2D forward model, as per the previous cases. The target is visibly small in relation to the geologic cross-section. The 2D DC forward solution, in dpdp array format, for this reference model, is presented in Figure 3.31a. As shown previously, in the 200m and 500m dpdp responses (see Figure 3.21 & Figure 3.25), the shallower, uppermost anomaly (dashed red circle) is clearly too shallow (top at n=3) and offset 300m west to represent the deep Kidd deposit, and represents an artefact relating to a 2D contact response – potentially leading to misinterpretation if relying on the

raw data alone. The deeper anomaly (solid red circle), appearing at n≈12, is similar in intensity (100 Ω-m), but noticeably smaller and poorly defined than the previous 500m model dpdp result – it is nonetheless correctly centred and at an appropriate depth over the target. It is clear, however, that due to its approaching similarity to the barren sulphide model (Figure 3.26) that the anomaly at 750m is rapidly becoming irresolvable in the raw data.

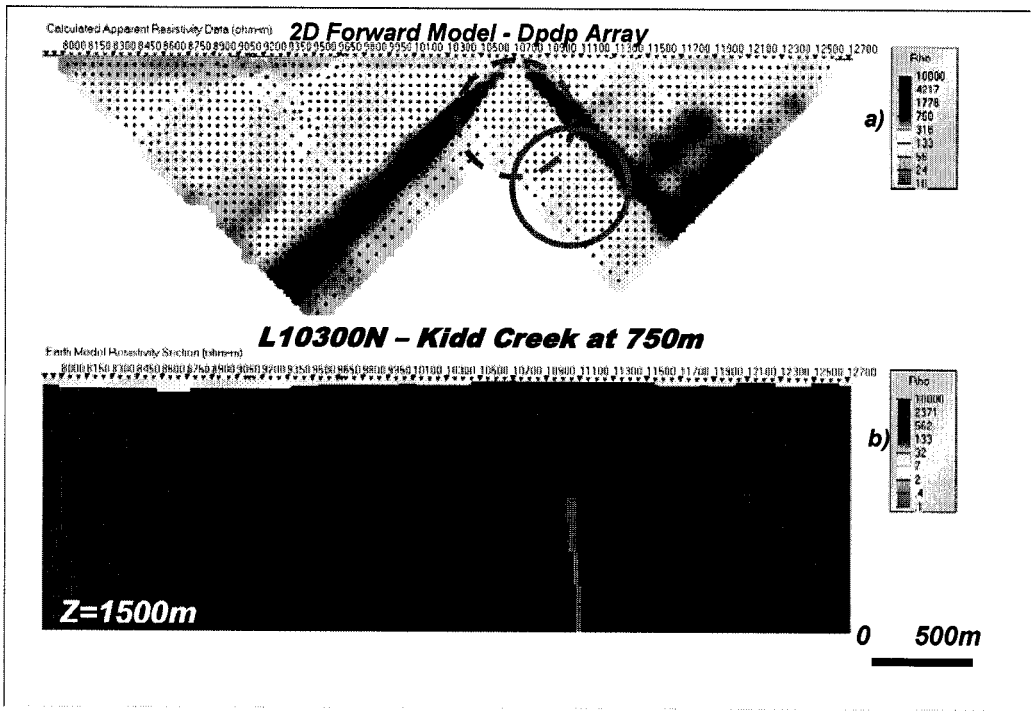

Figure 3.31: 2D DC Resistivity Forward Model, in Dpdp Array Format, for Kidd Creek at 750m Depth

The unconstrained and constrained 2D DC inversions of the 750m depth forward model data are shown in Figure 3.32 and Figure 3.33, below. The unconstrained inversion is remarkably similar to the previous 500m model result, and also correctly defines a weakly conductive target at greater depth. In fact, its depth of burial and dip-direction correspond well to the predicted Kidd Creek model. In particular, the inversion also correctly images the upper rhyolitic cap rock and surrounding mafic volcanics, as well as providing indications of significant vertical extent (>1km) to the conductor. However, although equivalent in

strength to the 500m response, the target resistivity is still significantly weaker (100 Ω-m vs. 10 Ω-m actual) and is also much wider than in the forward model reference – possibly reflecting the sensitivity to conductivity-thickness, described previously. Nevertheless, as with the 200m and 500m data, the unconstrained resistivity anomaly is clearcut – there is no doubt that the zone has been identified at depth. In marked contrast, the 2D inversion result in Figure 3.33c indicates that, with the exception of a slight, diffuse resistivity low decrease within the rhyolite host, there is virtually no resolvable anomaly detected in the constrained 2D inversions from the 750m forward modeling results.

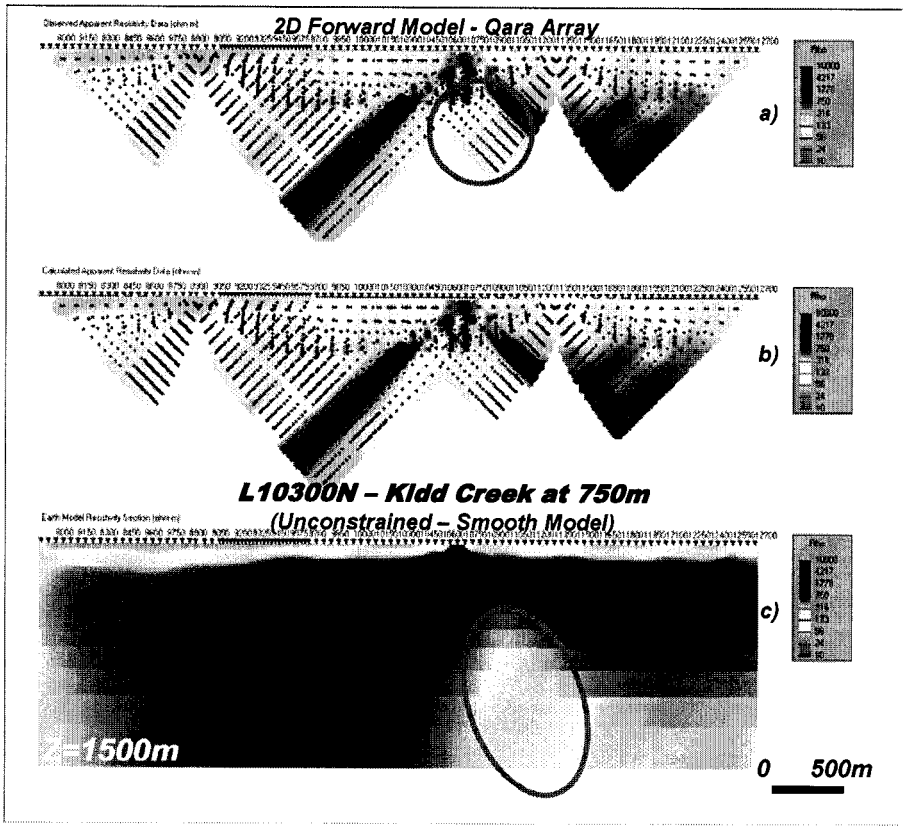

Figure 3.32: Smooth 2D Unconstrained DC Resistivity Inversion for Kidd Creek at 750m

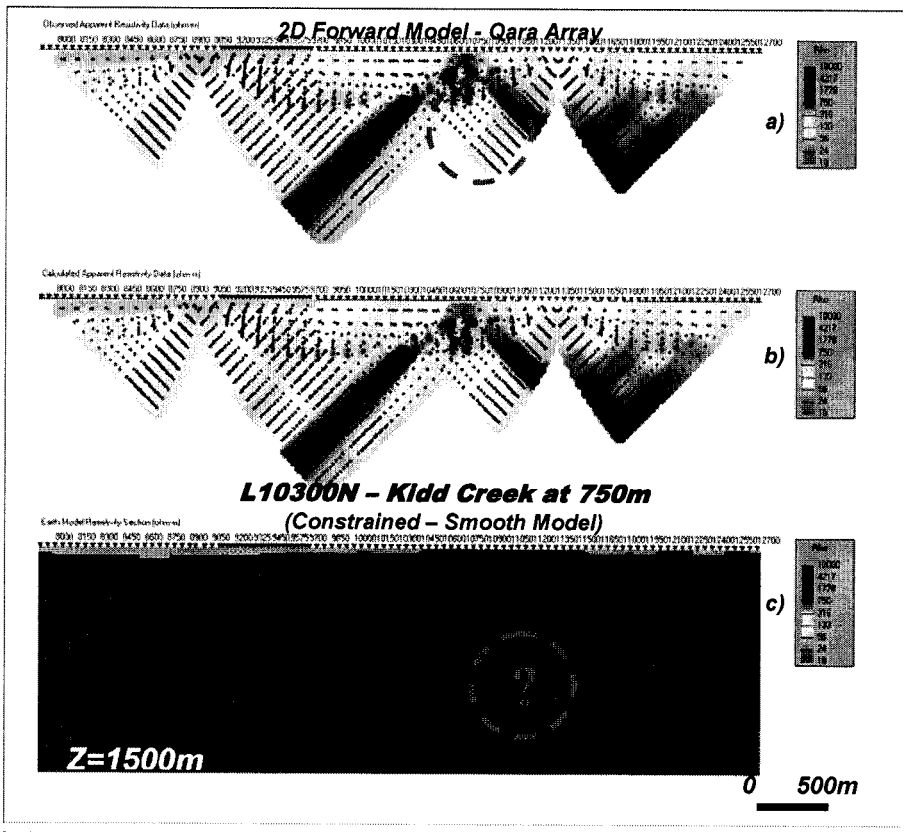

Figure 3.33: Smooth 2D Constrained DC Resistivity Inversion for Kidd Creek at 750m

e) *Depth = 1000m / DC Model and Inversion*

In order to confirm the depth investigation and resolution capability of the Titan DC resistivity surveys, 2D inversions were performed on a final 2D forward model, featuring Kidd Creek at 1km depths. As shown in Figure 3.34a (by the red dashed circle), the raw Center-pole array survey results are now virtually indistinguishable from the non-sulphide model results (Figure 3.28ac) – similarly (not shown) for the dipole-dipole array data. Furthermore, the unconstrained inversion of the 2D forward modeling results, in Figure 3.34bc, show that the deep anomaly (dashed red circle), is noticeably weaker in intensity (≈300 Ω-m) than in the previous 750m inversion, and is also more diffuse and poorly defined. These results suggests that, in spite of being detectible in the Titan 2D unconstrained inversions, at 1km, it would likely be irresolvable in the presence of geologic

noise. Finally, an analogous constrained 2D inversion failed and, as a result, is not shown – apparently because it was incapable of discerning measurable differences between the 2D forward and reference models.

We conclude that providing there is a sufficiently high contrast that, at 750m depths, an orebody similar to Kidd Creek, in spite of being poorly resolved/detected in the raw Titan-24 results, can nonetheless be successfully imaged in unconstrained 2D inversions, using default parameters. At 1km, however, in spite of being detected in the unconstrained inversions, it is unlikely that resistivity lows associated with Kidd Creek-like orebodies are resolvable using the present inversion algorithms. On the other hand, the absence of a resolvable anomaly in the constrained inversions confirms the earlier predictions: a) that the 500m depth represents the probable threshold of the depth-resolution limit for the constrained inversion, using the current algorithm, given the fact that the constrained inversion does not image a Kidd Creek-like orebody at 750m or 1km, and b) that, in spite of the constrained inversions better lateral resolution, the unconstrained inversion, nonetheless, appears to provide better depth of resolution/penetration than the constrained inversions, as similarly indicated in the earlier, 200m and 500m model inversions.

These conclusions regarding the depth of investigation of the Titan DCIP array differ significantly from generally accepted values, which are much less. For example, for dipole-dipole array, the penetration depth can be represented by the following formula (M. Chouteau, pers. comm., 11/2004), based on the work of Roy and Apparao (1971):

$$P \approx 0.19L(metres)$$

Where, P is the depth of penetration and is a direct function of L the largest receiver-transmitter separation. Hence, for the L = 3200m DCIP array size used at Kidd, the penetration P < 600m, which is 20% less than the 750m figure which has been approximately arrived at in this study.

However, although possibly widely accepted, the P=0.19L penetration factor is not rigorous, since it does not account for other, important factors such as a) size or geometry of target, b) physical property contrasts between host rock and target, c) the n-dimensionality or model complexity, d) the sampling density of the array, e) the data errors, and f) the inversion algorithm, as well as its related model-parameters. Clearly, the depth of penetration for a particular array can certainly be smaller than this P=0.19L figure, or possibly even larger.

Instead, the approach that we have adopted is similar to the method described by Oldenburg and Li (1999) and also White et al. (2003) who use 2D and 3D inversions to quantitatively determine the depth of penetration. In their paper Oldenburg and Li (1999) assert that inversions can provide first-order estimate of a depth region below which the earth structure is no longer constrained by the data, which in turn prevents over interpretation of the inversion results. In one of their examples, using their depth of investigation index (DOI), they determine that the depth resolution for dipole-dipole array varied between 0.125L and 0.38L. Note that this is 2X greater than the P=0.19L estimate – immediately putting it into question.

In the model-sensitivity examples presented here, in all cases, when compared directly against the "barren" Kidd Creek model, the DC resistivity inversions reveal a >10x magnitude anomaly above background. As a result, our model studies appear to satisfy the criteria set out by Oldenburg and Li (1999). It appears therefore that the expected benefits in penetration that were inherent in the design of the Titan DAS system, in terms of i) high data quality, ii) large data redundancy, iii) high resolution spatial oversampling and iv) large scale, distributed arrays are also supported in the results of the present inversion sensitivity analyses. Therefore, based on a Kidd Creek style target that is 2-dimensional in nature, the 750m penetration depth limit for the unconstrained DC results and 500m depth limit for the constrained inversion results are justifiable. Logically, we should also expect them to increase or decrease depending on the environ-

ment or array geometry used. Hence the utility of 2D and 3D sensitivity analyses, such as those performed here, over more misleading rule-of-thumbs.

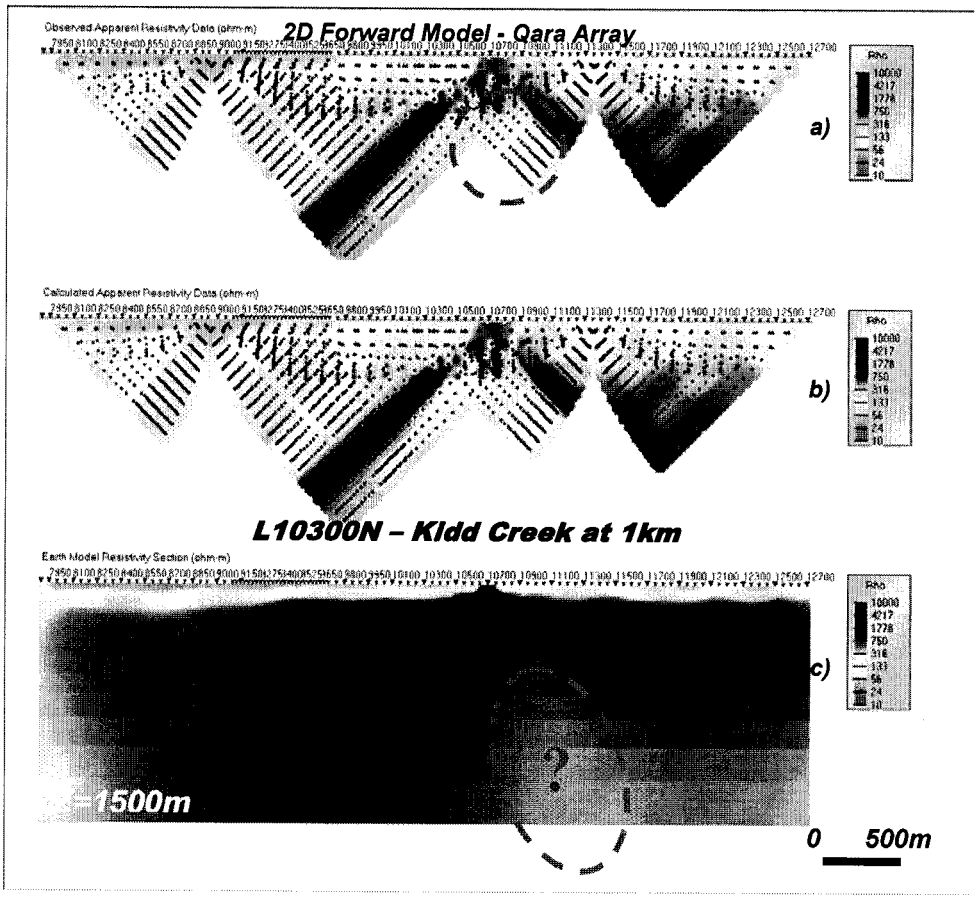

Figure 3.34: Smooth 2D Unconstrained DC Resistivity Inversion for Kidd Creek at 1000 m

3.3.2 IP Chargeability Models and Inversion

a) *Depth = 0m / IP Model and Inversion*

The model for the Kidd Creek deposit profile is shown in Figure 3.35, using the chargeability constraints presented in Table 3.5 below. This model is designed to simulate the theoretical Titan-24 IP response and resulting 2D inversions over Kidd Creek orebody, in its original state, before being mined out.

Table 3.5: Reference Chargeabilities for IP Models and Constrained Inversions

LITHOLOGY	RESISTIVITY	COLOUR
Overburden	0.5 mrad	Violet
Ultramafic volcanic	3 mrad	Dark Blue
Mafic volcanic	5 mrad	Navy
Sediments	10 mrad	Royal Blue
Rhyolite	20 mrad	Light Blue
Graphite/Massive Sulphide	75 mrad	Pink

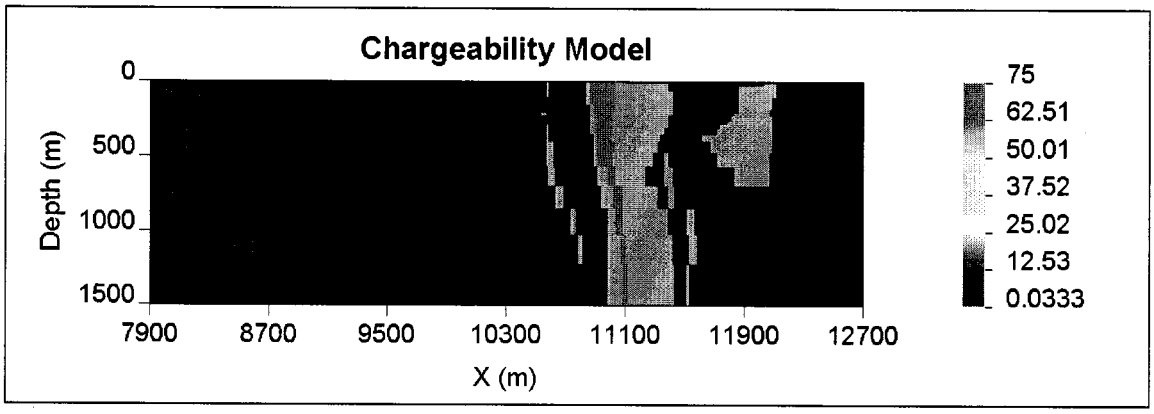

Figure 3.35: 2D Chargeability Reference Model for Kidd Creek at Surface.

The 2D IP chargeability forward model in superposed dpdp array format and calculated from the Gocad reference model, using the UBC *IPinv2d* platform (Oldenburg and Li, 1994), are both shown in Figure 3.36. Note that the 2D forward model chargeabilities have been scaled by a factor of 100x, to satisfy the UBC DCIPf2d forward modeling algorithm – these were later re-scaled for the subsequent inversions. A well defined, strong chargeability high is observed at the shallowest n-spacings, directly coincident with the up dip edge of Kidd Creek massive sulphide. Unlike the apparent resistivity forward modeling results, overprint anomalies are absent in the IP pseudosections results and the anomaly correctly characterizes a subcropping, wide-body (150-200m), depth-extensive, tabular and highly polarizeable body. In contrast, unlike the apparent resistivity

pseudosection, indications of dip are not obvious in the dpdp IP data. The analogous Center-pole array chargeability response is shown in Figure 3.37a, but is much less interpretable. Although a subcropping body is indicated and is centred on the predicted orebody, the chargeability high is weaker than expected, is broader at depth and its apparent dip direction is unexpected. Clearly, the interpretation of the Center-pole array data is reliant on 2D inversion.

An unconstrained 2D inversion of 2D forward model results, in Center-pole array, for this Kidd Creek (depth = 0m) model is shown in Figure 3.37bc. This inverse model was calculated using a relatively large alpha-s parameter (α_S = 0.001) in the UBC model norm function (see Section 2.3), which produces "sharp" resistivity images that emphasize high resolution over model smoothness. All other parameters used were the default UBC parameters, including a phase error equal to 0.5mrad that has been assigned for the input forward model data[8].

Note that, owing to the high level of data quality expected from Titan surveys (i.e., average IP error[9] at Kidd $\approx$ 0.1mrad), no additional "noise" (such as the 5% Gaussian, commonly used) has been added to these synthetic model data. This differs from standard practice (M. Chouteau, pers. comm., 11/2004) but is justifiable in light of the very high Titan data quality.

The IP inversion results in Figure 3.37c show a well defined, subcropping chargeability high feature, which corresponds well to the actual width, strength, depth of burial and dip-direction of the Kidd Creek deposit model. As well, the effect of 2D overprint signatures is not obvious – except for a small, unexplained "ghost" anomaly (dashed red circle), immediately east of the main IP anomaly. Moreover, in spite of the poorly resolved lateral chargeability structure, likely due to

---

[8] In the UBC IPinv2D code, the input data format requires both a chargeability value and a chargeability error, in the same units.

[9] Based on statistical analysis of all Titan IP data collected at Kidd Creek (7791 points), for data values having a maximum of 3 milliradians or less (includes7688/7791 pts = 99% of all Pz data) the Avg Pz error = 0.12 milliradians

poor model contrasts, adding little to potential mapping geo-lithologic contacts, significant vertical extent for the orebody is indicated (600m) – more so than in the analogous resistivity model. The depth of investigation for the IP inversion is unclear from the model, and furthermore, it appears that the inversion is not properly mapping the overburden across the length of the profile.

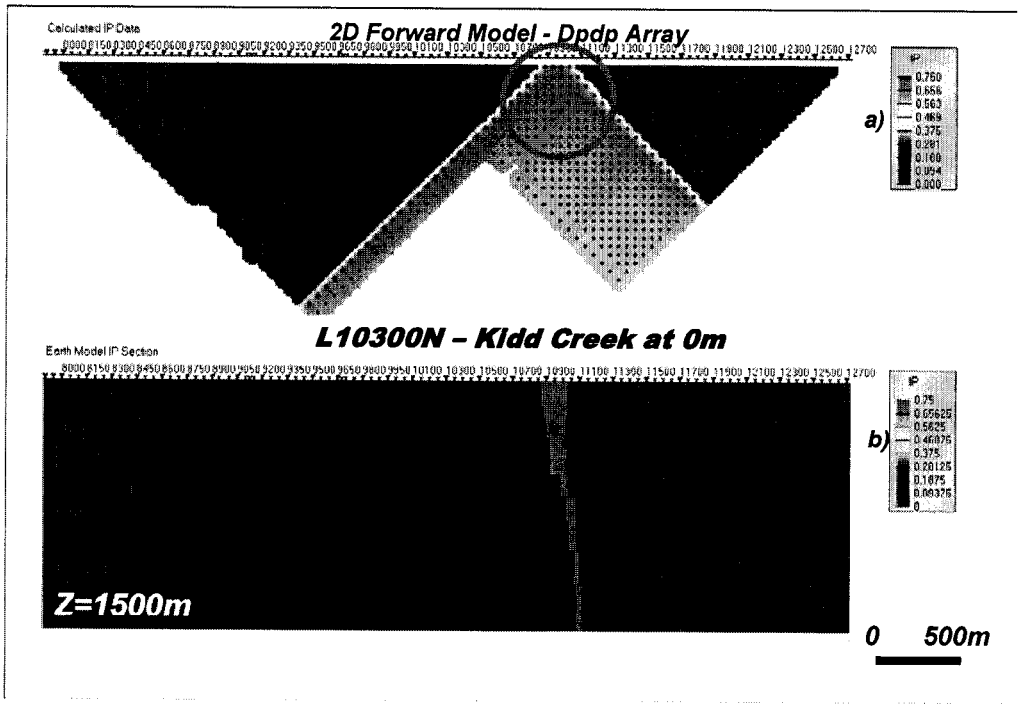

Figure 3.36: 2D Chargeability Forward Model, in Dpdp Array Format, for Kidd Creek at Surface.

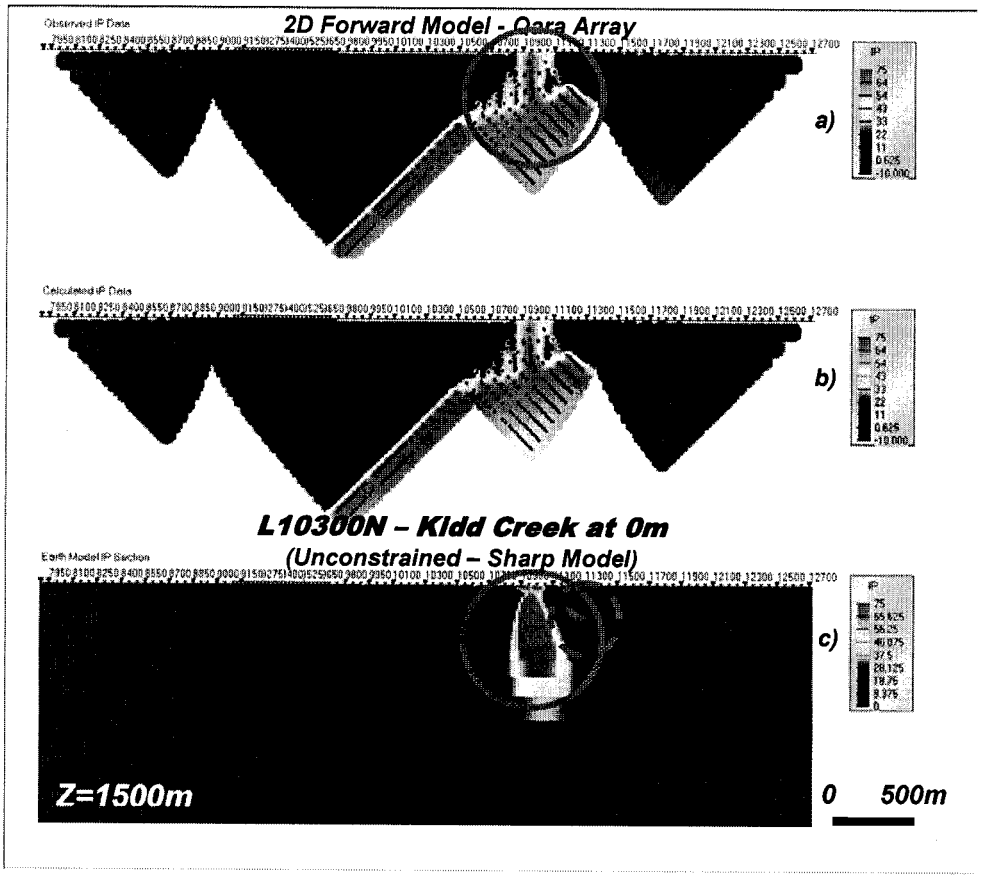

Figure 3.37: Sharp 2D Unconstrained Chargeability Inversion for Kidd Creek at Surface.

Another unconstrained 2D inversion of the same 2D forward model results is presented in Figure 3.38, for Kidd Creek at surface, which represents another comparable "smooth" model inversion – one which emphasizes model smoothness over resolution. This is achieved by using a default (small $\alpha_S \approx 0$) alpha-s parameter in the UBC model norm function (see Section 2.3). All other parameters were set to the UBC default values. The smooth inversion produces a large, strong IP high which also coincides in position and dip-direction to the predicted model, but is much larger and bares a poor resemblance - yet is quite typical of smooth, IP inversions obtained at Kidd Creek. Comparing Figure 3.38a and b, in spite of extending more deeply (900m vs. 600m) the smooth model fit to the data is also not as good as the sharp model, likely requiring a higher error floor for

convergence. These results suggest that a smooth large body is a poor representation of the data – a higher resolution solution is required. Consequently, for these reason, sharp inversions are generally preferred for unconstrained chargeability inversions in the present study.

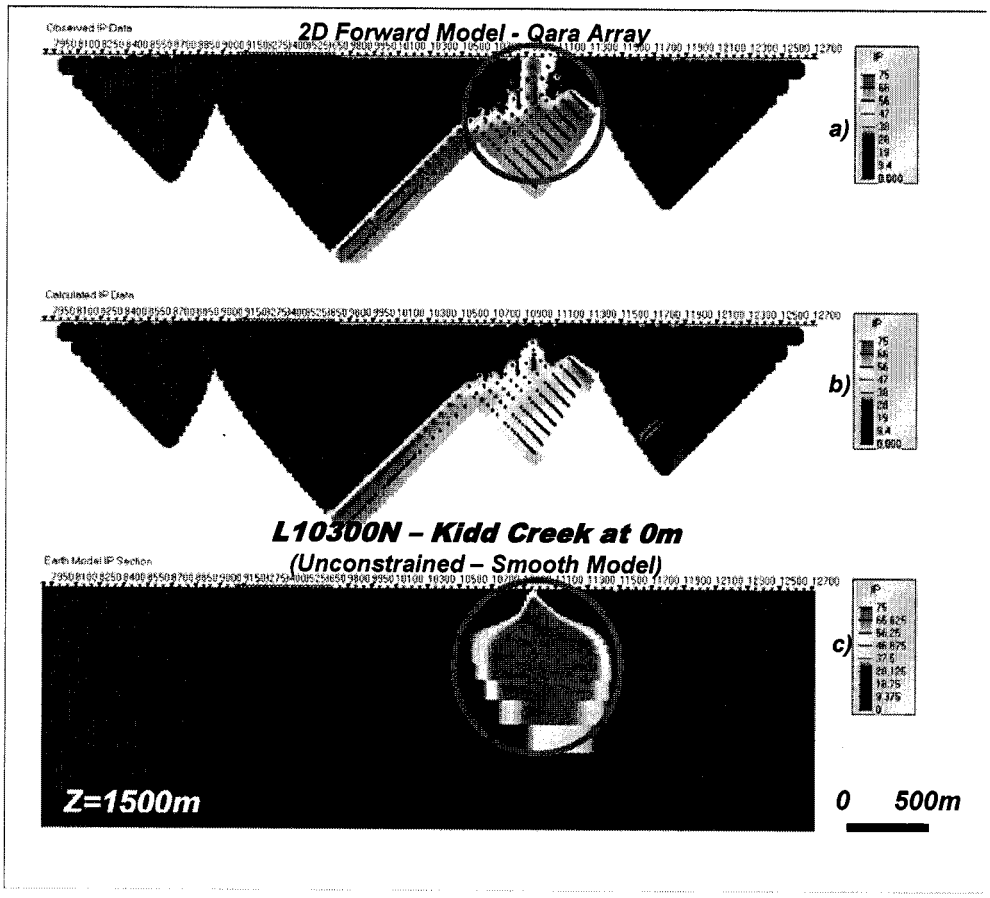

Figure 3.38: Smooth 2D Unconstrained Chargeability Inversion for Kidd Creek at Surface.

In a final comparative imaging test over the Kidd Creek orebody, simulated in its original (depth = 0m) state, a constrained 2D IP inversion of 2D forward model results, in Center-pole array format, was performed using a non-sulphide bearing rhyolite reference model for the Kidd horizon -shown in Figure 3.39. The constrained 2D inversion, shown in Figure 3.40, used modeling parameters identical to the first inversion (sharp model norm) but has been

weighted/guided by the geologic reference model and petrophysical constraints from Gocad. The 2D inversion returns a subcropping, strongly polarizeable body which corresponds well to the actual Kidd Creek orebody, in terms of depth of burial, vertical extent, dip angle, dip-direction, width at surface and position inside the rhyolite host rocks. However, as also seen in the DC resistivity inversion, the anomaly is also a complex, featuring two polarizeable centers (see solid red circles) – a stronger yet smaller zone at surface, and another, larger, weaker body centered at 700m depths (see Figure 3.40c), which differs from the original model. Moreover, like Kidd Creek, the modeled anomalous zone also appears to extend below 1.5km depth - however this is unexpected, given reasonable penetration limits of the Titan array DCIP surveys. Also, while some of the lithogeologic features in the original reference model have been preserved (i.e., sediments to west) in the constrained 2D inversion, the thinner rhyolitic units and basalts surrounding the main Kidd Creek horizon have been "painted" out of the cross-section, particularly with <500m depths. Notice also the false "ghost" anomalies (shown as dashed circles in Figure 3.40c). This evidence suggests that the constrained IP inversion is not sufficiently sensitive to "lithologic" chargeability contrasts, in the presence of stronger anomalous sources. On the other hand, we concluded that both the constrained and unconstrained inversions have nevertheless successfully been able to reproduce, with relative accuracy, the predicted zone of increased chargeability, within the rhyolite, which is unexplained by the geologic model, and would certainly command immediate interest.

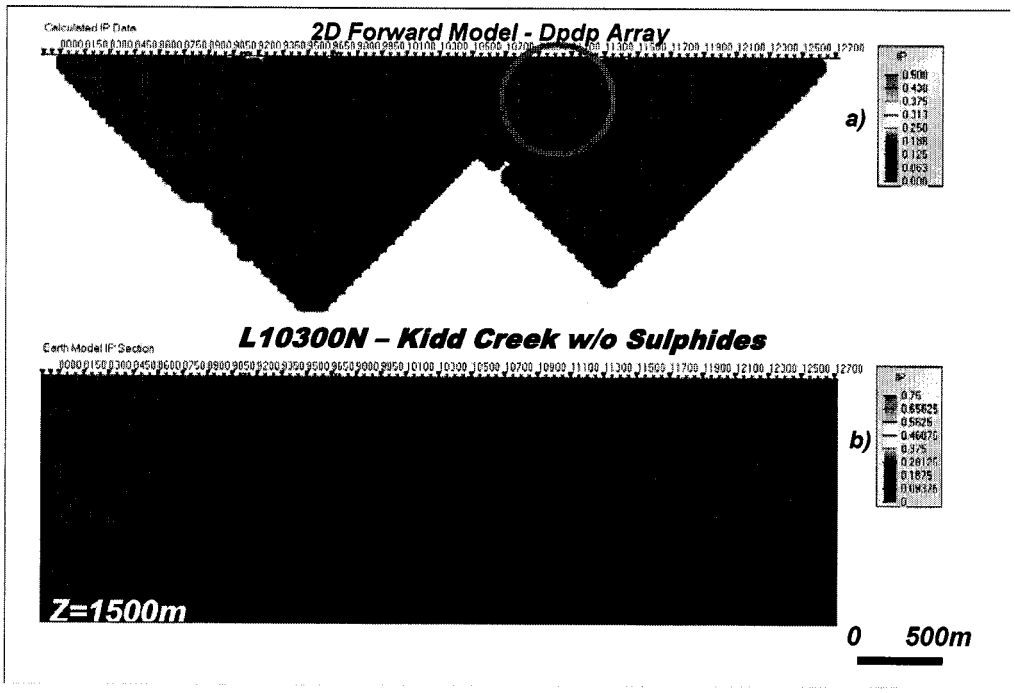

Figure 3.39: 2D IP Chargeability Forward Model for Kidd Creek without Massive Sulphides (IP reference model for constrained inversions)

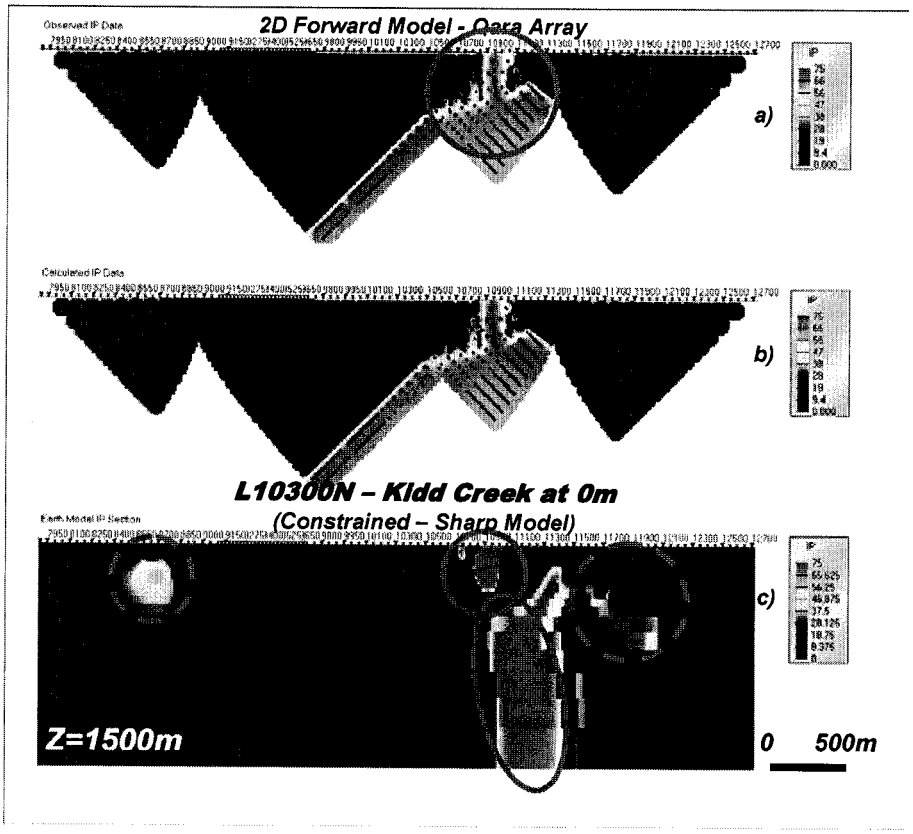

Figure 3.40: Sharp 2D Constrained DC Resistivity Inversion for Kidd Creek at Surface

b) *Depth = 200m / IP Model and Inversion*

The 2ND model shown in Figure 3.41, using identical chargeability parameters as previous, has been altered to simulate the Kidd Creek deposit at 200m depths, by replacing the values for sulphides with those for rhyolite in the reference model.

The 2D DC forward solution for this reference model is presented in Figure 3.41, in dpdp array format. In comparing the 200m depth response to the original, near surface forward model response (Figure 3.36), the IP anomaly is deeper (>n=3-6), significantly weaker (35mrad vs. 70 mrad) and more clearly asymmetric (east dip). Yet, unlike the analogous resistivity model, the IP anomaly is larger, more clear-cut, perfectly centred over the predicted target and

clearly implies a moderate-deeply buried target. This target should therefore be easily recognized in the raw results, without assistance from inversions, as might be expected.

The unconstrained 2D DC inversion, using sharp model parameters, of the 200m depth forward data is shown in Figure 3.37. A strong, highly polarizeable target is clearly defined at depth which corresponds very well to the depth of burial and dip-direction of the 200m Kidd Creek model provided. On the other hand, the anomalous body is more irregular shaped and less depth extensive than the predicted model – extending to a maximum depth of 600m. The unconstrained, sharp inversion also does not correctly images the upper rhyolitic cap rock and also generates ghost anomalies – a weak IP anomaly east of the inferred Kidd orebody (see small red circle), within a small rhyolite enclave. Nevertheless, the unconstrained chargeability anomaly is clear-cut – there is no doubt that the zone has been identified at 200m depths, with relative facility.

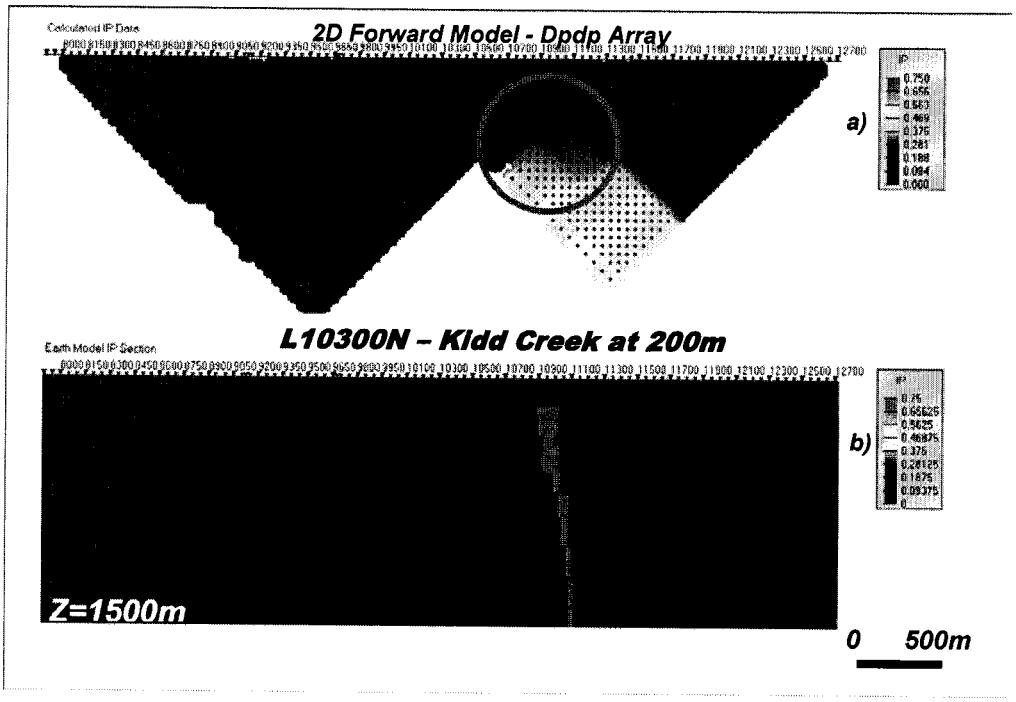

Figure 3.41: 2D Chargeability Forward Model, in Dpdp Array Format, for Kidd Creek at 200m Depth.

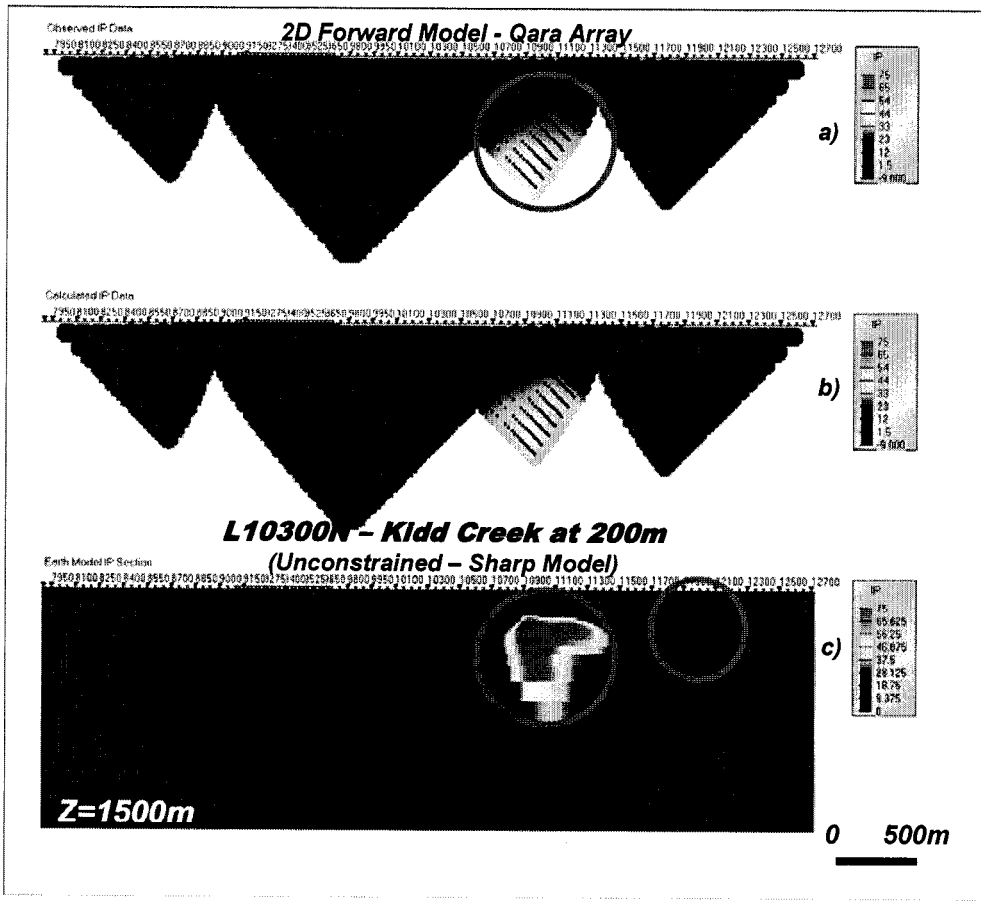

Figure 3.42: Sharp 2D Unconstrained Chargeability Inversion for Kidd Creek at 200m.

Constrained 2D inversion of the 2D forward IP results, using sharp and smooth model parameters, are shown in Figure 3.43 and Figure 3.44. These both use the same, non-mineralized reference model (Figure 3.39) and parameters that were tested earlier. The sharp model adheres more strictly to the reference model, whereas the smooth, constrained inversion initially uses the reference as a guide, but later is allowed to stray from it, as required, to obtain a satisfactory model convergence. The sharp inverse solution (Figure 3.43) correctly defines a weakly polarizeable target at depth (dashed circle) which corresponds very well to the depth of burial and position, but otherwise poorly describes the strength, dip-direction and vertical depth-extent of the 200m deep Kidd Creek model provided. In marked contrast, the smooth constrained inversion (Figure

3.44) defines a strongly polarizeable target at depth (dashed circle) which corresponds very well to the depth of burial, position, dip-direction and vertical depth-extent of the orebody. In fact, although its width is exaggerated, the smooth constrained inversion has done a better job at imaging the Kidd Creek orebody than the analogous unconstrained IP and also the DC results in general.

We conclude that, unlike the resistivity inversions, where unconstrained models were more successful at imaging deep targets, the inversion of the chargeability parameter benefits greatly from the Gocad-constraint, for medium-depth targets (<500m) - provided it is not forced to adhered strictly to a reference model which is significantly different than the real earth. This either relates to weaker contrasts between target and host for the chargeability in comparison with the resistivity (i.e., 5-25x max. for the IP, versus 10-1000:1 max. for the resistivity), or is possibly an artefact of the UBC inversion algorithm used.

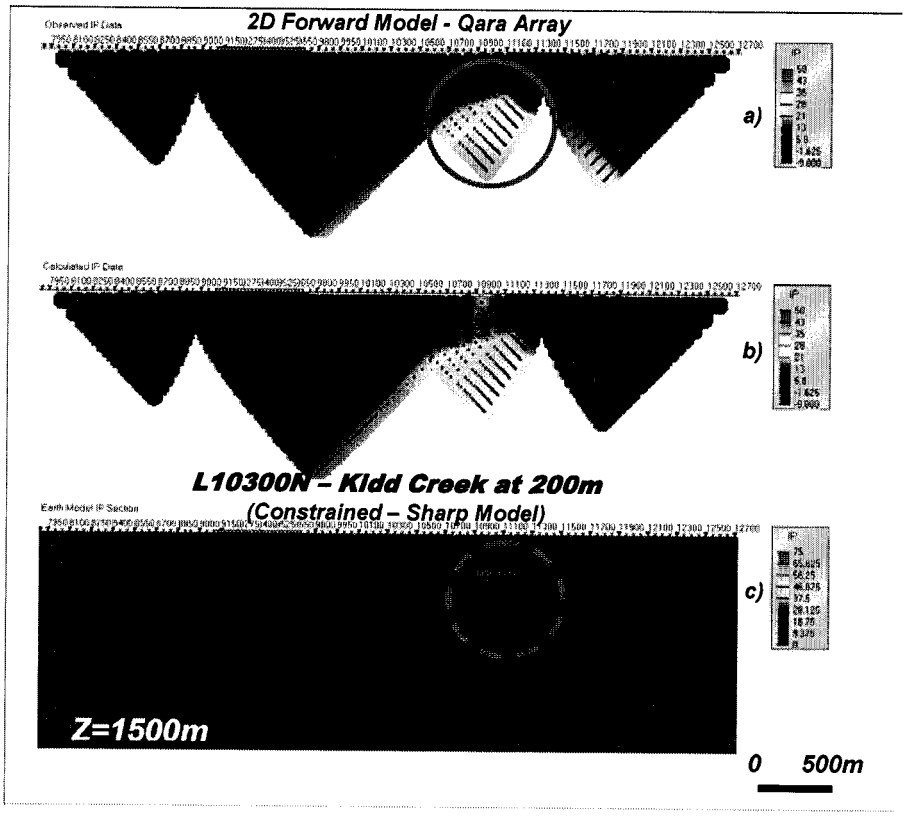

Figure 3.43: Sharp 2D Constrained IP Chargeability Inversion for Kidd Creek at 200m

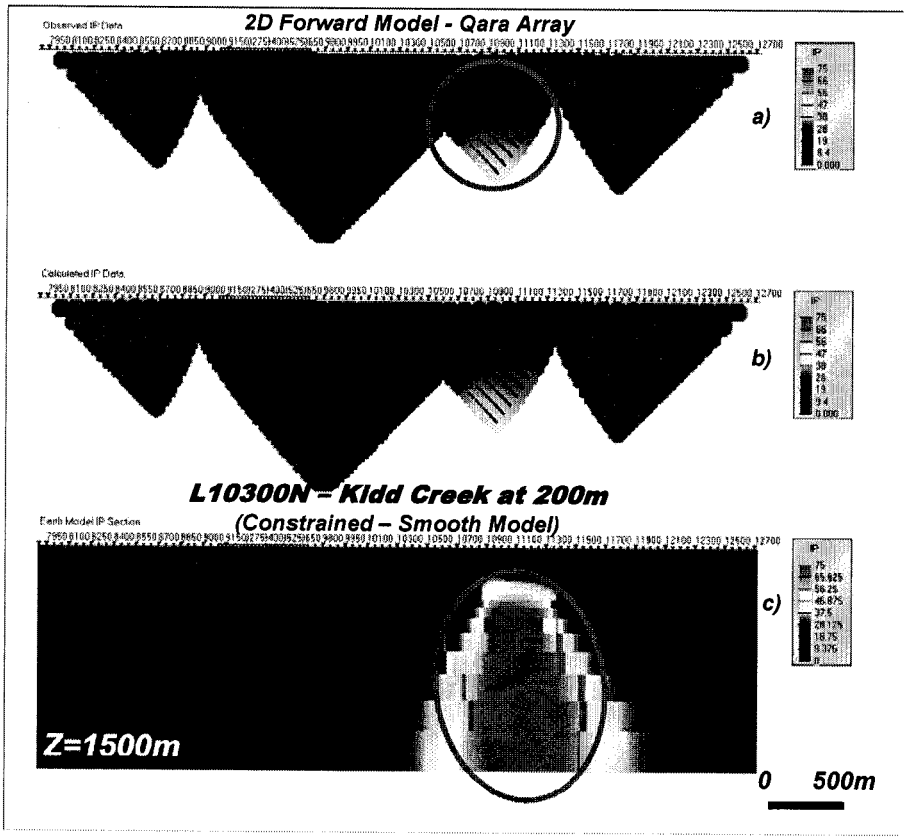

Figure 3.44: Smooth 2D Constrained IP Chargeability Inversion for Kidd Creek at 200m

c) *Depth = 500m / IP Model and Inversion*

A 3RD IP model, shown in Figure 3.45b, represents the Kidd Creek deposit which as been eroded to 500m depths below surface – again, by replacing massive sulphides for rhyolite in the reference model. The target is visibly small in relation to the geologic cross-section. The 2D IP forward solution, in dpdp array format, for this reference model, is presented in Figure 3.45a. It is similar to the 200m dpdp response (see Figure 3.41), but is significantly weaker (20mrad max.) suggesting, at first glance that while the 500m depth of burial poses no problem for detection in the Titan array DC data, a strongly polarizeable target might be mistaken for a large, lithologic response, i.e., notice the strong similarity with the dpdp response from the barren model shown in Figure 3.39. It appears, therefore, that the weaker contrasts, inherent in the chargeability, have significantly affected our ability to identify deeply buried IP targets in the raw Titan data.

In fact, the unconstrained 2D IP inversion of the 500m depth forward data, in Figure 3.46, fails to define the deep target from the predicted Kidd Creek model. Notice that the large (500 x 300m) anomaly at 200m depths (dashed circle) is clearly too shallow to represent the intended target at 500m. Indeed, the unconstrained IP inversion appears to be simply resolving, albeit accurately, the top of the barren rhyolite unit (20 mrad background). As proof, an identical inversion result from a barren rhyolitic model (all Kidd Creek sulphides replaced by rhyolite values), shown in Figure 3.47, identifies a similar feature at surface. It appears that, in marked contrast with the successful 200m depth inversion IP model, that the Titan surveys are unable to correctly image a Kidd Creek-like orebody, using unconstrained inversions of the IP parameter – either as a result of poor contrasts or as a result of the smooth conjugate algorithm used.

As final proof of the 500m limit to the depth of investigation of the IP parameter, a constrained 2D inversion is presented in Figure 3.48 – using the identical smooth inversion parameters which successfully imaged the 200m depth target in the previous constrained example (see Figure 3.44). It is clear that, in spite of mapping lateral chargeability contrasts, that a discernable IP anomaly, at depth, is absent from the model. We conclude, therefore, that due to the poor natural contrasts inherent in the IP parameter, possibly combined with the smoothing characteristics of the inversion algorithm, that the practical depth of investigation for the Titan IP surveys is between 200 and 500m – with 350m being a good estimate.

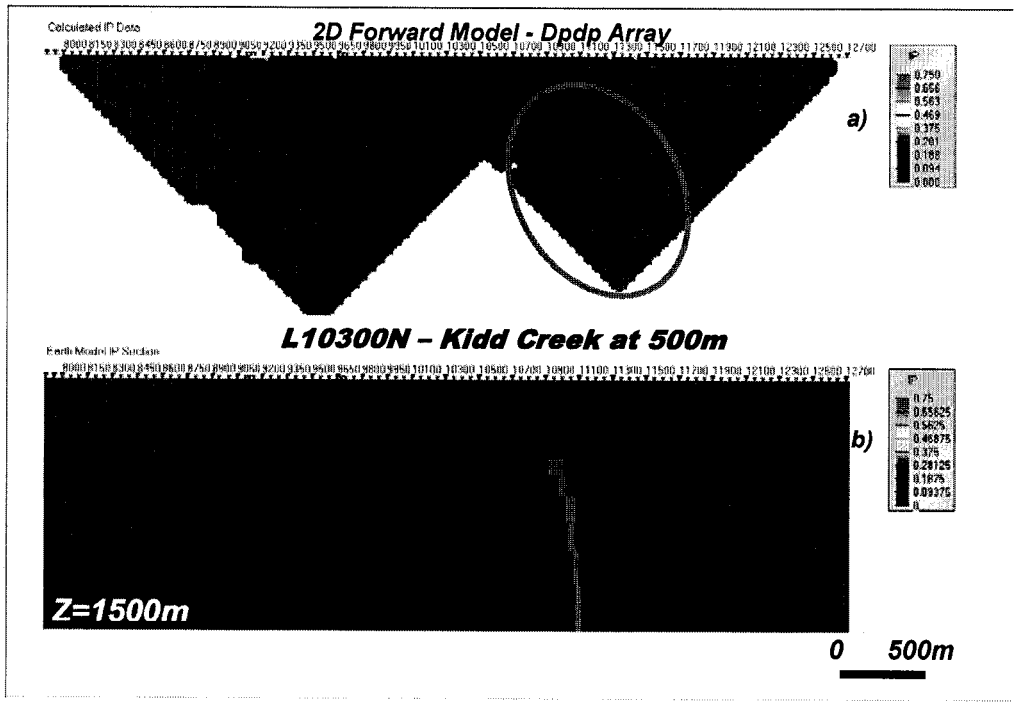

Figure 3.45: 2D Chargeability Forward Model, in Dpdp Array Format, for Kidd Creek at 500m Depth.

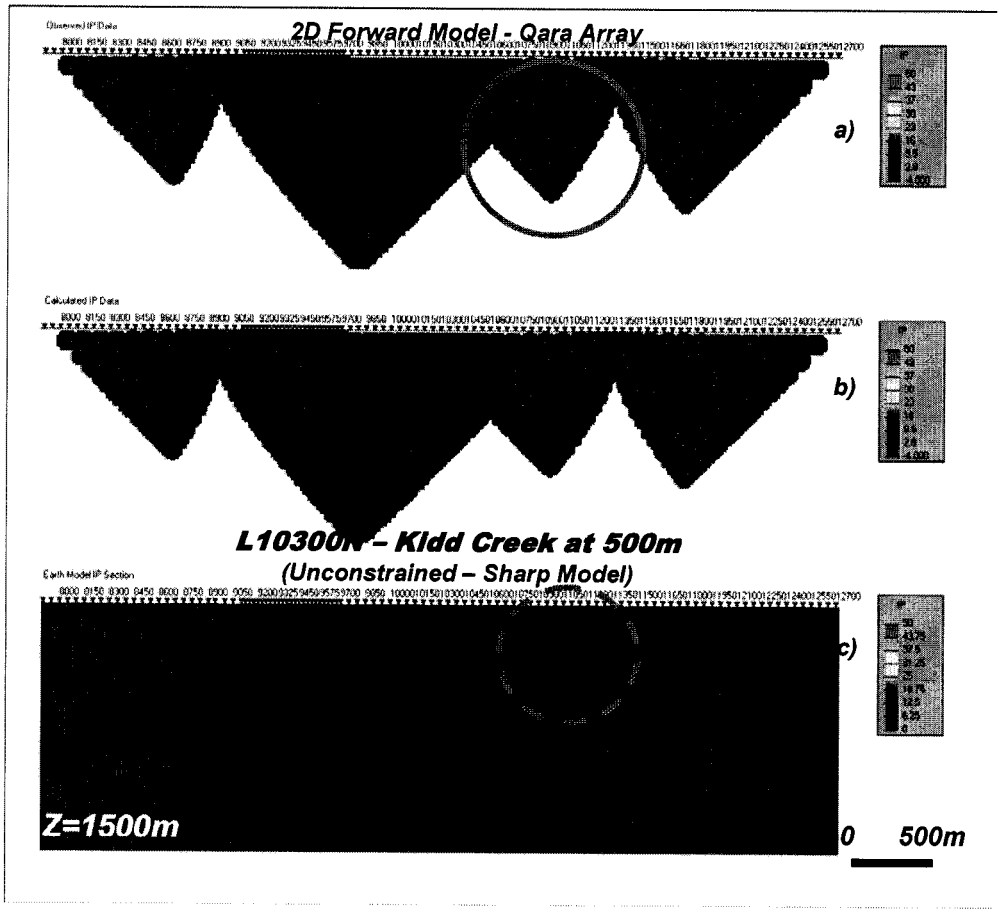

Figure 3.46: Sharp 2D Unconstrained Chargeability Inversion for Kidd Creek at 500m.

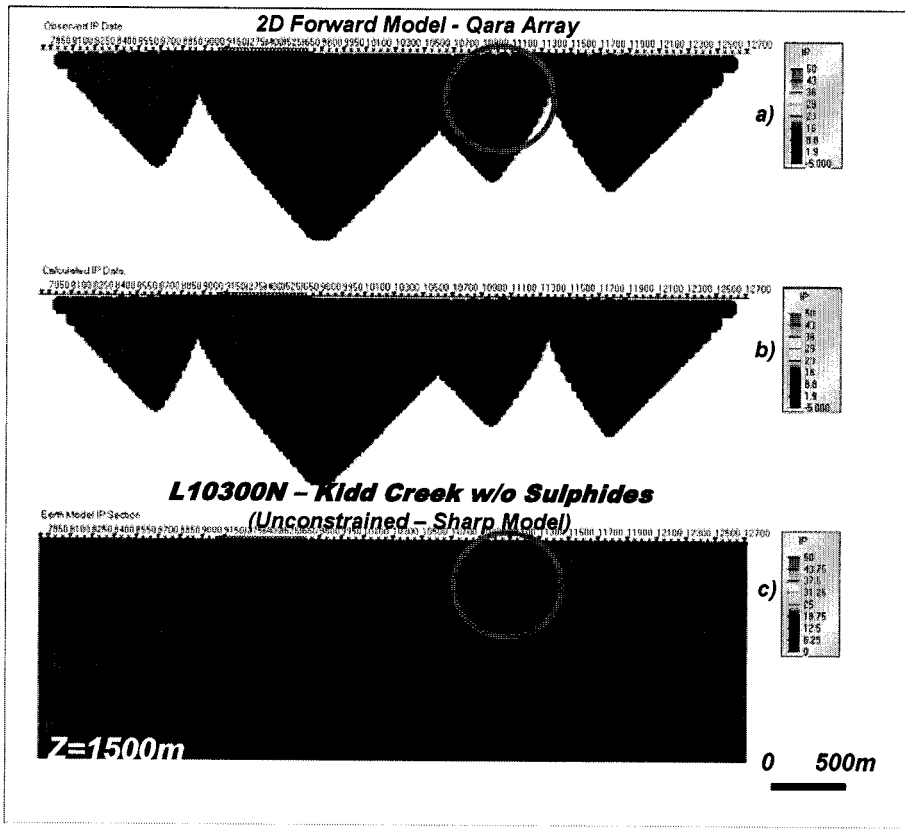

Figure 3.47: Smooth 2D Unconstrained IP Inversion for Kidd Creek without Massive Sulphides.

It is worthwhile noting that, just as in DC resistivity results (see Sec. 3.2.1), these conclusions regarding the depth of investigation for Titan IP surveys also differ significantly from generally accepted values, based on the work of Roy and Apparao (1971), i.e., for P ≈0.19L, P_{KIDD} < 600m (M. Chouteau, pers. comm., 11/2004). However, unlike the DC case, the estimated investigation for the Titan IP is nearly 50% less than the 600m figure.

It appears clear, therefore, that empirical, rule of thumb estimates for depth-penetration, are not reliable for more complex earth models. Furthermore, these IP model studies appear to satisfy the criteria set out by Oldenburg and Ly (1999). Therefore, based on a Kidd Creek style target that is 2-dimensional in nature, the 350m penetration depth limit for the unconstrained and constrained 2D inversion or Qara array Titan IP survey results appears justifiable.

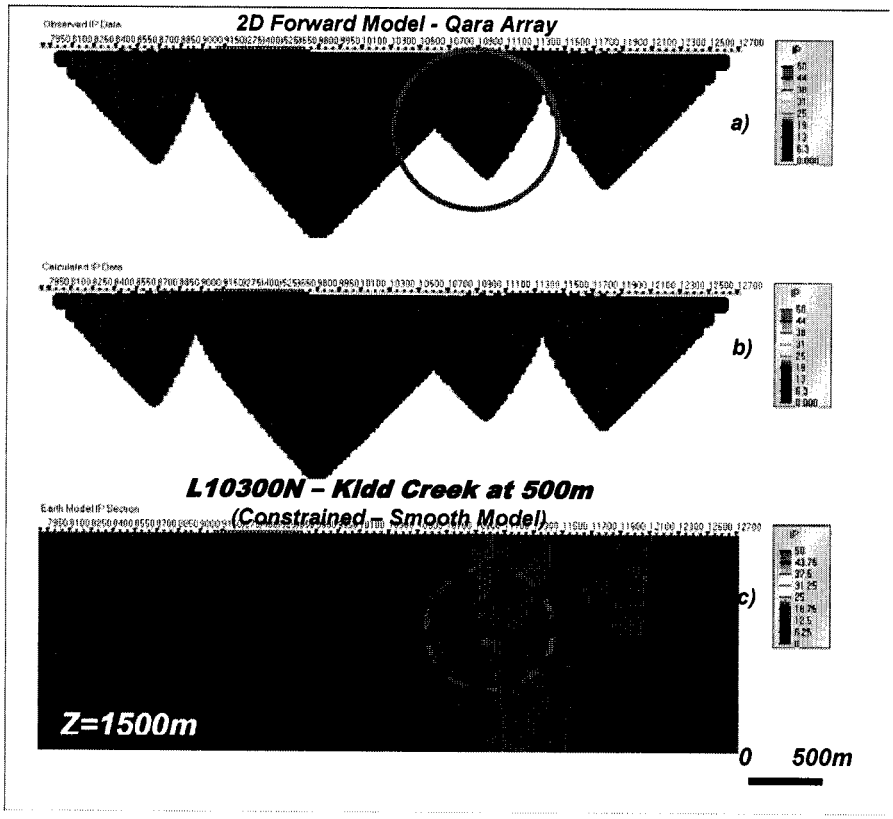

Figure 3.48: Smooth 2D Constrained IP Chargeability Inversion for Kidd Creek at 500m

3.3.3 2D MT Resistivity Modeling

The following series of examples present the calculated MT responses from the Kidd Creek deposit, in its original state, as a 2 dimensional body (infinite strike length), illustrating its progressively burial from surface to 2km depths. The 2D forward model profiles model shown use the same Gocad starting geologic model and the resistivity constraints used in the previous DC resistivity studies, and are presented in Table 3.6 below. In order to simulate the ore body's progressive burial in the following simulation, the model values for massive sulphide were replaced, from surface to a given depth (100, 200, 500, 1000, 2000m) with values for the barren rhyolites (1k ohm-m) – which is identical to the procedure followed for the DC and IP model sensitivity studies.

Using the Geotools 2D PW MT modeling algorithm, the forward models were calculated using the following parameters: The meshes were constructed using: a) run-mesh frequencies set at 10k, 1k, 100, 10 and 0.1 Hz, b) model resistivity projection to 10 to 10k ohm-m range, c) a minimum column width of 50m, inside the data range, increasing by 50% increments to 30km off each end, laterally, d) maximum 80 rows, with a minimum row-thickness of 10m to a depth of 1km, increasing by 10% increments to 30km depths. Mesh nodes were situated at each station for the PW models.

Note that, owing to the high level of data quality expected from Titan surveys (i.e., average rho error[10] at Kidd <0.01decades; avg phase error = <0.5 degrees), no additional "noise" (such as the 5% Gaussian, commonly used) has been added to these synthetic model data. This differs from standard practice (M. Chouteau, pers. comm., 11/2004) but is justifiable in light of the very high Titan MT data quality.

The PW MT forward model calculations return an apparent resistivity and phase, for the In-line (TM) and Cross-line (TE) components of the 2D response, at discrete frequencies in the 0.1 to 10,000 Hz bandwidth, at a logarithmic interval of 4 frequencies per decade. Unlike the DCIP case-study presented in Sec 3.3.1-3.3.2, inversions of the 2D MT forward modeling data were not calculated for this study, largely owing to the fact that the MT responses are more clear-cut and easily interpreted based on the raw data.

The results are presented in the industry standard frequency-pseudosection format, with increasing frequency along the abscissa Y axis, increasing station along the ordinate X axis, as shown in Figure 3.49c to Figure 3.49j. The stacked frequency pseudosection format shown features the TM apparent resistivity and phase at the top, and TE apparent resistivity and phase at

---

[10] Based on statistical analysis of Titan MT data collected along 10800N at Kidd Creek (1831 points). Avg apparent resistivity (rhoxy + rhoxy) error = 0.0047 decades; avg. phase (xy +yx) error = 0.36 degrees.

the bottom. Although, visually similar to 2D crossections, the pseudosections do not represent true depth sections, since the penetration is not uniform in the horizontal direction.

Table 3.6: Reference Resistivities for MT Models and Constrained Inversions

LITHOLOGY	RESISTIVITY	COLOUR
Mafic volcanic	10k ohm-m	Purple
Ultramafic volcanic	7k ohm-m	Navy-blue
Sediments	5k ohm-m	Blue
Rhyolite	1k ohm-m	Light blue
Overburden	30 ohm-m	Red
Graphite/Massive Sulphide	1-10 ohm-m	Pink

a) *Depth = 0m / MT Model*

The first model, shown in Figure 3.49a, is designed to simulate the theoretical Titan-24 MT response of the Kidd Creek orebody, in its original state, prior to being mined out. Below it, there are four pseudosections of data for this model (see Figure 3.49cegi), for each of the four components measured, as shown. Next to it, in Figure 3.49b, is the model for a barren rhyolite horizon without the Kidd Creek orebody, for comparison, along with each of its four component responses (Figure 3.49dfhj). All apparent resistivity pseudosections are logarithmically-zoned to a minimum-maximum range of 10 to 10k ohm-m, and the phase sections are linearly zoned, either from 0 to 90 degrees (Cross-line) or -180 to -90 degrees (In-line).

Distinctive features are worth noting in each of the pseudosections:

1. The In-line apparent resistivity pseudosections (Figs. C and D) exhibit vertical striping, consistent with "static" effects, due to near-surface heterogeneities and which are frequency independent. Looking closely, each variation in the near-surface structure, either geologic contacts or overburden, triggers a static In-line response – including characteristic

high/low resistivity features at the edge of each feature. The Kidd Creek orebody is defined as a "static"-like, narrow, subvertical resistivity low in Figure 3.49c (red ellipse), which is approximately the same width as the deposit. The barren model (Figure 3.49d) is uniformly moderately resistive (dashed ellipse) across the Kidd horizon. Elsewhere, away from the Kidd orebody, the two sections are nearly identical, which is consistent with the high lateral resolution nature of the In-line (TM) component response.

2. The In-line phase pseudosections below them (Figs. E and F) are similar and are also relatively immune to "static" effects. These more accurately map true variation in lateral resistivity structure. The Kidd Creek orebody is defined, in Figure 3.49e (red circle), as a narrow phase high at high to mid frequencies, whereas the barren rhyolite features a broad (1km wide), high frequency phase high (dashed oval) over the lower resistivity North Rhyolite unit. Similarly, to the apparent resistivities, away from the Kidd orebody, the phase sections are nearly identical.
3. The Cross-line apparent resistivity pseudosections (Figs. G and H) both display smooth variations across the geologic contacts and do not exhibit "static" effects. The Kidd Creek orebody is defined in Figure 3.49g as a resistivity low, at high to mid frequencies (red oval), which is broader (300m wide) than the orebody and widens to 500m at deeper skin-depths. In marked contrast, the barren model (Figure 3.49h – dashed oval) is uniformly resistive across the North Rhyolite. Unlike the In-line sections, the cross-line sections only resemble each other in the high frequency portions that are furthest away from the center. Indeed, the presence of the Kidd orebody is felt/detected at least 1km laterally, which is consistent with the sensitivity of the Cross-line component response.
4. The Cross-line phase pseudosections (Figs. I and J) are similar in their tendencies to the cross-line apparent resistivities. The Kidd Creek ore-

body is defined by a broad, high frequency phase high, followed by a phase low at mid-to-low frequencies. In contrast, the phase response across the North Rhyolite, in the barren model, is a weak, high frequency phase high, in response to the lower bulk resistivity in the rhyolitic horizon.

Clearly, from these results, in spite of the shallow cover, the Kidd Creek deposit would be discerned in all four components in the Titan MT raw data, in particular, the Cross-line apparent resistivity and phase. Its presence would also be felt 500-1000m away. These responses should also be easily distinguished from a barren rhyolitic horizon.

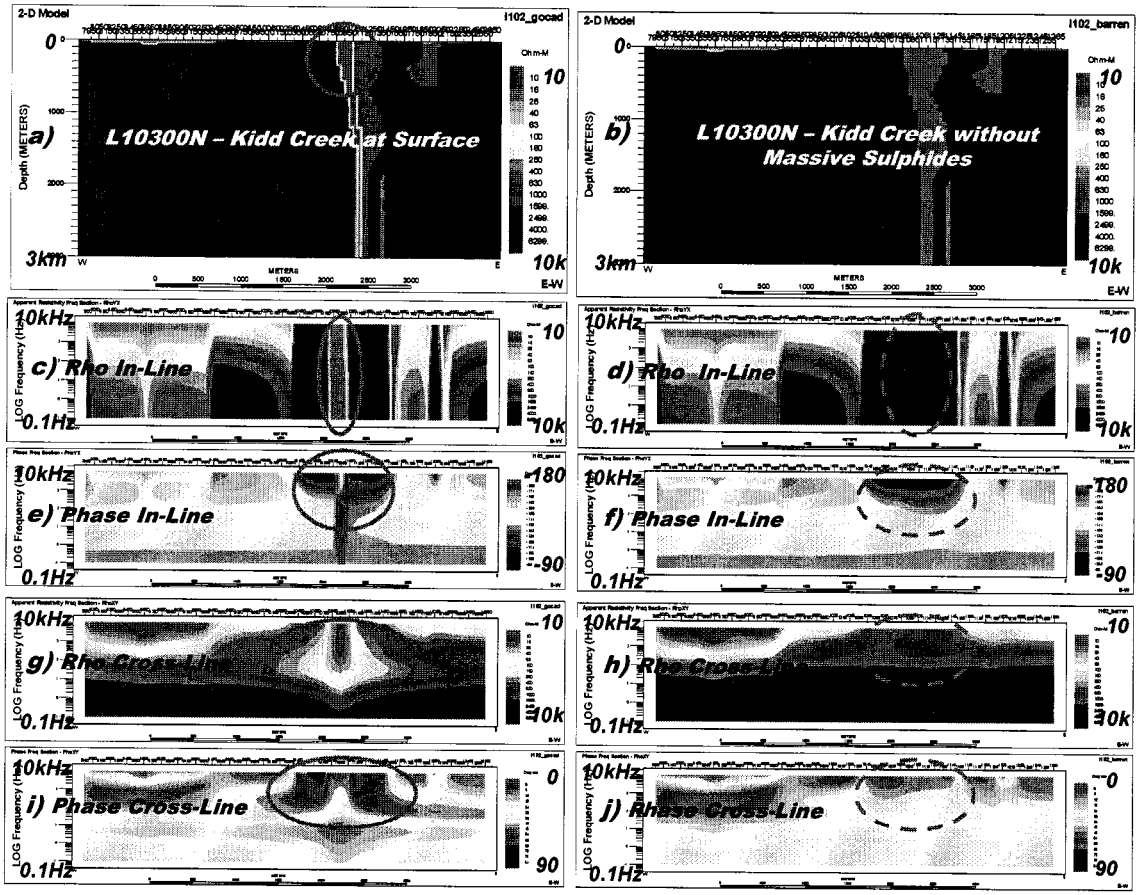

Figure 3.49: 2D MT Forward Models, for Kidd Creek at Surface and for Barren Rhyolite

b) Depth = 200m / MT Model

The second model, shown in Figure 3.50a, simulates the theoretical MT response of the Kidd Creek orebody, buried at 200m depths. As previously, below it, there are four pseudosections of data for this model (see Figure 3.50cegi), for each of the four components measured, as shown. Next to it, in Figure 3.50b, is the model for a barren rhyolite horizon without the Kidd Creek orebody, for comparison, along with each of its four component responses Figure 3.50dfhj). All apparent resistivity pseudosections are logarithmically-zoned to a minimum-maximum range of 10 to 10k ohm-m, and the phase sections are linearly zoned, either from 0 to 90 degrees (Cross-line) or -180 to -90 degrees (In-line).

Distinctive features are worth noting in each of the pseudosections:

1. The In-line apparent resistivity pseudosections (Figs. C and D) exhibit vertical striping, consistent with "static" effects, due to near-surface heterogeneities and which are frequency independent. Looking closely, each variation in the near-surface structure, either geologic contacts or overburden, triggers a static In-line response – including characteristic high/low resistivity features at the edge of each feature. Unlike the near-surface model, the 200m deep orebody response features only a weakly discernable resistivity low anomaly (see dashed ellipse in Figure 3.50c). In fact, the barren model (Figure 3.50d) is remarkably similar, while also featuring uniformly moderate resistivities across the rhyolitic horizon (dashed ellipse). The In-line mode is therefore insensitive to narrow, buried, subvertical conductors – even Kidd Creek-like orebodies at 200m – which is consistent with In-line/TM behaviour. Elsewhere, away from the Kidd orebody, the two sections are nearly identical, as previously shown.
2. The In-line phase pseudosections below them (Figs. E and F) are nearly identical and are also relatively immune to "static" effects. These more accurately map true variation in lateral resistivity structure. However, as

shown, the Kidd Creek orebody response, in Figure 3.50e (dashed oval) is also not discernable – in fact the pseudosection is nearly identical to the barren rhyolite response in Figure 3.50f. Clearly, the In-line component does not detect the massive sulphide orebody, buried at 200m, either.

3. The Cross-line apparent resistivity pseudosections (Figs. G and H) display smooth variations across the geologic contacts and do not exhibit "static" effects. In contrast with the In-line component response, the 200m deep orebody is defined in Figure 3.50g as a buried resistivity low, at mid frequencies (red oval), which is much broader (1km) than the orebody. In marked contrast, the barren model (Figure 3.50h – dashed oval) is uniformly resistive across the North Rhyolite.
4. The Cross-line phase pseudosections (Figs. I and J) feature similar tendencies as the cross-line apparent resistivities. The 200m deep Kidd orebody is defined by a broad (1km wide), mid-to-high frequency phase high, followed by a phase low at low frequencies. The phase response across the North Rhyolite, in the barren model is a weak, high frequency phase high, in response to the lower bulk resistivity in the rhyolitic horizon.

Clearly, from these results, at a 200m burial depth, the Kidd Creek deposit would be discerned in only two of four component in the Titan MT raw data - specifically, the Cross-line apparent resistivity and phase. However, its presence would also be felt >500-1000m away. These responses should also be easily distinguished from a barren rhyolitic horizon.

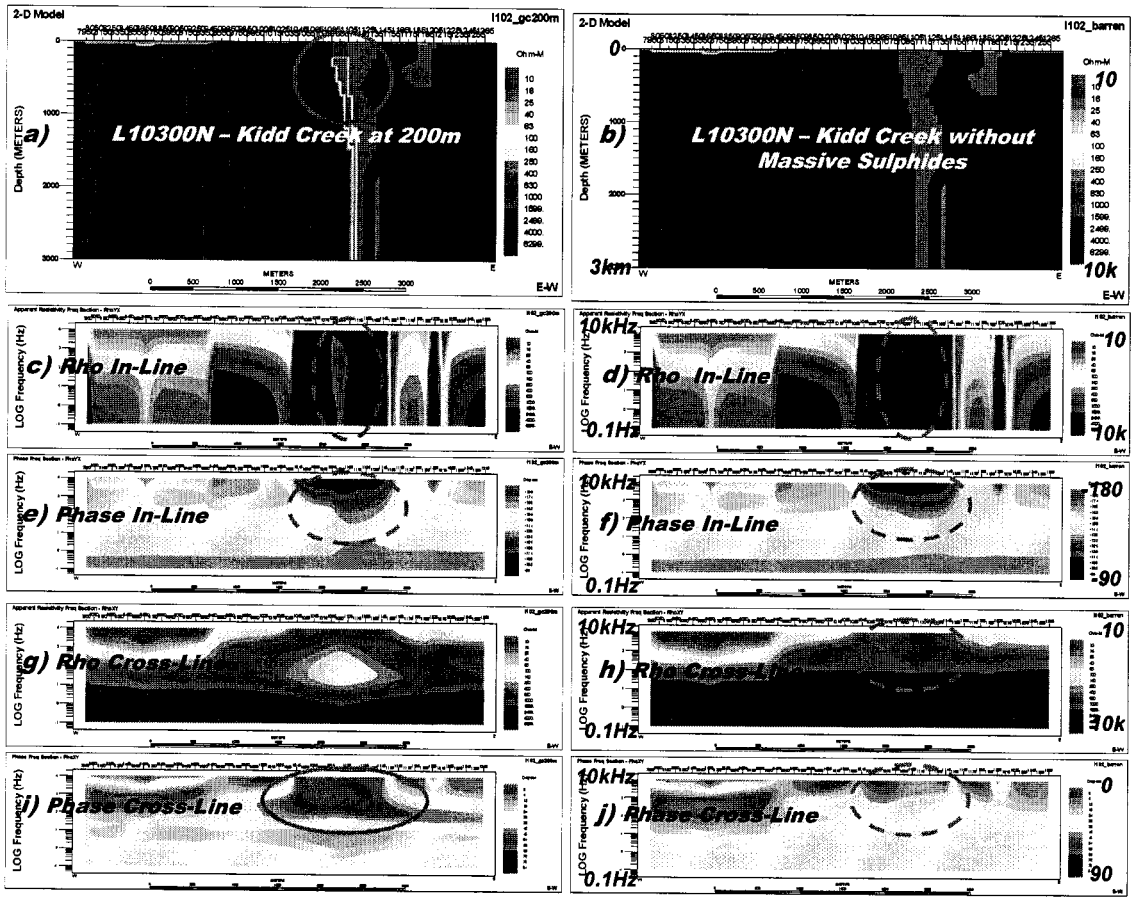

Figure 3.50: 2D MT Forward Models for Kidd Creek at 200m Depth and for Barren Rhyolite.

c) Depth = 500m / MT Model

The third model, shown in Figure 3.51a, simulates the theoretical MT response of the Kidd Creek orebody, buried at 500m depths. As previously, below it, there are four pseudosections of data for this model (see Figure 3.51cegi), for each of the four components measured, as shown. To the right, in Figure 3.51b, is the model for a barren rhyolite horizon without the Kidd Creek orebody, for comparison, along with each of its four component responses (Figure 3.51dfhj). All apparent resistivity pseudosections are logarithmically-zoned to a minimum-maximum range of 10 to 10k ohm-m, and the phase sections are linearly zoned, either from 0 to 90 degrees (Cross-line) or -180 to -90 degrees (In-line).

Distinctive features are worth noting in each of the pseudosections:

1. The In-line apparent resistivity pseudosections (Figs. C and D) exhibit vertical striping, consistent with "static" effects, due to near-surface heterogeneities and which are frequency independent. Looking closely, each variation in the near-surface structure, either geologic contacts or overburden, triggers a static In-line response – including characteristic high/low resistivity features at the edge of each feature. As with the previous 200m deep model, the 500m deep orebody feature a barely discernable resistivity low anomaly (see dashed ellipse in Figure 3.51c). In fact, the barren model (Figure 3.51d) is nearly identical, featuring uniformly moderate resistivities across the rhyolitic horizon (dashed ellipse). The In-line mode is therefore insensitive to narrow, buried, subvertical conductors – even Kidd Creek-like orebodies at 200 or 500m.
2. The In-line phase pseudosections below them (Figs. E and F) are relatively similar and also immune to "static" effects. These more accurately map true variation in lateral resistivity structure. However, as shown previously, the 500m-buried Kidd Creek orebody response, in Figure 3.51e (dashed oval) is also not discernable – in fact the pseudosection is identical to the barren rhyolite response in Figure 3.51f. Clearly, the In-line component does not detect the massive sulphide orebody, buried at 200 or 500m, either.
3. The Cross-line apparent resistivity pseudosections (Figs. G and H) display smooth variations across the geologic contacts and do not exhibit "static" effects. In contrast with the In-line component response, the 500m deep Kidd Creek orebody is defined in Figure 3.51g as a buried, weak/diffuse resistivity low, at mid-to-low frequencies (red oval), which is much broader (1.5km) than the predicted orebody. In marked contrast, like the previous cases, the barren model (Figure 3.51h – dashed oval) is uniformly resistive across the North Rhyolite.

4. The Cross-line phase pseudosections (Figs. I and J) feature similar characteristics as the cross-line apparent resistivities. The Kidd Creek orebody at 500m is defined by a broad (1.5km), moderate to weak, mid-frequency phase high, followed by a phase low at low frequencies – similar to the 200m response. The phase response in the barren model across the North Rhyolite is a weak, high frequency phase high, in response to the lower bulk resistivity in the rhyolitic horizon.

Clearly, from these results, at a 500m burial depth, the Kidd Creek deposit would be discerned in only two of four component in the Titan MT raw data – specifically, the Cross-line apparent resistivity and to a relatively greater extent in the phase. However, its presence would also be felt >500-1500m away. These responses should also easily distinguish it from a barren rhyolitic horizon.

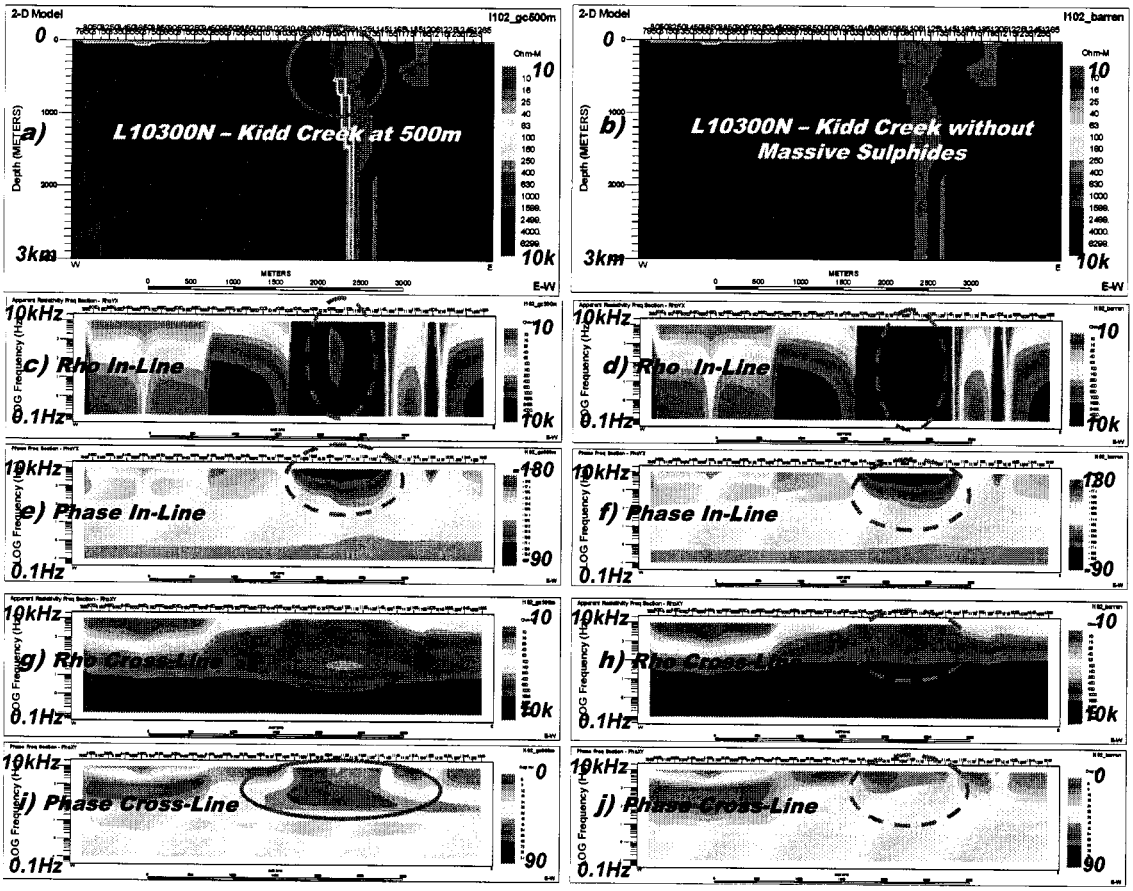

Figure 3.51: 2D MT Forward Models for Kidd Creek at 500m Depth and for Barren Rhyolite.

d) Depth = 1000m / MT Model

The fourth model, shown in Figure 3.52a, simulates the theoretical MT response of the Kidd Creek orebody, buried at 1000m depths. In this model, the resistivity for the massive sulphide has been lowered to 0.1 from 10 Ω-m, to make it more reasonably detectible at this depth – its colour range has also been adjusted from 10-10k ohm-m to 0.1-10k Ω-m. As in previous examples, shown below it are the four pseudosections of data for this model (see Figure 3.52cegi), for each of the four components measured. To the right, in Figure 3.52b, is the model for a barren rhyolite horizon without the Kidd Creek orebody, for comparison, along with each of its four component responses (Figure 3.52dfhj). All ap-

parent resistivity pseudosections are logarithmically-zoned to a minimum-maximum range of 10 to 10k ohm-m and the phase sections are linearly zoned, either from 0 to 90 degrees (Cross-line) or -180 to -90 degrees (In-line).

Distinctive features are worth noting in each of the pseudosections:

1. The In-line apparent resistivity pseudosections (Figs. C and D) exhibit vertical striping, consistent with "static" effects, due to near-surface heterogeneities and which are frequency independent. Looking closely, each variation in the near-surface structure, either geologic contacts or overburden, triggers a static In-line response – including characteristic high/low resistivity features at the edge of each feature. As with the previous 500m deep model, the Kidd Creek orebody at 1km does not feature a discernable In-line resistivity low anomaly (see dashed ellipse in Figure 3.52c). In fact, the barren model (Figure 3.52d) is identical, featuring uniformly moderate resistivities across the rhyolitic horizon (dashed ellipse). Hence, in spite of the 100x increase in conductivity, the In-line mode remains insensitive to narrow, buried, subvertical conductors – even Kidd Creek-like orebodies at 200m, 500m or 1km.
2. The In-line phase pseudosections below them (Figs. E and F) feature similar behaviour, but are relatively immune to "static" effects. These more accurately map true variation in lateral resistivity structure. However, as shown previously, the 1km deep Kidd Creek orebody response, in Figure 3.52e (dashed oval) is also not discernable – in fact the pseudosection is identical to the barren rhyolite response Figure 3.52f. Clearly, the In-line component does not detect the massive sulphide orebody, even if they are 100x more conductive, if they are buried below 200m, 500m or 1km, either.
3. The Cross-line apparent resistivity pseudosections (Figs. G and H) display smooth variations across the geologic contacts and do not exhibit "static" effects. In contrast with the In-line component response, the cross-line

data define the 1km deep Kidd Creek orebody in Figure 3.52g as a buried, moderate resistivity low at mid-to-low frequencies (red oval), which is much broader (≈3km) than the predicted orebody. As a result of the 100x increase in conductivity (from 10 to 0.1 Ω-m), the 1km resistivity low is markedly stronger and better resolved than the 500m depth target. As shown previously, the barren model (Figure 3.52h – dashed oval) is uniformly resistive across the North Rhyolite.

4. The Cross-line phase pseudosections (Figs. I and J) feature similar tendencies as the cross-line apparent resistivities. The Kidd Creek orebody at 1000m is defined by a broad (≈3km), moderately strong, low frequency phase high (red oval). It is equally better resolved than the previous 500m target, due to the stronger host/target contrast. The phase response across the North Rhyolite, in the barren model is a weak, high frequency phase high (dashed oval), in response to the lower bulk resistivity in the rhyolitic horizon.

Clearly, from these results, at a 1km burial depth, the Kidd Creek deposit would be discerned in only two of four component in the Titan MT raw data – specifically, the Cross-line apparent resistivity and to a relatively greater extent in the phase. However, its presence would also be felt >1000-1500m away. These responses should also be easily distinguished from a barren rhyolitic horizon.

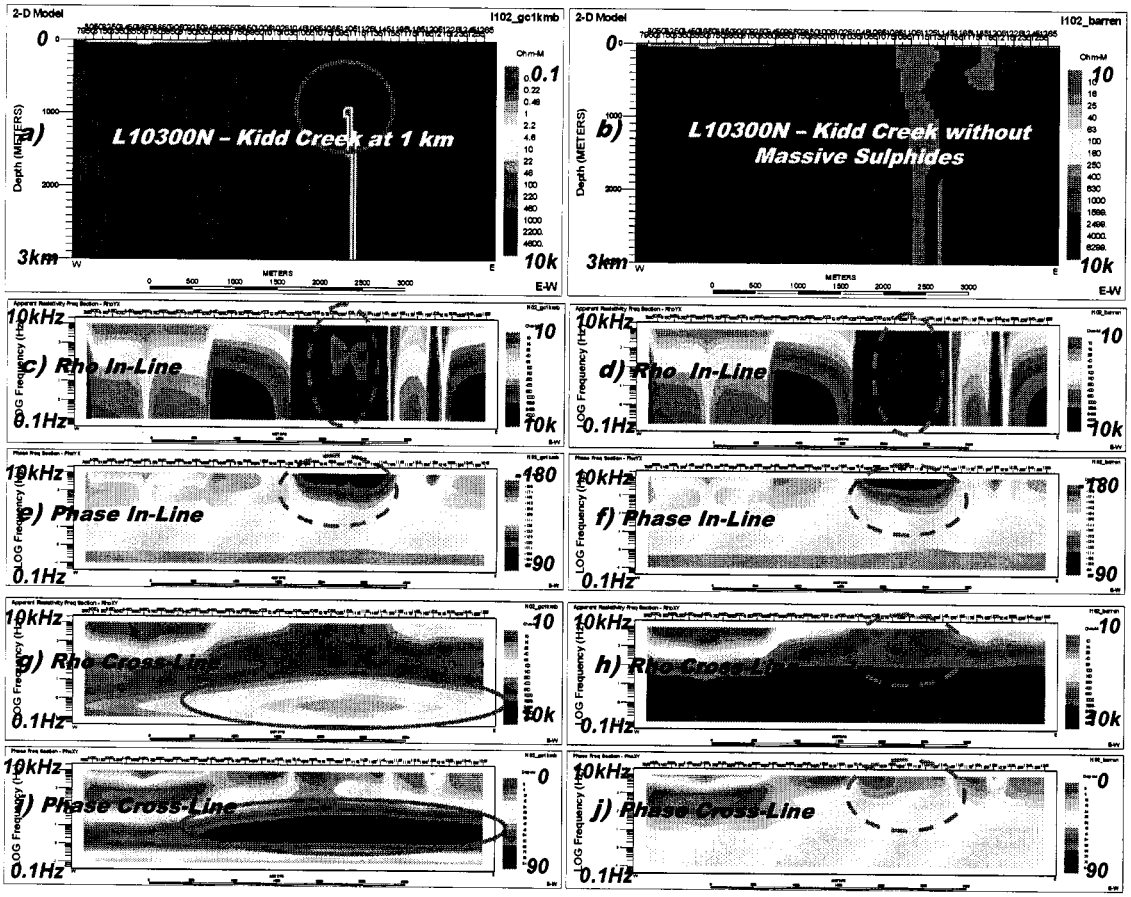

Figure 3.52: 2D MT Forward Models for Kidd Creek at 1 km Depth and for Barren Rhyolite

e) Depth = 2000m / MT Model

The fifth and final model, shown in Figure 3.53a, simulates the theoretical MT response of the Kidd Creek orebody, buried at 2km depths. Notice how the body is noticeably small, at this depth, relative to the cross-sectional geology. As with the previous model, the resistivity for the massive sulphide has been lowered to 0.1 from 10 Ω-m, to make it more reasonably detectible at this depth. As in the preceding example, below it, there are four pseudosections of data for this model (see Figure 3.53cegi), for each of the four components measured, as shown. Similarly, next to the 2km model, in Figure 3.53b, is the model for a barren rhyolite horizon without the Kidd Creek orebody, for comparison, along with

each of its four component responses (Figure 3.53dfhj). All apparent resistivity pseudosections are logarithmically-zoned to a minimum-maximum range of 10 to 10k ohm-m, and the phase sections are linearly zoned, either from 0 to 90 degrees (Cross-line) or -180 to -90 degrees (In-line).

Distinctive features are worth noting in each of the pseudosections:

1. The In-line apparent resistivity pseudosections (Figs. C and D) exhibit vertical striping, consistent with "static" effects, due to near-surface heterogeneities and which are frequency independent. Looking closely, each variation in the near-surface structure, either geologic contacts or overburden, triggers a static In-line response – including characteristic high/low resistivity features at the edge of each feature. As in the previous buried models, the Kidd Creek orebody at 2km does not feature a discernable In-line resistivity low anomaly (see dashed ellipse in Figure 3.53c). In fact, the barren model Figure 3.53d) is identical, featuring uniformly moderate resistivities across the rhyolitic horizon (dashed ellipse). The In-line mode is therefore insensitive to narrow, buried, subvertical conductors – even Kidd Creek-like orebodies at depths of 200m to 2km.
2. The In-line phase pseudosections below them (Figs. E and F) feature similar characteristics as the apparent resistivities but are relatively immune to "static" effects. These more accurately map true variation in lateral resistivity structure. However, as shown previously, the 2km deep Kidd Creek orebody response, in Figure 3.53e (dashed oval) is also not discernable – in fact the pseudosection is identical to the barren rhyolite response in Figure 3.53f. Clearly, the In-line component does not detect the massive sulphide orebody, buried at depths of 200m to 2km, either.
3. The Cross-line apparent resistivity pseudosections (Figs. G and H) display smooth variations across the geologic contacts and do not exhibit "static" effects. In contrast with the In-line component response, the 2km deep Kidd Creek orebody is defined in Figure 3.53g as a buried, mod-weak, dif-

fuse resistivity low at very low frequencies (red oval), which almost 2x as broad (≈4km) as the target-depth. However, in spite of the higher conductance target, its overall strength has diminished significantly – in the resistivity range is more similar to the 500m deep, 10 ohm-m model. Finally, as with the previous models, the barren model (Figure 3.53h – dashed oval) is uniformly resistive across the North Rhyolite.

4. The Cross-line phase pseudosections (Figs. I and J) are similar in character to the cross-line apparent resistivities. The Kidd Creek orebody at 2km is defined by a broad (≈4km), moderate strength, low frequency phase high (red oval). In contrast with the more muted apparent resistivity response, the phase still features a well-contrasted anomaly – although it is more layer-like. The phase response across the North Rhyolite, in the barren model is a weak, high frequency phase high (dashed oval), in response to the lower bulk resistivity in the rhyolitic horizon.

Clearly, from these results, at a 2km burial depth, the Kidd Creek deposit should be discernable in two of four components, at the lowest frequencies, in the Titan MT raw data – specifically, the Cross-line phase and to a relatively lesser degree in the apparent resistivity. In spite of the fact its presence would also be felt >1500m away, its broad, regional-like character could easily be misconstrued as a layered response. Furthermore, based on the Titan's low frequency bandwidth and the inversion depth limits to half the length of the profile (defined as its "aperture"), it appears that 2-2.5km also represents the practical limit to the depth of investigation of the Titan surveys at Kidd Creek mine site.

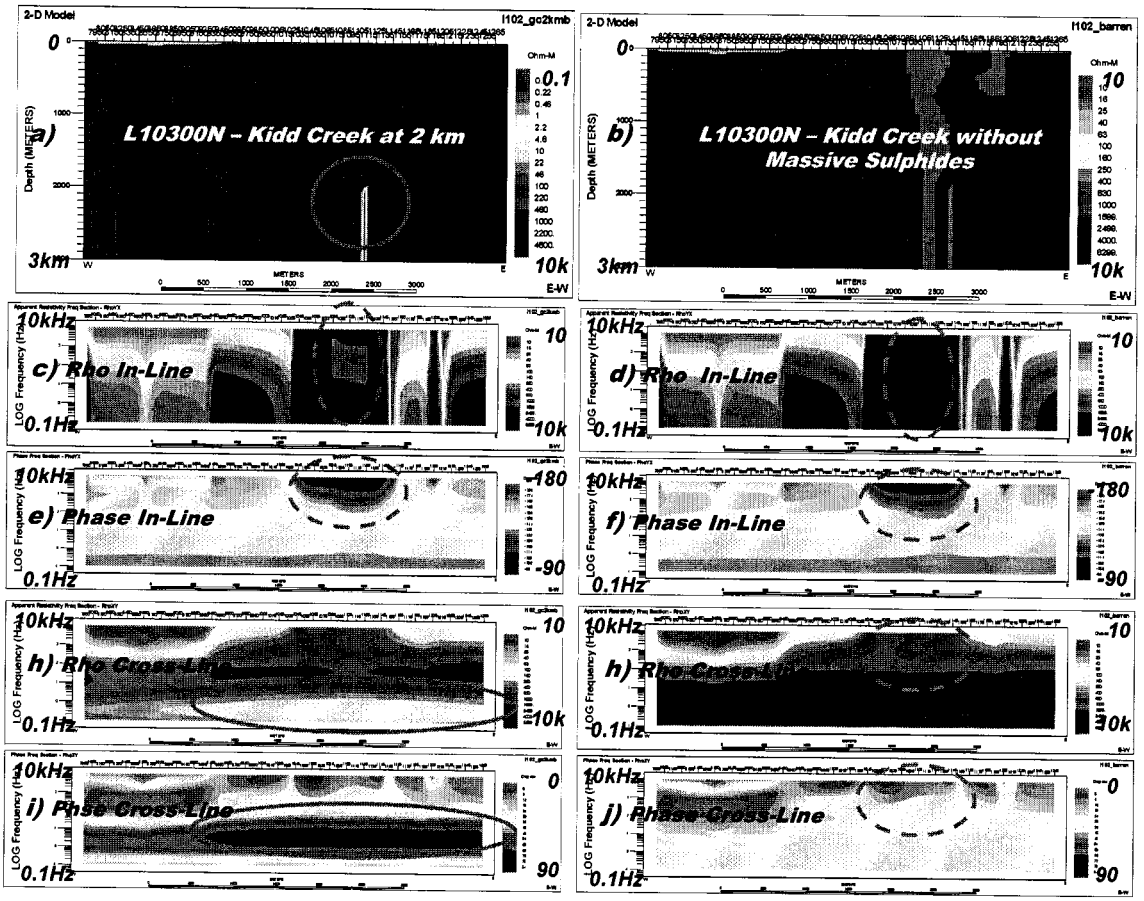

Figure 3.53: 2D MT Forward Models for Kidd Creek at 2km Depth and for Barren Rhyolite

3.4 Survey Results

The Titan-24 magnetotelluric and DC resistivity and induced polarization data at Kidd Creek were acquired in 11 survey days, between December 11TH and 22ND, 2001. In total, 23.4 line-km of MT and DCIP were acquired along 5 profiles, spaced 200m apart, and having a length of 4.0 to 4.8 km (Figure 1.2). The Titan arrays generally consisted of 32 in-line dipoles (channels) and 16 orthogonal, cross-line dipoles (see Figure 1.3), for a total array length of 3200m. Two arrays were required to complete each profile and each array was generally read in 1 survey day – first with DCIP, followed by MT. The array overlap was generally 10 stations for each profile.

The DCIP surveys used a station spacing of 100 metres. The Center-pole array central current pole was situated near the center of the array and the maximum AB size was 3600 metres. The survey procedure generally consisted of currents being injected between the in-line dipoles, generally at 100m spacings, sequentially from one end of the array to the other. At each current injection site, all array channels were recorded. The transmitted signal was a 30/256 Hz square wave at 100% duty cycle (~4sec Pos./Neg.) and currents varied between 1.5-17 amperes. Full waveform measurements were obtained at a receiver sampling rate of 480 samples per second, and 15-30 cycles were recorded. Although orthogonal dipole measurements were retained, only the in-line dipole data were studied. A total of 8414 dipole measurements were obtained. The data were reduced to a time-domain decay, and the results fit to a Halverson-Wait spectral model (see Sec. 2.1.2), using a 800 to 2133 millisecond window (see Figure 3.56) – the purpose of which is to fit the decays to a common 'IP standard', with a sufficient delay to avoid the effects of EM coupling, in early times. A voltage and phase (milliradians), with associated errors, was derived for each dipole measurement, and the results stored in a CSV (comma spaced value) ASCII file similar to a Geosoft DAT format.

The MT surveys were read using the same array as the DCIP, augmented by magnetic sensors, and with a remote-reference site situated 25km west, for noise rejection purposes. Both the in-line and orthogonal electric field dipoles were measured, with each alternating cross-line dipole being pared with two in-line dipoles to constitute a sounding site. A single orthogonal pair of magnetic sensors, centrally placed along the array, was used to normalize the electric field data into their respective E/H tensor impedances. Measurements spanned the 0.1 to 20,000 Hz bandwidth, but recordings were separated into the low, medium and high frequency bands, with sampling rates of 120, 9600 and 48k samples per second. The data were reduced to auto and cross-power spectral estimates, and output to unrotated, In-line (XY) and Cross-line (YX) tensor impedances,

along with their associated errors. Soundings consist of apparent resistivity and E/H phase, band-averaged to 8 points per frequency-decade. In total, 468 soundings were obtained, with a 10 station overlap per line. The MT data were stored in a EDI (electronic data exchange) format ASCII file, according to the SEG industry standard.

A more complete description of the Titan system and survey parameters is provided in the survey logistics report (Legault et al., 2002a). Both the raw and final-processed results, including preliminary 2D smooth inversion modeling, are also presented digitally in Oasis Montaj GDB database and cross-sectional MAP plot formats, in Legault et al., (2002b).

3.4.1 DCIP Surveys

The Titan apparent resistivity data for the five profiles surveyed at Kidd Creek are presented as stacked, Center-pole array pseudosections in Figure 3.54. The pseudosections are presented from bottom to top, representing south to north, and with the view looking north. The five pseudosections are similarly colour zoned, with the data spanning the 10 to 10,000 ohm-metre range. As shown in the pseudosections, the data are generally of an excellent data quality, due the high currents and bedrock resistivities. In general the calculated data error is <0.1% of the voltage and the data presented contain a maximum error of 5%. As shown, nearly 99% of the data have been retained. No "bull's-eyes" and few visible gaps in the pseudosections from bad data are observed, in particular for the lines closest to the mine-site, with the possible exception of the eastern-most edges of the profiles, where the effects of power lines are felt. These results prove the Titan arrays capability to obtain high quality data, in the presence of heavy conductive overburden, a noise-contaminated environment, and in winter conditions.

Although difficult to interpret on their own, in general, the Center-pole DC pseudosections indicate a general increase in resistivity and stronger contrasts

towards the east - consistent with the known geology and thinner overburden cover. Thicker portions of overburden occur in the central part of the profiles, but the Titan DC results seem to indicate no problems in easily penetrating into the bedrock. Moderate to weak resistivity lows also generally coincide with the position of the known rhyolitic horizons and graphitic units, which also appear to be depth extensive.

The Titan chargeability data are presented in stacked, Center-pole (center-pole) array pseudosections in Figure 3.55, with the view looking north. The five pseudosections are also similarly colour zoned, with the data spanning the -1 to 30 milliradian range, with occasional maxima exceeding 50 mrad. As shown in the pseudosections, the data are generally of an excellent data quality, due the high currents and bedrock resistivities. In general the calculated data error is <0.1milliradians, and averages 0.5mrads. The data presented contain a maximum error of 5mrad, and negative values below –5 have been removed. As shown, nearly 95% of the data have been retained. Few "bull's-eyes" and only minor gaps are visible in the pseudosections from bad data removed, which appears limited to lines closest to the mine-site and at easternmost edges of the profiles, where the effects of power lines are felt. Examples of typical DCIP chargeability decay curves are shown in Figure 3.56, for various current dipole sizes and receiver-transmitter separations. The quality of the decays and their low levels of noise-contamination are obvious in these curves. These results prove the Titan arrays capability to obtain high quality chargeability data, which only represent a small fraction of the voltage signal, in the presence of heavy conductive overburden, a noise-contaminated environment, and in winter conditions.

Although difficult to interpret on their own, in general, the Center-pole IP pseudosections also indicate a general increase in chargeability and stronger contrasts, consistent with the known geology and thinner overburden cover. Thicker portions of overburden occur in the central part of the profiles, but the Ti-

tan DC results seem to indicate no problems in easily penetrating into the bedrock. In fact, the physical property contrasts appear to be better defined than in the resistivity data. A larger mixture of weak to strong chargeability highs are defined, with the strongest generally coinciding with the position of the known rhyolitic and graphitic units, which also appear to be depth extensive.

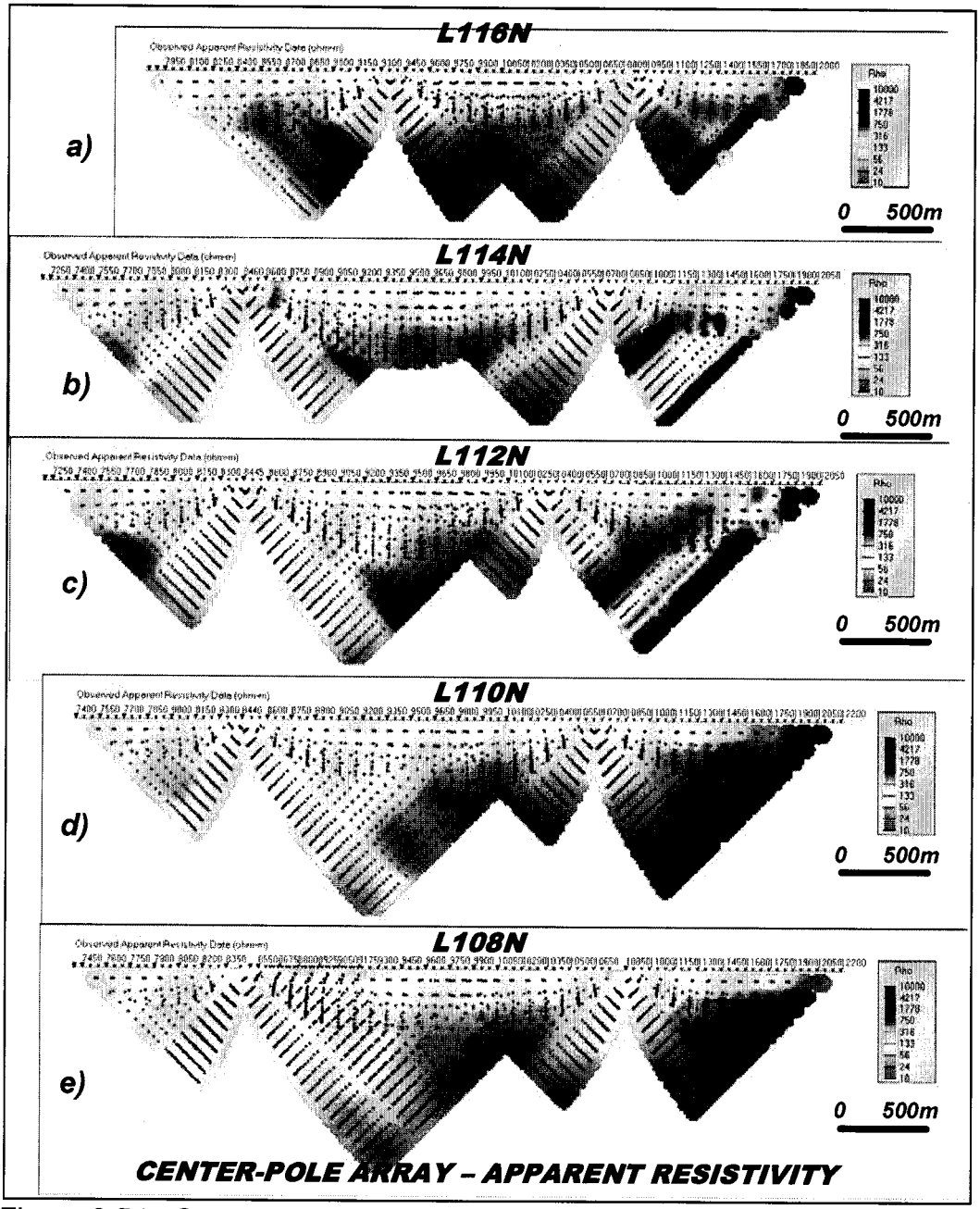

Figure 3.54: Center-pole Array DCIP Apparent Resistivity Pseudosections.

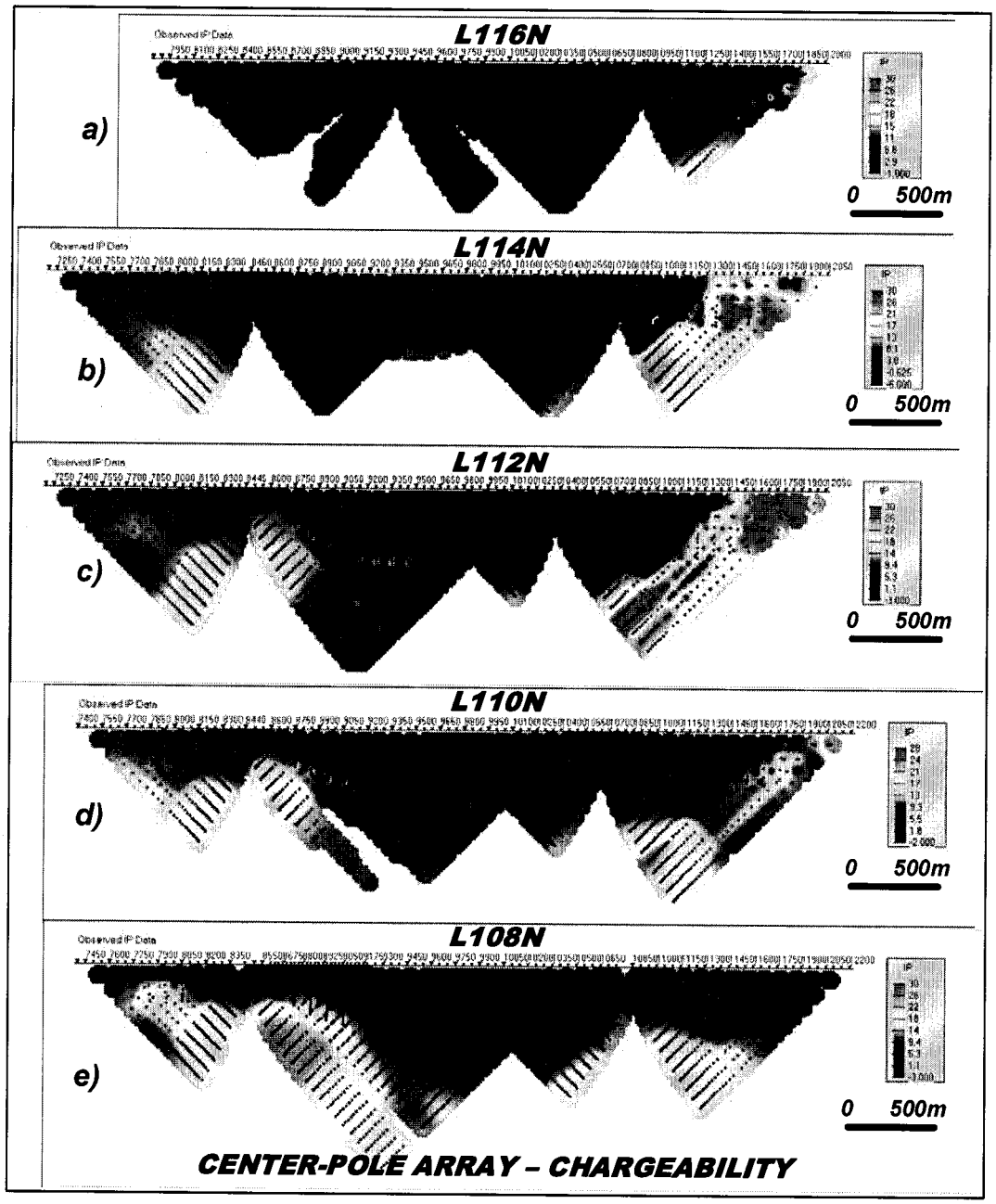

Figure 3.55: Center-pole Array DCIP Chargeability Pseudosections

In order to better visually interpret the data, the Titan apparent resistivity and chargeability data are presented along side each other, in Figure 3.57, in their dipole-dipole (dpdp) equivalent pseudosections, according to the superposition method described in Legault et al. (2002b) and more recently published in

Kingman and Garner (2003). The pseudosections are presented from bottom to top, representing south to north, and with the view looking north. The five pairs of pseudosections are similarly colour zoned identically to the previous Center-pole array format results. The superposed dipole-dipole pseudosections represent a=100m data, from two overlapping array pairs, providing separations of n=0.5 to 31.5 maximum, whose data redundancy provides them with 50m lateral resolution. These data have been presented Oasis cross-sectional map and database form in the logistics report (Legault et al., 2002a).

As shown in Figure 3.57, the dpdp data display much sharper contrasts than their Center-pole array equivalents, in part due to a 1st-derivative-like effect that "differencing" to superposed dipole-dipole causes, and also because the Center-pole plots are adversely affected by the mixture of gradient, pole-dipole and dpdp array signatures (see Figure 3.56) which is inherent in the Center-pole pseudosection presentation. However, this "differencing" also results in accentuating the noise higher levels in the dpdp pseudosections relative to the Center-pole data. In fact, while the DC dpdp pseudosections display coherent signatures to below n=30, the IP pseudosections are visibly distorted below n=15-20 – in sharp contrast to their high quality Center-pole equivalents. Quantified data errors are not carried through in the superposition calculations, however the errors in the input voltage and phase values are identical to the Center-pole results, i.e., 5% maximum for the primary voltage and ±5mrads, with values less than –5mrads omitted for the phase. As shown, in spite of the increased level of noise, better than 90-95% of the data have been retained. Indeed few "bulls eyes" and visible gaps are observed in the DC pseudosections, in particular, and in spite of the poorer quality, deep IP data, near surface and moderate depth features (≈350m equivalent depth) are still more easily discerned in the dpdp IP pseudosections. In fact, in terms of interpretability, the benefits of superposition appear to outweigh the drawbacks in terms of poorer signal-to-noise.

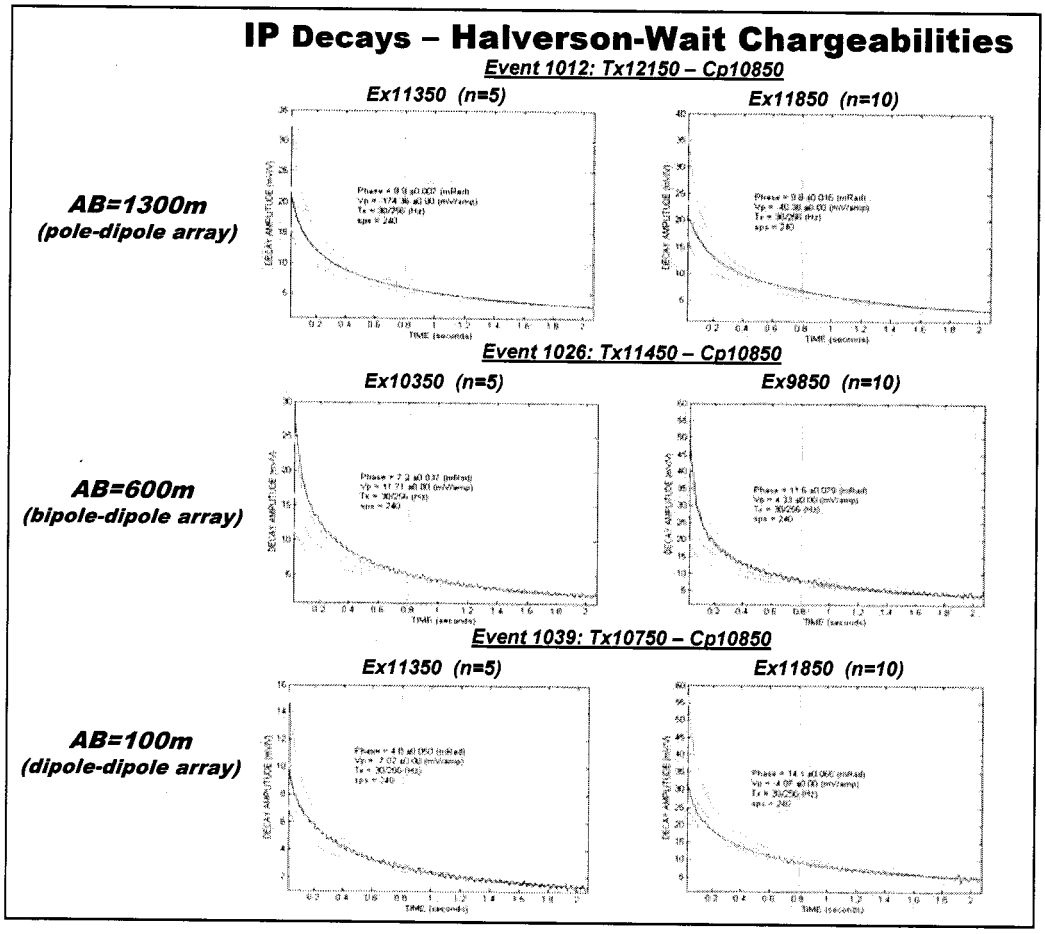

Figure 3.56: Titan-24 DCIP Chargeability Decay Curve Comparisons.

The apparent resistivity pseudosections also indicate a general increase in resistivity and stronger contrasts to the east - consistent with the known geology and thinner overburden cover. Thicker portions of overburden occur in the central part of the profiles, but sections appear to easily penetrate the bedrock. Major resistivity lows coincide with the position of the known rhyolitic horizons and graphitic units, which also appear to be depth extensive. In addition, minor resistivity lows, not discerned in the Center-pole results, from smaller bedrock conductive zones correlate with narrower rhyolites or remain unexplained. For the most part, resistivity lows coincide with analogous chargeability highs, indicating massive or stringer mineralization. Additional IP anomalies, uncorrelated to the DC results, indicate disseminated sulphide zones, which are unexplained in the

geologic model. For the most part, clear-cut anomalies are more easily interpreted in the upper portions of the pseudosection. Deeper signatures are likely also present, but are masked by combined anomaly overprints, from the near surface zones, as well as hidden in the noise. Clearly, 2D inversions are required to properly interpret the Titan DCIP data.

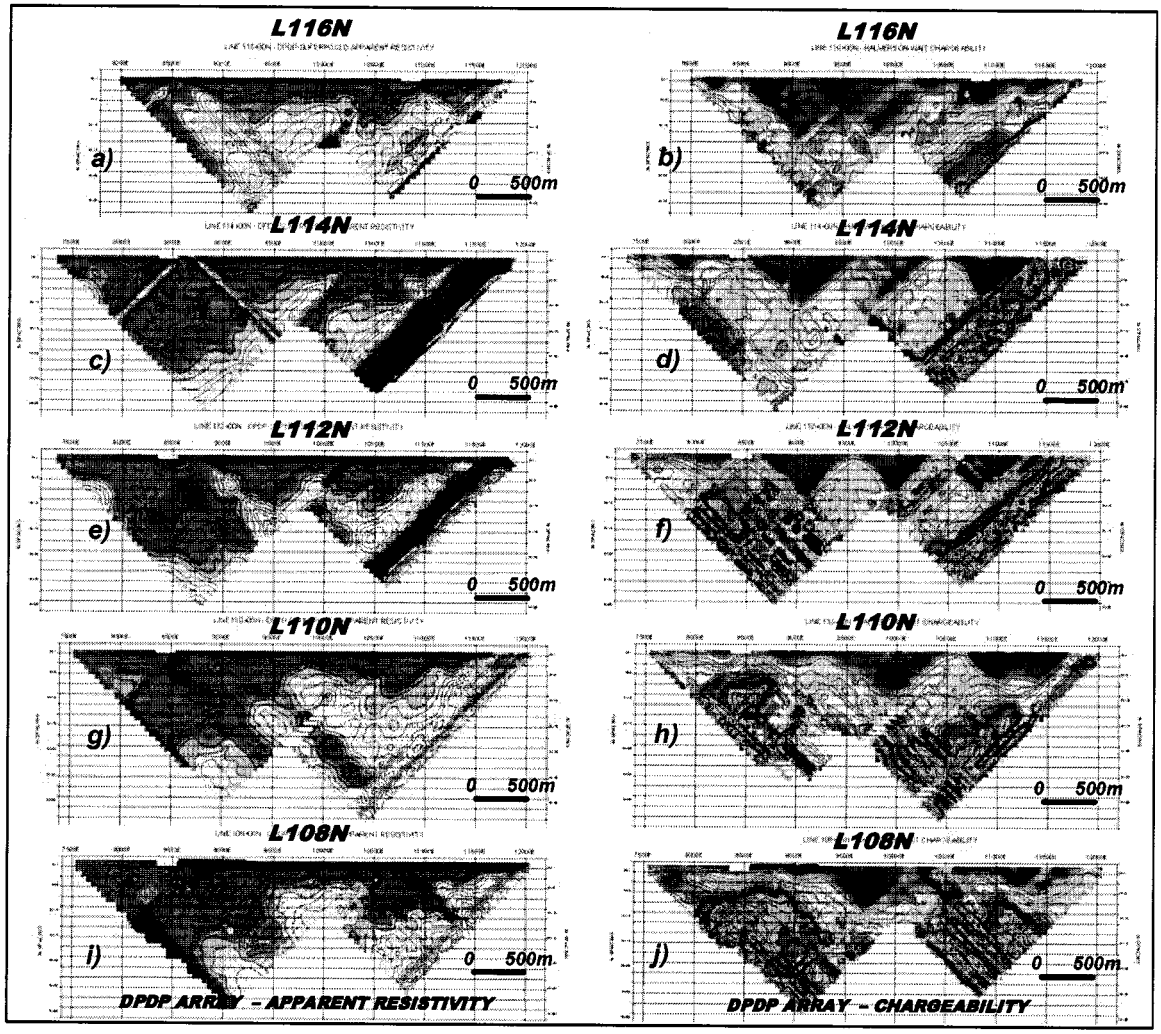

Figure 3.57: Superposed Dipole-Dipole Array DCIP Apparent Resistivity and Chargeability.

3.4.2 MT Surveys

a) Raw Unprocessed (non derotated) MT Data

The raw Titan MT apparent resistivity and phase data for the five profiles surveyed at Kidd Creek are presented as stacked, frequency pseudosections in Figure 3.58 for the In-line component data and Figure 3.59 for the Cross-line data. These data represent the scalar (Cagniard) values assuming the geoelectric strike is perpendicular to the survey line (see Section 2.2.3). The pseudosections are presented from bottom to top, representing south to north, and with the view looking north. The vertical scale represents frequency, spanning 5 decades, from 0.1 Hz, at the bottom of each pseudosections, to 10kHz at the top. The 10 apparent resistivity pseudosections, shown on the left of each figure, are similarly colour zoned, with the data spanning the 10 to 10,000 ohm-metre range. Typically, sounding curves span 3 decades of frequency, reflecting strong layered-earth contrasts. The impedance phase pseudosections are equal-area zoned to fit the data, which easily vary between 0-90 degrees, reflecting to the high resistivity contrasts shown in the sounding curves.

Visually, the data are generally of an excellent data quality, due in part to the noise rejection capabilities of the Titan array processing stream, and to high bedrock resistivities, as well as good natural field signal levels. In fact, weak natural fields in the 300-3kHz bandwidth, known as the "dead band", are typically absent from the sounding curves, as shown in Figure 3.60. As shown, very few edits were generally required for the data, and error bars for points in the sounding curves are not visible - indicating error levels <3degrees for the phase and <0.05 decades for the apparent resistivity. Few "bull's-eyes" and few visible gaps in the pseudosections from bad data are observed - in particular for the lines closest to the mine-site, with the possible exception of the easternmost edges of the profiles, where the effects of power lines and conductive graphites are felt. These results prove the Titan arrays capability to obtain high quality data, in the

presence of heavy conductive overburden, a noise-contaminated environment, and low natural field signal levels in winter conditions.

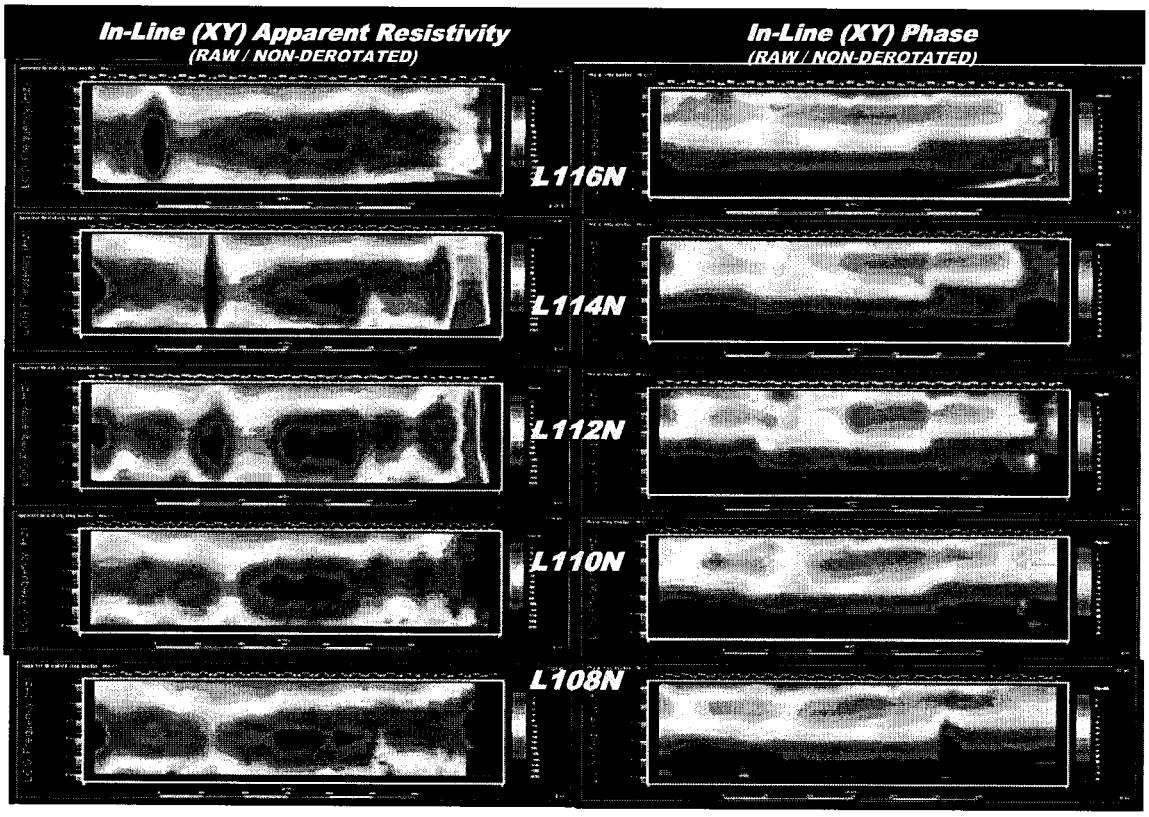

Figure 3.58: Raw (non-derotated) MT Resistivity and Phase for In-Line (XY) Component Pseudosections (view looking north.

Although difficult to interpret on their own, the MT pseudosections indicate a general increase in resistivity and stronger contrasts, consistent with the known geology and thinner overburden cover. Thicker portions of overburden occur in the central part of the profiles, but the Titan MT results clearly indicate no problems in easily penetrating into the bedrock. In fact, as shown in Figure 3.60, skin depth penetrations exceed 10km in nearly all soundings (based on the resolution of the deep crustal conductive response described by Hyndman and Hyndman (1968), Jones (1981) and Kurtz et al. (1993)). Static-like (frequency independent), moderate to weak resistivity lows also generally coincide with associated phase highs, relating to known rhyolitic horizons and graphic units, some which

also appear to be depth extensive. Resistivity signatures which are uncorrelated with associated phase responses are rare, suggesting that static shift from near-surface heterogeneities, such as conductive overburden pockets, are not significant.

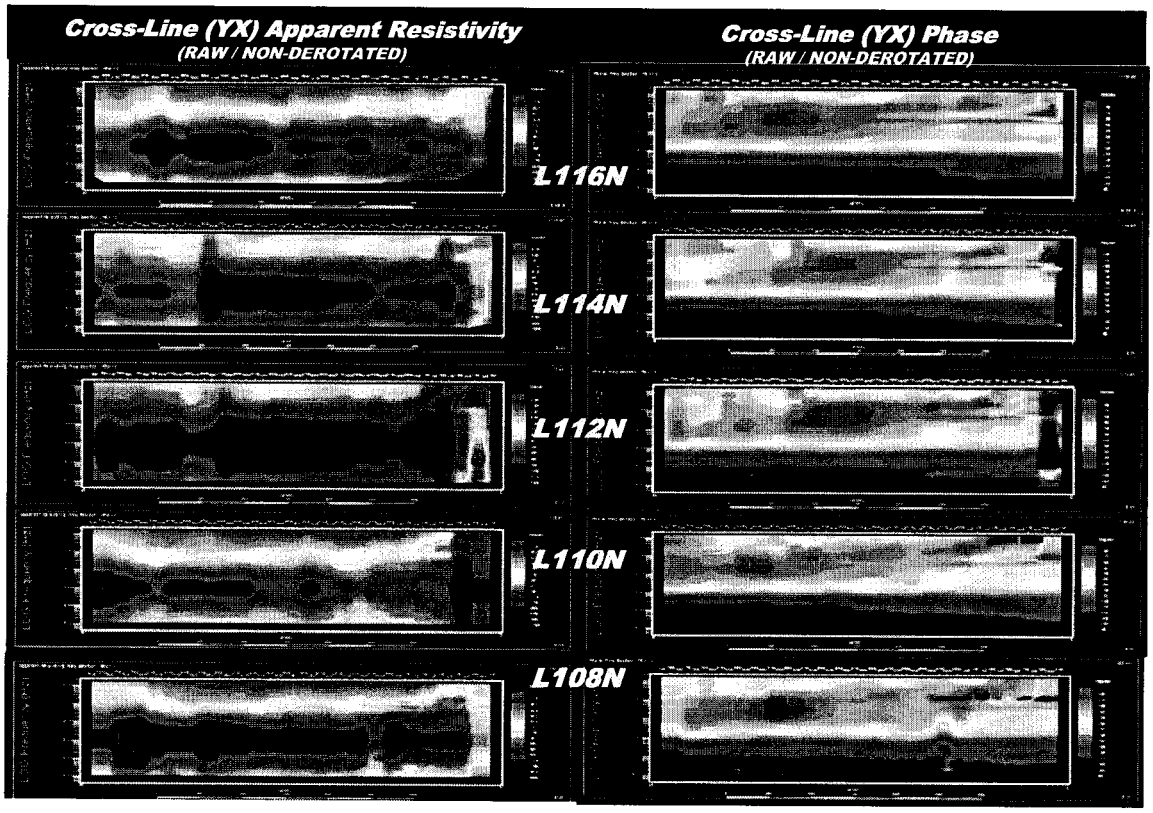

Figure 3.59: Raw (non-derotated) MT Resistivity and Phase for Cross-Line (YX) Component Pseudosections (view looking north).

Overall, however, the lateral contrasts are weak, in comparison with the DCIP evidence. Moreover, examining the pseudosections, both components look similar, lack contrasts and don't exhibit typical 2D In-line and Cross-line behaviour, particularly for the sounding to the west. Examining, many of the raw sounding curves, they appear isotropic (1-dimensional – see Figure 3.61a), where the In-Line and Cross-line component curves are very similar. In fact, this is directly attributable to the geology, which is oblique to our Titan profiles, particularly in the western survey area (see Figure 3.10). Figure 3.61 shows a typi-

cal Kidd Creek MT sounding curve, prior to and after mathematical de-rotation of the data, parallel and perpendicular to the geoelectric strike directions. As shown, after de-rotation, the two sounding curves become anisotropic. which contributes to stronger vertical and lateral resistivity contrasts – both of which are key elements in correctly defining the bedrock resistivity structure with 2D inversions.

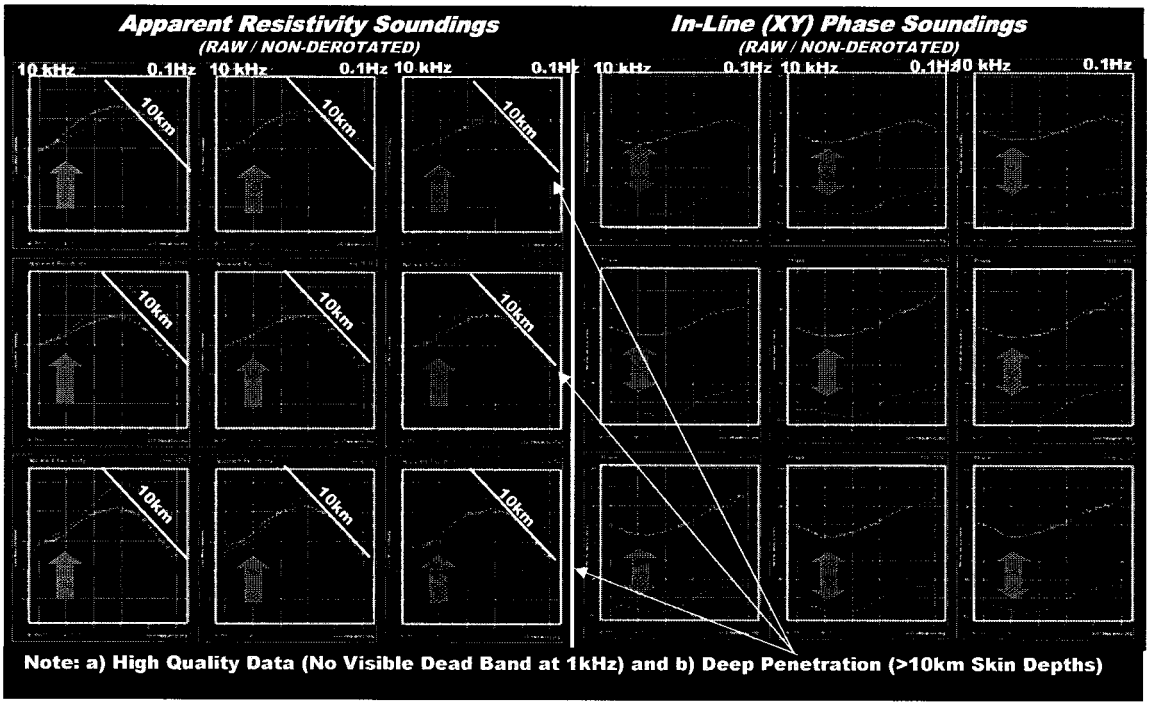

Figure 3.60: Examples of Raw MT Apparent Resistivity and Phase Sounding Curves at Kidd Creek

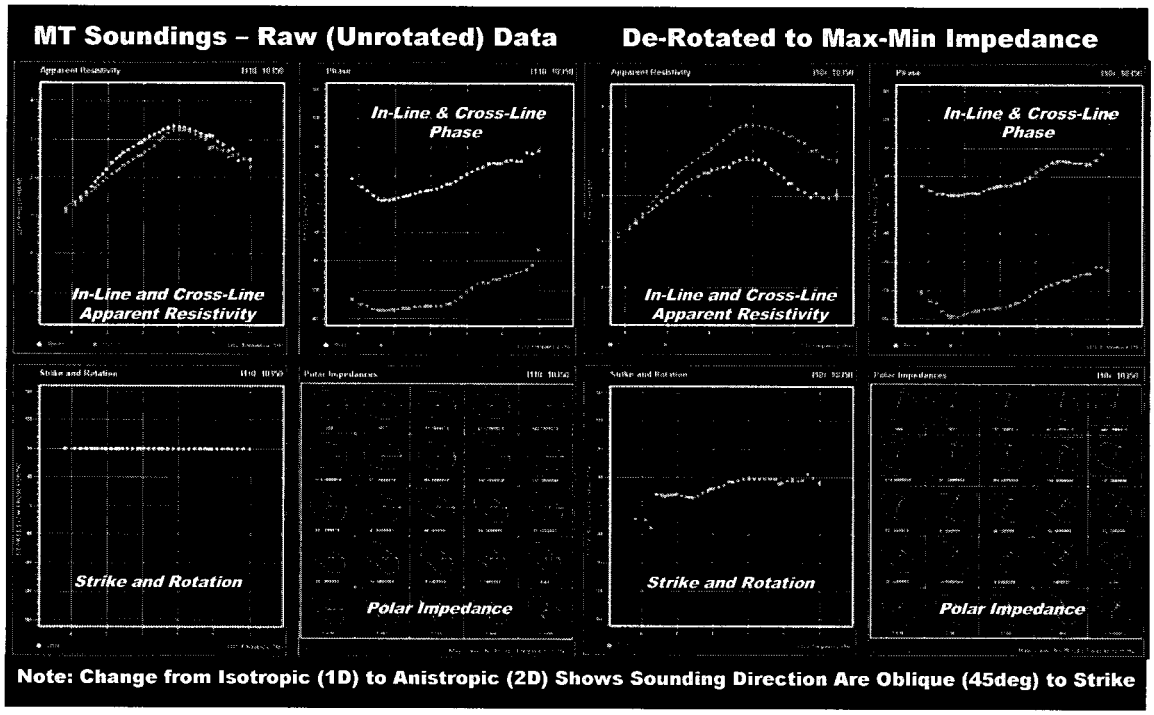

Figure 3.61: Tensor MT Parameters Before and After De-Rotation for a Typical Kidd Creek Sounding.

b) Final EVA processed (derotated) MT Data

The final, de-rotated MT pseudosections from Kidd Creek are presented in Figure 3.62 and Figure 3.63, for the TM and TE components respectively. In both figures, the stacked frequency pseudosections on the left represent the apparent resistivities and those on the right are the impedance phases – with northernmost to southernmost lines arranged from top to bottom, with the view looking north. The vertical scale also represents frequency - spanning 5 decades – from 0.1 Hz at the bottom of each pseudosection, to 10k Hz at the top. The colour zoning for pseudosections are identical to those shown previously, with the apparent resistivities spanning 10 to 10k ohm-m and the phases ranging from 0 to 90 degrees.

The EVA-derotated apparent resistivity and phase pseudosections show great similarity with the unrotated data, in terms of overall structure, except for

slightly stronger contrasts for the horizontal layering, as described in Figure 3.61, which is more evident in the phases. However, lateral contrasts are also not pronounced as they were in the non-rotated data, as compared to the DC resistivity, due to the dampening effects of the heavy clay overburden.

Of note, however, is the more well behaved nature of the EVA processed pseudosections, over the raw unrotated data, particularly near the easternmost ends of the lines where "phase rolling out-of-quadrant" (PROQ) data (Chouteau and Tournerie, 2000) were earlier prevalent. In fact, these effects were easily corrected following de-rotation using EVA processing, and are therefore examples where relaxing the assumption that the E- and H-fields are orthogonal, in eigenvector analysis (Eggers,1982); Spitz ,1985) provides an effective method for simplifying complex 3D data, as described in Section 2.2.4.

Although difficult to interpret on their own, the MT pseudosections define apparent resistivity lows and more subtle phase highs that correspond with known mineralization, including a) the Chance horizons to the west, b) the North Rhyolite horizon to the east and c) the Kidd 66 graphites to the north east. However, the absence of anomalous phase, in particular, "out-of-quadrant" data – exceeding 90 to >180 degrees – is perhaps significant from an exploration standpoint. This is due to the fact that these types of phases are indicative of 3D behaviour, typically relating to the channelling of currents into and around highly conductive features – sometimes observed below buried pipelines and mine tailings at surface, but sometimes also observed below massive sulphide deposits, as described at the Levack mine by Stevens and McNeice (1998), and Legault et al. (2003), at the Trilabelle Ni-Cu deposit (Livelybrooks et al., 1996) and in other volcanogenic massive sulphide environments, as described in Legault et al. (2002c). In all cases, although difficult to interpret using 2D inversion algorithms,

these types of anomalous MT responses nevertheless pointed to significant conductivity at depth. Hence, the absence of anomalously high and PROQ phase

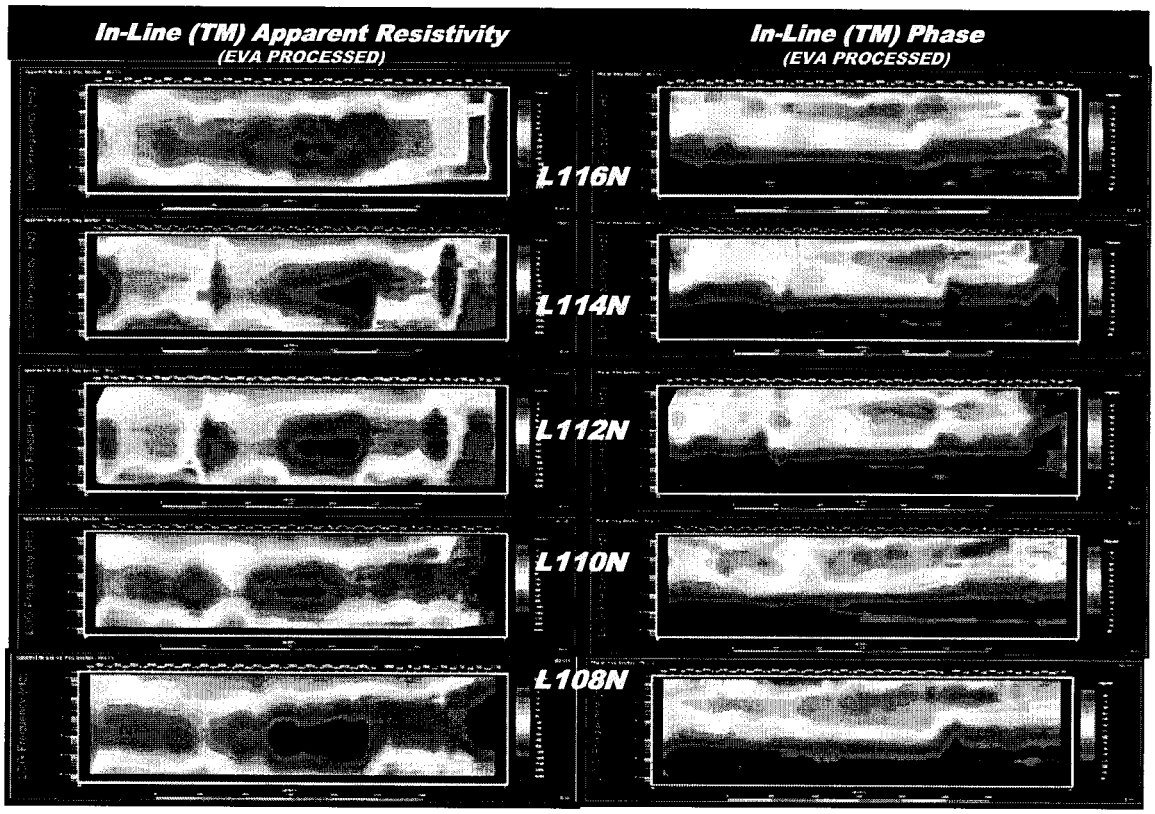

behaviour might lessen the potential for buried conductors in the Titan survey area, analogous to Kidd Creek.

Figure 3.62: EVA Processed (derotated) MT Resistivity and Phase for Cross-Strike (TM) Component Pseudosections (view looking north).

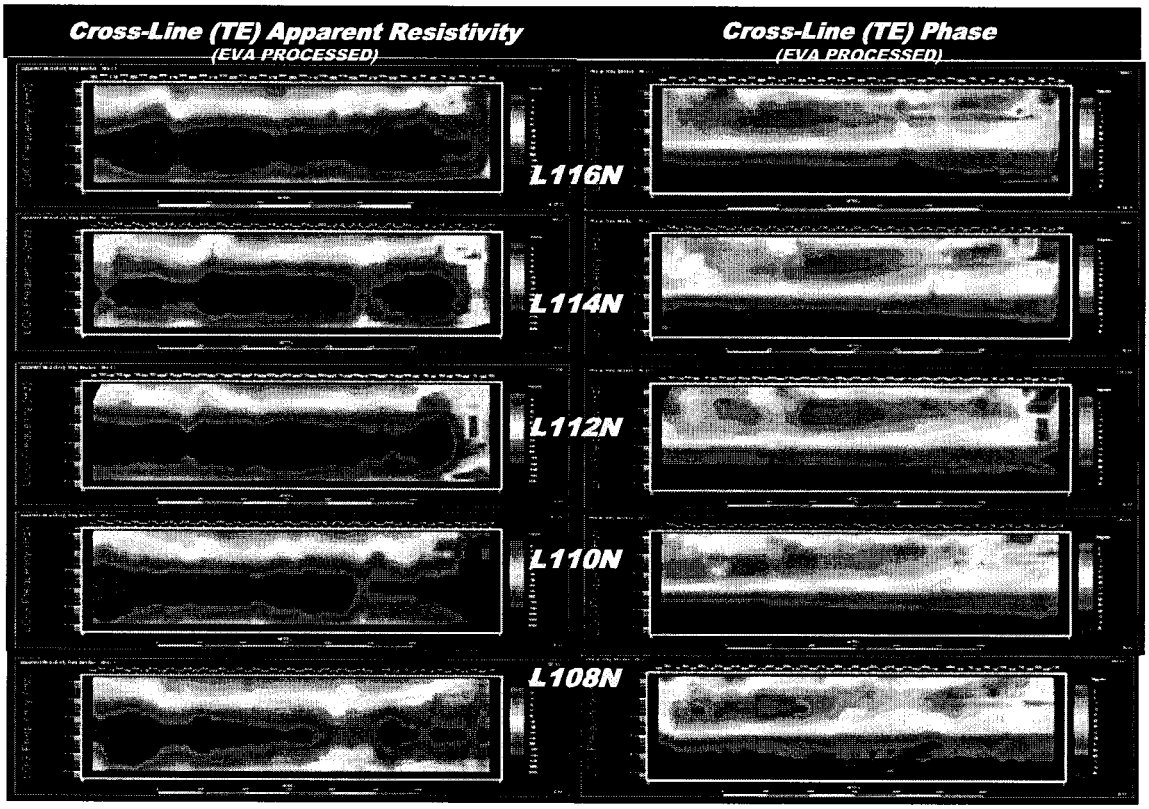

Figure 3.63: EVA Processed (derotated) MT Resistivity and Phase for Along-Strike (TE) Component Pseudosections (view looking north).

3.5 Unconstrained Inversions

3.5.1 DCIP Surveys

The results of unconstrained (non geologically referenced) 2D DCIP inversions are presented in Figure 3.64, for the "smooth" models and Figure 3.67, for the "sharp" models. As described in Section 2.3, "smooth" models emphasize model smoothness over data fit or resolution, but are effective in imaging lithologic-like geoelectric structures, where size, strength of contrast, vertical continuity and depth of investigation are important to distinguish in the data – well suited, in particular, to inversions of DC resistivity parameter, as demonstrated in the inversion sensitivity analyses, in Section 3.3.

In fact, this is borne out in the Kidd Creek Titan results where the smooth DC inversions, shown Figure 3.64acegi, appear to define the key rhyolitic and graphitic units, as moderate to strong resistivity lows – including indications of dip direction and vertical extent. The high degree of correlation between the DC resistivity and the geology is best observed inside the Gocad model, shown in Figure 3.65. As predicted in the sensitivity analyses, the DC inversions also appear to resolve the bedrock resistivity structure to below 750m depths. These results suggest that the unconstrained DC resistivity inversions provide an excellent lithologic mapping tool.

In marked contrast, the chargeability highs from the smooth unconstrained IP inversions, shown in Figure 3.64bdfhj, also generally coincide with corresponding DC resistivity lows, but their large, amorphous shapes appear to reveal little about the bedrock structure, as shown in Figure 3.66.

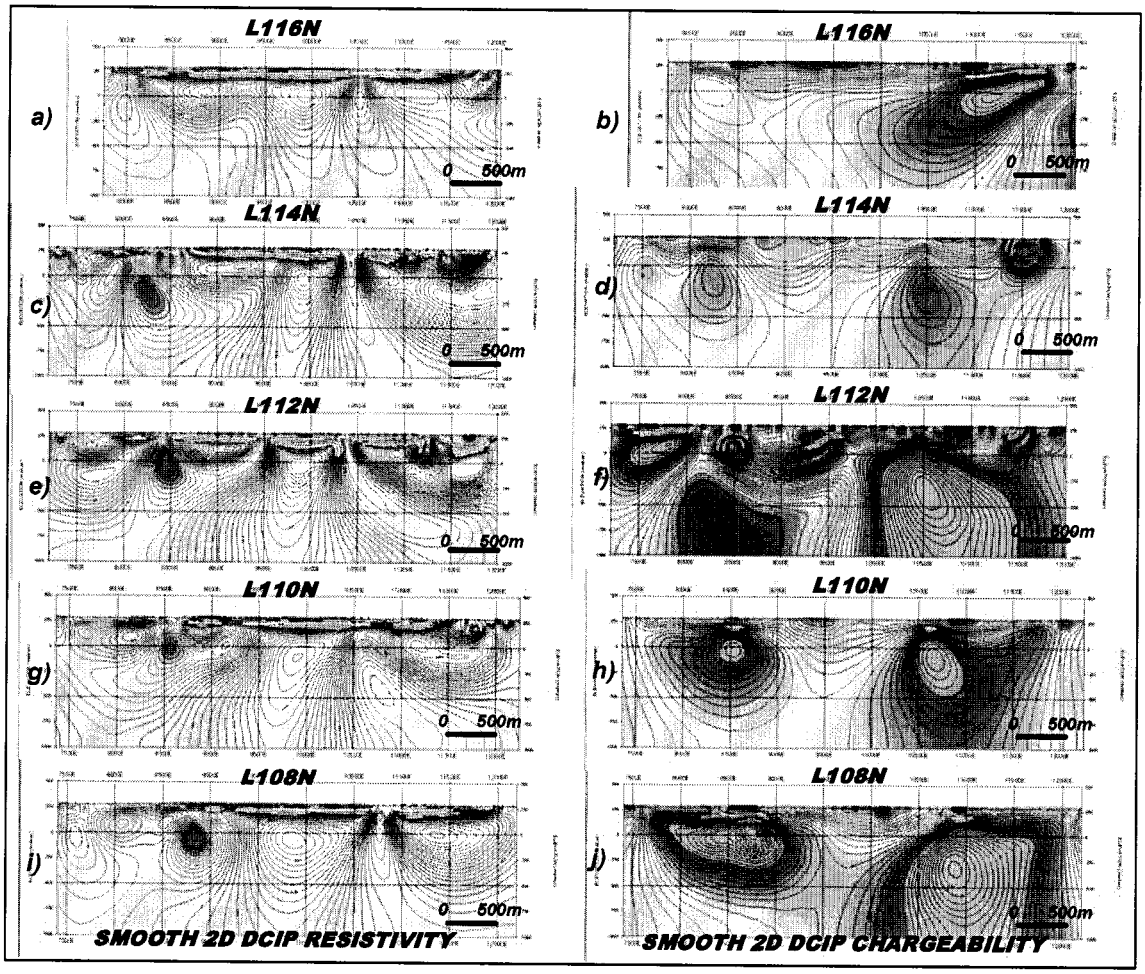

Figure 3.64: Unconstrained 2D DCIP Resistivity and Chargeability Inversions (Smooth Models) with view looking north

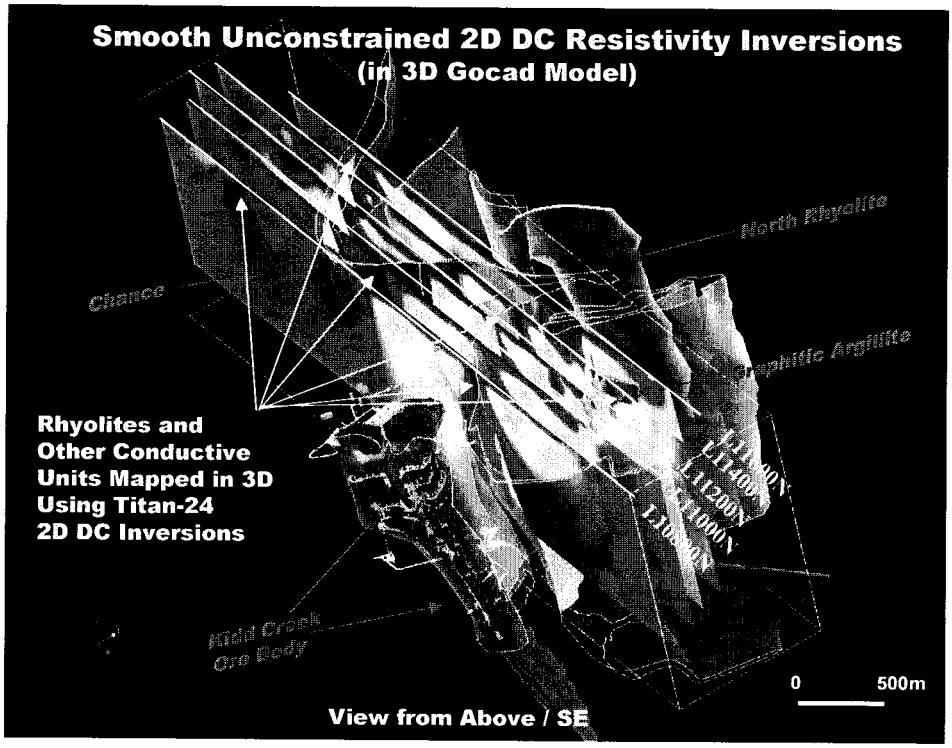

Figure 3.65: Smooth Unconstrained 2D DCIP Resistivity Inversions in Gocad

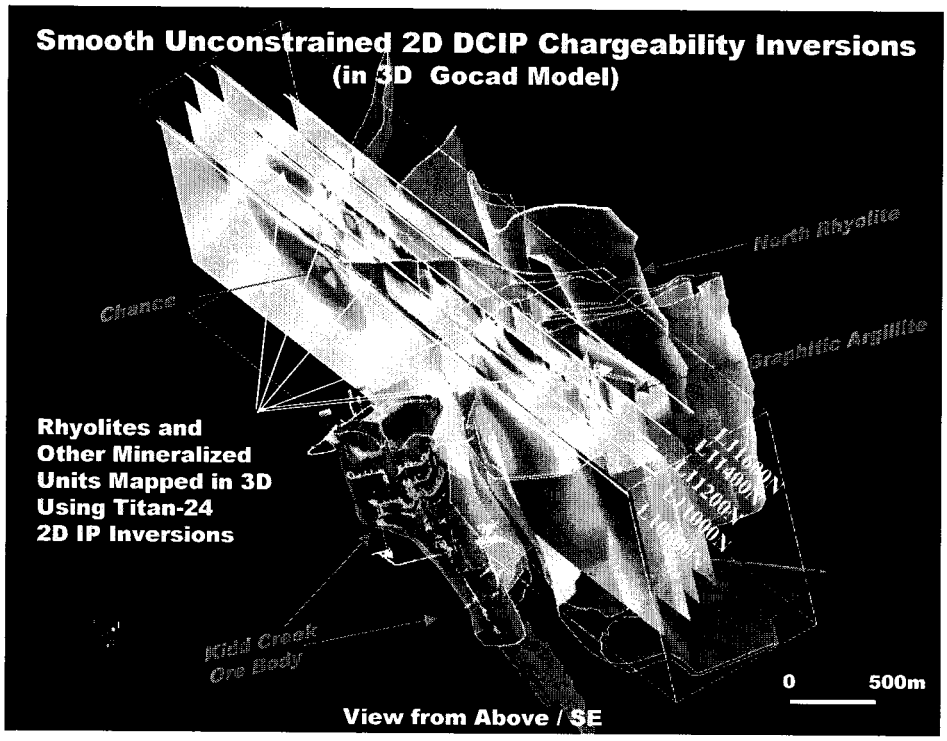

Figure 3.66: Smooth Unconstrained 2D DCIP Chargeability Inversions in Gocad

Figure 3.67 presents the "sharp" model, unconstrained DC and IP inversions at Kidd Creek. As described in Section 2.3, "sharp" models emphasize data resolution and fit over model smoothness, and as a results are effective in imaging small, orebody-like geoelectric structures– well suited, in particular, to inversions of IP chargeability parameter, as demonstrated in the inversion sensitivity analyses, in Section 3.3. The sharp DC and IP models, in addition to showing good correlation with the same resistivity lows and chargeability highs in the smooth unconstrained inversions, also detect and resolve additional smaller, multiple bodies – particularly in the IP. These appear to better explain, in particular for the IP, responses that have been ascribed to large, amorphous bodies in the smooth inversions. On the other hand, the vertical extent of these bodies is significantly smaller than obtained in the smooth models - rarely extending below 300-500m, as predicted in the sensitivity analyses in Section 3.3. Nevertheless, in spite of their poorer sensitivity to vertical extent as compared to the smooth inversions, the sharp models, due to their higher resolution, appear to successfully define additional anomalies which are unexplained by the geologic model, and merit further explanation and analysis in the following constrained inversions stages.

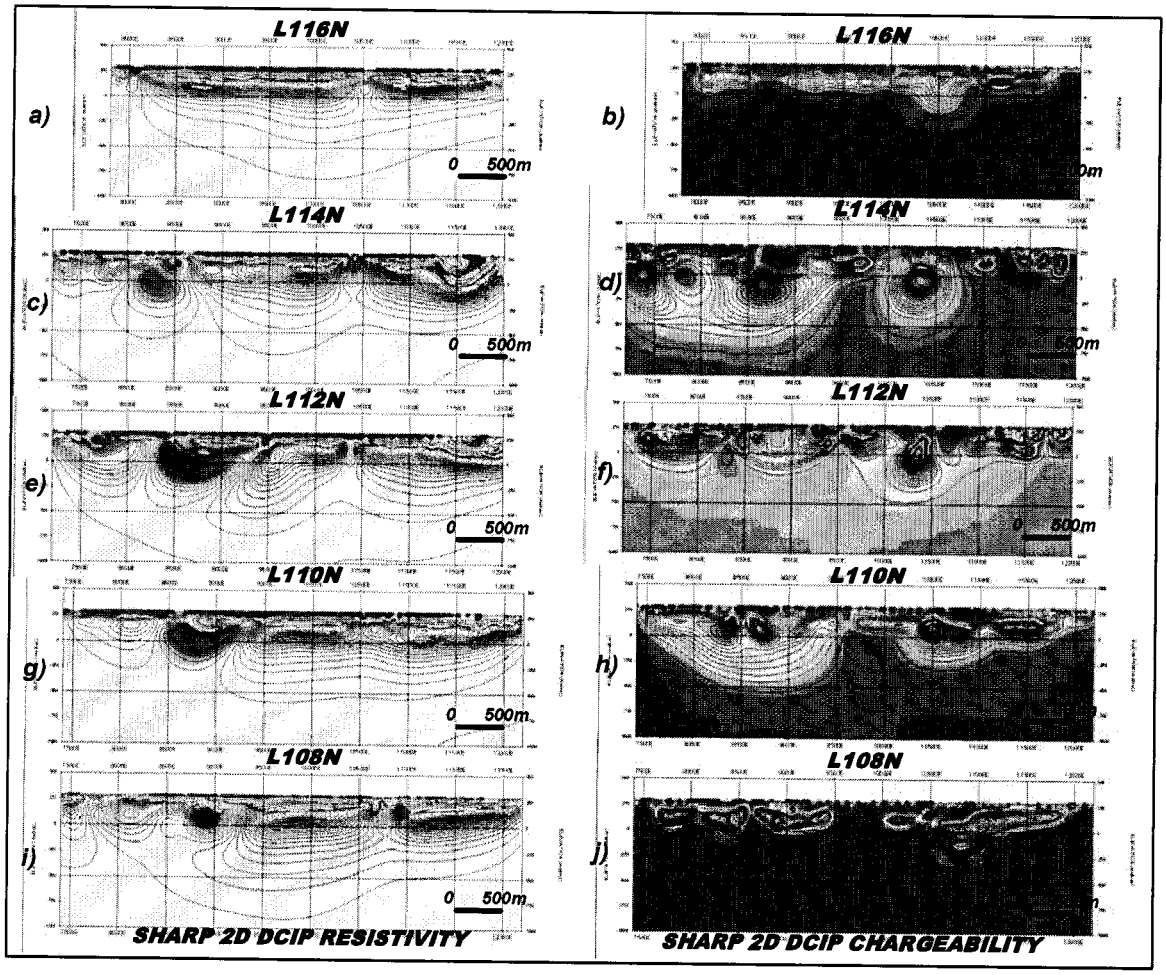

Figure 3.67: Unconstrained 2D DCIP Resistivity and Chargeability Inversions (Sharp Models) with view looking north.

3.5.2 MT Surveys

The results of unconstrained (non geologically referenced) 2D MT resistivity inversions are presented in Figure 3.68 for the preliminary, smooth-conjugate 2D models and Figure 3.69 for the advanced EVA-processed, PW inversions. The differences between the smooth-conjugate MT inversions and the EVA-PW MT inversions are analogous to the "smooth" and "sharp" model types described for the DCIP. The smooth-conjugate MT inversions were performed on the raw, non-derotated, MT data, using all four components (ρ_{XY}, ρ_{YX}, φ_{XY}, φ_{YX}) and were used as preliminary MT models in the interpretation.

As shown in Figure 3.68, the smooth conjugate MT results appear to detect much of the same conductivity structures as the unconstrained DC inversions, at least at surface, but, overall, to a much lesser degree of resolution, due to weak contrasts. This is particularly true at depths below 250-500m where few conductive features occur and most, near-surface zones pinch out – the sole exception being the L108N profile, which features a large (>500x500m), deeply buried (750m-1km) low resistivity zone below 11500E, which might represent an off-line/edge response to the Kidd Creek orebody, lying 500m south, or possibly gangue material surrounding the deposit, or metallic mine infrastructures.

The lack of resolution at depth can be attributed, in part, to the smoothing functions of the inversion algorithm used, but in all likelihood, is compounded by the mixture of In-line and Cross-line mode signatures, in the non-derotated data, caused by the oblique geology – as predicted earlier. In fact, as shown in Figure 3.70, the smooth conjugated MT inversions produce poorly defined images of the rhyolites and other conductive units, at depth in 3D, in comparison to the smooth DC inversions. Clearly, both an EVA-processed de-rotation as well as a less smooth/higher resolution 2D inversion algorithm are required for MT, particularly to resolve targets at depth.

Figure 3.69 presents the unconstrained PW MT inversions, which use a Gauss-Newton, finite-element algorithm, and are calculated using EVA processed data which performs, among other aspects, the de-rotation components into their respective geologic/geoelectric directions. The PW-EVA inversions were performed using all four components (ρ_{TM}, ρ_{TE}, φ_{TM}, φ_{TE}), by first using the unrotated RLM solution as the starting model for an initial, TM-mode only PW inversion, then using that solution as a starting model for the final TM-TE mode PW inversion. A full description of the EVA process is given in Section 2.2.4 and the EVA results, specific to the Kidd Creek Titan-24 unconstrained MT inversions, are presented in Appendix C.

It is worthwhile noting that when de-rotating ρ_{XY} and ρ_{YX} to the geological strike, the normal practice is, for 2D inversion, to project sites to a common direction profile, that is perpendicular to strike – thereby shortening the position of the sites by a factor of cos θ (M. Chouteau, pers. comm., 11/2004). This procedure has not, in fact, been applied to the Titan inversions in this study.

The PW inversions detect all the most significant subcropping conductive zones identified in the unconstrained DC resistivity inversions, as well as other, new buried conductive features, that were previously undetected in either of the smooth DC, IP and MT inversions. Their excellent correlation with the known geology is shown in the Gocad model (Figure 3.71). In addition, the PW inversions also appear to provide better differentiation of lateral and vertical resistivity contrasts at depths easily extending below 2km – well beyond the DC resistivity threshold of 750m. Line 108N and L114N both feature prominent, strong, low resistivity contrasts along the North Rhyolite. At least four new moderate to strongly conductive zones and several other weaker, buried conductivity targets are defined in the unconstrained PW MT inversions, from 500-2000m, which merit further investigation and comparison against the Gocad geologic model.

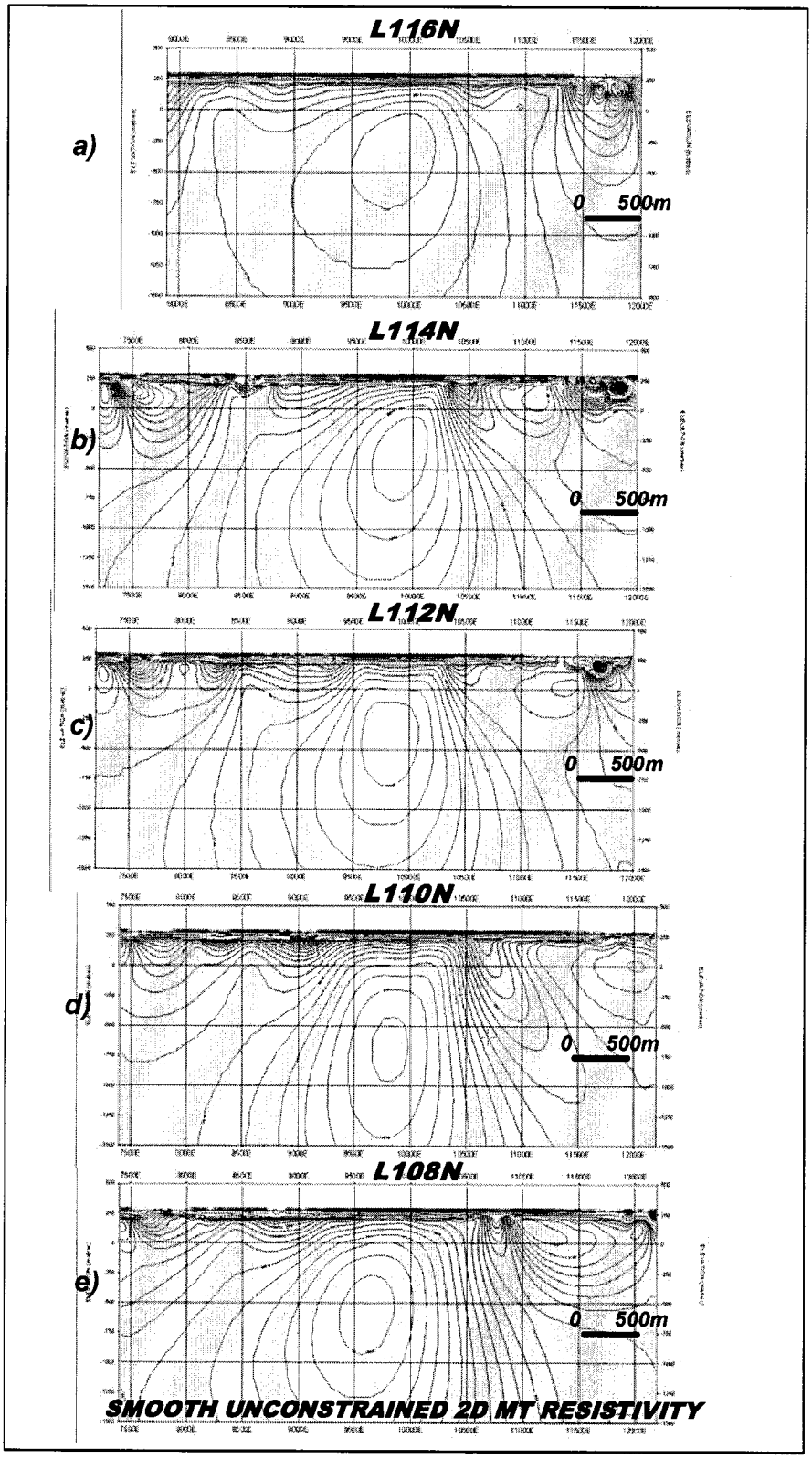

Figure 3.68: Smooth Unconstrained 2D MT Resistivity (Non De-rotated).

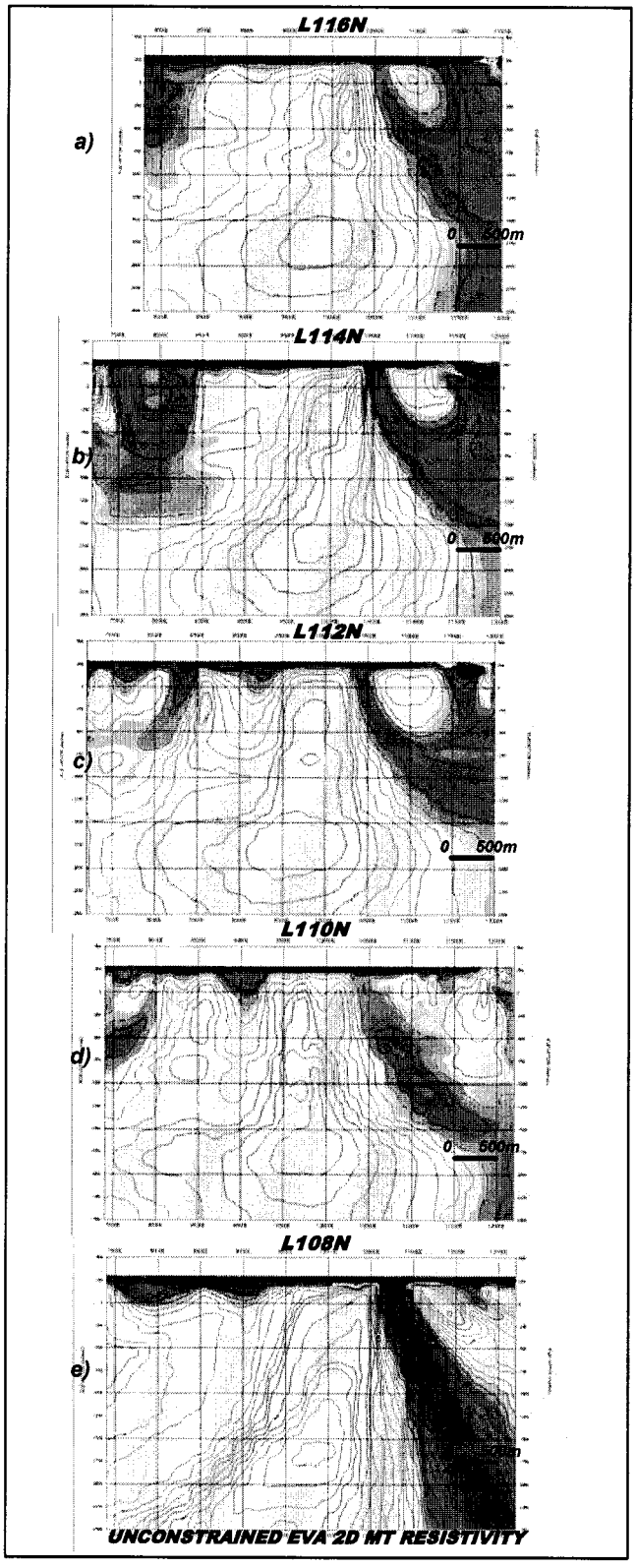

Figure 3.69: Unconstrained 2D PW MT Resistivity Inversions (EVA Processed).

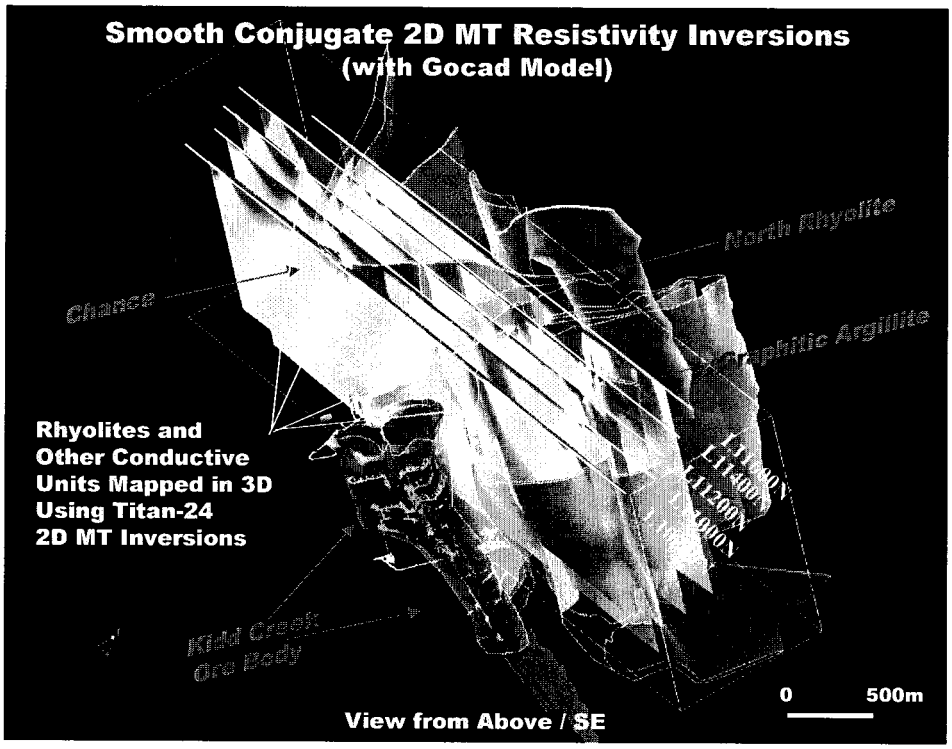

Figure 3.70: Smooth Unconstrained 2D MT Resistivity Inversions in Gocad Model

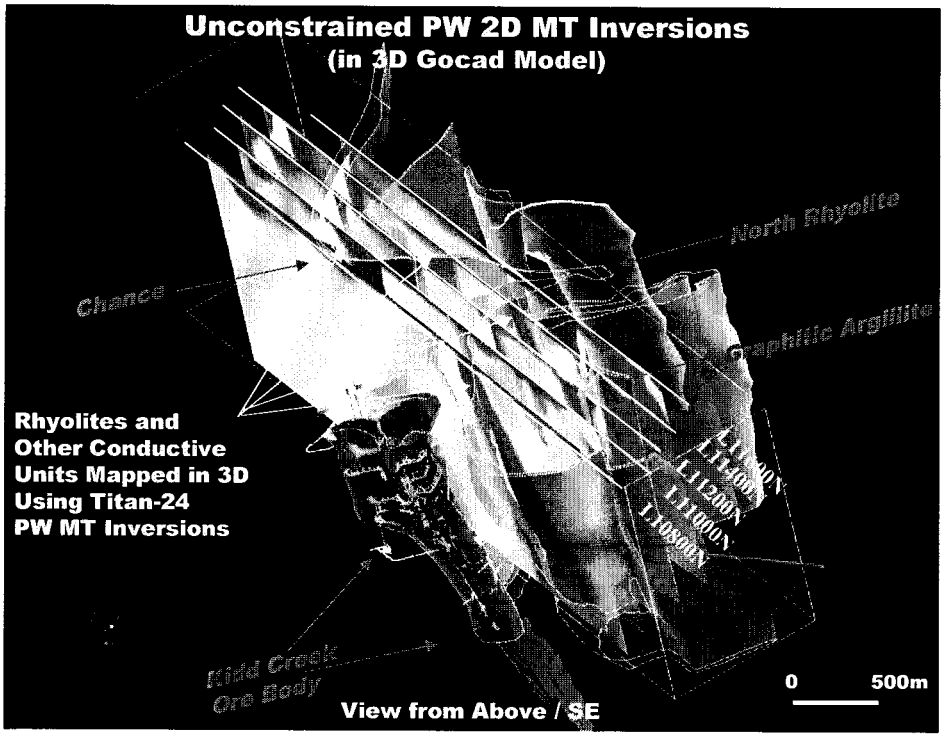

Figure 3.71: Unconstrained 2D PW MT Inversions (EVA Processed) in Gocad

3.6 Constrained 2D Inversions

3.6.1 DCIP Surveys

The results of constrained (geologically referenced) 2D DCIP inversions over the 5 Titan profiles are presented in Figure 3.72, for the resistivity and in Figure 3.73, for the chargeability, using a "sharp" model objective function. Each "sharp" model inversion is paired with its respective Gocad-reference resistivity model, whose physical property values are shown in Table 3.7 below. As described in Appendix B, the "sharp" DCIP models, designed to emphasize data fit or resolution over model smoothness, also produce constrained inversions which adhere most closely to the reference models. A close adherence is preferred for the Ratio-M and Delta-M analyses, in order to highlight differences between the inversion and predicted model, which represent targets for follow-up exploration. Notwithstanding, "smooth" constrained models, which by their nature are only loosely constrained by the Gocad model, were also calculated and are shown for comparison and review in Appendix B.

Table 3.7: Physical Properties used in Constrained 2D DCIP Inversions

LITHOLOGY	RESISTIVITY	CHARGEABILITY
Mafic volcanic =	10,000 ohm-m	3 mrad
Ultramafic volcanic =	7,000 ohm-m	5 mrad
Sediments =	5,000 ohm-m	10 mrad
Rhyolite =	1,000 ohm-m	20 mrad
Overburden =	30 ohm-m	0.5 mrad
Graphite/Massive Sulphide =	10 ohm-m	75 mrad

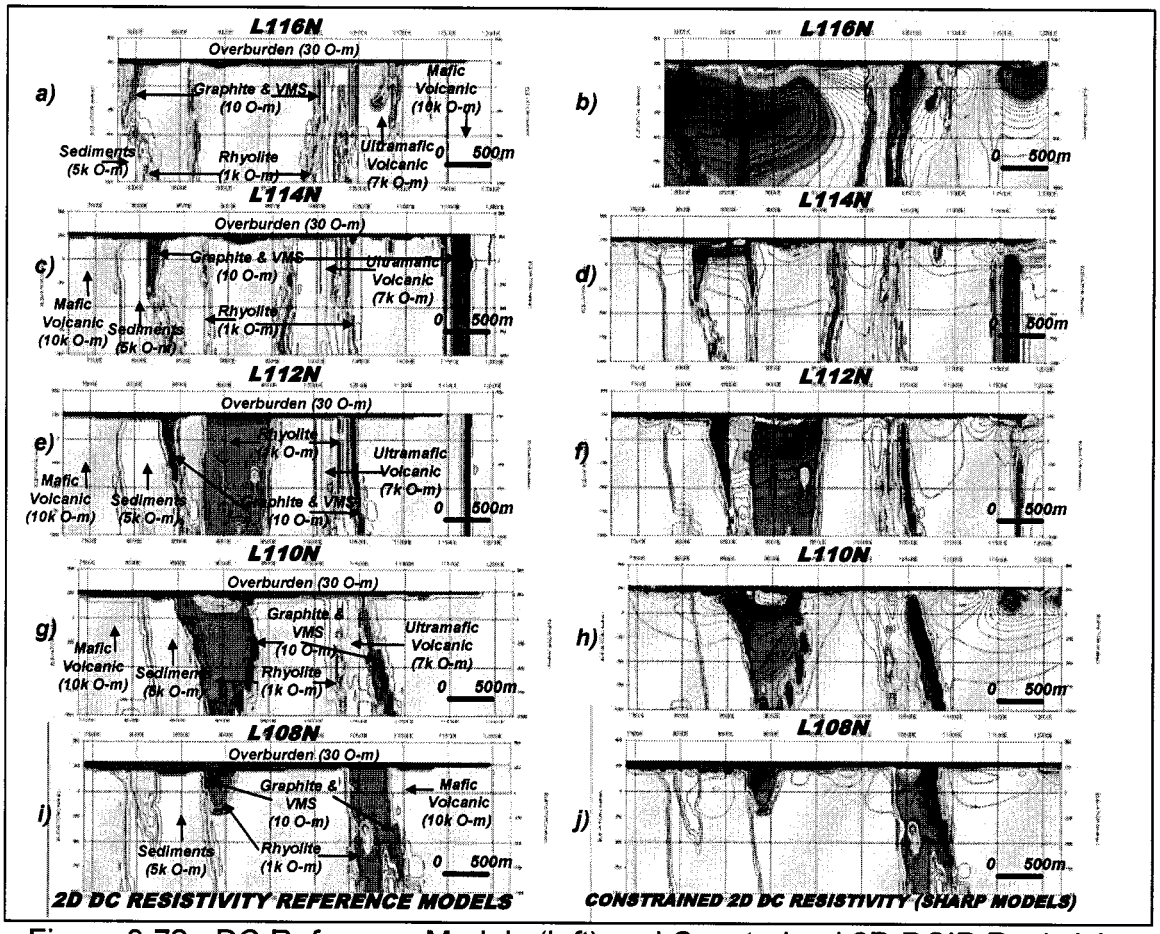

Figure 3.72: DC Reference Models (left) and Constrained 2D DCIP Resistivity Inversions (Sharp Models - right)

The sharp model, constrained DC resistivity inversions to the right in Figure 3.72bdfhj represent the conductivity structure required to satisfactorily explain the measured profile responses, while taking into account the known geologic structure, defined to the left in Figure 3.72acegi. Anomalous zones which occur outside the conductive rhyolite and graphitic units are easily differentiated in the cross-sections, by visually comparing them to the adjacent reference models. These include 2 prominent unexplained conductive anomalies, which occur to the north and south of the graphitic argillite, defined along L116N and L110N near 11500E, as well as 1 larger, lithologic like low resistivity zone lying at depth in the western third of L116N. Other, weaker anomalies outside the rhyolites, as

well as signatures coinciding with the rhyolites are much less easily defined, and require a Ratio-M analysis to accurately determine their significance (see further descriptions below). Still, prominent anomalous zones of conductivity, not predicted in the Gocad, are clearly obvious, in particular for the North Rhyolite along L116N and L108N, as well as the Chance rhyolites, along L110N and L112N. As well, based on the distribution of anomalies, maximum depth of investigation/resolution appears to be 500m, as predicted in the sensitivity analyses in Section 3.3.

The corresponding sharp model constrained 2D IP chargeability inversions are presented to the right in Figure 3.73, paired alongside their respective chargeability reference models to the left – again with the view looking south to north. Anomalous zones which occur outside the polarizeable rhyolite and graphitic units are easily differentiated in the cross-sections, by visually comparing them to the adjacent reference models. At least 4 prominent unexplained IP anomalies occur in the region surrounding the graphitic argillite near 11500E, including 1 large, lithologic or porphyry-like IP anomaly along L110N. Other, moderately strong IP anomalies are also defined in the sediments west of the Chance deposit. IP signatures which coincide directly with the rhyolites are masked, as a result, and require a Ratio-M to accurately determine their significance. Still, closely examining the cross-sections, at least 2 prominent IP anomalies, not predicted in the Gocad model, are defined in the Chance rhyolites, along L110N and L112N. As well, based on the distribution of anomalies, the maximum depth of investigation appears to be less than 500m for the constrained IP inversions, as predicted in sensitivity analyses in Section 3.3.

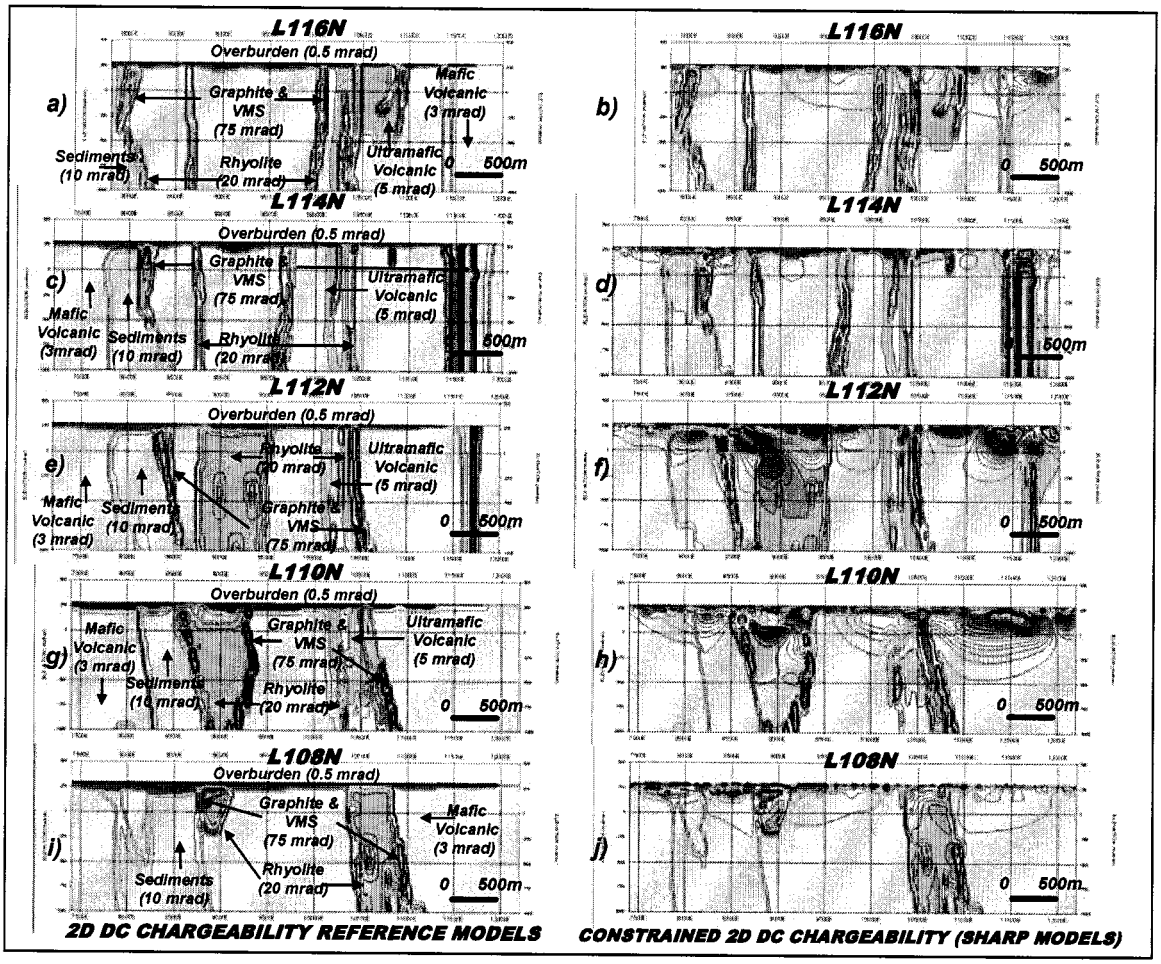

Figure 3.73: IP Reference Models and Constrained 2D DCIP Chargeability Inversions (Sharp Models)

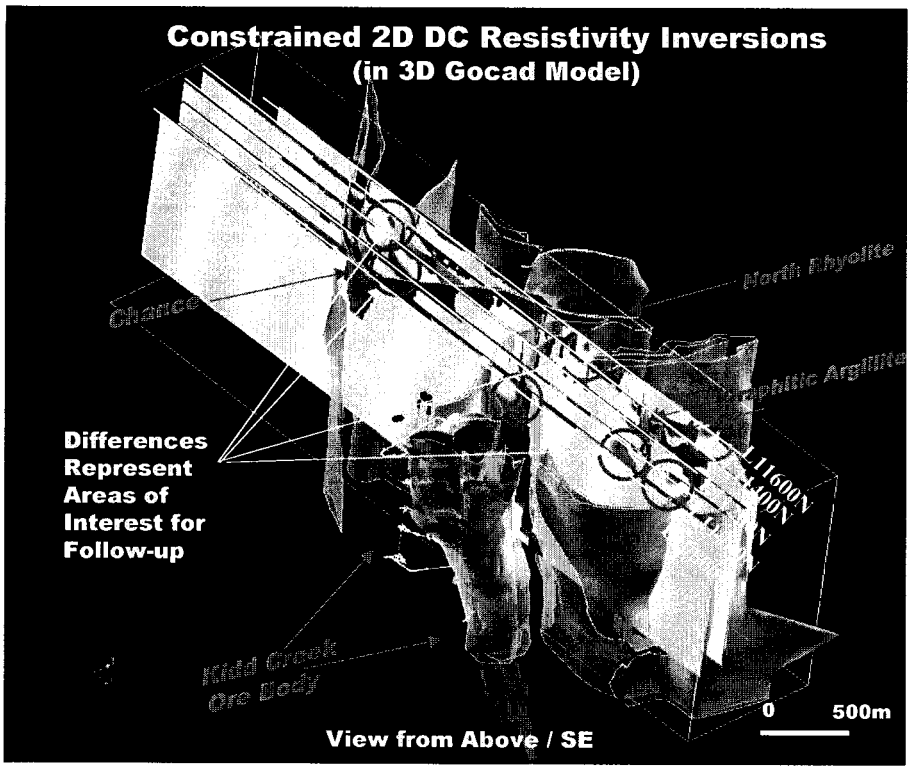

Figure 3.74: Sharp Constrained 2D DC Resistivity Inversions in Gocad Model

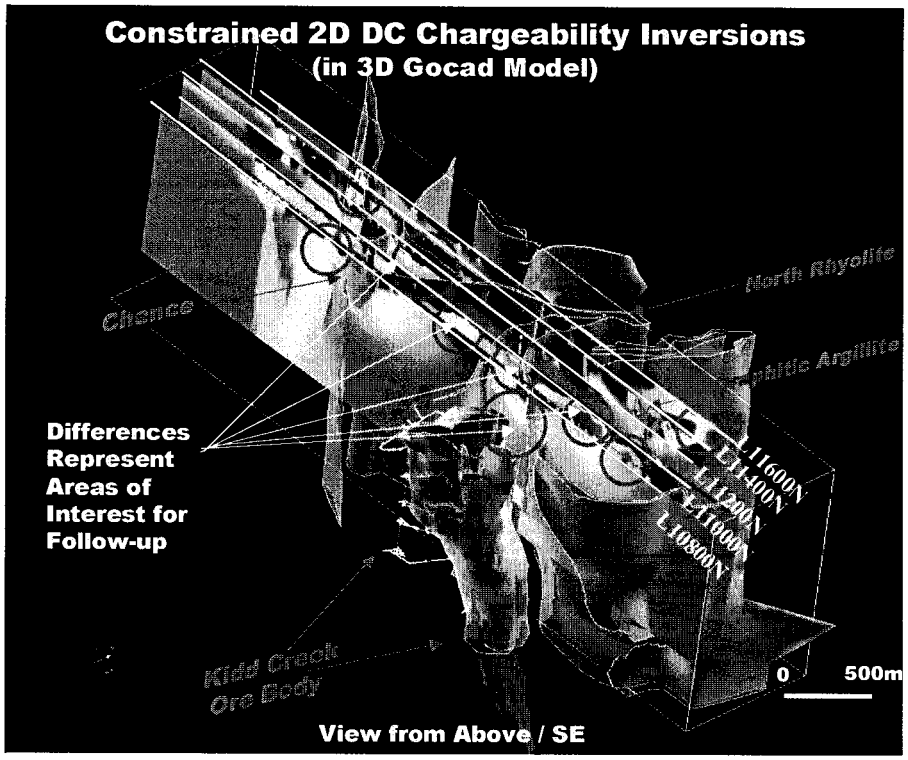

Figure 3.75: Sharp Constrained 2D IP Chargeability Inversions in Gocad Model

Finally, the end-result of the DCIP inversion process, the Ratio-M analyses of the constrained DC resistivity and the corresponding Delta-M analyses of the constrained IP chargeability sharp model inversion are presented in Figure 3.76 and Figure 3.77 as stacked cross-sections. These best highlight the differences between the actual vs. expected models. The two products were obtained by calculating the differences (log values for DC, linear subtraction for IP), directly, between the sharp constrained model and the reference model, using Gocad model files. The result is a quantitative portrayal of anomalous responses which are unexplained by the Gocad geologic model and which therefore merit additional follow-up.

Each cross-section is similarly colour-zoned:

a) cool colours (blue-white) represent values which are more resistive, in DC Ratio-M, or, alternately, less chargeable in the corresponding IP Delta-M, than the predicted Gocad model. Coolest colours represent values which are >10x more resistive or less polarizeable than expected;
b) neutral colours (green-yellow) correspond to values which are similar to the predicted Gocad model;
c) warm colours (red-purple) represent features which are more conductive or more polarizeable_than predicted in the Gocad model. Warmest colours represent values which are >10x less resistive or more polarizeable than expected.

Ratio-M and Delta-M analyses are stand-alone products, which do no require comparisons against the reference model to determine their significance. They are more easily compared and related across profiles, in comparison with the constrained inversions, and therefore more easily prioritized and rateable. In Figure 3.76, clear-cut Ratio-M anomalies are immediately obvious, including at least 8 prominent large conductive anomalies, concentrated along the key rhyolite and graphite horizons:

A) North Rhyolite: 3-4 zones, along L116N near 10500E, along L110N near 10600E, and along L108N, near 10400E and 10800E.

B) Chance Horizons: 3-4 zones, along L114N near 8500E, along L112N between 8500E and 9500E, along L110N near 8700E-9200E

C) Graphite: 2-3 zones, along L116N near 11900E, L110N near 11600E-12100E.

These unexplained zones generally all feature good vertical extension, occasionally to depths >750m, and are all partially buried (>50-100m) and therefore may have escaped detection previously. Smaller zones of significance are also differentiated, in particular a small body, buried at 100m depth along L108N near 8800E which may represent the Chance deposit. All these areas merit follow-up and are described in the following sections. In addition to weaker conductive anomalies, some areas are more resistive than expected, including the graphitic units to the northeast, near L114N/11700E and L116E/11600E. As well, most of the overburden is more resistive than expected, indicating that our estimate, based on preliminary unconstrained 2D inversion prior to entry into the Gocad model, was lower than the actual overburden resistivity. Similarly, 2 large area, buried weak resistivity lows, along L116N-L114N to the NW, and L110N to the east, either indicate poor reference estimates for the mafic volcanics and sediments locally, or potentially relate to alteration.

Based on the distribution of anomalies, most conductive features are partially buried (<50m) and most are resolved within 250-500m of the surface. Few are detected below 250m but many extend to depths below 750m. This seems to indicate that, for the DC parameter, the depths of investigation exceed the 500m maximum depth predicted for constrained inversions in the sensitivity analyses in Section 3.3 – possibly as a result of the lower data errors obtained in the surveys. Clearly, the Ratio-M analyses have proven useful in precisely defining areas of interest as well as at Kidd Creek.

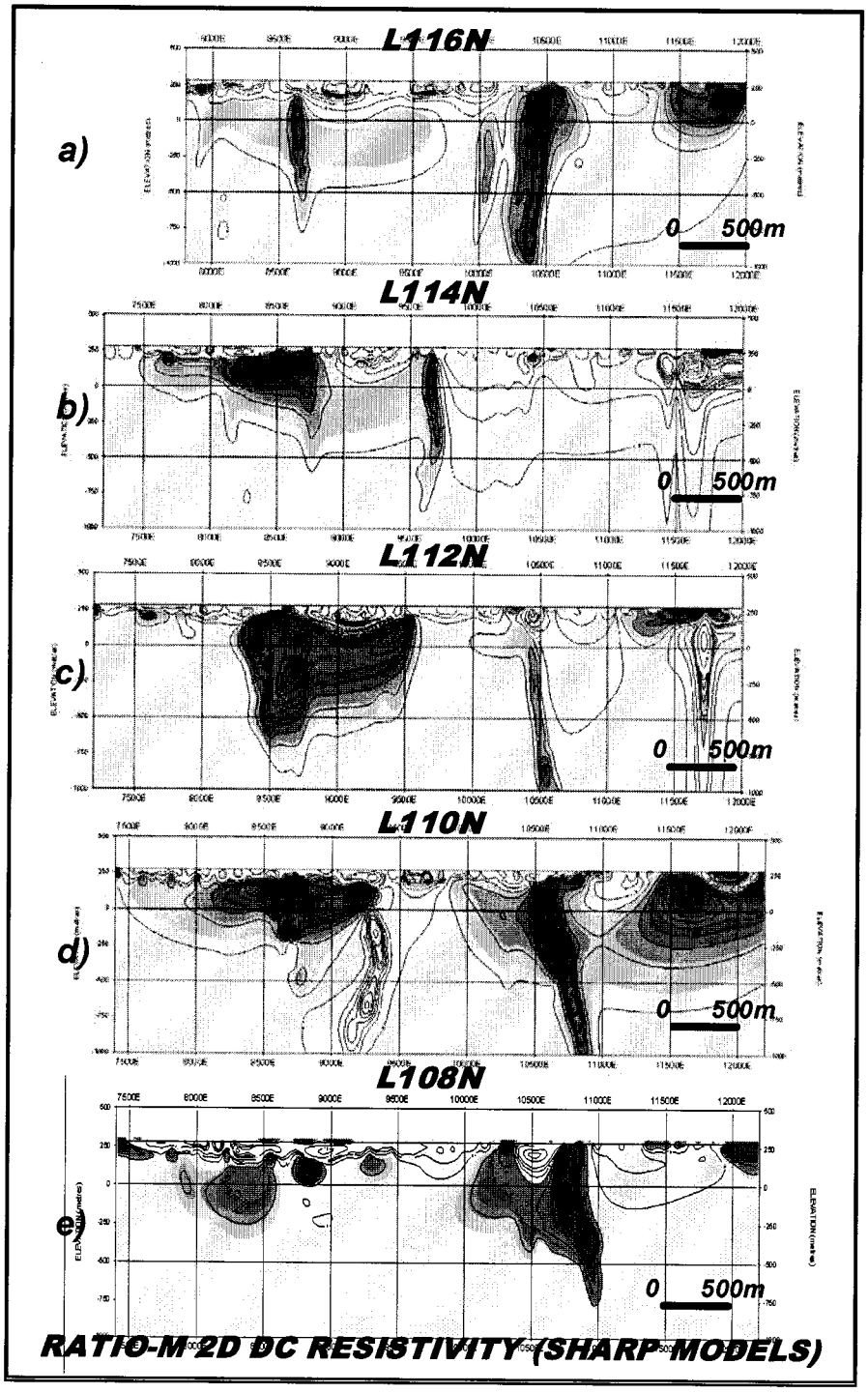

Figure 3.76: Constrained 2D DC Ratio-M Products (Sharp Models)

Figure 3.77 presents the Delta-M cross-sections for the constrained IP inversions along all five Titan profiles, shown with a view looking north. Delta-M anomalies are more numerous and are generally smaller than those defined in the Ratio-M. Moreover, they are more broadly distributed, spanning most geologic units. In fact, most are not concentrated along the key rhyolitic horizons, as indicated by the prevalence of dark blue vertical stripes (i.e., low IP), although many are closely associated.

At least 8 prominent moderate-large, strong chargeability anomalies are defined in Figure 3.77:

A) North Rhyolite: 1-2 zones, along L110N between 10000E-10600E.
B) Chance Horizons: 4-5 zones, along L114N near 8400E and 9600E, along L112N at 8000E and 8600E, along L110N near 8700E and 8900E
C) Graphite: 3-4 zones, along L116N between 11400E-11900E, L112N near 11400E and 11900E, L110N between 10800E-11900E, and L10800N, between 11000E-11700E.

For the most part, these unexplained zones are depth limited, and do not show vertical extensions below 250-350m – although this may be an artifact of the inversion (see Section 3.3) and may be underestimated. At least three extend below 500m, including the Chance at L114N/9700E and L112N/8700E, and the North Rhyolite, at L110N/10600E and L108N/10800E. Smaller zones of significance are also differentiated, in particular, two buried zones along the North Rhyolite, one at L116N/10400E, which is a weak anomaly buried at 500m depths, the other is a small, strong anomaly at 700m depths below L108N/10900E. However, both these anomalies are noticeably deeper than predicted possible in the sensitivity analyses, and may alternately represent artefacts of the inversion. Of note, the large porphyry-like anomalies to the east, along L110N and L108N, also correspond to broad, weak resistivity highs – possibly indicative of disseminate-mineralized alteration. All significant Delta-M

anomalies areas merit follow-up because they represent chargeability anomalies which are unexplained in the geologic model.

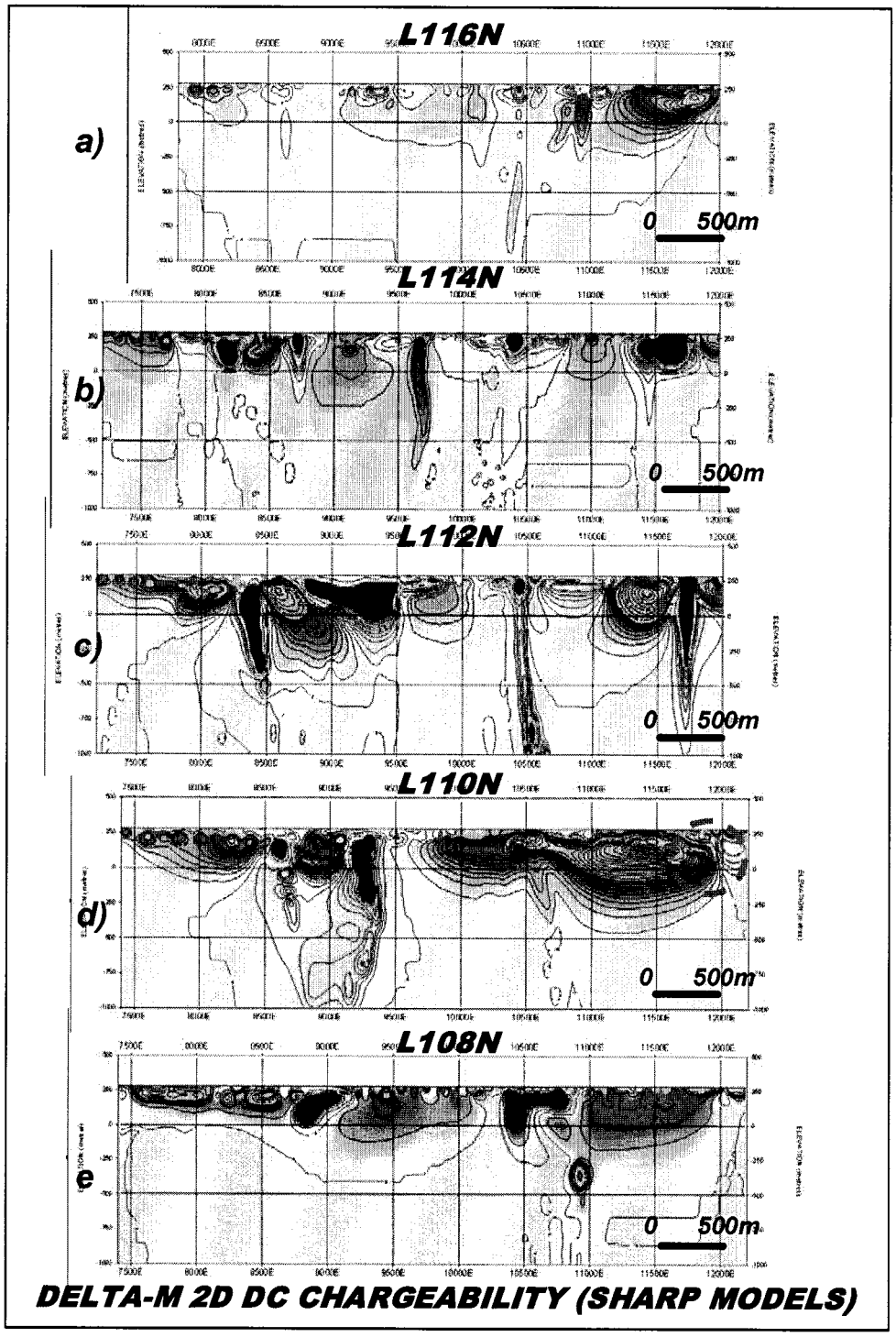

Figure 3.77: Constrained 2D IP Delta-M Products (Sharp Models)

In addition to weaker conductive anomalies, some areas are less polarizeable than expected, including the graphitic units and most of the rhyolitic horizons. This indicates that our reference IP estimates are too high, and that these horizons are not as strongly mineralized as perceived, i.e., their low resistivity results from high porosity not mineralization. Elsewhere, large, patch-like areas also reflect incorrect estimates for the mafic volcanic and sediments in particular. Clearly, more accurate, in situ chargeability values are required for the reference models. Based on the distribution of anomalies, most conductive features occur close to the surface, below the overburden, most are resolved within 250-350m of the surface and few are detected below 250m. These confirm the 250-500m maximum depths predicted in the sensitivity analyses in Section 3.3. Nevertheless, it is clear, the Delta-M analyses have proven useful in precisely defining areas of interest at Kidd Creek.

3.6.2 MT Surveys

The results of constrained (geologically referenced) 2D MT resistivity inversions over the 5 Titan profiles are presented in Figure 3.78, along with the Gocad reference models, and the corresponding Ratio-M's are shown in Figure 3.79. The inversions were calculated using the PW2dinv MT algorithm developed for Quantec by Prof. P. Wannamaker (de Lugao and Wannamaker, 1996). The resistivity reference models are identical to those used in the DC resistivity inversions, shown previously.

The constrained MT resistivity inversions define at least 10 prominent conductive anomalies, most of which lie along the key North Rhyolite, and Chance horizons, including: a) at least 4 shallow depth (<250m), b) 3 moderate to deep (250-1000m) zones, and c) 5 deep (>1km) elongate conductive zones – all of which occur along the North Rhyolite. Other, the significance of weaker anomalies outside the rhyolites, as well as signatures coinciding with the rhyolites are not easily determined and require a Ratio-M (see further descriptions below).

Still, prominent anomalous zones of conductivity, not predicted in the Gocad model, are clearly obvious, in particular for the North Rhyolite along L114N and L112N, as well as separate features along L110 and L108N, and at shallower depths along the Chance rhyolites, along L110N in particular. It is clear, based on the distribution of anomalies, that the maximum depth of investigation/resolution appears to exceed 1-2km, which also corroborates the figure predicted in the sensitivity analyses in Section 3.3.3.

Finally, Figure 3.79 presents the Ratio-M cross-sections for the constrained MT resistivity inversions along all five Titan profiles, shown with a view looking north. As was the case for the DC and IP, the Ratio-M for MT has helped clarify zones which remain unexplained in the Gocad Geologic model. Clear-cut Ratio-M anomalies are immediately obvious, including at least 7 prominent deep (>1.5km) conductive anomalies, 8 medium depth (500m-1.5km) anomalies and as many as 18 shallower depth (<500m) zones. These anomalies are concentrated along the key rhyolite horizons and graphites, and are prioritized for further exploration.

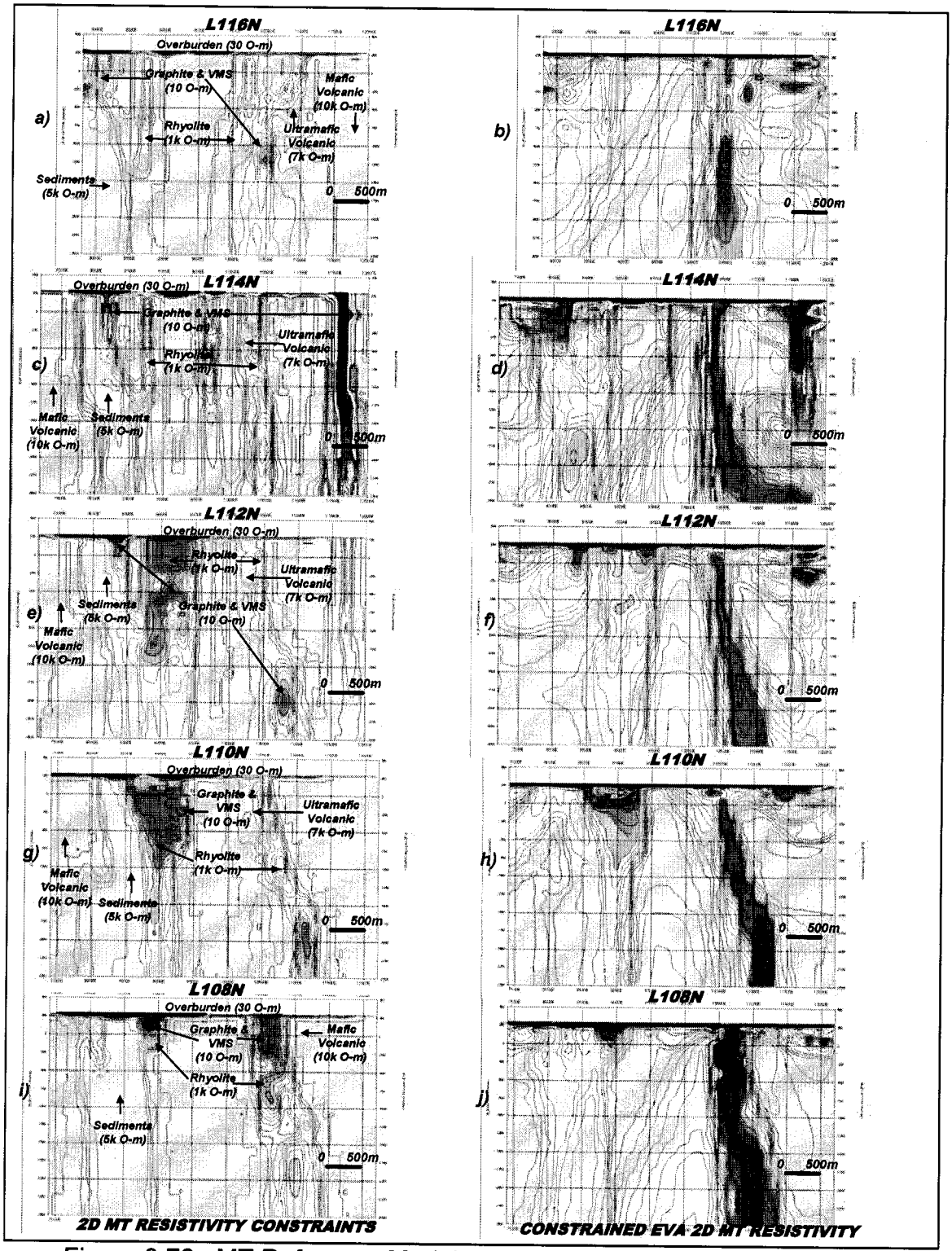

Figure 3.78: MT Reference Models and Constrained 2D MT Inversions

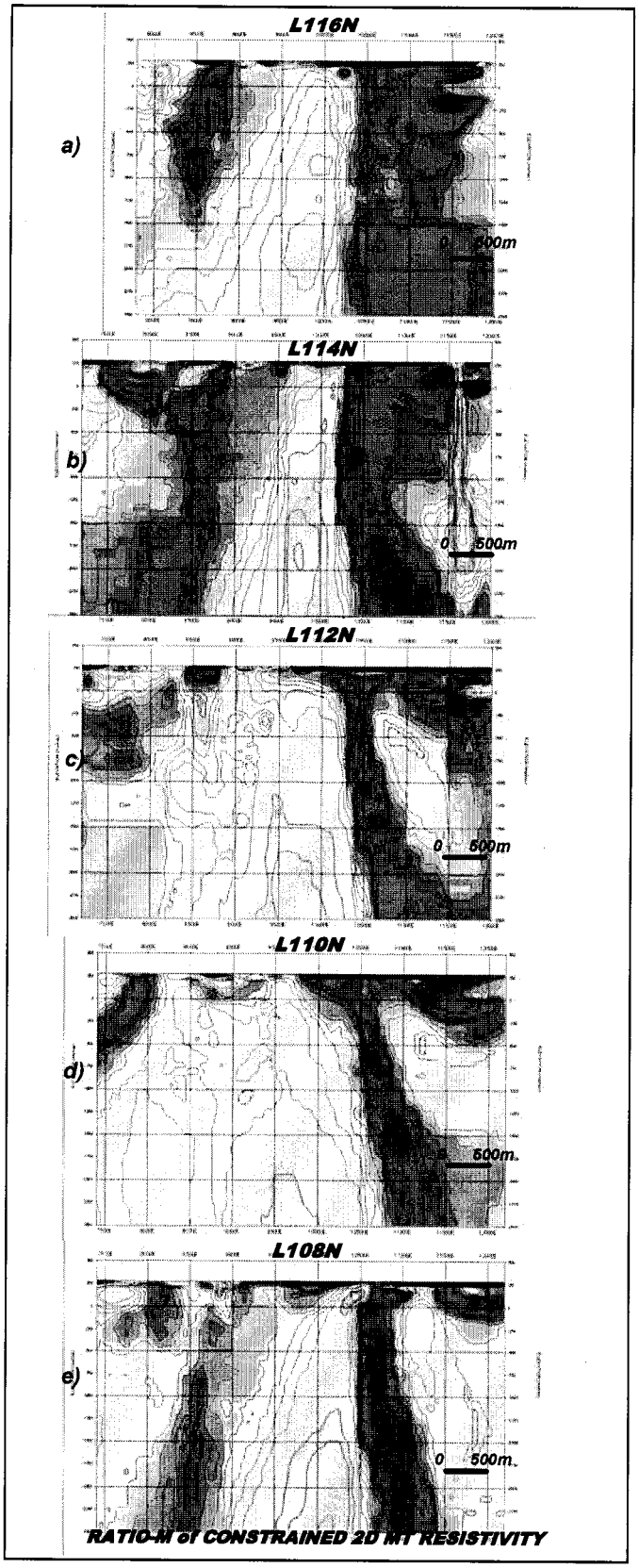

Figure 3.79: Ratio-M for Constrained 2D MT Resistivity Inversion

CHAPTER 4 CONCLUSIONS AND RECOMMENDATIONS

4.1 Overview

Titan-24, multi-channel, distributed acquisition surveys, by Quantec Geoscience Inc., were undertaken, in December, 2001, at Falconbridge Ltd.'s Kidd Creek zinc-copper mine. The Titan-24 system 2D interpretation capability, combined both conventional unconstrained 2D DC and MT inversion, as well as constrained-referenced 2D inversions, making use of the Gocad platform and petrophysical characterization. An integrated geologic and geophysical interpretation performed on these results consisted of geophysical inversion models that were constrained using the known geologic model, which had in turn been populated using in-situ physical properties. The constrained and predicted results were then compared, and the differences used to identify target anomalies that remain unexplained by the known geology. This thesis study undertook to present this new method of analysis whose goal was to identify potential drill targets, from surface to 2km depths.

Using joint surveys, combining tensor magnetotellurics (MT) and large-dipole/large-array DC-resistivity & induced polarization (DCIP), the survey objectives were to: a) map lithology, alteration and structure, b) define conductive and chargeable targets, associated with sulphides and/or graphite, along several known rhyolitic horizons, including the Chance and North Rhyolite horizons, to depths extending to +2km, c) penetrate thick conductive overburden, d) acquire high quality data in a noise-contaminated mine-site environment, and e) operate during the winter survey period, in order to test the system's all weather/four season performance characteristics.

The results of the unconstrained (non-geologically referenced) and Gocad-constrained inversions are presented and documented in this thesis The following is a list of the main observations and conclusions, as well as recommendations of the present study, divided into the various stages of the study, includ-

ing: a) the petrophysical analysis and assignment of the 2D inversion constraints, b) the Gocad model creation, c) the 2D sensitivity analysis, d) the Titan survey results, e) 2D inversion results and f) targeting. Due to their length, the topics are presented in reverse order, according to their relative importance in the study.

4.2 Observations and Conclusions:

4.2.1 2D Inversion Results

- The smooth unconstrained DC inversions appear to correlate very well with the known rhyolitic and graphitic horizons, defining them as resistivity lows. Indications of apparent dip and vertical extent, to below 750m are also indicated. The excellent degree of correlation is confirmed inside the Gocad model.
- In contrast, in spite of showing good correlation with DC resistivity lows, the smooth IP inversions produce large, amorphous, balloon-shaped anomalies which appear to bear little resemblance to the geology, as confirmed by the Gocad model.
- Sharp model, unconstrained DCIP inversions, due to their higher resolution, in addition to being well correlated with the smooth model inversions, also detect additional anomalous sources which are unexplained by the geologic/Gocad model.
- Preliminary smooth conjugate MT resistivity inversions show good correlation, at surface, with the smooth unconstrained DC inversions. However, at depths below 250-500m, few conductive features occur and most near-surface conductive zones pinch-out.

  The sole exception being the L108N profile, which features a large (>500x500m), deeply buried (750m-1km) low resistivity zone below 11500E, which is open at depth and which might, in fact, represent an off-line/edge response to either: a) the Kidd Creek orebody, situated 500m

south, b) its surrounding mineralized gangue material, or c) metallic mine infrastructure, lying below surface, underground.

- Unconstrained PW MT resistivity inversions of the EVA-processed data detect all the most significant subcropping conductive zones identified in the unconstrained DC resistivity inversions, as well as other, new buried conductive features, that were previously undetected in either of the smooth DC, IP and MT inversions.

  The unconstrained PW inversions also appear to provide better differentiation of lateral and vertical resistivity contrasts at depths easily extending below 2km – well beyond the DC resistivity threshold of 750m. At least four new moderate to strongly conductive zones, buried at depth and undetected in the DCIP results have been identified, as well as several other weaker, buried conductivity anomalies,

- Constrained inversions of the EVA-processed data detect all the most significant subcropping conductive zones identified in the unconstrained DC resistivity inversions, as well as other, new buried conductive features, that were previously undetected in either of the smooth DC, IP and MT inversions.

- Ratio-M and Delta-M analyses highlight the differences between the constrained inversion results and those predicted in the Gocad model.

  Differences between the observed inversions and the reference models are difficult to discern and quantify, visually, particularly where anomalies and mineralization overlap. The Ratio-M product, for the DC, and Delta-M, for the IP, are ideally suited to highlight these differences. The two products were obtained by calculating the differences (log values for DC, linear subtraction for IP), directly, between the sharp constrained model and the reference model values, using Gocad model files.

- Ratio-M and Delta-M analyses are stand-alone products, which do no require comparisons against the reference model to determine their significance. They are more easily compared and related across profiles, in comparison with the constrained inversions, and therefore more easily prioritized and rateable.
- The Ratio-M of the constrained DC resistivity inversions define at least 8 prominent large conductive anomalies, concentrated along the key rhyolite horizons and graphites, from surface to 750m depths. Including the North Rhyolite, along L116N, L110N and L108N, the Chance horizons, along L114N, L112N and L110N, and near the graphites, to the east, along L116N and L110N.
- The Delta-M of the constrained IP chargeability inversions define at least 8 prominent moderate to large chargeability anomalies, concentrated along the key rhyolite horizons and graphites, from surface to 500m depths. Including the North Rhyolite, along L110N, the Chance horizons, along L114N, L112N and L110N, and near the graphites, to the east, along L116N and L112N. Two large porphyry-like IP anomalies to the east, along L110N and L108N, also coincide with large, weak resistivity lows and may map disseminate mineralized alteration zones.

  The Delta-M anomalies tend to be smaller and more numerous than the Ratio-M features, and span nearly all geologic units across the sections. For the most part they are concentrated near the surface and do not feature significant depth-extensions below 250-350m.

- The Delta-M cross-sections display patch-like contrasts in chargeability, which is attributed to poorly referenced chargeabilities in the Gocad model. Large, deep IP lows along the rhyolites and graphites indicate that these horizons are not as strongly polarizeable as predicted.
- The Ratio-M of the constrained MT resistivity inversions define at least 15 significant conductive anomalies, from surface to 2000m depths. Most are

defined along the North Rhyolite horizon, including the strongest and most deeply buried. The Chance horizons also feature anomalous Ratio-M features, but these tend to be weaker and depth limited – effectively reducing their significance.

- The Titan system's ability to map lithology and structure in 3D, below a thick conductive overburden blanket, is affirmed by the unconstrained 2D DC inversion results, based on direct comparisons with the geology, inside the Gocad model.
- The PW MT inversions, in comparison with smooth MT and, in general, with DCIP inversions also, provide improved depth of investigation, vertical and lateral resolution, details on variations down-dip/plunge, dip-directions and also detects features that were not previously discerned, particularly at depths below 750m and potential extending to >2km.
- The unconstrained PW MT inversions define strong low resistivity contrasts along the North Rhyolite, across L108N and L114N. In addition, at least four new, buried, moderate to strong low resistivity zones, as well as several weaker responses, are defined in the 500-2000m depth range.
- The Ratio-M and Delta-M analyses are a quantitative method of rating/grading the constrained inversions. They also permit the identification of anomalies along the geologic strike, across the geologic boundaries and down-dip.

4.2.2 2D Sensitivity Analysis

- The Gocad model of the Kidd Creek deposit has been used to test the depth of investigation capability of the Titan DCIP and MT surveys, as well as their detection using 2D inversion.

  By extracting an east-west, 2D cross-section, for a profile 500m south and 500m east of our present survey coverage, from the Gocad model, 2D forward model simulations were calculated of the theoretical Titan-24 ar-

ray DC, IP and MT responses over the original, unmined Kidd Creek orebody, in order to understand and recognize the types of responses which might be expected from potential virgin orebodies of the same size. A sensitivity analysis was also performed by calculating theoretical 2D forward MT and DCIP responses for the equivalent of Kidd Creek, eroded to 200m below surface, 500, 1km and 2km depths. A non-mineralized model simulating a barren rhyolite horizon was also tested. These simulated DCIP data were subsequently inverted, using the UBC Dcinv2d^{TM} platform, in order to test the depth-imaging capability of the present inversion study, using both geologically constrained 2D inversions and unconstrained 2D inversions, for the DC and IP parameter. However, 2D MT inversions of the simulated results were not performed.

Part 1: 2D Forward Model Simulations (DC, IP, MT)

- The 2D forward modeling of the DC resistivity parameter shows that the Kidd Creek deposit produces discernable low resistivity anomalies in the raw data, at burial depths of 0m, 200m and 500m. The lattermost, 500m model data, however, produces a signature which is not significantly different from those from barren, non-mineralized rhyolite model. At burial depths of 750m and 1km, DC forward models of the Kidd Creek orebody are not significantly different from those of a barren, non-mineralized rhyolite model.

  The 2D forward model in DC resistivity, for Kidd Creek at surface, produces large, well-defined apparent resistivity low in dipole-dipole, which is nearly equal in magnitude to its intrinsic resistivity, slightly stronger than its Center-pole equivalent (≈2x), and extends from N≈1 to 32, as expected. The 2D forward model for Kidd Creek, buried at 200m, produces weaker, moderately well-defined apparent resistivity lows of similar magnitude in Dpdp and Center-pole (≈3x intrinsic resistivity), from N≈4-22, and a proper indication of dip. Using a higher conductance for Kidd Creek at a 500m

burial depth, the 2D forward DC resistivity model produces a weak, diffuse poorly defined apparent resistivity low, from N≈10-20, which is >100x weaker than its intrinsic resistivity. In fact, in comparison with the non-mineralized rhyolite model, the Kidd Creek at 500m depth produces a resistivity low anomaly which is only <3x stronger in magnitude. At 750m and 1km, the weakening effect is more significant.

- 2D forward modeling of the IP chargeability parameter shows that the Kidd Creek orebody produces discernable high chargeability anomalies in the raw data, at burial depths of 0m and 200m. At burial depths of 500m, 750m and 1km, forward models of the Kidd Creek orebody are not significantly different from those from a barren, non-mineralized rhyolite model.
- 2D forward models of the MT resistivity and phase show that the Kidd Creek deposit, at surface, produces discernable low resistivity and high phase anomalies in both the In-line and Cross-line components. At 200m and deeper, the Kidd Creek orebody is discerned only in the Cross-line component, particularly the phase, with no visible anomaly in the In-line component resistivity or phase, which resembles the barren model response. As the orebody deepens, the anomaly is detected at progressively lower frequencies, becomes weaker, particularly for the resistivity, and also broadens significantly, to a width almost equal to 2x its depth of burial. At 2km, the Cross-line phase and apparent resistivity anomalies are at the lowest point in the Titan frequency range.

Part 2: 2D Inversion Model Simulations (DC, IP)

- The unconstrained 2D DC resistivity inversions (not geologically referenced) of the forward models display well-defined anomalies, featuring the appropriate host-rock resistivity, burial depths, width, vertical extension and dip directions, for the Kidd Creek deposit simulated at burial depths of 0m, 200m, 500m and 750m. These inversions are also markedly dissimi-

lar to the one obtained from a barren, non-mineralized rhyolite model, which did not produce an obvious anomaly. In contrast, for Kidd Creek at 1km, the unconstrained 2D DC inversions produce a discernable anomaly but which is not significantly different from the barren, non-mineralized model. Overburden variations are also well resolved in unconstrained inversions, but lateral resistivity structures relating to non-mineralized geology are not retained.

- Unconstrained 2D IP chargeability inversions of forward models for the simulated Kidd Creek orebody demonstrate well-defined anomalies, with appropriate geometric parameters, for burial depths of 0m and 200m, which are markedly dissimilar from the barren, non-mineralized rhyolite. At depths of 500m, 750m and 1km, the unconstrained inversions produce signatures which are similar to the barren, non-mineralized model. Overburden variations and lateral resistivity structures relating to non-mineralized geology are not retained. Artefacts in the inversion, unrelated to the geology, are also obvious.
- The constrained 2D DC resistivity inversions (geologically referenced) of forward models produce discernable, anomalous resistivity low anomalies within the rhyolite unit, featuring the appropriate geometries, for the Kidd Creek deposit, buried at depths of 0m, 200m and 500m. Resistivity lows are weaker in comparison with the unconstrained anomalies. At 750m and 1km burial depths, the resulting constrained inversion are similar to that produced from a barren, non-mineralized rhyolite model. In contrast, overburden variations and lateral resistivity structures relating to non-mineralized geology are retained.
- The constrained 2D IP chargeability inversions of the simulated Kidd Creek orebody produce discernable high chargeability anomalies featuring appropriate geometries to 200m.

- Titan DCIP anomalies quickly become indistinguishable in the raw data at depths below 200m. In contrast, unconstrained inversions are capable of imaging anomalous features to depths in excess of 350-750m, depending on the physical property contrasts and specific parameter (ρ or Φ).
- Titan MT surveys are capable of detecting and resolving Kidd Creek size orebodies to depths up to 2km. Below this depth, their detection is hampered by the low frequency bandwidth of the Titan system, in addition to, in all likelihood, increased levels of noise and the "aperture" limits of the array during inversion –roughly equal to half the length of the model profile. This limit is likely 2-2.5km, based on the 4.8 km long arrays used.
- Unconstrained 2D DC inversions are capable of detecting and resolving Kidd Creek size orebodies to a maximum depth of 750m. Below this depth, the results are not significantly different from a barren, non-mineralized rhyolite model. We conclude that 750m is the maximum depth of investigation for Titan DC resistivity surveys.

  The unconstrained 2D inversions of the 2D DC resistivity forward models demonstrate that the Kidd Creek deposit could be readily resolved, in terms of host rock resistivity, burial depth, apparent conductivity-thickness, dip direction and vertical extension, in a Titan-24 study, for all burial depths between 0m and 750m – but likely not at 1km. The anomalous Kidd Creek signature could also be easily distinguished from barren, non-mineralized rhyolites, using standard inversion parameters and reasonable (5%) error levels, without geologic constraints. This suggests that the DC Titan-24 surveys are capable of detecting and resolving a target the size of Kidd Creek to a maximum burial depth of 750m, using unconstrained inversion of the DC resistivity.

  This figure is 20% greater than the P=0.19L rule-of-thumb figure commonly advocated for dipole-dipole arrays, but is easily within the range of values determined in other 2D and 3D model studies by other workers.

- Constrained 2D DC inversions are capable of detecting and resolving Kidd Creek size orebodies to a maximum depth of 500m. Below this depth, the results are not distinguishable from barren rhyolites. The marked difference with the deeper unconstrained threshold is likely the result of weaker model contrasts.

  The constrained 2D inversions of the 2D DC resistivity forward models of Kidd Creek at various depths of burial, indicate that a deposit of this type can be defined, for all burial depths between 0m and 500m – but 0.5km appears to be the maximum limit. Below this depth, constrained inversions indicate that a massive sulphide of Kidd Creek's size could not be distinguished from barren, non-mineralized rhyolite, based on reasonable levels (5%) of data error, using the smooth UBC 2D inversion modeling platform.

- Unconstrained and Constrained 2D IP inversion are capable of detecting and resolving Kidd Creek size orebodies to a maximum depth between 200 and 500m. At 500m depths and below, the results are not distinguishable from barren rhyolites. This is likely the result of weaker physical property contrasts for the chargeability parameter, as well as, possibly, the smoothing characteristics in the inversion algorithms used. We conclude that 350m is the practical limit to the depth of investigation for Titan IP chargeability surveys.

  We note that this figure is less than the P=0.19L rule of thumb figure commonly advocated but it is also within the range (albeit lower) of values determined in 2D and 3D model studies by other workers.

- Unconstrained DC inversions using "smooth" model parameters appear to best represent the actual resistivity structure, where size, strength, vertical continuity and depth of investigation are possibly better estimated than in "sharp" unconstrained DC models, where resolution are emphasized over model smoothness.

- Constrained inversions provide better vertical and lateral resolution, improved lithologic mapping and depth of investigation in comparison with unconstrained inversions. However, the apparent depth of investigation can be under-exaggerated.
- Unconstrained inversions provide stronger contrasts than constrained inversions, which results in relatively deeper investigation depths.
- Constrained inversions are capable of overcoming improper reference models, caused by either inaccurate geology or physical property constraints, and still be relied upon to return a reasonably accurate model.
- DCIP Inversions, particularly the chargeability, benefit from model constraints in targeting/imaging deep buried zones, provided they are not forced to adhere to a reference model which is significantly different from reality.

4.2.3 Gocad Model

- The known geology inside the Gocad model stops 800m short of the westernmost edge of the Titan survey coverage.
  The geologic information provided by Kidd Creek for the Gocad model includes geologic elements extending 1km east, and 500m further north and south of the existing survey coverage. However, except for overburden thickness information, the known geology does not extend further west than approx. 78+00E, which is 600m east of the westernmost tip of our survey lines – and so, beyond this point, a mafic volcanic geology has been assumed for this region of the Gocad model.
- The Gocad geologic model was constructed by interpolating geologic contacts across 6 successive level plans, spaced 200-400m apart, from surface to 1.8km depths. Geologic contacts were obtained from Dxf format line drawings. Drill holes were neither included nor used directly in the Gocad model construction.

- The Gocad model and resulting constrained inversions are not valid across the western 400-600m of the model cross-sections and also below 1.8km depths.

  Due to its design and in the absence of drill-hole data used directly in its construction, the Gocad model may contains significant level of uncertainty. This contrasts the geologically constrained 2D inversion models, which assume a uniform level of certainty.

  Although geologic contacts can be reliably interpolated from level plans, as was the case in the construction of the present Gocad model, it remains that the geologic constraints imposed are, at best, only truly accurate at 5 distinctive depths, spaced approximately 400m apart and extending to a maximum depth of 1.8km. Furthermore, because drill hole were not used in its construction, the level of certainty assigned to the position of geologic contacts is not properly quantified in the Gocad model. In contrast, although modern inversion algorithms are capable of applying weighting functions to the reference model, the current constrained geophysical inversions have assumed a uniform level of certainty in the reference models – which is possibly not the case. The re-inclusion of the drill-hole database may therefore be required to properly validate and assess the priority of unexplained geophysical responses.

4.2.4 Petrophysical Analysis

- The available physical property data, required to populate the Gocad model, were incomplete (particularly chargeability) and had to be drawn from several sources, both in-situ (borehole logging data) and indirect (archival laboratory studies and 2D inversions).

  The single-point resistance data, provided by Falconbridge, in the form of tabled statistical results, characterized only 3 (mafic volcanics, felsic volcanics and argillite/sediments) of the 8 units in the Gocad model. Details

concerning the SPR statistical populations and analyses are also unknown. The electric-array logging data for hole 4509, surveyed by Quantec Logging Services in January, 2002, characterized 5 (ultramafic, mafic, intermediate and felsic/rhyolite rocks, and argillite), with several being under-represented / under-sampled statistically (<0.1% total for mafic, argillite). Resistivities for the remaining 3 units (overburden, massive sulphide, graphite) and all chargeabilities were obtained in part from archival laboratory physical property analysis of representative Archean greenstone belt rocks (P. Alikaj, QIP) and direct comparisons with preliminary, unconstrained 2D inversions of Titan results at Kidd Creek.

- The borehole single-point resistance data, in spite of their relative similarity in data range (≈ 10k ohms), display a narrower range and contrasts which contradict the corresponding borehole electric array and 2D inversion results.

  The single-point resistance data fall into the 8k-12k ohm range, which is similar to the 10k-20k ohm-m range proposed for background rocks based on electric array logs and in our preliminary 2D resistivity models. However, not only are the SPR values display a large variances and a particularly narrow min-max range (<0.3 log-decades), the results suggest that the mafic volcanics are more resistive than the felsics. This contradicts the EAL data, which after subdividing out obvious zones of anomalous conductivity, indicate that the felsic rocks are nearly 2x more resistive than the mafic volcanics, 20x more resistive than the sediments and 300x more resistive than the conductive subunits.

- The SPR single point resistance data, which makes up the Kidd Creek database, are uncalibrated and also contaminated by effects caused by differences and down-hole changes in fluid conductivity and borehole diameter.

Unlike the electric array logs, which can be corrected for the effects of borehole fluid conductivity, single-point resistance data are uncalibrated and can not be corrected for the effects of variable ground contact resistances, borehole width and borehole fluid properties. These effects can lead to large (>100x) differences between the observed (apparent) and true formational resistivity.

- Unlike the resistivity parameter, which used in-situ measurements, the chargeability values used to populate the Gocad model were inferred from archival evidence and unconstrained 2D inversions – not from direct measurement of Kidd Creek rocks.
- The electric array logs indicate that the Kidd Creek rhyolites and dacite units contain both resistive and conductive intervals, the latter resulting from the presence of non-massive pyrrhotitic sulphides and graphites, which have not been accounted for in Gocad model.
- Initial constrained 2D resistivity and chargeability inversions, which were based on maximum values in the inferred physical property values for rhyolite, massive sulphide, graphite and overburden were unsatisfactory and unstable. A second set of constrained 2D inversions, using more moderate values in the range, seemed to produce more predictable and stable results.
- The single-point resistance data, by their nature and in spite of their similarity and range, are uncalibrated and do not accurately represent the formational resistivities required to populate the Gocad model and for referenced inversions.

  By definition, single-point resistance readings are a measure of the contact resistance between a mobile down-hole electrode and the grounding point at the surface, in units of ohms. Although contact resistance and resistivity profiles provide visually similar relative variations down-hole, they are not analogous, as relative amplitude and base-levels for SPR are

variably influenced by the quality of ground contacts obtained – resulting in the large variance and narrow range shown (<0.3 log-decades) in the Kidd data archive provided. As a result, in spite of their similar range in values to the electric array data, the SPR archive cannot be considered a reliable indicator of formational resistivity for rocks at Kidd Creek. Aside from laboratory measurements of rock samples or drill-core, which do not account for the influence of pore-fluid, electric array logs provide the only reliable alternative for formational resistivity characterizations.

- The present physical property analysis, which largely based on uncorrected electric array and single-point resistance logs, may underestimate the true formational resistivities of the rock units, due to the influence of the more conductive borehole fluid.

  In the same way that electric array surveys at surface are influenced by the overburden layer, the borehole electric array logs are affected by the presence of the conductive fluid in the drill hole. As a result, they represent "apparent" resistivities which may require an appropriate correction, in the case of narrow EAL spacings and large resistivity contrasts. However, for narrower holes, more resistive fluid, lower bulk resistivities and larger EAL spacings, the effect is lessened and the formational correction is minor. In fact, for the EAL results in hole 4509, this may indeed be the case, based on the close similarity in range between the borehole petrophysical and 2D resistivity inversion results. In the absence of available calliper and fluid conductivity data, the degree of correction required cannot be determined exactly.

- The physical property analyses indicate that many units in the Gocad model, particularly rhyolite, feature possibly bi-modal distributions in resistivity and therefore may not be validly represented by a single physical property value.

The electric array logs confirm that several of the Kidd Creek units, notably rhyolites, dacites, as well as possibly andesite, feature bi-modal distributions in resistivity, due to the presence of intercalations of non-massive yet conductive and polarizeable sulphides and/or graphite. As a result, not only are these units inaccurately defined by a single, representative resistivity or chargeability, as required in the Gocad model and constrained inversions, the statistical means are not diagnostic due to the possibly bimodal nature of the physical properties.

- The absence of reliable in-situ values for massive sulphide and graphite, mainly, and, to a lesser extent rhyolite and overburden, may strongly influence the accuracy, validity and reliability of constrained 2D inversions.

4.3 Recommendations

4.3.1 2D Inversion Results

- The constrained inversions could be greatly improved by using weighted reference models, based on geologic accuracy and reliability. Cell weighting is already included in the UBC dcip2d inversion platform.
- The EVA processing and unconstrained 2D MT inversions should account for the change in the projection, following de-rotation. Strictly speaking, when projecting sites to a common direction (perpendicular to strike) the position of the sites should be shortened by cos θ. This correction was neither accounted for in the current study nor applied for Titan survey data in general.
- The DCIP results should be inverted using 3D inversion algorithms. The MT inversion results should be tested using 3D models and inversions.

4.3.2 2D Sensitivity Analysis

- 2D sensitivity analyses should be extended to include other arrays, such as pole-dipole, other targets, such as smaller orebodies, and other ge-

ometries, such as 3D bodies, in order to better simulate real earth responses, particularly for the MT.

- More careful consideration should be given to adding appropriate levels of Gaussian noise to the synthetic data in order to make the inversions more robust.
- 2D inversions should be calculated for the MT forward models to test the sensitivity and accuracy of the model solutions, as per the DCIP case.

4.3.3 Gocad Model

- Future Gocad models should include and, if possible, be constructed directly from the drill-hole databases, rather than the digitized level-plan approach utilized presently, in order to: a) properly determine the confidence limits of geologic elements (geologic boundaries, known geology), b) properly constrain the geophysical inversions, by the use of weighting functions, and c) to properly validate and prioritize unexplained anomalies.
- The Gocad Model should be independently queried for fully integrated drill targets, using other information such as geochemistry and alteration.

4.3.4 Petrophysical Analysis

- Future programs requiring physical property analyses should include a larger statistical population of in-situ measurements, designed to adequately characterize all units in the Gocad model, including chargeability and resistivity, either through laboratory studies of hand samples or, preferably borehole electric array logging.
- Future borehole electric array studies should include caliper and fluid conductivity in order to accurately correct the data to a formational resistivity and chargeability value.
- The Gocad model should be reconciled with the borehole petrophysical surveys, in order to: a) account for discrepancies observed (i.e., notice-

able variations/zonations in conductivity and chargeability within a unit relating to known alteration or mineralization) and b) to ensure similar naming conventions for borehole and Gocad lithologies.

- Accurate physical property data for rhyolite, massive sulphide, graphite and, possibly, overburden is recommended for more reliable, quantitative analysis and target-evaluation of conductive anomalies detected, particularly based on the Ratio-M/Delta-M products.
- Induced polarization logging and physical property testing should be used to better characterize the IP reference constraints in the Gocad model.

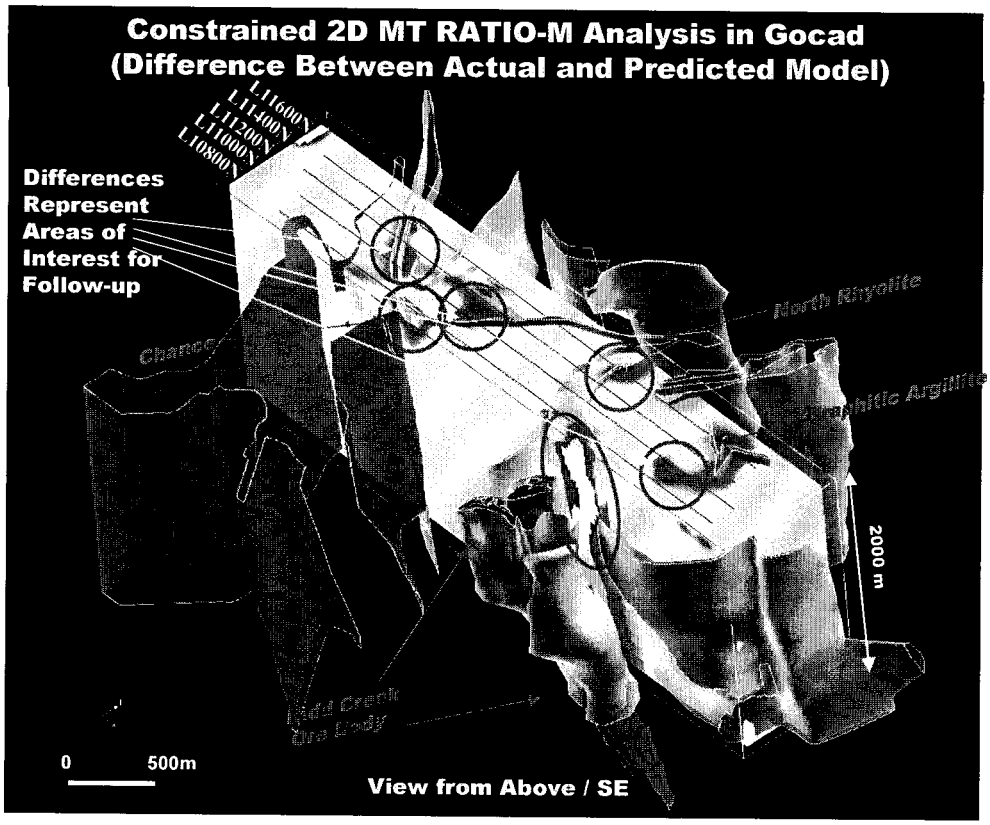

Figure 4.1: Constrained 2D MT Ratio-M Values in 3D Gocad Model.

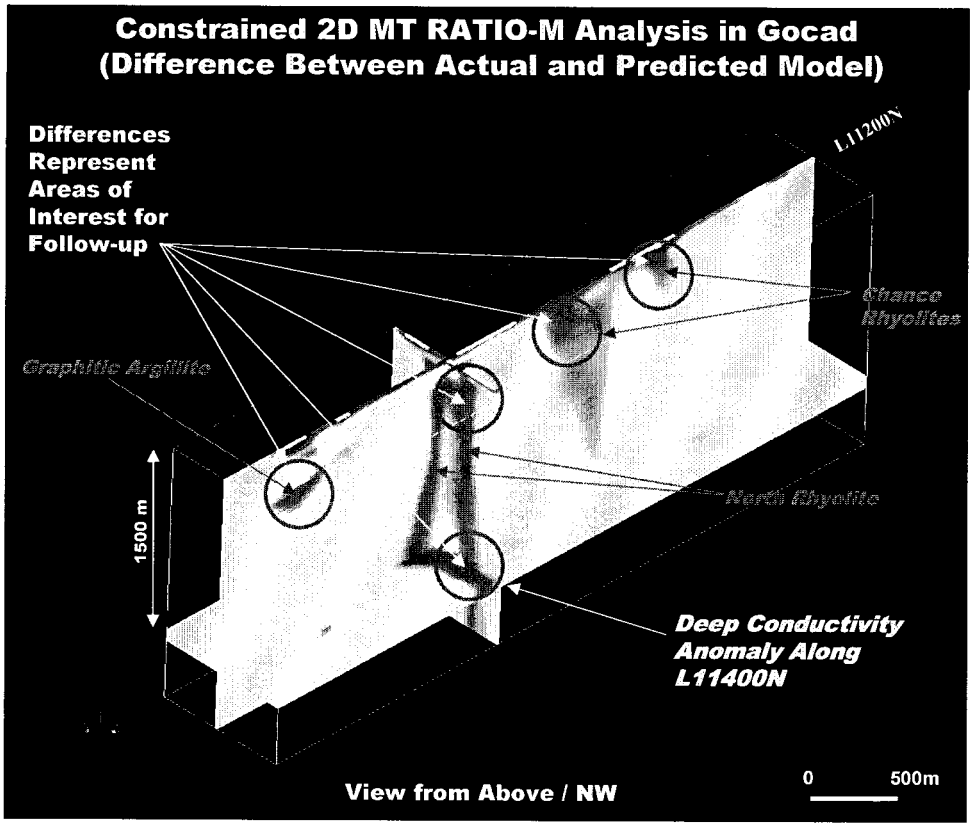

Figure 4.2:Constrained 2D MT Ratio-M in 3D Showing Deep Anomaly in Gocad.

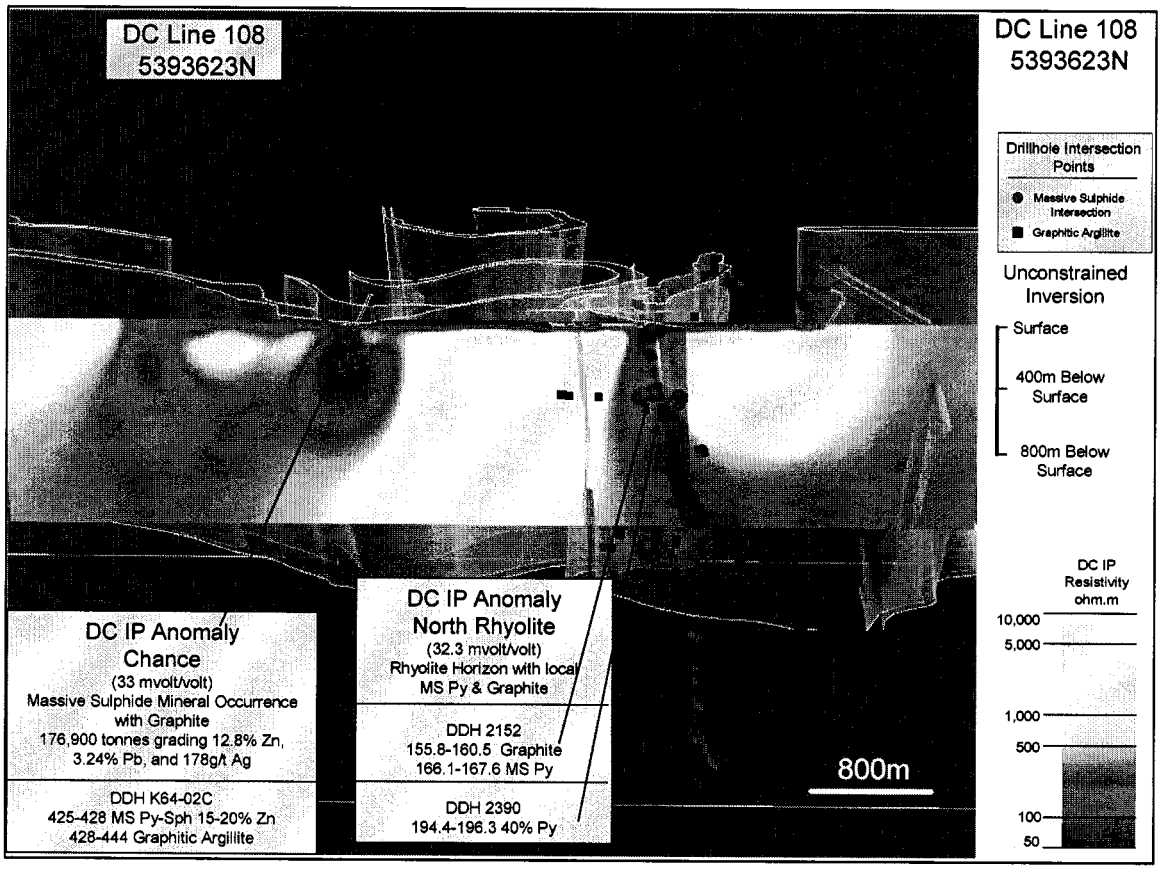

Figure 4.3: Titan 2D DC Results inside Gocad Model showing Drill Results (courtesy Falconbridge Ltd.)

CHAPTER 5 REFERENCES

CAGNIARD, L. (1953). Basic theory of the magnetotelluric method of geophysical prospecting. Geophysics, v. 18, pp. 605-635.

CHOUTEAU, M. (1985). Magnetotelluric measurements in La Malbaie area (Québec): the anomalous vertical magnetic field. Canadian Journal of Earth Sciences, v. 22, pp. 1530-1536.

CHOUTEAU, M. and TOURNERIE, B. (2000). Analysis of magnetotelluric data showing phase rolling out of quadrant (PROQ). 70TH annual international meeting: society of exploration geophysics, pp. 344-346.

COGGON, H. (1973). Comparison of IP electrode arrays. Geophysics, v.38, p 737-761.

DE LUGAO, P. P., and WANNAMAKER, P. E. (1996). Calculating the two-dimensional magnetotelluric Jacobian in finite elements using reciprocity: Geophysical Journal International, v. 127, pp. 806-810.

EGGERS, D.E. (1982). An eigenstate formulation of the magnetotelluric impedance tensor. Geophysics, v. 47, pp. 1204-1214.

FALCONBRIDGE LTD. (2002). Copper - Kidd Creek: Geology Description. In Falconbridge Ltd. website. [On line] http://www.falconbridge.ca/our_business/copper_kidd_creek.html. (web page consulted on August 1ST, 2004).

FISCHER, G. (1985). Some remarks on the behaviour of the magnetotelluric phase. Geophysical Prospecting, v. 33, pp. 716-722.

GARLAND, D. (1979). Introduction to Geophysics (Mantle, Core and Crust). W.B. Saunders Company, Toronto, 494 p.

GOLDSTEIN, M.A., and STRANGWAY, D.W. (1975). Audio frequency magnetotellurics with a grounded dipole source. Geophysics, v. 40, pp. 669-683.

HALVERSON, M.O., ZINN, W.G., MCALISTER, E.O., ELLIS, R., and YATES, W.C. (1981). Assessment of results of broad-band spectral IP field tests. In: Advances in Induced Polarization and Complex Resistivity, pp. 295–346, University of Arizona.

HANNINGTON, M.D., BARRIE, T., and BLEEKER, W. (2004). The giant Kidd Creek volcanogenic massive sulphide deposit, western Abitibi Subprovince, Timmins, Ontario, Canada: local geology. In: Natural Resources Canada, Mineral Resources Division website. [On line] http://www.nrcan.gc.ca/gsc/mrd/projects/kiddcreek/localgeo_e.html. (web page consulted on July 1ST, 2002).

HOOVER, D.B., FRISCHKNECHT, F.C., and TIPPENS, C.L. (1976). Audiomagnetotelluric sounding as a reconnaissance exploration technique in Long Valley, California. Journal of Geophysical Research, v. 81, pp. 801-809.

HYNDMAN, R.D., and HYNDMAN, D.W. (1968). Water saturation and high electrical conductivity in the lower continental crust. Earth and Planetary Science Letters, v. 4, pp. 427-432.

JOHNSON, I.M. (1984). Spectral induced polarization parameters as determined through time-domain measurements. Geophysics, v. 49, pp. 1993-2003.

JONES, A.G. (1981). On a type classification of lower crustal layers under Precambrian regions. Canadian Journal of Earth Sciences. v. 49, pp. 226-233.

JONES, A.G. (1983). On the equivalence of the "Niblett" and "Bostick" transformations in the magnetotelluric method. Letter to the editor, Geophysics v. 53, pp. 72-73.

KAUFMAN, A.A., and KELLERr, G.V. (1981). The Magnetotelluric Sounding Method. Elsevier, New York, 595 pp.

KELLER, G.V., and FRISCHKNECHT, F.C. (1966). Electrical Methods in Geophysical Prospecting. Pergamon Press, New York, 519 pp.

KINGMAN, J. (2000a). Halverson-Wait model. Quantec Geoscience internal memorandum, Dated 31-10-2000, 2 pp.

KINGMAN, J. (2000b). Quantec Geoscience chargeability scale and units standards. Quantec Geoscience Inc. internal memorandum, Dated 28-11-2000, 9 pp.

KINGMAN, J., and GARNER, S. (2003). Benefits of large channel capacity systems in electrical geophysics. Extended Abstracts of papers of the ASEG 16TH geophysical conference and exhibition, Adelaide, Australia, 4 pp. [On line]. http://www.vnce.com.au/sferic/Library/ASEG2003.benefits.pdf. (web page consulted on December 1ST, 2004).

KURTZ, R.D., CRAVEN, J.A., NIBLETT, E.R., and STEVENS, R.A. (1993). The conductivity of the crust and mantle beneath the Kapuskasing Uplift: electrical anisotropy in the upper mantle. Geophysical Journal International, v. 113, pp. 483-498.

LANGORE, L., ALIKAJ, P., GJOVREKU, D. (1989). Achievements in copper sulphide exploration in Albania with IP and EM methods. Geophysical Prospecting, v. 37, p 925 - 941.

LEGAULT, J.M., MORALES, M., PELECHATY, and DAWSON, D.J.W. (2002a). Geophysical survey logistics report regarding the Quantec Titan-24 distributed array system tensor magnetotelluric and DCIP resistivity surveys over the Kidd Creek mine project, Kidd Twp., near Timmins, ON, on behalf of Ontario Ministry

of Northern Development and Mines and Falconbridge Ltd (OMET project 13-2001a). Toronto: Quantec Geoscience Inc. internal report, 89p, QG-215.

LEGAULT, J.M., GORDON, R., REDDIG, M., and SLAMA E. (2002b). Geophysical survey interpretation report regarding the Quantec Titan-24 distributed array system tensor magnetotelluric and DCIP resistivity surveys over the Kidd Creek mine project, Kidd Twp., near Timmins, ON, on behalf of Ontario Ministry of Northern Development and Mines and Falconbridge Ltd (OMET project 13-2001a). Toronto: Quantec Geoscience Inc. internal report, 99p, QG-215.

LEGAULT, J.M., GORDON, R., REDDIG, M., and SLAMA E. (2002c). Geophysical survey interpretation report regarding the Quantec Titan-24 distributed array system tensor magnetotelluric and DCIP resistivity surveys over the Dixie and Ben Lake projects, near Red Lake, ON, on behalf of Ontario Ministry of Northern Development and Mines and Tribute Minerals Corp. (OMET project 13-2001c). Toronto: Quantec Geoscience Inc. internal report, 80p, QG-220.

LEGAULT, J.M., MORALES, P., DOERNER, W., and SLAMA E. (2003). Geophysical survey interpretation report regarding the Quantec Titan-24 distributed array system tensor magnetotelluric and DCIP resistivity surveys over the Norman and Levack mine projects, near Sudbury, ON, on behalf of Ontario Ministry of Northern Development and Mines and FNX Mining Ltd. (OMET project 13-2001d). Toronto: Quantec Geoscience Inc. internal report, 89p, QG-219.

LIVELYBROOKS, D., MARESCHAL, M., BLAIS, E., and SMITH, J.T. (1996). Magnetotelluric delineation of the Trilabelle sulphide body in Sudbury, Ontario. Geophysics, v. 61, no. 4. pp. 971-986.

MORRISON, K., and MCGAUGHEY, J. (2001). The Gocad common earth model: A revolution in exploration data integration. In Mira Geoscience website. [On line]. http://www.mirageoscience.com/publications/mira_earth_decision_sci-

ences, and Gocad research presentations. (web page consulted on August 1ST, 2004).

OLDENBURG, D.W., and LI, Y. (1999). Estimating depth of investigation in DC and IP surveys. Geophysics, v. 64, pp. 403-416.

OLDENBURG, D.W., and LI, Y. (1994). Inversion of induced polarization data Geophysics, v. 59, pp. 1327-1341.

OLDENBURG, D.W., LI, Y., and JONES, F. (1998). Tutorial: Inversion (Res/IP) Methodology. In: The UBC Geophysical Inversion Facility Tutorials. [On line]. http://www.geop.ubc.ca/ubcgif/tutorials/invtutorial/index.html. (web page consulted on August 1ST, 2004).

OPAWICA EXPLORATIONS LTD. (2004). Chance-Whitestar property: Drilling 2000. In Opawica Explorations website. [On line]. http://www.opawica.com/ (web page consulted on August 1ST, 2004).

PELTON, W.H., WARD, S.H., HALLOF, P.G., SILL, W.R. and NELSON, P.H. (1978). Mineral discrimination and removal of inductive coupling with multifrequency IP. Geophysics, v. 43, pp. 588-609.

PRUGGER, A.F., and WOODS, D.V. (1984). The pattern of anomalous geomagnetic variation fields over the mid-continent gravity high. Journal of Geophysical Research, v. 89, pp. 7773-7782.

QUANTEC GEOSCIENCE LTD. (2004). Titan-24 Deep Electrical Earth Imaging Technology. In Quantec Geoscience website. [On line]. http://www.quantec geoscience.com/titanInfo.html. (web page consulted on August 1ST, 2004).

REDDIG, R. (2002). Geophysical interpretation report, Titan-24 distributed array MT and DCIP resistivity surveys over the Red Lake mine project, on behalf of Ontario Ministry of Northern Development and Mines and Goldcorp Ltd. (OMET

project 13-2001b). Toronto: Quantec Geoscience Inc. internal company report, 79p, QG-218.

RODI, W.L., and MACKIE, R.L. (2001). Nonlinear conjugate gradients algorithm for 2D magnetotelluric inversion. Geophysics, v. 66, pp. 174-187.

ROY, A., and APPARAO, A. (1971). Depth of investigation in direct-current methods. Geophysics, v. 36, pp. 943-959.

RUTLEY, R,, OLDENBURG, D.W., and SHETKHMAN, R. (2001). 2D and 3D IP/resistivity for the inversion of Isa style targets. Extended Abstracts of papers of the ASEG 15TH geophysical conference and exhibition, Brisbane, Australia, 4 pp.

SHEARD, N. (1998). MIMDAS: A new direction in geophysics. Proceedings of the ASEG 13th International Conference, Hobart, Tasmania.

SEIGEL, H.0. (1959). Mathematical formulation and type curves for induced polarization. Geophysics, v. 24, pp. 547-565.

SPITZ, S. (1985). The magnetotelluric impedance tensor properties with respect to rotations. Geophysics, v. 50, pp. 1610-1617.

STEVENS, K.M., and MCNEICE, G. (1998). On the detection of ni-cu ore hosting structures in the Sudbury igneous complex using the magnetotelluric method. 68TH annual international meeting: society of exploration geophysics, pp 751-755.

STRANGWAY, D.W., and KOZIAR, A. (1979). Audio frequency magnetotelluric sounding - a case history of the Cavendish geophysical test range. Geophysics, v. 44, pp. 1420-1446.

STRANGWAY, D.W., SWIFT, C.M., and HOLMER, P.C. (1973). The application of audio frequency magnetotellurics to mineral exploration. Geophysics v. 38, pp. 1159-1175.

TELFORD., W.M., GELDART, L.P., SHERIFF, R.E., and KEYS, D.A. (1976). Applied Geophysics. Cambridge University Press, New York, 860 pp.

TORRES-VERDIN, C., and BOSTICK, F.X. (1992). Principles of spatial surface electric field filtering in magnetotellurics: electro-magnetic array profiling (EMAP). Geophysics, v. 57, pp. 603-622.

VOZOFF, K. (1972). The magnetotelluric method in the exploration of sedimentary basins. Geophysics, v. 37, pp. 98-141.

WHITE, R.M.S., COLLINS, S., and LOKE, M.H. (2003). Resistivity and IP arrays, optimised for data collections and inversion. Exploration Geophysics, v. 34, pp. 229-332.

WORD, D.R., GOSS, R., and CHAMBER, D.M. (1986). An EMAP case study. Abstracts of papers of the 56th annual meeting of the SEG, Houston, p. 383.

WORD, D.R., SMITH, H.W., and BOSTICK, F.X. (1971). Crustal investigations by the magnetotelluric tensor impedance method. In: Geophysical Monograph Series, v. 14: The Structure and Physical Properties of the Earth's Crust, Heacock, J.G., ed., pp. 145-167.

YOUNG, C.T. (1981). Principles of Phoenix Geophysics real time remote reference magnetotelluric system. Phoenix Geophysics, Denver, vers. 3.2, 51 pp., based on: Magnetotelluric measurements of conductivity anomalies in northern Wisconsin (1977). Ph.D. dissertation, Department of Geology and Geophysics, University of Wisconsin, Madison.

CHAPTER 6 BIBLIOGRAPHY

ADAM, A., SZARKA, L., and Vero, J. (1989). Natural and man-made EM variations in the Komlo coalfield. Physics of the Earth and Planetary Interiors, v. 53, pp. 207-213.

ALPEROVITCH, I.M. and other workers (1982). Magnetotellurics in Oil Exploration in the USSR. SEG Publications, Tulsa, 65 pp.

ANDRIEUX, P., and WIGHTMAN, W.E. (1984). The so-called static corrections in magnetotelluric measurements. Abstracts of papers of the 54th annual meeting of the SEG, Atlanta, p. 270.

BARTEL, L.C., and JACOBSON, R.D. (1987). Results of a controlled-source audiofrequency magnetotelluric survey at the Puhimau thermal area, Kilauea Volcano, Hawaii. Geophysics, v. 52, pp. 665-667.

BERDICHEVSKY, M.N., and DMITRIEV, V.I. (1976). Basic principles of interpretation of magnetotelluric curves. In: Geoelectric and Geothermal Studies, Adam, A., ed., Akademini Kiado, pp. 165-221.

BERDICHEVSKY, M.N., DMITRIEV, V.I., LEBEDEVA, N.A., and BARASHOV, I.S. (1984). Magnetotelluric sounding of crustal conduction zones. Izvestiya, Physics of the Solid Earth, v. 20, pp. 683-688.

BERDICHEVSKY, M.N., VANYAN, L.L, and DMITRIEV, V.I. (1989). Methods used in the U.S.S.R. to reduce near-surface inhomogeneity effects on deep magnetotelluric sounding. Physics of the Earth and Planetary Interiors, v. 53, pp. 194-206.

BERDICHEVSKY, M.N., and ZHDANOV, M.S. (1984). Advanced Theory of Deep Geomagnetic Sounding. Elsevier, New York, 362 pp.

BOSTICK, F.X. (1977). A simple and almost exact method of MT analysis. In: Workshop on Electrical Methods in Geothermal Exploration, Snowbird, Ut., USGS contract no. 14080001-8-359.

BOSTICK, F.X. (1986). Electromagnetic array profiling (EMAP). Abstracts of papers of the 56th annual meeting of the SEG, Houston, p. 383.

CARLSON, N.R., ZONGE, K.L., and HUGHES, L.J. (1986). Applications of CSAMT to oil and gas exploration: a case history. Abstracts of papers of the 48th annual meeting of the EAEG, Ostende, p. 83.

CHOUTEAU, M. (1982). Magnetotelluric survey across the Abitibi Greenstone Belt: Preliminary Results. Earth Physics Branch, E.M.R., internal report, 26 pp.

CHOUTEAU, M. (1985). The highly conductive structure of Ste-Mathilde (Québec): Interpretation from magnetotelluric soundings. CIM Bulletin, v. 78, pp. 69-74.

CHOUTEAU, M., and BOUCHARD, K. (1988). Two-dimensional terrain correction in magnetotelluric surveys. Geophysics, v. 53, pp. 854-862.

CSORGEI, J., LADA, F., and VERO, L. (1986). Magnetotelluric measurements for exploration of non structural hydrocarbon deposits. Abstracts of papers of the 48th annual meeting of the EAEG, Ostende, p. 83.

DOBRIN, M.B. (1976). Introduction to Geophysical Prospecting. McGraw-Hill, New York, 730 pp.

DUNCAN, P.M., HWANG, A., EDWARDS, R.N.. and GARLAND, G.D. (1980). The development and application of a wide band electromagnetic sounding system using a pseudo-noise source. Geophysics, v. 45, pp. 1276-1296.

EDWARDS, R.N., GOMEZ-TRAVINO, E., and Nobes, D. (1982). A magnetometric resistivity (MMR) survey at research area RA-4, Atikokan, Ontario. Work done by the University of Toronto for AECL.

FISCHER, G. (1989). A strong topographic valley effect of AMT and VLF-R measurements. Geophysical Journal, v. 96, pp. 469-475.

FISCHER, G., SCHNEGG, P.-A., PEGUIRON, M., and LEQUANG, B.V. (1981). An analytic one-dimensional magnetotelluric inversion scheme. Geophysical Journal of the Royal Astronomical Society, v. 67, pp. 237-278.

FUJII, T., KOMORI, H., and HONKURA, Y. (1989). A portable ELF-MT system for shallow resistivity sounding. Physics of the Earth and Planetary Interiors, v. 53, pp. 270-277.

GAMBLE, T.D., GOUBAU, W.M., and CLARKE, J. (1979). Magnetotellurics with remote magnetic reference. Geophysics, v. 41, pp. 53-68.

GOLDBERG, S., and ROTSTEIN, Y. (1982). A simple form of presentation of magnetotelluric data using the Bostick transform. Geophysical Prospecting, v. 30, pp. 211-216.

GRANT, F.S., and WESTt, G.F. (1965). Interpretation Theory in Applied Geophysics. McGraw-Hill, Toronto, 584 p.

GROOM, R.W., and BAILEY, R.C. (1989). Some effects of multiple inhomogeneities in magnetotellurics. Geophysical Prospecting, v. 37, pp. 697-712.

HATTINGH, M. (1989). The use of data-adaptive filtering for noise removal on magnetotelluric data. Physics of the Earth and Planetary Interiors, v. 53, pp. 239-254.

JIRACEK, G.R., REDDIG, R.P., and KOJIMA, R.K. (1989). Application of the Rayleigh-FFT technique to magnetotelluric modeling and correction. Physics of the Earth and Planetary Interiors, v. 53, pp. 365-375.

JONES, A.G. (1983). The problem of current channelling: a critical review. Geophysical Surveys, v. 6, pp. 79-122.

JONES, A.G. (1988). Static shift of magnetotelluric data and its removal in a sedimentary basin environment. Geophysics, v. 53, pp. 967-978.

KANASEWICH, E.R. (1981). Time Sequence Analysis in Geophysics. University of Alberta Press, Edmonton, 480 p.

KU, C.C., HSU, M.S., and LIM, S.H. (1972). The topographic effect in electromagnetic fields. Canadian Journal of Earth Sciences, v. 10, pp. 645-656.

KURTZ, R.D., MACNAE, J.C., and WEST, G.F. (1989). A controlled-source, time-domain electromagnetic survey over an upthrust section of Archean crust in the Kapuskasing Structural Zone. Geophysical Journal International, v. 99, pp. 195-203.

LAKANEN, E. (1986). Scalar audiomagnetotellurics applied to base-metal exploration in Finland. Geophysics, v. 51, pp. 1628-1646.

LILLEY, F.E.M., and WOODS, D.V. (1978). The channelling of natural electric currents by orebodies. Bulletin of the Australian Society of Exploration Geophysics, v. 9, pp. 62-63.

MURUKAMI, Y. (1985). Two representations of the magneto-telluric sounding survey. Geophysics, v. 50, pp. 161-164.

NEWMAN, G.A., WANNAMAKER, P.E., and HOHMANN, G.W. (1985). On the detectibility of crustal magma chambers using the magnetotelluric method. Geophysics v. 50, pp. 1136-1143.

OLDENBURG, D.W. (1979). One-dimensional inversion of natural source magnetotelluric observations. Geophysics, v. 44, pp. 1218-1244.

PADILHA, A.L., TRIVEDI, N.B., DA COSTA, J.M., VITORELLO, I., DUPIS, A., and CAVOIT, C. (1989). Audiomagnetotelluric study in northeast region of Parana Basin, South America. Geophysics, v. 54, pp. 824-831.

PARK, S.K. (1985). Distortion of magnetotelluric sounding curves by three-dimensional structures. Geophysics, v. 50, pp. 785-797.

PARK, S.K., and LIVELYBROOKS, D.W. (1989). Quantitative interpretation of rotationally invariant parameters in magnetotellurics. Geophysics, v. 54, pp. 1483-1490.

PARK, S.K., ORANGE, A.S., and MADDEN, T.R. (1983). Effects of three-dimensional structure on magnetotelluric sounding curves. Geophysics, v. 48, pp. 1402-1405.

PORSTENDORFER, G. (1975). Principles of Magneto-Telluric Prospecting. Geoexploration Monographs, series 1, no. 5, 118 pp.

RANGANAYAKI, R.P. (1984). An interpretive analysis of magnetotelluric data. Geophysics, v. 49, pp. 1730-1748.

REDDIG, R.P., and JIRACEK, G.R. (1984). Topographic modeling and correction in magnetotellurics. Abstracts of papers of the 54th annual meeting of the SEG, Atlanta, p. 270.

REDMAN, J.D., HSU, D., and STRANGWAY, D.W. (1980). Audio frequency magnetotelluric measurements on the Eye-Dashwa Lakes Pluton, Atikokan, Ontario. AECL Technical Report, RW/GPH-057-81, 19 pp.

SANDBERG, S.K., and HOHMANN, G.W. (1982). Controlled-source audiomagnetotellurics in geothermal exploration. Geophysics, v. 47, pp. 100-116.

SASAKI, Y. (1989). Two-dimensional joint inversion of magnetotelluric and dipole-dipole resistivity data. Geophysics, v. 54, pp. 254-262.

SHOEMAKER, C.L., SHOHAM, Y., and HOCKEY, R.L. (1986). Interpretation of natural source electromagnetic array data. Abstracts of papers of the 56th annual meeting of the SEG, Houston, p. 383.

SLANKIS, J.A., TELFORD, W.M., and BECKER, A. (1972). 8 hz telluric and magnetotelluric prospecting. Geophysics, v.37, pp. 862-878.

SPIES, B.R. (1989). Depth of investigation in electromagnetic sounding methods. Geophysics, v. 54, pp. 872-888.

SPIES, B.R., and EGGERS, D.E. (1986). The use and misuse of apparent resistivity in electromagnetic methods. Geophysics, v. 51, pp. 1462-1471.

STERNGERG, B.K., WASHBURNE, J.C., and PELLERIN, L. (1988). Correction for the static shift in magnetotellurics using transient electromagnetic soundings. Geophysics, v. 53, pp. 1459-1468.

STODT, J.A., HOHMANN, G.W., and TING, S.C. (1981). The telluric-magnetotelluric method in two- and three-dimensional environments. Geophysics, v. 46, pp. 1137-1147.

STRANGWAY, D.W., REDMAN, J.D., HOLLADAY, S., and HORNE, C. (1980). Audio frequency magnetotelluric soundings at the Whiteshell nuclear research

establishment and Chalk River nuclear laboratories. AECL, Technical Record, TR-71, 58 pp.

SWIFT, C.M., Jr. (1981). Theoretical MT and turam response from two-dimensional inhomogeneities. Geophysics, v. 36, pp. 12-18.

TING, S.C., and HOHMANN, G.W. (1981). Integral equation modeling of three-dimensional magnetotelluric response. Geophysics, v. 46, pp. 182-197.

TZANIS, A., and BEAMISH, D. (1989). A high-resolution spectral study of audio-magnetotelluric data and noise interactions. Geophysical Journal, v. 97, pp. 557-572.

VAN NGOC, P., BOYER, D., and CHOUTEAU, M. (1978). Mapping of apparent pseudo-resistivities by telluric-telluric profiling associated with magnetotellurics. Geophysical Prospecting, v. 26, pp. 218-246.

WAESELYNCK, M. (1974). Magnetotellurics - principle and outline of the recording technique - a case history. Geophysical Prospecting, v. 22, pp. 107-121.

WAIT, J.R. (1959). Overvoltage Research and Geophysical Applications. Pergammon Press.

WANNAMAKER, P.E., STODT, J.A., and RIJO, L. (1986). Two-dimensional topographic responses in magnetotellurics modeled using finite elements. Geophysics, v. 51, pp. 2131-2144.

WANNAMAKER, P.E., HOHMANN, G.W.. and WARD, S.H. (1984). Magnetotelluric responses of three-dimensional bodies in layered earths. Geophysics, v. 49, pp. 1517-1534.

WARD, S.H. (1959). AFMAG - airborne and ground. Geophysics, v. 24, pp. 761-789.

WARD, S.H. (1983). Controlled source electrical methods for deep exploration. Geophysical Surveys, v. 6, pp. 137-152.

WARD, S.H., RYU, J., GLENN, W.E., HOHMANN, G.W., DEY, A., and SMITH, B.D. (1974). Electromagnetic methods in conductive terrain. Geoexploration, v. 12, pp. 121-183.

WEST, R.C., and WARD, S.H. (1988). The borehole controlled-source audio-magnetotelluric response of a three-dimensional fracture zone. Geophysics, v. 53, pp. 215-230.

YAMASHITA, M., and HALLOF, P.G. (1985). CSAMT case histories with a multi-channel, CSAMT system and discussion of near-field data correction. Paper presented at the 55th annual meeting of the SEG, Washington, 13 pp.

YOUNG, R.A., and LUCAS, J.E. (1988). Exploration beneath volcanics, Snake River plain, Idaho. Geophysics, v. 53, pp. 444-452

APPENDICES
(SEE ATTACHED DOCUMENT ON CD-ROM)